

Anonymous Referee #1

This paper describes the construction of an important and comprehensive long-term dataset for key trace gases in the stratosphere. It is important to have a peer-reviewed and citable description of datasets like this GOZCARDS dataset. The manuscript serves this purpose very well, and I support publication in ACP.

My main criticism concerns the length of the manuscript. Over 100 journal pages, almost 30 figures, plus appendix and supplement are a tall order. I wish the authors would have made the effort to be more concise. At this point it is probably difficult to make the paper much shorter, but I have some suggestions:

Response: This main criticism has been addressed by significantly reducing the size of the paper, following most of the reviewer comments/suggestions; we certainly appreciate all the reviewer efforts regarding suggestions to help address the length issue.

We decided to present the merging methodology in this paper but also included some original analyses (after having released the data for community analyses) in order to make it more relevant for ACP. We also include useful details such as data screening procedures, not always described well enough in past papers, in order to assist anyone potentially wanting to duplicate this dataset (and for completeness) – but now relegate most of this to the Appendix. We also believe that ACP papers (and this paper in particular) should not deal primarily with methodology - so we were not inclined to remove everything of interest regarding early sample results using GOZCARDS. One can get criticized the other way sometimes and get suggestions to try publishing in AMT instead, if one deals only or mainly with methodology (or techniques or validation). While this paper is still somewhat long because of the dual goal (methodology and some results + the description of a multi-species effort), we feel that at this point, a 23% reduction in the main text (and our cutting out 3.5 Figures out of the original 27) without eliminating most newer discussions/results is a reasonable compromise.

1 Major comments

GOZCARDS HCl sample results: Given recently published results, e.g. Mahieu et al. 2014, I feel that it is not necessary to discuss the HCl variations at various levels in such detail. I think Figures 7 and 8 already present all the relevant information. Figures 9 and 10, to me, are not needed (a look at Fig. 7 gives almost the same information). The discussion on pages 5865 last paragraph to 5868 first paragraph is also not necessary. I think it provides no really new or essential information, and is not necessary for the main topic of the paper, which is description of the overall dataset. Moving the important citations to the early part of section 3.3 would be enough, in my opinion.

Response: We have made significant cuts here. However, showing that the HCl behavior is turning around in the later years is useful and new (and in our view, informative for ACP audience, and as a brief update to the Mahieu et al. work, which mainly looked at columns - and stopped in 2011). We believe that it is most useful to show (keep) the 2 left panels of Fig. 10 to show the non-linearity and connection to surface total chlorine changes. So we took out two thirds of Figs. 9 & 10 (combined) [we are just left with the new Fig. 9] and shortened the text significantly (by about 45% - see the new discussion before Sect. 4).

GOZCARDS H₂O sample results, pages 5873 to 5876: This reads almost like a review paper. Again, I think many readers will be familiar with the overarching issues, and would appreciate a briefer and more concise discussion. Figures 15 and 17 already give a very good description of long and shorter term water vapour variations, even without much text. Is Figure 16 really needed? Are all the (confusing and overall similar) thin and dashed lines needed in a dataset description paper?

Response: Agreed, we have significantly shortened this H₂O discussion (by almost 40% for section 4.3) and we simplified Fig. 16 (now with no thin lines), without taking it out altogether, as one can refer to this as a useful diagnostic for testing model variability.

GOZCARDS Ozone sample results: Since GOZCARDS is primarily a stratospheric ozone profile dataset, I wonder if the long comparison and discussion with the Ziemke and Chandra 2012 column dataset is really that helpful. As the authors show, this dataset seems to definitely have a problem, and generally TOMS and OMI are not recommended for long-term trend analyses any more. It seems to me that this part of the current paper dates back a few years. There are several more recent analyses of ozone profile trends (Tummon et al. ACPD 2014, Harris et al. ACPD 2015, WMO 2014). I feel it would be much better to tie in the GOZCARDS data with these publications, and drop the comparison with the Ziemke and Chandra column data. At the same time, the discussion could be shortened, and number of figures in this part could be reduced.

Response: We think that cutting out the column ozone discussion completely would remove a significant analysis as we have not really seen published work on this subject, despite what some may view or characterize as “common knowledge” regarding TOMS/OMI column data time series analyses. This ozone discussion may “date back” a bit, but it is new evidence nevertheless (many papers discuss “old data”), and the ozone topic is the primary reason to tie this paper to the SP²N special issue (on ozone only). The reviewer states “as the authors show”, and we did feel we needed to show something on this topic, as we did not see such a mention (to the ZC12 work) in the WMO Report, for example. Unless specific published references already exist to clearly make our point and/or to imply that other column series are superior to TOMS/OMI, we plan to retain the flavor of this ozone-related “sample result”. For brevity, however, we remove Fig. 23 and Fig. 25 and retain only Fig. 24 (Fig. 22 in the update); this preserves our point regarding comparison issues for GOZCARDS stratospheric column relative changes versus those provided by ZC12, but more succinctly. Overall, the Sect. 5.3 text has been cut by 37%.

Also, adding something really new to the ozone profile trends discussions at this point would likely require substantial efforts and a separate manuscript, given the assessments and discussions provided for GOZCARDS ozone profiles in WMO (2014) and in several other references – as mentioned in our ozone section. We think that briefly referencing/highlighting recent trend studies using GOZCARDS is sufficient, as there are a lot of details in those papers.

Summary and conclusions could also be shortened. There, and in several other places, it seems to me that the manuscript resulted from adding newer references to an older previous manuscript version, and discussing them later / separately. E.g. Section 5.5.2 about diurnal ozone variations seems like a tag-on coming from more recent interest and publications on this topic. The reference to Mahieu et al. 2014 paper on page 5893 restarts the discussion again, making the paragraph unnecessarily long.

Response: Agreed. We have shortened this summary significantly; the whole summary section was cut by 31%.

The water vapour summary on pages 5894 and 5895 is also very long. It should be shortened and focused.

Response: Agreed. We have shortened this summary significantly; the whole summary section was cut by 31%.

Overall, the manuscript would benefit greatly from a thorough attempt at removing redundancies and shortening plus focusing on the main topics: Data set generation and sample results.

Response: Agreed. We have shortened the main text significantly (by 23% - and deleted 3.5 Figures), also following another set of referee comments – but keeping in mind our introductory response (sample results are viewed as a useful contribution to ACP).

2 Minor comments

page 5851, lines 15 to 17: I find this sentence confusing and hard to understand. Maybe change to: In the upper stratosphere, however, SAGE II is not used after June 2000, when the (NCEP temperature-dependent) data conversion from a density/altitude to a mixing ratio/pressure grid exhibits a shift in the Southern Hemisphere. Instead HALOE data are used as a transfer reference from SAGE II before 2000 to the datasets starting in 2004.

Response: Agreed, but this portion and the whole Abstract were shortened (per other referee comments), so the upper stratospheric details are now left out of the Abstract.

page 5852, line 15: Here, and in most places, WMO 2011 should be supplemented by WMO 2014, or replaced by it. WMO 2014 was published in December 2014.

Response: Agreed; in places, as appropriate, we have added the WMO (2014) reference (although in the first mention listed here, we removed the WMO reference for brevity).

page 5854, line 6: Probably good to add "converted to mixing ratio versus pressure using their enclosed NCEP temperature profiles, and" after "were"

Response: Agreed; we essentially used the above additional text.

page 5854, line 8: Add a typical number of MLS profiles per day.

Response: Agreed, done (about 3500 profiles).

By the way, also related to the next paragraph: How is the standard error of the mean calculated in Figure A1(b)? From the Appendix and the Figure caption I get the impression that it is calculated by standard deviation divided by the square root of the number of profiles. This assumes that all the profiles are uncorrelated. This may be true for the few and far spread occultation profiles, but for the many close emission profiles it is probably not true.

Response: Yes, this is how it is calculated (standard definition); the correlation issue is not trivial to accurately estimate, and the main result (many more data points from emission measurements) still would lead to these relatively much smaller errors (probably within a factor of two or better). Correlation occurs for some MLS bands (radiance) more than others but mainly along-track; in particular, the MLS measurement calibration (which can introduce some correlation) occurs on a much shorter timescale (a few minutes/profiles) than the typical profile

separation in a monthly 10° zonal average, which mixes in many uncorrelated data points from separate orbits.

page 5854, lines 15, 16: cross-sections (UV, visible, near IR, far IR, microwave) could also be an issue.

Response: Agreed, but this is implicitly included in the retrievals and their assumptions; if we were to produce all the potential reasons, this list would be quite long (e.g., see the MLS validation/characterization papers). Thus, and for brevity, we did not try to list all error sources.

page 5855, 1st paragraph: Maybe add WMO 2014 as well?

Response: Agreed, done.

page 5856: I am missing a mention of SAGE screening. Maybe mention the discussion in the Appendix here.

Response: The main data screening procedures have now been collected/summarized in Table A1 (Appendix A). We found a few species-specific details to be more appropriate for the species sections, but Table A1 is mentioned in these sections also.

page 5860+5861: I find this whole discussion lengthy and difficult to understand. Could it not be shortened? Is it not simply like this: First AURA-MLS and ACE-FTS are shifted to have the same average level in 2004 and 2005. This level is equal to their combined average level. Then HALOE (which has fewer data in 2004 and 2005) is also shifted to this level.

Response: No, this is not the way we adjust the third dataset and this will not provide the same answer as our procedure, as we wish to give equal weight to each of the three datasets (also note that the number of points changes with latitude and HALOE can often have more points than ACE-FTS, especially in the tropics). Shifting the 3rd dataset to the average of the first two is not the same as weighting them all three equally to get an average reference that depends on all three series. We describe our iterative procedure, which does use this equal weighting philosophy (since the first 2 series give a temporary merged result, then weighted by 2/3 with the 3rd series weighted by 1/3 for the last adjustments). Since a simplification was sought here, text cuts (by close to 30%) were implemented for the 1st part of Sect. 3.2 (Fig. 1 description of the HCl and H₂O merging process), with little reduction in the main message. However, an oversimplification would be dangerous, for what is an essential description of the process. The Appendix has a mathematical explanation that should help, and this process can be carefully tested on sample datasets (and we have done this - also when considering the simplifications offered by the reviewers). The iterative process is what we decided upon as the best path, and it does take a few sentences to explain this. Note that this explanation paragraph is not a major portion of the full paper (or even the HCl section), but we did shorten this section. We also added some clarification words in the caption to Figure 1, which we hope can help.

page 5865, line 23: With the addition of the Mahieu et al. 2014 references, and one or two additional sentences, section 3.3 could end right here. The rest of the section, until page 5868 line 15, is not needed, in my opinion.

Response: We made some significant cuts here. However, showing that the HCl behavior is turning around in the later years is useful and new (and in our view, informative for ACP audience, and as a brief update to the Mahieu et al. work, which mainly looked at columns - and

stopped in 2011). We believe that it is most useful to show (keep) the 2 left panels of Fig. 10 to show the non-linearity and connection to surface total chlorine changes. Thus, we took out two thirds of Figs. 9 and 10 (combined) and shortened the text accordingly; we are left with the new Fig. 9.

page 5868, around line 25: Is it certain that these low H₂O values are wrong? Is there a reference for that? Could H₂O from the gas phase have gone into Pinatubo aerosols, which consist of a sulfuric acid + water mixture? I have not done the numbers, so maybe this just shows my ignorance.

Response: The water vapor averages are lower than usual and other tropical measurements from UARS MLS (for 22 hPa) do not typically dip lower than 3 ppmv (including 3 std. devs. from the monthly means, which are above 3.5 ppmv). The Pinatubo-related stratospheric SO₂ amounts are quite small compared to the 0.5 to 1 ppmv needed for these water vapor differences in 1992. In particular, Read et al. (GRL, June 1993) indicate that enhanced lower stratospheric SO₂ profile values (measured by UARS MLS) were only of order 10 ppbv in Sep. 1991. Thus, conversion to sulfuric acid aerosols would not be expected to deplete water vapor substantially on a large scale, even if shortly after the eruption it may have had some (more localized) impact. However, we added the following sentence: "While this method may exclude some good data points, the lowest values (< 3 ppmv) do get screened out; such outliers are not corroborated by 22 hPa UARS MLS data (with most values > 3 ppmv).

page 5873, line 15 to page 5876, line 6: This is very lengthy, half a water vapour review paper. I think it should be shortened substantially. A few key messages, no literature review.

Response: Agreed, we eliminated most references and shortened this significantly (section 4.3 is now almost 40% shorter), also in response to comments from another referee.

page 5877, lines 1 to 7: I am missing clarity here. There are two aspects: 1.) SAGE retrieval needs density profiles. For V6.2 these came from NCEP operational, for V7 these came from MERRA. The effect of the different sources on SAGE ozone (number density vs. altitude) is very small 2.) Conversion to mixing ratio vs. pressure needs temperature/ pressure profiles. There, a large artefact arises in the SH upper stratosphere when NCEP is used instead of MERRA. If GOZCARDS would use MERRA here (and not the NCEP that comes with SAGE V6.2) the problem would be much smaller. I think this needs to be made clearer.

Response: Agreed, we have reworded the relevant sentences (before Sect. 5.1.1).

page 5878, line 20: Give some references for SAGE-HALOE comparisons, e.g. E. Remsberg et al., and others.

Response: While the data versions in the past have often differed slightly, we do not know or find which Remsberg reference the referee might be thinking of; but we did add the SPARC (1998 Report) reference, providing overall agreement with our own results (shown in the Supplementary material).

page 5879, line 27: I don't think SAGE ozone drifts. What drifts is NCEP / the conversion to mixing ratio versus pressure. Please correct.

Response: Agreed, we clarified this further by rearranging the sentences and rewording (see discussion of Fig. 17, before Sect. 5.2).

page 5881, line 17 to page 5887 line 21: Two very long subsections (review papers) that present lots of references, but very little really new information. Please shorten substantially.

Response: Agreed, we shortened this substantially (also per comment of another referee). These combined two ozone sections are now shorter by about 28% (5.2.2 is shorter by nearly 20% and 5.3 by 37%). Also, two ozone Figures were deleted from the “sample results” section (5.3).

Anonymous Referee #2

This manuscript describes the GOZCARDS data set comprised of several key stratospheric constituents. The goal of GOZCARDS is to combine data from multiple satellites into a consistent record suitable for long-term analysis. This paper describes the methodology used in constructing the data set, as well as provides analysis examples for each of the primary constituents. Continued long-term stratospheric time series analysis depends on our ability to combine data from multiple instruments, and as such documentation and validation of the methods used to construct this data set are very important to the research community. The manuscript is appropriate for publication in ACP with some notable revisions.

General Comments:

Overall the analysis and approach is good. However, I fear the length of the manuscript (27 figures, plus appendix and supplemental material) makes the paper in its current form very difficult to digest. I feel some of the analysis confuses the main point of the paper, which is the methods used to construct the data set, and the consistency between the source data sets used by GOZCARDS which directly affects the uncertainty of the final product. While I understand shortening the manuscript at this point is easier said than done, I suggest the authors consider whether some of the detailed analysis in particular can be removed, and possibly put into a separate manuscript. Though I'm not sure it would help significantly with length, in several sections the manuscript could be written more concisely. I will make a few suggestions in my specific comments, but general suggestions include writing in present active tense as much as possible, limiting qualitative descriptors, especially when the actual results follow in parentheses, and using tables as much as possible.

Response: This main criticism has been addressed by significantly reducing the size of the paper, following most of the reviewer comments/suggestions). However, we note that this paper is really the culmination of a 5-year effort to produce the datasets and to provide some results and overview of the possibilities, which are enhanced as well by other recent (or upcoming) papers analyzing ozone or HCl variations, for example. The paper has been shortened, largely following the suggestions from the reviewers and we certainly appreciate all the reviewer efforts regarding suggestions to help address the length issue.

We decided to present the merging methodology in this paper but also included some original analyses (after having released the data for community analyses) in order to make it more relevant for ACP. We also include useful details such as data screening procedures, not always described well enough in past papers, in order to assist anyone potentially wanting to duplicate this dataset (and for completeness) – but now relegate most of this to the Appendix. We also believe that ACP papers (and this paper in particular) should not deal primarily with methodology - so we were not inclined to remove everything of interest regarding early sample results using GOZCARDS. One can get criticized the other way sometimes and get suggestions to try publishing in AMT instead, if one deals only or mainly with methodology (or techniques or validation). While this paper is still somewhat long because of the dual goal (methodology and some results + the description of a multi-species / multi-year effort), we feel that at this point, a

23% reduction in the main text (and our cutting out 3.5 Figures out of the original 27) without eliminating most newer discussions/results is a reasonable compromise.

For example, Tables 1 and 2 are very informative, and easy to refer back to as needed. Can the general data screening information be put into a table? It is convenient to have all the filtering information in one place, but there are many details that are covered in the relevant publications that are not needed in the narrative. The authors might put the filtering information in a table, sticking just to the actual filtering and not including all the details as to what each filter is doing, for example: UARS MLS precision > 0, MMAF_STAT = "G", "t", "T", Quality=4, per Livesey et al (2003).

Conversely, if the authors do want to describe what each filter means (precision > 0 ensures only a negligible contribution to the retrieval from a priori, as an example), they might consider putting it in the Appendix as the SAGE filtering is done. Either way the information is presented in one place, but not in the main portion of the paper. There are other bits of information that seem to be repeated multiple times, such as the ACE_FTS data processing problems in 2010, that can be noted in the tables or in the data provenance information, rather than repeatedly in the text.

Response: Agreed, we have put the general screening in a Table (Table A1) in the Appendix but have kept some small discussion in the main text for the less well documented screening issues.

The description of the merging process seems overly complicated. For HCl and H₂O, if I understand correctly, the reference level is the average between mean HALOE values from August 2004-Nov 2005 (all that exist), mean ACE-FTS values over the same time period (all that exist), and mean AURA MLS values, but only averaged over the months that ACE-FTS has data. However, since the figures and discussion are keyed to a multi-step process, I do not recommend any large changes, just look for opportunities to simplify the text when possible. Also in the wording, keep in mind that the multi-instrument mean used as reference is not necessarily the correct answer, it is just a common reference. If AURA MLS were perfect, for example, it would still be adjusted in this procedure. In later discussion when referring to data sources that are biased low or high, I believe it is important to clearly state that they are biased high or low relative to the reference level.

Response: Since a simplification was sought here, text cuts (by close to 30%) were implemented for the 1st part of Sect. 3.2 (Fig. 1 description of the HCl and H₂O merging process), with little reduction in the main message. However, an oversimplification would be dangerous, for what is an essential description of the process. The Appendix has a mathematical explanation that should help, and this process can be carefully tested on sample datasets (we have done this - also when considering incorrect simplifications offered by the reviewers). The iterative process is what we decided upon as the best path, and it does take a few sentences to explain this. Note that this explanation paragraph is not a major portion of the full paper (or even the HCl section), but we did shorten this section. We also added some clarification words in the caption to Figure 1, which we hope can help.

Specific Comments/Wording Suggestions (many are minor and not mandatory)

p5850. General in abstract, don't need abbreviations unless you are using the abbreviation multiple times in the abstract (i.e. don't need MERRA and ESDR).

Response: Agreed, we deleted the terms "ESDR" and "MERRA" from the Abstract.

L9-L10: I'm not sure about the word debiased, it implies the full bias is removed, but in fact only the relative bias is removed. What about "To merge ozone records we first adjust each time series by its mean offset with respect to SAGE II during periods of measurement overlap to remove relative bias, and then average. For other species we use a multi-instrument mean computed during overlap periods as the reference."

Response: Agree to the "relative to SAGE II" modification (simple), but not on the 2nd simplification, which uses more words but does not state accurately enough what is done (we prefer to leave the details for the main text rather than oversimplify). Also, our slight revision is shorter than the above suggestion.

L17-18: and lower stratospheric Aura MLS data

Response: Agreed, done.

L20: On 6-8 year time scales [in general work to consolidate space by limiting the use of parentheses].

Response: Agreed, done.

L25-p5851 L2: this could be shortened: "Short-term tendencies of lower stratospheric and column HCl vary, with increases from 2005-2010 at northern mid-latitudes and deep tropics, but decreases after 2011 in northern mid-latitudes and increases at southern mid-latitudes."

Response: Agreed, done (even slightly more succinctly).

p5851 L17 I think you can end the sentence at reference and the meaning is clear [saving little bits of space]. L17: remove next sentence, this is confusing and not needed in the abstract.

Response: Agreed, done.

p5852 L10: of independent ground-based data (as in analysis of independent...)

Response: Agreed, done.

L19-20: A slow recovery of the ozone layer towards pre-1985 levels is expected...

Response: Agreed, done.

L22: High quality ozone and other constituent datasets are needed to document past variability and to constrain... [suggestion to reduce word count].

Response: Agreed, done.

p5853 L8: here is an example of how one might consolidate the words a bit: ... on a common latitude/pressure grid, using the following high quality satellite limb sounding instruments:[move list starting on line 15, and rest of paragraph, up.] Then change last sentence to "All source data sets still have shortcomings or imperfections, but in creating the GOZCARDS Earth Systems Data Record (ESDR) we maintain the integrity of the original data and do not arbitrarily

disregard data, nor do we attempt to fill in spatial or temporal gaps in the record." The sentence on ways to fill in data is beyond scope of paper and is not needed.

Response: Agreed, done.

P5854 L7: see Sect. 5.1.1 L8: profiles in two narrow latitude bands every day.

Response: Agreed, done.

L11-14: consolidate here [you've just introduced the source files and grid, so no need to refer back to these ideas]: Next we merge the GOZCARDS source data files by computing average biases between different source files during periods of overlap, and then adjusting each source file to a common reference to remove the relative biases. Non-zero biases ...

Response: Agreed, consolidation was done.

L16: such as differences in radiance measurement system or wavelength range, the retrieval algorithm, or in the vertical, temporal or spatial resolution. [no need to refer to Level 1 or Level 2, especially if you have to then define what you mean]

Response: Agreed, done.

L17: remove sentence starting "A useful reference" and start next sentence as Toohey et al. (2013) studied ...

Response: Agreed, done.

L21: '... vs. averages of output sampled at sub-orbital track locations'

Response: Agreed, done.

P5855 L4-5: remove clause "these analyses ... discussed later"

Response: Agreed, done.

L8: SI2N initiative (...) [remove 'which stands for'] L18: replace 'main' with 'source' [since source data sets already defined]

Response: Agreed, done.

L19-20: Section 6 briefly mentions GOZCARDS N₂O, HNO₃ and temperatures...

Response: Agreed, done.

P5856-5857 L5: As mentioned before, the filtering done according to various data teams can be summarized either in a table or in the appendix. **The special filtering for ACE-FTS is appropriate for the text body.** Also there is no discussion of SAGE here, or reference to the appendix that I saw. I suggest moving this information out of the main text body, but if it is not moved, SAGE should be mentioned.

Response: Agreed; as mentioned earlier, most of the data screening is now described in Table A1 (Appendix).

P5857 ACE-FTS: this discussion was a little confusing, and could be simplified. "When analyzing ACE-FTS data we found it necessary to remove occasional large outlier values that

could significantly impact the monthly zonal means. Our outlier screening procedure ... for each year of data."

Response: Agreed, done.

L12: What do the authors mean by independent zonal means from the ACE-FTS team? Is this a data set that the ACE-FTS filtered using their own method and it compares well? I'm not clear on how the zonal means supplied by the team are independent.

Response: Yes, the ACE-FTS team used a slightly different method; we added a brief clarification for this sentence.

L17: remove 'in the tropics' because the limits are extended in all latitude bands L17: remove parentheses around good.

Response: Agreed, done, and with slightly more consolidation.

L21-22: such data sparseness can increase trend uncertainties, for example.[I don't follow the rest of this sentence, comparisons with AURA gave confidence in trend results from ACE-FTS?]

Response: To remove confusion and length, and as this is not critical information, we have largely cut this out.

L24: add this last filter to the table or appendix, as it is standard.

Response: Agreed, this is now in Table A1 (Appendix).

L28: have been set to -999 in the GOZCARDS files.

Response: Agreed, done.

Section 3.1: This section is a bit confusing. First extra screening is covered, then the band deterioration on MLS, then validation studies, then more screening, more on the band deterioration and then more validation studies. Suggest adding "Froidevaux et al. (2008) found anomalously high MLS HCl vs. aircraft data at 147 hPa at low latitudes; these values are not included in the GOZCARDS HCl data set." to the screening info after the HALOE aerosol screening. Then summary of validation work. Then 'Finally, AURA MLS HCl data are not recommended for trend analysis at pressures < 10 hPa (reference?) even if monthly ... measurements. Aura MLS switched to backup band 14 after primary HCl band 13 showed signs of rapid degradation in early 2006. For pressures 10 hPa and above, the long-term band 14 data are considered robust, but drift in band 14 HCl in the upper stratosphere led us to not include AURA MLS HCl upper stratospheric source data in the GOZCARDS record.

Response: Agreed, we have rearranged and shortened this section.

Section 3.2: [the first two sentences don't add new information, but it would be helpful in Table 2 to note that the AURA MLS is included only from 10 hPa and below] 'Although not included in the final merged product, we do use the 2004-2005 absolute Aura HCl measurements at pressures less than 10 hPa to compute the offsets for the ACE-FTS and HALOE source files in a consistent manner at all pressure levels. Figure 1 ...

Response: Agreed, done.

P5860 L14: remove phrase in () L18: remove "too"

Response: Agreed, done.

L29: the average of the months when data from both instruments exist (i.e. at ACE-FTS temporal sampling).

Response: Agreed, done.

P5861 L4: we weight L11: thus removing any relative bias

Response: Agreed, done.

L15-16: checked against independent data sets from two institutions? This needs more detail, or to be removed. Did the authors compare to two other merged data sets?

Response: No, this was an independent computational check within our team (among co-authors at different places), but in the interest of shortening the text, we have removed this detail.

L29: is biased low relative to the reference mean and needs to be increased by the offset value.

Response: Agreed, done.

P5862 L7: detailed examples of upper and lower stratospheric offsets

Response: Agreed, done.

L 18-20: This seems a general data information statement, and should be moved up to the ACE-FTS screening section, if it needs to be mentioned explicitly.

Response: Agreed, done.

P5863 L17: ... merged values is given by the range of available ...

Response: Agreed, done.

L18: remove sentence 'We have made such a calculation...'

Response: Agreed, done.

L23: in relation to the reference values

Response: We have changed to: "biased significantly more than others, in a relative sense."

P5864 L4 ... comparisons; although not an official product, users can readily...

Response: Agreed, done.

L6-16: this seems a more general description of the GOZCARDS files. Should some or all of this information be covered elsewhere, before getting into individual constituent discussion? Maybe at the end of the data screening/binning section.

Response: Agreed, done.

Section 3.3 This section is very long, and seems like a good place to make some larger cuts. As a reader interested in the GOZCARDS data, I am most interested in GOZCARDS comparisons with other results. I would suggest at the very least removing Figure 10. The authors can simply state, as they have, that analysis showed the short-term drifts in the period from 2006-2011 to be

most hemispherically asymmetric. I would suggest ending this section at P5866 L27 (end sentence with GOZCARDS lower stratospheric HCl trends agree quite well.) This shows what GOZCARDS can do, which is what users need from this paper.

Response: We made some significant cuts here (Sec. 3.3 is cut by 33% per word count). However, showing that the HCl behavior is turning around in the later years is useful and new (and in our view, informative for ACP audience, and as a brief update to the Mahieu et al. work, which mainly looked at columns - and stopped in 2011). We believe that it is most useful to show (keep) the 2 left panels of Fig. 10 to show the non-linearity and connection to surface total chlorine changes. Thus, we took out two thirds of Figs. 9 and 10 (combined) and shortened the text accordingly; we are just left with the new Fig. 9.

P5865:

L1: Remove sentence 'The GOZCARDS HCl ...' this was covered already, and is in the Tables.

Response: Agreed, done.

L4: ... documented by satellite-based ...

Response: Agreed, done.

L12: ... for the one and a half year band 13 AURA MLS data record ...

Response: Agreed, done.

P5866: L2 less negative trends.

Response: Agreed, done.

L13: Is putting Fig 9a, 9b and 9c in parentheses required? It seems a bit odd, but it might be a journal requirement. If not, I would suggest removing the ().

Response: The Journal did this – but we have reworded this in the new version.

L12-13: remove 'For the results'

Response: Agreed, done.

L17: and both positive and negative values

Response: Agreed, done.

P5868 Section 4.1: consider writing in active voice. '... we screened HALOE H₂O data for high aerosol extinction values, closely following the screening used in the Stratospheric ...'

Response: Agreed, done.

P5869 L7: (Version 20 or VPMC) could be used ...

Response: Agreed, done.

L16-17: do the authors mean the resulting UARS MLS source data span 1991-1993?

Response: Yes, we clarified this.

L20: The validation results here are confusing. Is it necessary to talk about V2.2 and V3.3 AURA MLS validation? Sticking to V3.3 might limit some of the confusion.

Response: Yes, we have limited this more to the V3.3 discussion, although not exclusively so, for proper referencing of important past validation work.

p5871 L3: Sentence #2, this sentence could be removed, as the reason given for not including SAGE H₂O seems good enough, that speculation to retrieval problems after the volcano are not needed.

Response: Agreed, done.

L9-L16: Do the authors mean care should be taken because there are missing bands in the GOZCARDS? Since space is at a premium in this paper, I would consider taking this paragraph out. Most users should be aware of sampling issues when averaging without full coverage and it's already been made clear that missing values are not filled in GOZCARDS.

Response: A user came to us with this specific (sort of "blind plotting") result/issue, and thus, we feel that it is worthwhile to include a note especially for the lower altitude region (not to have users, even a minority of them, rediscover the wheel in this case). The merged dataset does not readily provide flags or latitudinal coverage information for the source datasets, and users would need to do more work to track this particular issue down (maybe they should, agreed...). We prefer to keep this cautionary note (latitudinal inhomogeneity issues in early/occultation datasets), given also the interest in H₂O at lower altitudes; however, we shortened this text significantly.

L18: remove "(mentioned earlier)"

Response: Agreed, done.

P5872 L10: with a large drift in the difference time series.

Response: Agreed, done.

L15: if the two time series

Response: Agreed, done.

L16: consider removing this sentence 'The main point here...' [this is understood]

Response: Agreed, done.

L19: end sentence at ACE-FTS data [don't need to mention again data ending in 2010]

Response: Agreed, done.

P5873 Section 4.3 This section is well written, but it reads like a completely new paper, and possibly could be part of a new manuscript. For the purposes of this paper however it seems far too detailed, especially considering the overall length of the paper. One suggestion would be to use the first sentence of the section, then skip to Fig 15 through the end of the section.

Response: Agreed, the literature review has been removed, as it is not that directly relevant or necessary. Overall, Sect. 4.3 is almost 40% shorter now.

P5876 L14: remove commas around "is needed"

Response: Agreed, done.

P5877 L12 were discarded L24: It is known

Response: Agreed, done.

P5880 L 11: remove 'as described in Sect 5.1'

Response: Agreed, done.

L13: remove sentence 'The monthly means ... ' I think the construction of monthly means after screening is applied follows from section 5.1 and doesn't need to be restated.

Response: Agreed, done.

P5882

L9-11: Isn't the sentence starting 'Biases' at the end of line 9 repeating what was said in the line above? It might be possible to shorten the diurnal section, just noting that the data are simply not co-located in time (sunset to 1:30am is a large time range). Solving this issue really requires model output which isn't feasible for this work (at least this version).

Response: Yes, the redundant sentence was removed and some trimming of the rest was implemented although the point is that the relative bias adjustments include diurnal effects and one does not really need model output (with their own uncertainties) to do such adjustments, thus taking care of diurnal sampling effects, at least to first order. All datasets are basically adjusted to the SAGE II average local times (sunset and sunrise combined). Also, MLS (and ACE-FTS to a large extent) do not have significantly different (local time) sampling patterns year after year (see also the stability issue below).

L21: Only at 3.2 hPa and above, correct?

Response: Yes, we clarified this.

L18-27: This paragraph is a little confusing. Why is stability of measurements coming up now (assuming the authors are not still considering diurnal ozone variations). Is this not a consideration for all constituents?

Response: This was meant to focus on the diurnally-changing region. We clarified this, but also removed the last two sentences for brevity - as the stable sampling patterns of various instruments should be known.

P5886 L3 - end of section: The Ziemke Chandra results have always been anomalous, and it is probably not worthwhile pursuing this comparison. Updated column ozone comparisons could be made with SBUV MOD (which do not agree with ZC12); SBUV is considered the better "trend-quality" data set. However, given space constraints, it is not clear that a column ozone analysis is needed. The authors could easily end the section after the review of the GOZCARDS profile comparisons that have already been done.

Response: We think that cutting out the column ozone discussion completely would remove a significant analysis as we have not really seen published work on this subject, despite what some may view or characterize as "common knowledge" regarding TOMS/OMI column data time series analyses. This ozone discussion is new evidence nevertheless and it is the primary reason to tie this paper to the SF²N special issue (which is on ozone, not on other species). Unless

specific published references already exist to clearly make our point and/or to imply that other column series are superior to TOMS/OMI, we plan to retain the flavor of this ozone-related “sample result”. For brevity, however, we remove Fig. 23 and Fig. 25 and retain only Fig. 24 (Fig. 22 in the update); this preserves our point regarding comparison issues for GOZCARDS stratospheric column relative changes versus those provided by ZC12, but more succinctly. Overall, the Sect. 5.3 text has been cut by 37%.

P5888 L23: We now briefly mention the N₂O, HNO₃ and temperature GOZCARDS records that were part of the delivery...

Response: Agreed, done.

P5889 L6 end sentence after data record [again don't need to repeat this information about ACE-FTS if it is mentioned in the general data screening section and/or Tables].

Response: Agreed, done.

L11-14: wording is confusing. Suggest 'Until then the GOZCARDS N₂O record will include AURA MLS N₂O though the end of 2012 only, to avoid the discontinuities resulting from the shift to 190 GHz band N₂O in the current V3.3 data.

Response: Yes, we have reworded and shortened this discussion.

L19-20: Is this sentence referring to the first validation studies mentioned? If so, combine these sentences. 'Validation results for the first few years of AURA MLS and ACE-FTS N₂O shows agreement mostly within 5% in the stratosphere (Lambert et al., 2007; Strong et al., 2008)'.

Response: We have shortened this brief validation discussion.

L25: is illustrated in Fig. S15, showing generally highly correlated fields and insignificant drifts.

Response: Agreed, done.

P 5890 L5 remove parentheses.

Response: Agreed, done.

L19: can remove 'the quality of'

Response: Agreed, done.

P5891 L2: and 2012 agree mostly within 10-15%

Response: Yes, modified slightly.

L15-18: remove parentheses.

Response: Agreed, done.

Summary and Conclusions: This section is also quite long, and will have to be changed to reflect changes made, particularly in the summary sections for each constituent. In the interest of space, a higher level summary, focusing primarily on the data set methodology, would suffice.

Response: We have shortened this summary section significantly (a total cut of 31%); however, we believe that sample results have their place in such a summary for ACP (and for many people who have or take time to read mostly Abstract and/or Summary).

1 **Global Ozone Chemistry And Related Datasets for the**
2 **Stratosphere (GOZCARDS): methodology and sample results**
3 **with a focus on HCl, H₂O, and O₃**

4 **L. Froidevaux¹, J. Anderson², H.-J. Wang³, R. A. Fuller¹, M. J. Schwartz¹,**
5 **M. L. Santee¹, N. J. Livesey¹, H. C. Pumphrey⁴, P. F. Bernath⁵,**
6 **J. M. Russell III², and M. P. McCormick²**

7 ¹Jet Propulsion Laboratory, California Institute of Technology, Pasadena, CA, USA

8 ²Hampton University, Hampton, VA, USA

9 ³Georgia Institute of Technology, Atlanta, GA, USA

10 ⁴The University of Edinburgh, Edinburgh, UK

11 ⁵Old Dominion University, Norfolk, VA, USA

12 *Correspondence to:* L. Froidevaux (lucief@jpl.nasa.gov)

13

14

15

16

17

18

19

20

21

22

23

24 **Abstract**

25 We describe the publicly available data from the Global OZone Chemistry And Related Datasets
26 for the Stratosphere (GOZCARDS) project, and provide some results, with a focus on hydrogen
27 chloride (HCl), water vapor (H₂O), and ozone (O₃). This dataset is a global long-term
28 stratospheric Earth System Data Record, consisting of monthly zonal mean time series starting as
29 early as 1979. The data records are based on high quality measurements from several NASA
30 satellite instruments and ACE-FTS on SCISAT. We examine consistency aspects between the
31 various datasets. To merge ozone records, the time series are debiased relative to SAGE II values
32 by calculating average offsets versus SAGE II during measurement overlap periods, whereas for
33 other species, the merging derives from an averaging procedure during overlap periods. The
34 GOZCARDS files contain mixing ratios on a common pressure/latitude grid, as well as standard
35 errors and other diagnostics; we also present estimates of systematic uncertainties in the merged
36 products. Monthly mean temperatures for GOZCARDS were also produced, based directly on
37 data from the Modern-Era Retrospective analysis for Research and Applications.

38 The GOZCARDS HCl merged product comes from HALOE, ACE-FTS and lower
39 stratospheric Aura MLS data. After a rapid rise in upper stratospheric HCl in the early 1990s, the
40 rate of decrease in this region for 1997-2010 was between 0.4 and 0.7%/yr. On 6-8 yr timescales,
41 the rate of decrease peaked in 2004-2005 at about 1%/yr, and has since levelled off, at ~0.5%/yr.
42 With a delay of 6-7 years, these changes roughly follow total surface chlorine, whose behavior
43 versus time arises from inhomogeneous changes in the source gases. Since the late 1990s, HCl
44 decreases in the lower stratosphere have occurred with pronounced latitudinal variability at rates
45 sometimes exceeding 1-2%/yr. Recent short-term tendencies of lower stratospheric and column
46 HCl vary substantially, with increases from 2005-2010 for northern mid-latitudes and deep
47 tropics, but decreases (increases) after 2011 at northern (southern) mid-latitudes.

48 For H₂O, the GOZCARDS product covers both stratosphere and mesosphere, and the same
49 instruments as for HCl are used, along with UARS MLS stratospheric H₂O data (1991-1993).
50 We display seasonal to decadal-type variability in H₂O from 22 years of data. In the upper
51 mesosphere, the anti-correlation between H₂O and solar flux is now clearly visible over two full
52 solar cycles. Lower stratospheric tropical H₂O has exhibited two periods of increasing values,

53 followed by fairly sharp drops (the well-documented 2000-2001 decrease and a recent drop in
54 2011-2013). Tropical decadal variability peaks just above the tropopause. Between 1991 and
55 2013, both in the tropics and on a near-global basis, H₂O has decreased by ~5-10% in the lower
56 stratosphere, but about a 10% increase is observed in the upper stratosphere and lower
57 mesosphere. However, such tendencies may not represent longer-term trends.

58 For ozone, we used SAGE I, SAGE II, HALOE, UARS and Aura MLS, and ACE-FTS data to
59 produce a merged record from late 1979 onward, using SAGE II as the primary reference. Unlike
60 the 2 to 3% increase in near-global column ozone after the late 1990s reported by some,
61 GOZCARDS stratospheric column O₃ values do not show a recent upturn of more than 0.5 to
62 1%; continuing studies of changes in global ozone profiles, as well as columns, are warranted.

63 A brief mention is also made of other currently available, commonly-formatted GOZCARDS
64 satellite data records for stratospheric composition, namely those for N₂O and HNO₃.

65 **1 Introduction**

66 The negative impact of anthropogenic chlorofluorocarbon emissions on the ozone layer,
67 following the early predictions of Molina and Rowland (1974), stimulated interest in the trends
68 and variability of stratospheric ozone, a key absorber of harmful ultraviolet radiation. The
69 discovery of the ozone hole in ground-based data records (Farman et al., 1985) and the
70 associated dramatic ozone changes during southern hemisphere winter and spring raised the level
71 of research and understanding regarding the existence of new photochemical processes (see
72 Solomon, 1999). This research was corroborated by analyses of aircraft and satellite data (e.g.,
73 Anderson et al., 1989; Waters et al., 1993), and of independent ground-based data. Global total
74 column ozone averages in 2006-2009 were measured to be smaller than during 1964-1980 by
75 ~3%, and larger more localized decreases over the same periods reached ~6% in the southern
76 hemisphere midlatitudes (WMO, 2011). Halogen source gas emissions have continued to
77 decrease as a result of the Montreal Protocol and its amendments. Surface loading of total
78 chlorine peaked in the early 1990s and subsequent decreases in global stratospheric HCl and ClO
79 have been measured from satellite-based sensors (Anderson et al., 2000; Froidevaux et al., 2006;
80 Jones et al., 2011) as well as from the ground (e.g., Solomon et al., 2006, Kohlhepp et al., 2012).
81 A slow recovery of the ozone layer towards pre-1985 levels is expected (WMO, 2011; 2014).

82 High quality long-term datasets for ozone and related stratospheric species are needed to
83 document past variability and to constrain global atmospheric models. The history of global
84 stratospheric observations includes a large suite of satellite-based instruments, generally well-
85 suited for the elucidation of long-term global change. A review of differences between past and
86 ongoing satellite measurements of atmospheric composition has been the focus of the
87 Stratosphere-troposphere Processes And their Role in Climate (SPARC) Data Initiative; results
88 for stratospheric H₂O and O₃ intercomparisons have been described by Hegglin et al. (2013) and
89 Tegtmeier et al. (2013), respectively, to be followed by a report on many other species.
90 Systematic biases reported in these papers mirror past validation work.

91 Under the Global OZone Chemistry And Related Datasets for the Stratosphere (GOZCARDS)
92 project, we have created monthly zonally averaged datasets of stratospheric composition on a
93 common latitude/pressure grid, using high quality data from the following satellite instruments:
94 the Stratospheric Aerosol and Gas Experiments (SAGE I and SAGE II), the Halogen Occultation
95 Experiment (HALOE) which flew aboard the Upper Atmosphere Research Satellite (UARS), the
96 UARS Microwave Limb Sounder (MLS), the Atmospheric Chemistry Experiment Fourier
97 Transform Spectrometer (ACE-FTS) on SCISAT, and Aura MLS. Table 1 provides
98 characteristics of the original datasets; validation papers from the instrument teams and other
99 related studies give a certain degree of confidence in these data. However, the existence of
100 validation references does not imply that there are no caveats or issues with a particular
101 measurement suite. In this project, we have strived to optimize data screening and mitigate some
102 undesirable features, such as the impact of outlier values or the effects of clouds or aerosols. All
103 source data sets still have imperfections, but in creating the GOZCARDS Earth System Data
104 Record (ESDR) we maintain the integrity of the original data and do not arbitrarily disregard
105 data, nor do we typically attempt to fill in spatial or temporal gaps in the record.

106 Based on original profiles from the various instruments, GOZCARDS “source” monthly
107 zonal mean values were derived. After data screening, monthly average profiles were created by
108 vertical interpolation onto the GOZCARDS pressure levels, followed by binning and averaging
109 into monthly sets. In order to accommodate the lower vertical resolution of some limb viewers,
110 such as UARS MLS, the GOZCARDS pressure grid was chosen as

111 $p(i) = 1000 \times 10^{-\frac{i}{6}}$ (hPa) (1)

112 with i varying from 0 to a product-dependent top; this grid width corresponds to ~ 2.7 km. The
113 high resolution SAGE O₃ profiles were converted to mixing ratio versus pressure using their
114 associated NCEP temperature profiles, and smoothed vertically onto this grid. Given the
115 sampling of solar occultation instruments, which usually provide 15 sunrise and 15 sunset
116 profiles in two narrow latitude bands every day (versus the denser sampling from MLS, with
117 almost 3500 profiles/day), we used 10°-wide latitude bins (18 bins from 80°S-90°S to 80°N-
118 90°N) to construct monthly zonal means. Next, we merged the GOZCARDS source data by
119 computing average relative biases between source datasets during periods of overlap, and then
120 adjusting each source dataset to a common reference to remove relative biases. Non-zero biases
121 always exist between data from different instruments for various reasons, such as systematic
122 errors arising from the signals or the retrieved values, different vertical resolutions, or sampling
123 effects. Toohey et al. (2013) studied sampling biases from a large suite of satellite-based
124 stratospheric profiling instruments, based on simulations using fully-sampled model abundance
125 averages versus averages of output sampled at sub-orbital locations. Larger sampling errors arise
126 from occultation than from emission measurements, which often sample thousands of profiles
127 per day. Toohey et al. (2013) found that sampling biases reach 10-15%, notably at high latitudes
128 with larger atmospheric variability. Sofieva et al. (2014) have also discussed sampling
129 uncertainty issues for satellite ozone datasets.

130 We have observed very good correlations between GOZCARDS and other long-term ozone
131 data, such as the Stratospheric Water vapor and OzOne Satellite Homogenized (SWOOSH) data
132 (S. Davis, personal communication, 2012) and homogenized Solar Backscatter Ultraviolet
133 (SBUV) data. Dissemination of trend results arising from analyses of GOZCARDS and other
134 merged ozone datasets was planned as part of WMO (2014) and the SI²N (Stratospheric
135 Processes And their Role in Climate (SPARC), International Ozone Commission (IOC),
136 Integrated Global Atmospheric Chemistry Observations (IGACO-O₃), and the Network for the
137 Detection of Atmospheric Composition Change (NDACC)) initiative. Profile trend results have
138 been provided by Tummon et al. (2015), Harris et al. (2015), as well as Nair et al. (2013, 2015).

139 This paper starts with a discussion of data screening issues (Sect. 2 and Appendix A), and
140 then describes the GOZCARDS data production methodology, followed by some atmospheric

141 results for HCl (Sect. 3), H₂O (Sect. 4), and O₃ (Sect. 5). We provide specific diagnostics that
142 indicate generally good correlations and small relative drifts between the source datasets used to
143 create the longer-term GOZCARDS merged time series. Section 6 briefly mentions GOZCARDS
144 N₂O and HNO₃, as well as temperatures derived from Modern-Era Retrospective analysis for
145 Research and Applications (MERRA) fields. The version of GOZCARDS described here is
146 referred to as ESDR version 1.01 or ev1.01.

147

148 **2 GOZCARDS source data and data screening**

149 Data provenance information regarding the various measurements used as inputs for
150 GOZCARDS is provided in Appendix A (Sect. A.1).

151 **2.1 GOZCARDS data screening and binning**

152 The screening of profiles for GOZCARDS has largely followed guidelines recommended by
153 the various instrument teams and/or relevant publications, **and we have documented these issues**
154 **and procedures in Appendix A (Table A1)**. Unless otherwise noted, we only provide monthly
155 means constructed from 15 or more (good) values in a given latitude/pressure bin. For ACE-FTS
156 data, we also found it necessary to remove occasional large outlier values that could significantly
157 impact the monthly zonal means. Our outlier screening removed values outside 2.5 times the
158 standard deviation, as measured from the medians in each latitude/pressure bin, for each year of
159 data. This was deemed close to optimum by comparing results to Aura MLS time series, which
160 typically are not impacted by large outliers, and to ACE-FTS zonal means screened (in a slightly
161 different way) by the ACE-FTS instrument team. Up to 5% of the profile values in each bin in
162 any given month were typically discarded as a result, but the maximum percentage of discarded
163 values can be close to 10% for a few months of ACE-FTS data, depending on year and species.
164 Moreover, because of poor ACE-FTS sampling, the threshold for minimum number of good
165 ACE-FTS values determining a monthly zonal mean was allowed to be as low as 10 for mid- to
166 high latitudes, and as low as 6 for low latitudes (bins centered from 25°S to 25°N). Zonal mean
167 data from ACE-FTS become too sparse in some years if such lower threshold values are not
168 used. **Finally, no v2.2 ACE-FTS data are used after September 2010 (or after December 2009 for**

169 ozone) because of a data processing problem that affected this data version; a newly reprocessed
170 ACE-FTS dataset was not available before we made the GOZCARDS data public.

171 Placing profiles on a common pressure grid is straightforward when pressures are present
172 in the original files, as is the case for most data used here. Also, the vertical resolutions are
173 similar for most of the instruments used for GOZCARDS. The UARS MLS, HALOE, and Aura
174 MLS native pressure grids are either the same as or a superset of the GOZCARDS pressure grid,
175 so these datasets were readily sampled for the construction of monthly means. For ACE-FTS,
176 pressures are provided along with the fixed altitude grid, and we used linear interpolation versus
177 $\log(\text{pressure})$ to convert profiles to the GOZCARDS grid. More details are provided later for
178 SAGE I and SAGE II O_3 , for which density versus altitude is the native representation.

179 The binning of profiles occurs after the screened values are averaged (in each
180 latitude/pressure bin). Note that for the species discussed here, sunset and sunrise occultation
181 values in the same latitude bin during a given month are averaged together. Negative monthly
182 means are set to -999.0 in the GOZCARDS files; while negative mixing ratios smaller (in
183 absolute value) than the associated standard errors can in theory be meaningful, negative
184 monthly means are unlikely to be very useful scientifically. Quantities other than mixing ratios
185 are provided in the netCDF GOZCARDS files, which are composed of one set of individual
186 yearly files for all source datasets, and one set of yearly files for the merged products. The main
187 quantities are monthly averages, plus standard deviations and standard errors. The GOZCARDS
188 source files also provide the number of days sampled each month as well as minimum and
189 maximum values for the source datasets. Other information includes average solar zenith angles
190 and local solar times for individual sources. Finally, formulae for monthly standard deviations of
191 the merged data are given in Appendix A, where sample time series of the standard deviations
192 and standard errors (not systematic errors) for both source and merged data are also shown.

193

194 **3 GOZCARDS HCl**

195 **3.1 GOZCARDS HCl source data records**

196 We used HCl datasets from HALOE, ACE-FTS and Aura MLS to generate the monthly zonal
197 mean source products for GOZCARDS HCl. In addition to the procedures mentioned before, a

198 first-order aerosol screening was applied to the HALOE HCl profiles: all HCl values at and
199 below a level where the 5.26 μm aerosol extinction exceeds 10^{-3} km^{-1} were excluded. Regarding
200 Aura MLS HCl, Froidevaux et al. (2008a) found anomalously high values versus aircraft data at
201 147 hPa at low latitudes; these values are not used in the production of the merged HCl product.
202 Also, the ongoing standard MLS HCl product is retrieved using band 14 rather than band 13,
203 which targeted HCl for the first 1.5 years after launch, but started deteriorating rapidly after Feb.
204 2006. As the remaining lifetime for band 13 is expected to be short, this band has been turned on
205 only for a few days since Feb. 2006. MLS HCl data are not recommended for trend analyses at
206 pressures < 10 hPa. However, for pressures ≥ 10 hPa, band 14 HCl is deemed robust, because of
207 the broader emission line in this region, in comparison to the measurement bandwidth.

208 Past validation studies have compared MLS HCl (v2.2), ACE-FTS (v2.2) and HALOE (v19)
209 datasets using coincident pairs of profiles; such work was described by Froidevaux et al. (2008a)
210 for MLS HCl validation and by Mahieu et al. (2008) for ACE-FTS HCl validation. The MLS
211 version 3.3/3.4 HCl data used here (see Livesey et al., 2013) compare quite well with v2.2 HCl
212 (average relative biases are within 5%). HALOE HCl values were found to be biased low by
213 $\sim 10\text{-}15\%$ relative to both MLS and ACE-FTS, especially in the upper stratosphere; this low bias
214 versus other (balloon- and space-based) measurements had been noted in past HALOE validation
215 studies (Russell et al., 1996). Also, HALOE (v19) and ACE-FTS (v2.2) HCl data tend to lose
216 sensitivity and reliability for pressures less than ~ 0.4 hPa.

217 **3.2 GOZCARDS HCl merged data records**

218 *Although Aura MLS HCl data for pressures less than 10 hPa do not contribute to the time*
219 *dependence of the merged HCl product, the 2004-2005 absolute Aura HCl measurements in this*
220 *region are used to compute the offsets for the ACE-FTS and HALOE zonal mean source data in*
221 *a consistent manner versus pressure.* Figure 1 illustrates the merging process for HCl at 32 hPa
222 for the 45°S latitude bin (covering 40°S-50°S). Given that there exists very little overlap between
223 the three sets of measurements in the same months in 2004 and 2005, especially in the tropics, a
224 simple 3-way averaging of the datasets would lead to significant data gaps. Our methodology is
225 basically equivalent to averaging all three datasets during this period, and we use Aura MLS as a
226 transfer dataset. This was done by first averaging ACE-FTS and Aura MLS data, where the

227 datasets overlap, and then including the third dataset (HALOE) into the merging process with the
228 temporary merged data. As the HALOE HCl values are generally lower than both the MLS and
229 ACE-FTS values, the merged HCl dataset is generally further away from HALOE than it is from
230 either ACE-FTS or Aura MLS. The top left panel in Fig. 1 shows GOZCARDS source data for
231 HALOE, ACE-FTS, and Aura MLS during the overlap period, from August 2004 (MLS data
232 start) through November 2005 (HALOE data end). The top right panel illustrates the result of
233 step 1 in the merging procedure, with the temporary merged data values (orange) resulting from
234 the adjustment of ACE-FTS and Aura MLS values to the mean reference (black dashed line);
235 this reference is simply the average of the two series for all months when both values exist. The
236 middle left panel shows step 2, namely the values (brown) obtained from merging HALOE
237 values with the temporary merged values from step 1; the temporary merged values are weighted
238 by $2/3$ and HALOE values by $1/3$ (giving the black dashed line as mean reference), so this is
239 equivalent to averaging the three datasets with a weight of $1/3$ each. A simple mathematical
240 description of the above procedure is provided in Appendix A. The middle right panel shows the
241 source data along with the final merged values during the overlap period, whereas the bottom
242 panel shows the full time period, after the additive offsets are applied to the whole source series,
243 thus removing relative biases; the three adjusted series are then averaged together wherever
244 overlap exists, to obtain the final merged dataset. We tested this procedure by using one or the
245 other of the two occultation data as the initial one (for step 1) and the results were not found to
246 differ appreciably. We also found that the use of multiplicative adjustments generally produces
247 very similar results as additive offsets. Some issues were found on occasion with multiplicative
248 offsets, when combining very low mixing ratios, but additive offsets can also have drawbacks if
249 the merged values end up being slightly negative, notably as a result of changes that modify the
250 already low HCl values during Antarctic polar winter. This occurs on occasion as additive offsets
251 tend to be weighted more heavily by larger mixing ratios found during non-winter seasons; as a
252 result, we decided not to offset lower stratospheric HCl source datasets in the polar winter at
253 high latitudes for any of the years. Further specifics and procedural details regarding the merging
254 of HCl data are summarized in Appendix A.

255 In Fig. 2, we display the offsets that were applied to the three HCl source datasets as a result
256 of the merging process in each latitude/pressure bin; a positive value means that a dataset is

257 biased low relative to the reference mean and needs to be increased by the offset value. These
258 offsets show that in general, ACE-FTS and Aura MLS HCl values were adjusted down by 0.1-
259 0.2 ppbv (a decrease of about 2-10%), while HALOE HCl was adjusted upward by 0.2-0.4 ppbv.
260 Offset values tend to be fairly constant with latitude and the sum of the offsets equals zero. The
261 generally homogeneous behaviour versus latitude is a good sign, as large discontinuities would
262 signal potential issues in the merging (e.g., arising from large variability or lack of sufficient
263 statistics). Figure S1 provides more detailed examples of upper and lower stratospheric offsets
264 versus latitude, including standard errors based on the variability in the offsets during the overlap
265 period (error bars provide an indication of robustness). Another indication of compatibility
266 between datasets is provided by a comparison of annual cycles. Figure S2 provides average
267 annual cycle amplitudes obtained from simple regression model fits to HALOE, ACE-FTS, and
268 Aura MLS series over their respective periods. While there are a few regions where noise or
269 spikes exist (mainly for ACE-FTS), large annual amplitudes in the polar regions occur in all time
270 series; this arises from HCl decreases in polar winter, followed by springtime increases.

271 A more detailed analysis of interannual variability and trend consistency is provided from
272 results in Fig. 3, which shows an example of ACE-FTS and Aura MLS time series. We have
273 used coincident points from these time series to compare the deseasonalized anomalies (middle
274 panel in Fig. 3) from both instrument series; correlation coefficient values (R values) are also
275 computed. Very good correlations are obtained and no significant trend difference between the
276 anomalies (bottom panel in Fig. 3) exists for ACE-FTS versus Aura MLS HCl. A view of these
277 correlations and drifts at all latitudes/pressures is provided in Fig. 4, where the top panel gives R
278 values for deseasonalized anomalies, and the bottom panel gives the ratio of the difference trends
279 over the error in these trends. The results in Fig. 4 confirm that there are significant trend
280 differences between the upper stratospheric HCl time series from ACE-FTS and Aura MLS (as a
281 reminder, we did not use Aura MLS HCl for pressures less than 10 hPa). Fig. 4 also shows very
282 low correlation coefficients from the deseasonalized HCl series in the uppermost stratosphere,
283 because Aura MLS HCl exhibits unrealistically flat temporal behavior, whereas ACE-FTS HCl
284 varies more. In the lower stratosphere, there is generally good agreement between the ACE-FTS
285 and Aura MLS HCl time series, with R values typically larger than 0.7 and difference trend to

286 error ratios smaller than 1.5. The few low R values for 100 hPa at low latitudes likely reflect
287 more infrequent ACE-FTS sampling and some (possibly related) outlier data screening issues.

288 Figure S3 illustrates GOZCARDS merged 46 hPa HCl variations versus time; there is clearly
289 a much more complete global view (with no monthly gaps) after the launch of Aura MLS. Gaps
290 at low latitudes in 1991 and 1992 are caused by post-Pinatubo aerosol-related issues in the
291 HALOE record, and gaps in later years arise from the decrease in coverage from UARS. In the
292 upper stratosphere, there are more gaps compared to 10 hPa and below, as a result of the much
293 poorer tropical coverage from ACE-FTS and the elimination of MLS data in this region.

294 An indication of systematic errors in the merged values is given by the range of available
295 monthly mean source data. For each bin, we compute the ranges of monthly means above and
296 below the merged values that include 95% of the available source data monthly means. These
297 error bars are not usually symmetric about the merged values, especially if one dataset is biased
298 significantly more than others, in a relative sense. We did not have enough datasets here to
299 consider a more statistical approach (such as the standard deviations among source datasets).
300 Figure 5 shows the result of such a systematic error calculation at 46 hPa for the 35°S latitude
301 bin. The lower shaded region range gives the lower bound, determined by HALOE data, and the
302 upper limit of the grey shading originates from ACE-FTS data. Figure 6 shows contour plots of
303 these estimated systematic errors in HCl. These are fairly conservative error bars; however, even
304 the source data averages at the 95% boundaries have their own systematic errors (rarely smaller
305 than 5%), so our estimates do not really encompass all error sources. Error bars representing a
306 range within which 95% of the source data values reside (see Figs. 5 and 6) can be a useful guide
307 for data users or model comparisons; although this is not an official product, users can readily
308 calculate such ranges (or we can provide these values).

309 **3.3 GOZCARDS HCl sample results and discussion**

310 Stratospheric HCl is important because it is the main reservoir of gaseous chlorine and it can be
311 used to follow the chlorine budget evolution over the past decades. This includes a significant
312 increase before the mid-1990s as a result of anthropogenic chlorofluorocarbon (CFC) production,
313 followed by a slower decrease as a result of the Montreal Protocol and subsequent international

314 agreements to limit surface emissions that were correctly predicted to be harmful to the ozone
315 layer (Molina and Rowland, 1974; Farman et al., 1985).

316 In Fig. 7, we provide an overview of the HCl evolution since 1991, based on GOZCARDS
317 average merged HCl for 3 different latitude regions at 4 pressure levels, from the upper
318 stratosphere to the lower stratosphere. In the upper stratosphere (at 0.7 hPa shown here), the
319 rapid early rise in HCl was followed by a period of stabilization (1997-2000) and subsequent
320 decreases. Rates of decrease for stratospheric HCl and total chlorine have been documented
321 using satellite-based upper stratospheric abundances, which tend to follow tropospheric source
322 gas trends with a time delay of order 6 years, with some uncertainties in the modeling of this
323 time delay and related age of air issues (Waugh et al., 2001; Engel et al., 2002; Froidevaux et al.,
324 2006). As summarized in WMO (2011), the average rate of decrease in stratospheric HCl has
325 typically been measured at -0.6 %/yr to -0.9 %/yr, in reasonable agreement with estimated rates
326 of change in surface total chlorine; see also the HCl upper stratospheric results provided by
327 Anderson et al. (2000) for HALOE, Froidevaux et al. (2006) for the one and a half year band 13
328 Aura MLS data record, and Jones et al. (2011) and Brown et al. (2011) for a combination of
329 HALOE and ACE-FTS datasets. The WMO (2011) summary of trends also includes results from
330 column HCl data at various NDACC Fourier transform infrared (FTIR) measurement sites; see
331 Kohlhepp et al. (2012) for a comprehensive discussion of ground-based results, showing some
332 scatter as a function of latitude. Figure 7 demonstrates that a global-scale decline in mid- to
333 lower stratospheric HCl is visible since about 1997. We also notice that at 68 hPa in the tropics,
334 the long-term rate of change appears to be near-zero or slightly positive. In addition, there are
335 shorter-term periods in recent years when an average increasing “trend” would be inferred rather
336 than a decrease; in particular, see the northern hemisphere from 2005 through 2012 at 32 hPa.

337 We created deseasonalized GOZCARDS merged monthly zonal mean HCl data at different
338 latitudes and we show in Fig. 8 the linear rate of change that results from simple fits through
339 such series. The long-term trends (1997 - 2013 for lower and 1997 - 2010 for upper stratosphere)
340 are generally negative and between about -0.5%/yr (upper stratosphere) and -1%/yr (lower
341 stratosphere). Some separation between northern and southern hemisphere results is observed in
342 the lower stratosphere, with less negative trends in the northern hemisphere. Also, the scatter
343 increases from 68 hPa to 100 hPa, where some positive trends occur at low latitudes; however,

344 we have less confidence in the 100 hPa results, given the larger scatter and errors (and smaller
345 abundances) in that region. Without trying to assign exact linear trends from these simple
346 analyses, we observe considerable latitudinal variability in lower stratospheric HCl short-term
347 behavior, especially after 2005. Such lower stratospheric changes in HCl have been captured in
348 column HCl FTIR data (Mahieu et al., 2013, 2014). The latter reference shows that total column
349 (FTIR) results and GOZCARDS lower stratospheric HCl trends agree quite well, and the authors
350 imply that a relative slowdown in the northern hemispheric circulation is responsible for
351 observed recent changes in the lower stratosphere. However, we note (Fig. 7) that changes in
352 lower stratospheric HCl appear to be fairly short-term in nature, with an apparent reversal in
353 behavior occurring at both northern and southern midlatitudes since 2011 (e.g., at 32 hPa).
354 Lower stratospheric changes are distinct from the upper stratospheric long-term decrease, which
355 we expect to continue, as long as the Montreal Protocol and its amendments are followed and
356 total surface chlorine keeps decreasing.

357 In Figure 9, we provide simple rates of upper and lower stratospheric change in HCl for 6-yr
358 sliding time periods (e.g., a 2004 value means a 2001-2006 average) for various latitudes. These
359 results indicate that there has been an acceleration in the rate of decrease of upper stratospheric
360 HCl between 2000 and 2004, followed by a period with somewhat smaller rates of change. This
361 is roughly in agreement with curves showing the rates of change for surface total chlorine based
362 on National Oceanic and Atmospheric Administration (NOAA) surface data (Montzka et al.,
363 1999), as shown in Fig. 9 (top panel) with the Earth System Research Laboratory Global
364 Monitoring Division data, time shifted by 6 or 7 years to account for transport delays into the
365 upper stratosphere. Chlorine source gases have indeed shown a reduction in their rate of decrease
366 during the second half of the past decade, as discussed by Montzka et al. (1999) and summarized
367 in WMO (2011, 2014). Reasons include the initial rapid decrease in methyl chloroform, slower
368 rates of decrease from the sum of CFCs in recent years, and increases in
369 hydrochlorofluorocarbons (HCFCs). The lower stratospheric HCl behavior in Fig. 9 (bottom
370 panel) shows rates of change in partial column density between 68 hPa and 10 hPa. These
371 changes show more variability with latitude than in the upper stratosphere for short (6-yr) time
372 periods, and a hemispheric asymmetry exists, peaking in 2009, when positive tendencies are seen
373 in the northern hemisphere, as opposed to decreases in the south (Mahieu et al., 2014). These

374 results do not depend much on whether 6-yr or 8-yr periods (not shown) are used, but longer
375 periods smooth out the rates of change; interannual variations, such as those arising from the
376 quasi-biennial oscillation (QBO), will affect short-term results. Temporal patterns in the upper
377 and lower stratosphere are qualitatively similar, and rates of change in surface emissions will
378 impact both regions, but carefully disentangling this from changes in dynamics or in other
379 species (e.g., CH₄) that can affect chlorine partitioning will require more analyses and modeling.

380 **4 GOZCARDS H₂O**

381 **4.1 GOZCARDS H₂O source data records**

382 We used water vapor datasets from HALOE, UARS MLS, ACE-FTS, and Aura MLS to generate
383 the monthly zonal mean source products for GOZCARDS H₂O. In addition to the data screening
384 procedures mentioned in Appendix A, we screened HALOE H₂O data for high aerosol extinction
385 values, closely following the screening used for merged H₂O in the Stratospheric Water vapor
386 and OzOne Satellite Homogenized (SWOOSH) dataset (S. Davis, personal communication,
387 2012). This method (see Fig. S4) screens out anomalous HALOE H₂O values that occurred
388 mainly in 1991-1992, when the aerosol extinction near 22 hPa exceeded $5 \times 10^{-4} \text{ km}^{-1}$; for
389 pressure levels at and below 22 hPa, we have excluded the corresponding H₂O values. **While this
390 method may exclude some good data points, the lowest values (< 3 ppmv) do get screened out;
391 such outliers are not corroborated by 22 hPa UARS MLS data (with most values > 3 ppmv).**
392 Also, for upper mesospheric HALOE data, care should be taken during high latitude summer
393 months, as no screening was applied for the effect of polar mesospheric clouds (PMCs). High
394 biases (by tens of percent) in H₂O above ~70 km have been shown to occur as a result of PMCs
395 in the HALOE field of view (McHugh et al., 2003). Indeed, monthly means larger than 8-10
396 ppmv are observed in GOZCARDS H₂O merged data and in HALOE source data for pressures
397 less than ~0.03 hPa. A more recent HALOE data version (V20 or VPMC) could be used to
398 largely correct such PMC-related effects, although this was not implemented for GOZCARDS
399 H₂O. Aura MLS and ACE-FTS measurements, obtained at longer wavelengths than those from
400 HALOE, do not yield such large H₂O values; a rough threshold of 8.5 ppmv could also be used
401 (by GOZCARDS data users) to flag the pre-2005 merged dataset.

402 UARS MLS stratospheric H₂O for GOZCARDS was obtained from V6 (or V600) H₂O data.
403 This data version is identical to the original prototype (named V0104) from Pumphrey (1999),
404 who noted that UARS MLS H₂O often exhibits drier values (by 5-10%) than HALOE H₂O (see
405 also Pumphrey et al., 2000). The resulting UARS MLS H₂O source data span the period from
406 Sep. 1991 through April, 1993; a significant fraction of this dataset in the tropics at 100 hPa is
407 flagged bad, as a result of diminishing sensitivity.

408 Summarizing past validation results, SPARC WAVAS (2000) analyses pointed out the
409 existence of a small low bias in HALOE stratospheric H₂O versus most other measurements,
410 except for UARS MLS. Lambert et al. (2007) showed agreement within 5-10% between Aura
411 MLS version 2.2 H₂O and other data, including ACE-FTS H₂O. From the mid-stratosphere to the
412 upper mesosphere, excellent agreement between ground-based data from the Water Vapor
413 Millimeter-wave Spectrometer and H₂O profiles from Aura MLS and ACE-FTS has been
414 demonstrated by Nedoluha et al. (2007, 2009, 2011). Changes from MLS v2.2 to v3.3 led to an
415 increase of 0.2-0.3 ppmv in stratospheric H₂O (Livesey et al., 2013). Recent comparisons by
416 Hurst et al. (2014) of MLS v3.3 H₂O data versus Cryogenic Frost point Hygrometer time series
417 above Boulder show excellent overall agreement, indicating that systematic uncertainties for
418 lower stratospheric MLS data may be as low as ~5%; this reinforces MLS H₂O validation work
419 by Read et al. (2007) and Voemel et al. (2007). Aura MLS stratospheric H₂O v3.3 values are
420 slightly larger (by up to ~5%) than the multi-instrument average from a number of satellite
421 datasets, as discussed in satellite intercomparisons by Hegglin et al. (2013), who observed only
422 small disagreements in interannual variations from various series for pressures less than 150 hPa.

423 **4.2 GOZCARDS H₂O merged data records**

424 The merging process for H₂O is nearly identical to the method used for HCl. The main difference
425 is an additional step that merges UARS MLS data with the already combined datasets from
426 HALOE, ACE-FTS, and Aura MLS, by simply adjusting UARS MLS values to the average of
427 the previously merged series during the early (1991-1993) overlap period; see Fig. S5 for an
428 illustration. Typically, this requires an upward adjustment of UARS MLS H₂O data, as these
429 values are biased low versus most other datasets; nevertheless, the short but global record from
430 UARS MLS helps to fill the time series. After considering the channel drift issues for SAGE II

431 H₂O (and following past advice from the SAGE II team itself), we decided to use caution and did
432 not include that dataset for GOZCARDS, as trend results could be affected. Other minor
433 procedural merging details or issues for H₂O are included in the Supplement. Also, data users
434 should be aware of anomalous effects arising in merged average series from non-uniform
435 latitudinal sampling when no MLS data exist, in regions with large latitudinal gradients, as for
436 H₂O at 147 hPa, the largest pressure for merged GOZCARDS H₂O. Latitudinal averages can be
437 biased in certain months and month-to-month variability is increased because of relatively poor
438 global sampling (in this region) prior to Aug. 2004, after which Aura MLS data are used.

439 In Fig. 10, we display the average offsets that were applied to the four H₂O source datasets;
440 these offsets follow previously known relative data biases. For example, low biases in UARS
441 MLS H₂O, especially in the mesosphere, were discussed by Pumphrey (1999) and the UARS
442 MLS offsets (see Fig. 10) correct that dataset upward. The application of offsets derived for
443 HALOE and UARS MLS raises the H₂O time series from these instruments, whereas negative
444 offsets lower the H₂O source data from ACE-FTS and Aura MLS. As we found for HCl, the
445 offset values generally display small variations versus latitude and are therefore fairly stable
446 systematic adjustments to the time series. Figure S6 displays the amplitudes of the fitted annual
447 cycles for HALOE, ACE-FTS, and Aura MLS. As for HCl, similar patterns emerge for these
448 datasets. Wintertime descent into the polar vortex regions is responsible for large annual cycles
449 at high latitudes, especially in the mesosphere; also, the seasonal impact of dehydration in the
450 lower stratospheric Antarctic region causes a large annual cycle in Aura MLS high southern
451 latitude data. Figure 11 provides some statistical information, as done for HCl in Sect. 3.2,
452 regarding the correlations and trend differences between ACE-FTS and Aura MLS. There are a
453 few regions with noisier relationships. While slow increases in H₂O are generally observed by
454 both instruments in the stratosphere and mesosphere, the tropical region near 0.1 hPa shows a
455 slight decreasing trend for the ACE-FTS points, thus leading to larger discrepancies; it is not
456 clear what the source of these discrepancies is. While the tropical ACE-FTS data are generally
457 sampled with a significantly lower temporal frequency, the same applies for all pressure levels;
458 however, a few outlier points can have a much larger impact when sampling is poorer. There are
459 also a few other spots, such as near 65°S and 65°N and near 5 hPa, with a large drift in the
460 difference time series; this may be caused by a combination of poorer sampling by ACE-FTS

461 and higher atmospheric variability, which can lead to more scatter. At the highest latitudes in the
462 lower stratosphere, the observed slope differences are more within error bars, but the larger
463 variability means that a longer record is needed to determine if the time series trend differently.
464 The merged dataset tends to be much closer to Aura MLS in terms of trends because there are
465 many more months of Aura MLS than ACE-FTS data; the overall impact of
466 ACE-FTS data on the merged H₂O series is fairly small.

467 Figure S7 provides a visual representation of the merged GOZCARDS H₂O fields at
468 3 hPa and 68 hPa, respectively. Well-known features are displayed in these plots, given the good
469 global coverage in the post-2004 period in particular. In the upper stratosphere, descent at high
470 latitudes during the winter months leads to larger H₂O values, and low latitude QBO features are
471 also observed. In the lower stratosphere, one observes dehydration evidence at high southern
472 latitudes in the winter months, as well as a low latitude seasonal “tape recorder” signal; this
473 phenomenon is driven by tropopause temperatures and has been measured in satellite data since
474 the early 1990s (Mote et al., 1996; Pumphrey, 1999). A vertical cross-section of this lower
475 stratospheric tropical (20°S to 20°N) tape recorder in GOZCARDS merged H₂O for 1991-2013
476 is shown in Fig. 12; periods of positive anomalies alternate with negative anomalies, including
477 the post-2000 lows, as well as the most recent decreases in 2012-2013 (see also next section).

478 As we discussed for HCl, we have estimated systematic errors for the merged H₂O product.
479 This is illustrated by the contour plots in Fig. 13; these ranges encompass at least 95% of the
480 monthly mean source data values from HALOE, UARS MLS, ACE-FTS, and Aura MLS above
481 or below the merged series. These errors typically span 5 to 15% of the mean between 100 and
482 0.1 hPa; errors larger than 30% exist in the tropical upper troposphere (147 hPa), and large
483 values in the upper mesosphere arise from the low bias in UARS MLS H₂O.

484 **4.3 GOZCARDS H₂O sample results and discussion**

485 Stratospheric H₂O variations have garnered attention because of the radiative impacts of water
486 vapor in the UTLS and the connection to climate change (Solomon et al., 2010), as well as the
487 stratospheric chemical significance of H₂O oxidation products. Individual water vapor datasets
488 have been used here to produce a merged stratospheric H₂O record spanning more than two
489 decades. We do not attempt here to characterize trends or to imply that recent tendencies will

490 carry into the next decade or two. Rather, as variability is also of interest to climate modelers, we
491 focus here on observed decadal-type (longer-term) variability in stratospheric water vapor.

492 Figure 14 illustrates monthly, annual, and longer-term changes in stratospheric water vapor,
493 based on GOZCARDS merged H₂O; this shows the well-known H₂O minimum in the lower
494 tropical stratosphere as well as an increases in the upper stratosphere (as a result of methane
495 oxidation). As we know from past studies (e.g., Randel et al., 2004), medium- to long-term
496 changes in H₂O are large-scale in nature. However, lower stratospheric H₂O variations are more
497 accentuated at low latitudes, in comparison to near-global (60°S-60°N) results. It has long been
498 known (e.g., from the *in situ* balloon-borne measurements of Kley et al., 1979) that the
499 hygropause is typically located a few km higher than the thermal tropopause. We observe that
500 the tropical stratosphere is drier at 68 hPa than at 100 hPa (near the tropopause). According to
501 the 22-year GOZCARDS data record, annually-averaged H₂O values in the tropics (20°S-20°N)
502 have varied between about 3.2 and 4.2 ppmv at 68 hPa. The rapid drop between 2000 and 2001
503 is observed at 100 and 68 hPa, with some dilution of this effect at higher altitudes. There is a
504 clear difference in long-term behavior between the upper stratosphere, where changes in methane
505 should have the clearest influence, and the lower stratosphere, where cold point temperatures and
506 dynamical changes have a significant impact. To first-order, the last few years show ~10% larger
507 values in the upper stratosphere than in the early 1990s, while the opposite holds in the lowest
508 stratospheric region, where a decrease of order 10% is observed over the same period. Figure 14
509 also shows that month-to-month and seasonal variations are usually somewhat larger than the
510 long-term changes in the lower stratosphere, most notably at 100 hPa.

511 In order to provide longer-term variability diagnostics for water vapor, we show in Fig. 15 the
512 minimum to maximum spread in annual averages (tropics and mid-latitudes) from Fig. 14 for the
513 22-yr period. We observe that the tropical variability is largest just above the tropopause (here
514 this means at the 68 hPa GOZCARDS level), where it reaches ~27% (1 ppmv). Such diagnostics
515 of variability should be useful for comparisons to various chemistry climate models.

516 The longer-term variability in water vapor increases above the stratopause and reaches close
517 to 30% in the uppermost mesosphere, as seen in Fig. 16(a); this plot shows the monthly and
518 annual near-global (60°S-60°N) H₂O variations at 0.01 hPa. Large seasonal changes in this
519 region are driven by vertical advection associated with the mesospheric circulation, with each

520 hemisphere's summertime peaks contributing to the maxima (two per year) in these near-global
521 averages; such seasonal variations were compared to model results by Chandra et al. (1997),
522 based on the first few years of HALOE H₂O data. The strong upper mesospheric variability in
523 annual-mean H₂O is known from previous studies of ground-based and satellite H₂O data
524 (Chandra et al., 1997; Nedoluha et al., 2009; Remsberg, 2010), and this region is where the solar
525 (Lyman α) influence on H₂O is strongest. Figure 16(b) displays the near-global variations in
526 annual upper mesospheric H₂O from 0.1 to 0.01 hPa. We clearly see increased variability in the
527 uppermost mesosphere, and decreases in the mixing ratios as a result of H₂O photodissociation.

528 **5 GOZCARDS ozone**

529 A number of discussions relating to signs of ozone recovery have been presented before
530 (Newchurch et al., 2003; Wohltmann et al., 2007; Yang et al., 2008; Jones et al., 2009; Hassler
531 et al., 2011; Salby et al., 2011, 2012; Ziemke and Chandra, 2012; Gebhardt et al., 2014;
532 Kuttipurath et al., 2013; Kirgis et al., 2013; Nair et al., 2013, 2015; Shepherd et al., 2014, Frith et
533 al., 2014). While there are some indications of small increases in O₃ in the past 10-15 years,
534 further confirmation of an increase in global O₃ and its correlation with column increases is
535 needed in order to more clearly distinguish between long-term forcings, notably from the 11-yr
536 solar cycle, slow changes in halogen source gases, temperature changes, and shorter-term
537 variability. Continuing, good long-term ozone datasets are clearly needed for such studies.

538 **5.1 GOZCARDS ozone source data records**

539 We used ozone datasets from SAGE I, SAGE II, HALOE, UARS MLS, ACE-FTS, and Aura
540 MLS to generate the monthly zonal mean source products for GOZCARDS. Due to time
541 constraints, we did not use the newer SAGE II version 7 ozone (see Damadeo et al., 2013) as
542 part of the GOZCARDS merged dataset. Our studies indicate that there are systematic
543 differences of only a few percent between SAGE II V6.2 and V7 O₃ on their native coordinates
544 (number density versus altitude). However, these 2 versions exhibit some differences if the data
545 are converted to mixing ratios on pressure surfaces. These differences result mainly from
546 different temperatures (and their trends) between MERRA and analyses from the National
547 Centers for Environmental Prediction (NCEP), used by SAGE II V7 and V6.2 retrievals,

548 respectively. The main differences between MERRA and NCEP temperatures occur in the upper
549 stratosphere for time periods before 1989 and after mid-2000 (see further details in Sect. 5.2).

550 **5.1.1 Treatment of SAGE ozone profiles**

551 Both SAGE I and SAGE II used solar occultations during satellite sunrise and sunset to measure
552 vertical profiles of ozone, along with other composition data and aerosol extinction (McCormick
553 et al., 1989; Cunnold et al., 1989). It takes about 1 month for SAGE I and II to provide near
554 global coverage (about 80°N to 80°S), with some dependence on season. The SAGE I
555 measurements started in February 1979 and stopped in November 1981, while SAGE II provided
556 data between October 1984 and August 2005. In the middle of July 2000, SAGE II had a
557 problem in its azimuth gimbal system. Although this was corrected by November 2000, the
558 instrument operation was switched to a 50% duty cycle, with either sunrise or sunset occultations
559 occurring in monthly alternating periods, until the end of the mission.

560 It is known that there were altitude registration errors in SAGE I (V5.9) data (Veiga et al.,
561 1995; Wang et al., 1996). To correct this problem, an empirical altitude correction method based
562 on Wang et al. (1996) had been applied to SAGE I (V5.9) data; these corrected SAGE I V5.9
563 profiles, which had been evaluated in previous trend studies (e.g. SPARC, 1998; WMO, 2003),
564 were used to create the GOZCARDS SAGE I product (denoted as version V5.9_rev). We did not
565 use reprocessed version 6.1 SAGE I data (L. W. Thomason, personal communication, 2012)
566 because the altitude registration problems had not been completely fixed and new altitude
567 correction criteria should be derived and validated.

568 Ozone data screening details for the original SAGE I and SAGE II datasets are provided in
569 Appendix A. The number density profiles were converted to mixing ratios on pressure levels by
570 using NCEP temperature and pressure data provided with each profile. Derived ozone profiles
571 were then interpolated to fixed pressure levels on the following grid:

$$572 \quad p(i) = 1000 \times 10^{-\frac{i}{30}} \text{ (hPa)} \quad i = 0, 1, 2, \dots \quad (2)$$

573 Ozone values at each of the 5 levels centered on every GOZCARDS pressure level were then
574 averaged (weighted by pressure) to derive mixing ratios at each GOZCARDS pressure level. By
575 doing this, the SAGE profiles were smoothed to a vertical resolution comparable to that of the

576 other satellite instruments used in this GOZCARDS work. Monthly zonal means were then
577 computed for the SAGE ozone datasets on the GOZCARDS-compatible grid.

578 **5.1.2 Comparisons of ozone zonal means**

579 Ozone differences between SAGE II and other satellite data are shown in Fig. S8. Zonal mean
580 differences between SAGE II and HALOE are generally within 5% for 1.5 to 68 hPa at mid-
581 latitudes, and for 1.5 to 46 hPa in the tropics; relative biases are larger outside those ranges and
582 increase to ~10% near the tropopause and also near 1 hPa. This good level of agreement was
583 demonstrated in the past (e.g., SPARC, 1998). SAGE II data show better agreement with UARS
584 and Aura MLS in the upper stratosphere and lower mesosphere, within 5% up to 0.68 hPa and
585 for latitudes outside the polar regions. Aura MLS O₃ compares better with SAGE II data than
586 does UARS MLS in the tropics for pressures larger than 68 hPa; the high bias in UARS MLS O₃
587 at 100 hPa has been discussed previously (Livesey et al., 2003). There are no months that include
588 both SAGE II and ACE-FTS data in the northern hemisphere tropics (see the gap in Fig. S8,
589 bottom right panel), largely due to the poorer coverage from ACE-FTS in the tropics. ACE-FTS
590 O₃ shows the largest positive bias (greater than 10%) with respect to SAGE II, for pressures less
591 than 1.5 hPa. The high bias in upper stratospheric ACE-FTS ozone has been mentioned in past
592 validation work using ACE-FTS data (e.g., Froidevaux et al., 2008b; Dupuy et al., 2009). The
593 biases shown here are also consistent with recent O₃ intercomparison studies from a
594 comprehensive array of satellite instruments by Tegtmeier et al. (2013). It has been known for
595 some time that the HALOE and SAGE II ozone datasets, which govern the main variations of the
596 GOZCARDS merged ozone values before 2005, agree quite well (within 5%) in absolute value,
597 and also in terms of temporal trends (Nazaryan et al., 2005), and versus ozonesondes (mostly
598 above ~20 km or ~50 hPa). Larger percentage differences occur in the lowest region of the
599 stratosphere at low latitudes, and especially in the upper troposphere, where HALOE values
600 become significantly smaller than SAGE II data, which are already biased low (by ~50%) versus
601 sondes (Wang et al., 2002); see also Morris et al. (2002), as well as results of SAGE II and
602 HALOE comparisons versus solar occultation UV-Visible spectrometer measurements from long
603 duration balloons (Borchi et al., 2005). We should note here that in this GOZCARDS merging
604 work, we have largely avoided the upper tropospheric region.

605 Zonal mean differences between SAGE II and Aura MLS show some latitudinal structure
606 between 1 and 3 hPa, with larger (5-10%) biases in the southern hemisphere, especially for 0 to
607 30°S (see Fig. S8). There are no such features between SAGE II and HALOE or UARS MLS.
608 We found that this results from anomalous NCEP temperatures after 2000, which affect SAGE II
609 data converted from number density/altitude to GOZCARDS VMR/pressure coordinates.
610 Figure 17 shows an example of the ozone series from SAGE II and other satellite data for 10°S to
611 20°S from 1 to 6.8 hPa. At 1 hPa, the SAGE II ozone values (converted to mixing ratios) drift
612 relative to HALOE and are elevated after mid-2000; this can be attributed to abnormal NCEP
613 temperature trends compared to MERRA and HALOE during the same time period (for detailed
614 views, see Figs. S9 and S10). Similar features are found down to pressures near 3 hPa. These
615 issues relating to anomalous upper stratospheric NCEP temperature trends were noted by
616 McLinden et al. (2009). Because such artifacts are confirmed by using either MERRA or
617 HALOE temperatures, we decided not to include in the merging process any SAGE II O₃ values
618 after June 30, 2000 for pressures equal to or less than 3.2 hPa. SAGE II ozone is not significantly
619 affected by the conversion to mixing ratio/pressure coordinates at 4.6 and 6.8 hPa (Fig. 17).

620 **5.2 GOZCARDS ozone merged data records**

621 **5.2.1 Methodology for GOZCARDS merged ozone**

622 Ozone measurements from SAGE I, SAGE II, HALOE, UARS MLS, Aura MLS and ACE-FTS,
623 were used to establish a near-continuous monthly zonal mean record from late 1979 through
624 2012 for the GOZCARDS merged O₃ product (ESDR version 1.01). The SAGE II dataset was
625 used as a reference standard, since it has the longest period of measurements and has been
626 extensively validated. A GOZCARDS ozone merged data record is constructed by combining
627 these measurements after removing systematic biases with respect to SAGE II. This is done by
628 applying additive offsets to all other instrument series, as determined from average differences
629 between monthly zonal means and SAGE II during overlap time periods. The merged data are
630 then derived by averaging all available adjusted datasets. Because there are gaps in overlap
631 between SAGE II and ACE-FTS monthly mean data in some latitudes (Fig. S7), and as SAGE II
632 ozone VMRs obtained from the vertical grid transformation were affected by anomalous NCEP
633 temperatures after mid-2000 for pressures smaller than or equal to 3.2 hPa, a two-step approach

634 is used to generate the merged product. First, SAGE II data are used as reference for pressures
635 larger than 3.2 hPa to adjust HALOE, UARS MLS and Aura MLS based on overlapping months
636 between 1991 and Nov. 2005; see the method overview schematic in Fig. 18. For $p \leq 3.2$ hPa,
637 SAGE II O₃ is still used as a reference through June 2000, and HALOE and UARS MLS data are
638 adjusted accordingly. This eliminates the effect of anomalous NCEP temperatures on SAGE II
639 ozone and leads to more accurate offsets based on HALOE values, after they have been adjusted
640 to SAGE II. Adjusted HALOE data (HALOE* in Fig. 18) are then used as a reference to derive
641 estimated offsets for Aura MLS O₃, using the overlap period with HALOE from Aug. 2004 to
642 Nov. 2005. In step 2, a new reference value is derived by averaging all available data from
643 SAGE II, HALOE*, UARS MLS* and Aura MLS*. This value is used to adjust ACE-FTS ozone
644 based on all overlapping months between March 2004 and Nov. 2005. By including Aura MLS
645 in the dataset created in step 1, we obtain more complete spatial and temporal coverage than
646 possible with SAGE II and HALOE, and ensure that there are overlapping months between this
647 combined dataset and ACE-FTS source data. At the end of step 2, the final merged ozone is
648 derived by averaging the temporary merged dataset from step 1 with the adjusted ACE-FTS data.

649 **5.2.2 Further considerations regarding GOZCARDS merged ozone data**

650 Even in the absence of diurnal variations, measurements from occultation sensors can yield
651 larger sampling errors than those from densely-sampled emission measurements (Toohey et al.,
652 2013). Diurnal changes in ozone can affect data comparisons and could impact data merging.
653 Recently, Sakazaki et al. (2013) presented diurnal changes measured by the Superconducting
654 Submillimeter-Wave Limb-Emission Sounder (SMILES) and Parrish et al. (2014) analyzed
655 ground-based microwave O₃ profile variations versus local time in conjunction with satellite
656 data. Ozone diurnal variations range from a few percent in the lower stratosphere to more than
657 10% in the upper stratosphere and lower mesosphere (see also Ricaud et al., 1996; Haeefele et al.,
658 2008; Huang et al., 2010). SAGE II and other occultation instruments observe ozone at local
659 sunrise or sunset, and the retrieved values are generally closer to nighttime values in the upper
660 stratosphere and mesosphere. To characterize systematic differences between satellite data,
661 coincident profiles with small differences in space and time are most often used; an example of
662 mean differences and standard deviations between SAGE II and Aura MLS using both
663 coincident profile and zonal mean methods is provided in Fig. S11. SAGE II and coincident

664 Aura MLS nighttime O₃ values agree within ~5% between 0.46 and 100 hPa, except in the
665 tropical lower stratosphere where comparisons are noisier. Differences between zonal mean
666 SAGE II and Aura MLS data are very close to differences from averaged coincident values,
667 except for pressures less than 2 hPa, where differences increase from a few to ~10% at 0.3 hPa,
668 consistent with what one expects from the diurnal cycle. Although zonal mean differences are
669 likely to be less representative of “true” differences, by combining SAGE II with Aura MLS data
670 adjusted by zonal mean biases, we provide a series adjusted to the average of sunrise and sunset,
671 as measured by SAGE II. If Aura MLS data were adjusted by biases obtained using the
672 coincident method, an upper stratospheric offset of more than several percent and artificial trends
673 due to such a diurnal cycle effect could be introduced. The use of long-term datasets with
674 consistent sampling should be an advantage for trend detection, even in a region with diurnal
675 changes. Also, our avoidance of SAGE II upper stratospheric O₃ after mid-2000 mitigates
676 potential artifacts arising from changing SAGE II sunrise/sunset sampling patterns over time.

677 Figure 19 displays the average ozone offsets obtained from the biases relative to SAGE II. A
678 high bias in upper stratospheric ACE-FTS O₃ relative to other datasets is evident from the
679 negative ACE-FTS offsets (as large as 25%). Most of the other instrument offsets are in the 5-
680 10% range; lowering O₃ from UARS MLS, HALOE, and Aura MLS in the lower mesosphere is
681 required to match SAGE II. Sampling differences and data sparseness may be mostly responsible
682 for larger offsets at high latitudes; in these regions, the merged data are less amenable to long-
683 term analyses because of data gaps and larger variability (especially prior to 2004).

684 As shown in the Supplement (Fig. S12), we observe strong similarities (e.g., peaks at
685 midlatitudes near 10 and 1.5 hPa) in the O₃ annual cycle amplitude patterns from SAGE II,
686 HALOE, ACE-FTS, and Aura MLS over their respective measurement periods. Middle
687 stratospheric peaks are a result of the annual cycle in oxygen photolysis, whereas temperature
688 variations drive the annual cycle in the upper stratosphere (Perliski et al., 1989). This sort of
689 comparison provides some reassurance regarding the consistency of various datasets. Figure 20
690 provides diagnostics similar to those given for HCl and H₂O, namely correlation coefficients and
691 significance ratios for the slopes of the deseasonalized anomaly time series from SAGE II versus
692 HALOE as well as from ACE-FTS versus Aura MLS (for 1992 through 1999, and 2005 through
693 2009, respectively). These diagnostic results for ACE-FTS and Aura MLS are of a quality that is

694 comparable to the HALOE/SAGE II results; poorer fits occur mostly at high latitudes and in the
695 upper stratosphere. Poorer correlations at upper altitude appear largely tied to a decrease in the
696 amount of valid data in this region (especially at high latitudes), coupled with a relatively small
697 variability. For regions with poorer agreement between ACE-FTS and Aura MLS, we often see
698 small variability in the series from Aura MLS but larger changes (scatter) in the ACE-FTS series.
699 Larger differences in trends between SAGE II and HALOE were noted by Nazaryan et al. (2005)
700 at low latitudes near 50 km; this is also indicated by our simple linear fits (not shown here) to the
701 GOZCARDS source datasets from these two instruments and the existence of poorer agreements
702 in Fig. 20 for the slope of the difference series in that region. The existence of good correlations
703 in interannual ozone variations between a large number of satellite measurements was discussed
704 by Tegtmeier et al. (2013). Regarding temporal drifts, Nair et al. (2012) have shown that small
705 drifts (mostly within about $\pm 0.5\%/yr$ for the 20-35 km region) exist between most of the datasets
706 from six ozone lidar sites and coincident HALOE, SAGE II, and Aura MLS measurements;
707 similar results were obtained by Kirgis et al. (2013). Other recent studies (in particular, by
708 Hubert et al., 2015) corroborate the very good stability of the datasets used for GOZCARDS,
709 which relies most heavily on O₃ data from SAGE II and Aura MLS. While we feel justified in
710 the use of the longer-term time series chosen for GOZCARDS O₃, data users should still note the
711 existence of a few regions with poorer correlations or trend agreement (and, therefore, larger
712 uncertainties) between different satellite ozone datasets, as indicated in Fig. 20. Long-term
713 merged datasets from GOZCARDS and other sources should undergo continued scrutiny from
714 the community, as done recently for trends by Tummon et al. (2015) and Harris et al. (2015).
715 Sample cross-sectional views of two slices through the GOZCARDS merged O₃ field are
716 provided in the Supplement (Fig. S13). Figure 21 shows estimated systematic errors from our
717 calculation of the 95% ranges for the monthly mean source data used here, both above and below
718 the merged values. In this case, as SAGE II is used as a reference dataset, the applied offsets
719 (Fig. 20) correlate quite well with this plot depicting the ranges about SAGE II values. Minimum
720 error bars can be slightly lower than 5% for the middle stratosphere at low latitudes, where ozone
721 values are largest. This view of systematic error bars is consistent with results by Tegtmeier et al.
722 (2013), based on the larger set of data analyzed for the SPARC Data Initiative. They also found

723 that the regions with lowest errors (scatter) are in the middle stratosphere at low to mid-latitudes,
724 where most monthly mean satellite data fit within $\pm 5\%$ of the multi-instrument mean.

725 **5.3 GOZCARDS ozone sample results and discussion**

726 Nair et al. (2013) used regression analyses to compare profile trend results from GOZCARDS
727 merged O₃ at northern midlatitudes versus a combined O₃ dataset from lidar and coincident
728 satellite data at the Observatoire de Haute Provence (OHP), France. They showed that good
729 consistency exists for the decreasing ozone time period, from the early 1980s to 1997, and for the
730 upper stratospheric increase since 1997, but some differences exist in the lower stratosphere
731 during this second time period, when the GOZCARDS results show a near-zero trend in
732 comparison to small positive trends from the combined (and more localized) dataset. The above
733 results for the declining time period agree broadly with earlier work (for the 1979-1997 period)
734 by Jones et al. (2009). Gebhardt et al. (2014) analyzed ozone profile trends from SCIAMACHY
735 on ENVISAT, and compared this to trends from Aura MLS, Optical Spectrograph and InfraRed
736 Imager System (OSIRIS) on the Odin satellite, and sondes; their results include the detection of
737 localized ozone increases in the mid-stratosphere at low latitudes; see also Bourassa et al. (2014),
738 who analyzed merged SAGE II and (OSIRIS) observations for 1984-2013, as well as results
739 from Kyrölä et al. (2013) on combined SAGE II and Global Ozone Monitoring by Occultation of
740 Stars (GOMOS) records for 1984-2012, and Eckert et al. (2014), who investigated ENVISAT
741 MIPAS trends for 2002-2012. The shortness of data records since 1997, coupled with relative
742 variability and potential drifts between various measurements may explain some differences in
743 recent trend results, notably for the post-1997 period. More comprehensive analyses from the
744 SI²N initiative have focused on an intercomparison of profile changes from a variety of datasets,
745 including GOZCARDS and other merged records (Tummon et al., 2015; Harris et al., 2015).

746 Here, we investigate ozone column results based on the global GOZCARDS data, given the
747 work by Ziemke and Chandra (2012), hereafter referenced as ZC12. These authors analyzed total
748 column and stratospheric column data from satellites, and their analyses yielded a rather strong
749 near-global (60°S-60°N) average ozone increase since 1998. Their stratospheric columns
750 depend on the convective-cloud differential (CCD) method and use Total Ozone Mapping
751 Spectrometer (TOMS) and Ozone Monitoring Instrument (OMI) column data over convective

752 clouds near the tropopause (see also Ziemke et al., 2005). In Fig. 22, we compare changes in
753 60°S-60°N ZC12 column ozone data (J. Ziemke, personal communication, 2013) to changes in
754 GOZCARDS O₃ columns above 68 hPa for that region; note that GOZCARDS values do not
755 provide for a continuous long-term time series down to pressures of 100 hPa or more in the
756 SAGE I years (1979-1981). To eliminate biases between stratospheric columns as calculated
757 using the CCD methodology and the GOZCARDS fixed bottom pressure approach, we reference
758 all stratospheric columns to the 1980 total column value. These column series include SAGE I
759 data and are linearly interpolated between 1981 and 1984, when no GOZCARDS source datasets
760 exist. We observe that relative changes in GOZCARDS columns follow the ZC12 curves within
761 a few DU in the downward phase until about 1992, but the 1992-1997 decrease in total columns
762 does not compare very well. Some of this discrepancy may occur because total columns capture
763 a stronger decrease from levels below 68 hPa, not fully represented in GOZCARDS. Focusing on
764 the late period (from Aura MLS and ACE-FTS), we also show the GOZCARDS columns above
765 68 hPa, referenced to 2007 instead of 1980. There is a good match in the variations between
766 GOZCARDS and ZC12 columns during 2005-2010, in agreement with the fact that very good
767 correlations were obtained by ZC12 between Aura MLS columns and stratospheric column data
768 from the CCD technique. ZC12 values for stratospheric and total columns are in good agreement,
769 although the stratospheric values have gaps when not enough data were present for near-global
770 estimates. The increase in ZC12 data from 1997 to 1998 is not matched very well by
771 GOZCARDS; this is also true if we remove the 11-yr solar cycle from both datasets (not shown
772 here), as done by ZC12. We also note that recent analyses by Shepherd et al. (2014), who used a
773 chemistry-climate model constrained by meteorology to investigate causes of long-term total
774 column O₃ variations, show a partial return, in 2010, towards 1980 ozone column values, but not
775 nearly as much as implied by ZC12. We note that long-term halogen source gas reductions that
776 have occurred since the mid-1990s should only lead to column ozone increases of a few DU
777 since 1997 (Steinbrecht et al., 2011). It is likely that the discrepancies seen here lie in the various
778 datasets and their merging; for example, it would be worthwhile to check if homogenized SBUV
779 column O₃ data show results that are substantially different from those of ZC12. Discrepancies
780 could also arise from differences in ozone column calculations or coverage, because of different
781 methodologies, grids or sampling to properly determine near-global results.

782 **6 Other GOZCARDS data records**

783 We now briefly mention the N₂O, HNO₃, and temperature GOZCARDS records that were part of
784 the delivery for public dissemination in 2013. For N₂O and HNO₃, the somewhat simpler
785 merging procedure consisted of averaging the source datasets from ACE-FTS and Aura MLS
786 over the overlap time period (Aug. 2004 through Sep. 2010) to obtain the additive offsets for
787 each of the two individual records. We then simply used the correspondingly-adjusted and
788 averaged series to create the merged results; this procedure is the same as we described for the
789 first step in the HCl (or H₂O) merging process.

790 **6.1 N₂O**

791 This data set starts in August 2004, when the Aura MLS data record began; the only dataset after
792 Sep. 2010 is the Aura MLS N₂O (version 3.3) data record. Because of degradation in the main
793 target MLS N₂O band (near 640 GHz) after the first few months of 2013, the N₂O standard MLS
794 product is being reprocessed for the whole Aura MLS period using an alternate measurement
795 band; currently, there are no official GOZCARDS N₂O data after 2012.

796 Excellent agreement (mostly within 5%) exists between stratospheric ACE-FTS and Aura
797 MLS N₂O profiles (see Lambert et al., 2007; Strong et al., 2008; Livesey et al., 2013). Plots
798 showing the average offsets applied to both MLS and ACE-FTS N₂O series as a function of
799 latitude and pressure are provided in Fig. S14. These plots are in agreement (in magnitude and in
800 sign) with the above-referenced studies; the two datasets yield typical offsets (one half of the
801 average differences) of less than 5%. Also, very good temporal agreement between these two
802 time series (for 2004-2010) is illustrated by the quality of the N₂O diagnostic information
803 displayed in Fig. S15, showing generally highly correlated fields and insignificant drifts.

804 Figure 23 shows sample contour plots for the N₂O merged field (2004-2012); as seen from the
805 bottom panel (100 hPa), wintertime descent brings low N₂O values down at high latitudes inside
806 the polar vortices. N₂O is a conserved tracer in the lower stratosphere and its variations near the
807 tropopause have implications regarding age of air. Variations in upper stratospheric N₂O are
808 clearly affected by seasonal and dynamical effects; this is evident from the striking semi-annual,
809 annual and QBO-related patterns displayed in Fig. 23 for the 6.8 hPa level (top panel).

810 **6.2 HNO₃**

811 As for N₂O, we merged the HNO₃ data from ACE-FTS (version 2.2) and Aura MLS (version
812 3.3) from Aug. 2004 onward, and included only the adjusted MLS dataset after Sep. 2010. The
813 average offsets applied to MLS and ACE-FTS time series as a function of latitude and pressure
814 for HNO₃ are provided in Fig. S16. The typical offsets (one half of the average differences) for
815 HNO₃ are less than ~10% (and less than 0.5 ppbv). Despite somewhat larger percent absolute
816 differences than for N₂O between Aura MLS and ACE-FTS HNO₃, there is very good agreement
817 as a function of time between these two datasets in the stratosphere. This is illustrated by the
818 HNO₃ diagnostic information provided in Fig. S17; the poorest correlations are obtained at or
819 below the tropical tropopause.

820 Comparisons of v3.3 Aura MLS and v2.2 ACE-FTS nitric acid profiles have shown good
821 agreement (see also Livesey et al., 2013), as the MLS HNO₃ v3.3 values are now generally larger
822 than in v2.2, for which validation results were provided by Santee et al. (2007). Wolff et al.
823 (2008) also compared MLS (v2.2) and ACE-FTS (v2.2) coincident profiles, and obtained similar
824 results; in addition, they demonstrated that very good agreement exists between the HNO₃
825 profiles from ACE-FTS and coincident profiles from MIPAS on Envisat. Also, comparisons
826 between Aura MLS HNO₃ (v3.3) profiles and wintertime HNO₃ profiles retrieved by a Ground-
827 based Millimeter-wave Spectrometer (GBMS) in Thule, Greenland, during the first 3 months of
828 2010, 2011, and 2012 show agreement mostly within 10-15% (Fiorucci et al., 2013).

829 Figure 24 (top two panels) displays the HNO₃ fields at 46 hPa from the UARS MLS period
830 (1991-1997) as well as from the 2004-2013 period, for which a merged GOZCARDS product
831 was produced, based on Aura MLS and ACE-FTS source datasets. Also shown (bottom two
832 panels) are time series for 45°N and 32 hPa from both these periods; the bottom right panel
833 includes the source and merged time series. We have performed additional investigations (not
834 shown here) which lead us to believe that small upward adjustments to the UARS MLS HNO₃
835 values (by about 10%) are needed to better cross-correlate these datasets across the two distinct
836 time periods; such relative biases are within the expected systematic errors. This is based on a
837 consideration of ground-based Fourier Transform infrared column HNO₃ data covering the full
838 time period, as well as past GBMS HNO₃ profile retrievals. Also, Aura MLS and ACE-FTS

839 HNO₃ data match ground-based and other correlative data quite well, and typically better than
840 the intrinsically poorer quality UARS MLS HNO₃ data. However, obtaining an optimum global
841 set of adjustments for the UARS MLS nitric acid field will be limited by the number of sites with
842 such ground-based data as well as by the different vertical resolutions for these datasets versus
843 MLS. More collaborative work regarding such analyses is needed in order to find the optimum
844 adjustments to help tie together these two time periods for this species. Although we did not
845 deliver the UARS MLS HNO₃ source data files for GOZCARDS, we could provide these
846 monthly zonal mean series upon request, keeping the above caveats in mind.

847 **6.3 Temperature**

848 Finally, in terms of the initial set of delivered GOZCARDS products, and for the convenience of
849 stratospheric composition data users, we have used temperatures (T) from the Modern-Era
850 Retrospective Analysis for Research and Applications (MERRA) to produce a monthly mean
851 GOZCARDS temperature data set from 1979 onward. MERRA is a NASA Goddard reanalysis
852 (Rienecker et al., 2011) for the satellite era using Goddard Earth Observing System Data
853 Assimilation System version 5 (GEOS-5); T is from the DAS 3d analyzed state MAI6NVANA,
854 version 5.2 files (such as MERRA300.prod.assim.inst6_3d_ana_Nv.20110227.hdf). Data from
855 four daily MERRA files (for 00, 06, 12, and 18 hr UT) were averaged to provide daily mean
856 temperature fields (appropriate for a mean time of 09 hr). Vertical interpolation was performed
857 onto the GOZCARDS pressure grid, which, for temperature, covers 30 pressures levels from
858 1000 hPa to 0.0147 hPa. Averaged values were stored for the 10° GOZCARDS latitude bins, and
859 daily results were binned to create the GOZCARDS monthly temperature data set (version 1.0).

860 **7 Summary and conclusions**

861 We have reviewed the GOZCARDS project's production of merged data records of stratospheric
862 composition, mainly for HCl, H₂O, and O₃, using carefully screened satellite data, starting in
863 1979 with SAGE I and continuing through Aura MLS and ACE-FTS data periods. The source
864 data have a high degree of maturity and we have reinforced our confidence in their usefulness
865 through investigations of various diagnostics (offsets, annual cycles, correlations and trend
866 differences of deseasonalized series). These records are publicly available as GOZCARDS
867 ESDR version 1.01 and can be referenced using DOI numbers (Froidevaux et al., 2013b,

868 Anderson et al., 2013, and Wang et al., 2013, for the above species, respectively). The other
869 GOZCARDS data records also have references, namely Schwartz et al. (2013) for the MERRA-
870 based temperature records, and Froidevaux et al. (2013c, 2013d) for N₂O and HNO₃,
871 respectively. Table 2 provides a summary of the GOZCARDS monthly mean datasets. Yearly
872 netCDF files are available for public access (<http://mirador.gsfc.nasa.gov>). The merging
873 methodology follows from a determination of mean biases (for each pressure level and 10°
874 latitude bin) between monthly mean series, based on the overlap periods. For ozone, SAGE II
875 data are the chosen reference, whereas for other species, the merging basis is equivalent to an
876 average of the datasets during the periods of overlap. The merged data files contain the average
877 offset values applied to each source data time series, along with standard deviations and standard
878 errors. The GOZCARDS README document (Froidevaux et al., 2013a) provides more details
879 about data file quantities, including local time and solar zenith angle information, and a list of
880 days with available data. We also display here estimated systematic errors about the merged
881 values; we find that mixing ratio errors are typically within 5% to 15% and are consistent with
882 the magnitude of observed relative biases.

883 The GOZCARDS HCl merged record in the upper stratosphere enables long-term tracking of
884 changes in total stratospheric chlorine. The long-term increase in HCl prior to the late 1990s, and
885 the subsequent gentler decrease in the 21st century, are delayed manifestations of changes in the
886 sum of the surface source gas abundances as a result of regulations from the Montreal Protocol
887 and its amendments. From 1997 to 2010, the average rate of change in upper stratospheric HCl
888 (50°S to 50°N) was about -0.4 to -0.7%/yr (with the smaller rates of decrease after 2003). In the
889 lower stratosphere, where Aura MLS data are weighted heavily, recent short-term variations
890 have shown a flattening out and, in particular for northern midlatitudes and at 50-70 hPa for the
891 deep tropics, a significant reversal and increasing trend (see also Mahieu et al., 2014), compared
892 to the decrease from the late 1990s to about 2004. However, lower stratospheric HCl tendencies
893 appear to be reversing again in recent years (2011-2014), with decreases at northern
894 midlatitudes and some increasing tendencies at southern midlatitudes. In the future, we expect to
895 see long-term global HCl decreases in both the upper and lower stratosphere.

896 For water vapor, we have used data from the same instruments as for HCl, with the same
897 methodology, except for the addition of 1991-1993 UARS MLS data. The H₂O data record

898 shows large mesospheric variations that are anti-correlated with the solar flux over the past two
899 11-yr solar cycles. Net long-term trends in lower stratospheric H₂O are quite small if one
900 considers the past 22 years, but there has been considerable interannual variability, including the
901 steep drop from 2000 to 2001, as mentioned in past work. While H₂O tendencies have been
902 generally positive after 2001, the 68 and 100 hPa levels show some steep decreases (by 0.5-0.8
903 ppmv) from 2011 to 2013 (see also Urban et al., 2014). Over the past 22 years, long-term global
904 H₂O increases of order 10% are observed in the upper stratosphere and lower mesosphere,
905 whereas a decrease of nearly 10% has occurred in the lower stratosphere (near 70-100 hPa).
906 However, there is no regular monotonic change on decadal timescales, especially in the tropical
907 lower stratosphere, where fairly sharp decreases followed by steadier increases may be a
908 recurrent pattern (see also Fueglistaler, 2012); this complicates the detection of any small
909 underlying trend. As one might expect from the well-documented temperature influence on the
910 tropical lower stratosphere, H₂O variability (based on maximum minus minimum yearly
911 averages) is largest in the tropics and just above the tropopause. More accurate studies of
912 seasonal to decadal water vapor variability will be enabled by continuing such merged H₂O
913 datasets in the future. A reduction in model spread for stratospheric H₂O is likely easier to
914 achieve than tighter upper tropospheric model results; for the upper troposphere, see the
915 data/model comparisons (H₂O and ice water content) by Jiang et al. (2012).

916 For ozone, we have used measurements from SAGE I, SAGE II, HALOE, UARS MLS, Aura
917 MLS and ACE-FTS to produce a merged record starting in 1979, after adjusting the series to
918 SAGE II. We observed temporal drifts in the SAGE II series, after conversion to the
919 GOZCARDS mixing ratio/pressure grid, as a result of the NCEP temperature data used in this
920 conversion, mostly in the upper stratosphere after June 2000 (see also McLinden et al., 2009). To
921 mitigate this issue, we used HALOE upper stratospheric O₃ as a reference for July 2000 to
922 November 2005, after adjusting the HALOE series to SAGE II. The resulting GOZCARDS
923 merged O₃ data for northern midlatitudes have been used in regression analyses (Nair et al.,
924 2013) to reveal decreases in the whole stratosphere for 1984-1996. Nair et al. (2015) extended
925 this work and found increasing trends in upper stratospheric GOZCARDS O₃ since 1997, but no
926 significant positive trends in the lower stratosphere. Other studies of GOZCARDS O₃ profile
927 trends have been discussed as part of the WMO (2014) and SI²N assessments (Tummon et al.,

928 2015; Harris et al., 2015). Here, we looked at the consistency of column data between
929 stratospheric GOZCARDS O₃ and work by Ziemke and Chandra (2012), who noted that a fairly
930 rapid change (“recovery”) in near-global ozone columns from TOMS and OMI could be inferred
931 since the mid-1990s. We show that the similarly analyzed GOZCARDS column data does not
932 show an upturn of more than 0.5-1% since that period. Reasons for these differences could
933 include data coverage or merging-related issues in either dataset, or inaccuracies in globally-
934 averaged stratospheric columns. A recent global total ozone study (Shepherd et al., 2014) also
935 points to less of a return towards 1980 levels than implied by ZC12.

936 We also briefly described the creation of N₂O and HNO₃ GOZCARDS data records, based on
937 Aura MLS and ACE-FTS. The agreement between these two instruments’ datasets for these
938 species was shown to be generally very good. For HNO₃, UARS MLS HNO₃ source datasets in
939 the GOZCARDS format are available from the authors. However, a small upward adjustment (of
940 order 10%) to the UARS MLS values is likely needed based on our preliminary work comparing
941 these series to HNO₃ column results from FTIR measurements. More detailed work should help
942 determine if global adjustments can indeed be made to UARS MLS HNO₃ data; lacking this, one
943 should ensure that error bars reflect likely biases that can affect the continuity between HNO₃
944 datasets before and after 2000, given the multi-year gap in satellite coverage for this species.

945 **There is a Supplement related to this article.**

946 *Acknowledgements.* Work at JPL was performed under contract with the National Aeronautics
947 and Space Administration (NASA). We dedicate this work to the memory of Professor Derek
948 Cunnold (Georgia Institute of Technology) who was a member of the original NASA
949 MEaSURES (Making Earth System Data Records for Use in Research Environments)
950 GOZCARDS proposal. The GOZCARDS data generation could not have been possible without
951 the past work from instrument teams for SAGE I, SAGE II, HALOE, UARS MLS, Aura MLS,
952 and ACE-FTS, and related data usage documentation. At JPL, we thank Joe Waters for his
953 leadership role in making MLS instruments and datasets possible and Bill Read for his key role;
954 thanks to Vince Perun for MERRA-related work, and to Brian Knosp and Robert Thurstans for
955 database and computer management assistance. We also thank Kaley Walker and Ashley Jones
956 for comments regarding ACE-FTS data, Gloria Manney and William Daffer for help in making

957 the original ACE-FTS data profiles available, and Joe Zawodny and Larry Thomason for their
958 contributions and comments regarding SAGE data. We acknowledge the work of the GMAO
959 team responsible for MERRA data used to generate the GOZCARDS temperatures, specifically,
960 Steven Pawson and Jianjun Jin for discussions and cross-checks regarding temperature data. We
961 acknowledge Jerry Ziemke for the ozone column data (from Ziemke and Chandra, 2012), and
962 Sean Davis for discussions on data usage and screening, and the creation of long-term series. For
963 early HNO₃-related work connecting ground-based data to MLS datasets, we thank Giovanni
964 Muscari and Irene Fiorucci. We are thankful for the NOAA Earth System Research Laboratory
965 (ESRL) Global Monitoring Division (GMD) website information and data on total surface
966 chlorine. We obtained solar flux data for the Ottawa/Penticton sites from the NOAA National
967 Geophysical Data Center (NGDC) website (www.ngdc.noaa.gov), for which we also
968 acknowledge the National Research Council of Canada.

969 **References**

- 970
- 971 Anderson, J. G., Brune, W. H., and Proffitt, M. H.: Ozone destruction by chlorine radicals within the
972 Antarctic vortex: The spatial and temporal evolution of ClO–O₃ anticorrelation based on in situ ER-2
973 data, *J. Geophys. Res.*, 94, 11,465-11,479, 1989.
- 974 Anderson, J., Russell, J. M., Solomon, S., and Deaver, L. E.: HALOE confirmation of stratospheric
975 chlorine decreases in accordance with the Montreal Protocol, *J. Geophys. Res.*, 105, 4483-4490, 2000.
- 976 Anderson, J., Froidevaux, L., Fuller, R. A., Bernath, P. F., Livesey, N. J., Pumphrey, H. C., Read, W. G.,
977 and Walker, K. A.: GOZCARDS Merged Data for Water Vapor Monthly Zonal Means on a Geodetic
978 Latitude and Pressure Grid, version 1.01, Greenbelt, MD, USA: NASA Goddard Earth Science Data and
979 Information Services Center, accessible from doi:10.5067/MEASURES/GOZCARDS/DATA3003, 2013.
- 980 Barath, F., Chavez, M. C., Cofield, R. E., Flower, D. A., Frerking, M. A., Gram, M. B.,
981 Harris, W. M., Holden, J. R., Jarnot, R. F., Kloezeman, W. G., Klose, G. J., Lau, G. K.,
982 Loo, M. S., Maddison, B. J., Mattauch, R. J., McKinney, R. P., Peckham, G. E., Pickett, H. M., Siebes,
983 G., Soltis, F. S., Suttie, R. A., Tarsala, J. A., Waters, J. W., and Wilson, W. J.: The Upper Atmosphere
984 Research Satellite Microwave Limb Sounder Experiment, *J. Geophys. Res.*, 98, 10751-10762, 1993.
- 985 Bernath, P. F., McElroy, C. T., Abrams, M. C., Boone, D., Butler, M., Camy-Peyret, C.,
986 Carleer, M., Clerbaux, C., Coheur, P.-F., Colin, R., DeCola, P., DeMaziere, M., Drummond, J. R.,
987 Dufour, D., Evans, W. F. J., Fast, H., Fussen, D., Gilbert, K., Jennings, D. E., Llewellyn, E. J., Lowe, R.
988 P., Mahieu, E., McConnell, J. C., McHugh, M., McLeod, S. D., Michaud, R., Midwinter, C., Nassar, R.,
989 Nichitiu, F., Nowlan, C., Rinsland, C. P., Rochon, Y. J., Rowlands, N., Semeniuk, K., Simon, P., Skelton,
990 R., Sloan, J. J., Soucy, M.-A., Strong, K., Tremblay, P., Turnbull, D., Walker, K. A., Walkty, I., Wardle,
991 D. A., Wehrle, V., Zander, R., and Zou, J.: Atmospheric Chemistry Experiment (ACE): Mission
992 overview, *Geophys. Res. Lett.*, 32, L15S01, doi:10.1029/2005GL022386, 2005.
- 993 Bhatt, P. P., Remsberg, E. E., Gordley, L. L., McInerney, J. M., Brackett, V. G., and
994 Russell, III, J. M.: An evaluation of the quality of Halogen Occultation Experiment ozone profiles in the
995 lower stratosphere, *J. Geophys. Res.*, 104 (D8), 9261-9275, 1999.
- 996 Borchi, F., Pommereau, J.-P., Garnier, A., and Pinharanda, M.: Evaluation of SHADOZ sondes, HALOE
997 and SAGE II ozone profiles at the tropics from SAOZ UV-Vis remote measurements onboard long
998 duration balloons, *Atmos. Chem. Phys.*, 5, 1381-1397, 2005.

999 Bourassa, A. E., Degenstein, D. A., Randel, W. J., Zawodny, J. M., Kyrölä, E., McLinden, C. A., Sioris,
 1000 C. E., and Roth, C. Z., Trends in stratospheric ozone derived from merged SAGE II and Odin-OSIRIS
 1001 satellite observations, *Atmos. Chem. Phys.*, 14, 6983-6994, doi:10.5194/acp-14-6983-2014, 2014.

1002 Brown, A. T., Chipperfield, M. P., Boone, C., Wilson, C., Walker, K. A., and Bernath, P.: Trends in
 1003 atmospheric halogen containing gases since 2004, *J. Quant. Spec. Rad. Trans.*, 112, 2552-2566, 2011.

1004 Chandra, S., Jackman, C. H., Fleming, E. L., and Russell, J. M.: The seasonal and long term changes in
 1005 mesospheric water vapor, *Geophys. Res. Lett.*, 24, No. 6, 639-642, 1997.

1006 Chu, W. P., and McCormick, M. P.: Inversion of Stratospheric Aerosol and Gaseous Constituents From
 1007 Spacecraft Solar Extinction Data in the 0.38-1.0 μm Wavelength Region, *Appl. Opt.*, 18, No. 9, 1404-
 1008 1413, 1979.

1009 Cunnold, D. M., Chu, W. P., Barnes, R. A., McCormick, M. P., and Veiga, R. E.: Validation of SAGE II
 1010 ozone measurements, *J. Geophys. Res.*, 94, 8447-8460, 1989.

1011 Damadeo, R. P., Zawodny, J. M., Thomason, L. W., and Iyer, N.: SAGE version 7.0 algorithm:
 1012 application to SAGE II, *Atmos. Meas. Tech.*, 6, 3539-3561, doi:10.5194/amt-6-3539-2013, 2013.

1013 Dupuy, E., Walker, K. A., Kar, J., Boone, C. D., McElroy, C. T., Bernath, P. F.,
 1014 Drummond, J. R., Skelton, R., McLeod, S. D., Hughes, R. C., Nowlan, C. R., Dufour, D. G., Zou, J.,
 1015 Nichitiu, F., Strong, K., Baron, P., Bevilacqua, R. M., Blumenstock, T., Bodeker, G. E., Borsdorff, T.,
 1016 Bourassa, A. E., Bovensmann, H., Boyd, I. S., Bracher, A., Brogniez, C., Burrows, J. P., Catoire, V.,
 1017 Ceccherini, S., Chabrillat, S., Christensen, T., Coffey, M. T., Cortesi, U., Davies, J., De Clercq, C.,
 1018 Degenstein, D. A., De Maziere, M., Demoulin, P., Dodion, J., Firanski, B., Fischer, H., Forbes, G.,
 1019 Froidevaux, L., Fussen, D., Gerard, P., Godin-Beekmann, S., Goutail, F., Granville, J., Griffith, D.,
 1020 Haley, C. S., Hannigan, J. W., Hopfner, M., Jin, J. J., Jones, A., Jones, N. B., Jucks, K., Kagawa, A.,
 1021 Kasai, Y., Kerzenmacher, T. E., Kleinbohl, A., Klekociuk, A. R., Kramer, I., Kullmann, H.,
 1022 Kuttippurath, J., Kyrölä, E., Lambert, J.-C., Livesey, N. J., Llewellyn, E. J., Lloyd, N. D., Mahieu, E.,
 1023 Manney, G. L., Marshall, B. T., McConnell, J. C., McCormick, M. P., McDermid, I. S., McHugh, M.,
 1024 McLinden, C. A., Mellqvist, J., Mizutani, K., Murayama, Y., Murtagh, D. P., Oelhaf, H., Parrish, A.,
 1025 Petelina, S. V., Piccolo, C., Pommereau, J.-P., Randall, C. E., Robert, C., Roth, C., Schneider, M., Senten,
 1026 C., Steck, T., Strandberg, A., Strawbridge, K. B., Sussmann, R., Swart, D. P. J., Tarasick, D. W., Taylor,
 1027 J. R., Tetard, C., Thomason, L. W., Thompson, A. M., Tully, M. B., Urban, J., Vanhellefont, F.,

1028 Vigouroux, C., von Clarmann, T., von der Gathen, P., von Savigny, C., Waters, J. W., Witte, J. C., Wolff,
1029 M., and Zawodny, J. M.: Validation of ozone measurements from the Atmospheric Chemistry Experiment
1030 (ACE), *Atmos. Chem. Phys.*, 9, 287–343, doi:10.5194/acp-9-287-2009, 2009.

1031 Eckert, E., von Clarmann, T., Kiefer, M., Stiller, G. P., Lossow, S., Glatthor, N., Degenstein, D. A.,
1032 Froidevaux, L., Godin-Beekmann, S., Leblanc, T., McDermid, S., Pastel, M., Steinbrecht, W., Swart, D.
1033 P. J., Walker, K. A., and Bernath, P. F.: Drif-corrected trends and periodic variations in MIPAS IMK/IAA
1034 ozone measurements, *Atmos. Chem. Phys.*, 14, 2571-2589, doi:10.5194/acp-14-2571-2014, 2014.

1035 Engel, A., Strunk, M., Muller, M., Haase, H.-P., Poss, C., Levin, I., and Schmidt, U.: The temporal
1036 development of total chlorine in the high latitude stratosphere based on reference distributions of mean
1037 age derived from CO₂ and SF₆, *J. Geophys. Res.*, 107, 4136, doi:10.1029/2001JD000584, 2002.

1038 Farman, J. C., Gardiner, B. G., and Shanklin, J. D.: Large losses of total ozone in Antarctica reveal
1039 seasonal ClO_x/NO_x interaction, *Nature*, 315, 207-210, 1985.

1040 Fiorucci, I., Muscari, G., Froidevaux, L., and Santee, M. L.: Ground-based stratospheric O₃ and HNO₃
1041 measurements at Thule, Greenland: an intercomparison with Aura MLS observations, *Atmos. Meas.*
1042 *Tech.*, 6, 2441–2453, doi:10.5194/amt-6-2441-2013, 2013.

1043 Frith, S. M., Kramarova, N. A., Stolarski, R. S., McPeters, R. D., Bhartia, P. K., and Labow, G. J.: Recent
1044 changes in total column ozone based on the SBUV Version 8.6 Merged Ozone Data Set, *J. Geophys.*
1045 *Res.*, 119, 9735-9751, doi:10.1029/2014JD021889, 2014.

1046 Froidevaux, L., Livesey, N. J., Read, W. G., Salawitch, R. J., Waters, J. W., Drouin, B., MacKenzie, I. A.,
1047 Pumphrey, H. C., Bernath, P., Boone, C., Nassar, R., Montzka, S., Elkins, J., Cunnold, D., and
1048 Waugh, D.: Temporal decrease in upper atmospheric chlorine, *Geophys. Res. Lett.*, 33, L23813,
1049 doi:10.1029/2006GL027600, 2006.

1050 Froidevaux, L., Jiang, Y. B., Lambert, A., Livesey, N. J., Read, W. G., Waters, J. W., Fuller, R. A.,
1051 Marcy, T. P., Popp, P. J., Gao, R. S., Fahey, D. W., Jucks, K. W., Stachnik, R. A., Toon, G. C.,
1052 Christensen, L. E., Webster, C. R., Bernath, P. F., Boone, C. D., Walker, K. A., Pumphrey, H. C.,
1053 Harwood, R. S., Manney, G. L., Schwartz, M. J., Daffer, W. H., Drouin, B. J., Cofield, R. E., Cuddy, D. T.,
1054 Jarnot, R. F., Knosp, B. W., Perun, V. S., Snyder, W. V., Stek, P. C., Thurstans, R. P., and Wagner, P. A.:
1055 Validation of Aura Microwave Limb Sounder HCl measurements, *J. Geophys. Res.*, 113,
1056 doi:10.1029/2007JD009025, D15S25, 2008a.

1057 Froidevaux, L., Jiang, Y. B., Lambert, A., Livesey, N. J., Read, W. G., Waters, J. W.,
1058 Browell, E. V., Hair, J. W., Avery, M. A., McGee, T. J., Twigg, L. W., Sumnicht, G. K., Jucks, K. W.,
1059 Margitan, J. J., Sen, B., Stachnik, R. A., Toon, G. C., Bernath, P. F., Boone, C. D., Walker, K. A.,
1060 Filipiak, M. J., Harwood, R. S., Fuller, R. A., Manney, G. L., Schwartz, M. J., Daffer, W. H., Drouin, B. J.,
1061 Cofield, R. E., Cuddy, D. T., Jarnot, R. F., Knosp, B. W., Perun, V. S., Snyder, W. V., Stek, P. C.,
1062 Thurstans, R. P., and Wagner, P. A.: Validation of Aura Microwave Limb Sounder stratospheric and
1063 mesospheric ozone measurements, *J. Geophys. Res.*, 113, doi:10.1029/2007JD008771, D15S20, 2008b.
1064

1065 Froidevaux, L., Fuller, R., Schwartz, M., Anderson, J., and Wang, R.: README Document for the
1066 Global OZoneChemistry And Related trace gas Data records for the Stratosphere (GOZCARDS) project,
1067 Goddard Earth Sciences Data and Information Services Center (GES DISC), <http://disc.gsfc.nasa.gov>,
1068 NASA Goddard Space Flight Center, Code 610.2, Greenbelt, MD 20771 USA, 2013a.

1069 Froidevaux, L., Anderson, J., Fuller, R. A., Bernath, P. F., Livesey, N. J., Russell III, J. M., and
1070 Walker, K.A.: GOZCARDS Merged Data for Hydrogen Chloride Monthly Zonal Means on a Geodetic
1071 Latitude and Pressure Grid, version 1.01, Greenbelt, MD, USA: NASA Goddard Earth Science Data and
1072 Information Services Center, accessible from doi:10.5067/MEASURES/GOZCARDS/DATA3002,
1073 2013b.

1074 Froidevaux, L., Fuller, R. A., Lambert, A., Livesey, N. J., Bernath, P. F., Livesey, N. J., and Walker,
1075 K.A.: GOZCARDS Merged Data for Nitrous Oxide Monthly Zonal Means on a Geodetic Latitude and
1076 Pressure Grid, version 1.01, Greenbelt, MD, USA: NASA Goddard Earth Science Data and Information
1077 Services Center, accessible from doi:10.5067/MEASURES/GOZCARDS/DATA3013, 2013c.

1078 Froidevaux, L., Fuller, R. A., Santee, M. L., Manney, G. L., Livesey, N. J., Bernath, P. F., and Walker,
1079 K.A.: GOZCARDS Merged Data for Nitric Acid Monthly Zonal Means on a Geodetic Latitude and
1080 Pressure Grid, version 1.01, Greenbelt, MD, USA: NASA Goddard
1081 Earth Science Data and Information Services Center, accessible from
1082 doi:10.5067/MEASURES/GOZCARDS/DATA3008, 2013d.

1083 Fueglistaler, S.: Step-wise changes in stratospheric water vapor? *J. Geophys. Res.*, 117, D13302,
1084 doi:10.1029/2012JD017582, 2012.

1085 Gebhardt, C., Rozanov, A., Hommel, R., Weber, M., Bovensmann, H., Burrows, J. P., Degenstein, D.,
1086 Froidevaux, L., and Thompson, A. M.: Stratospheric ozone trends and variability as seen by

1087 SCIAMACHY from 2002 to 2012, *Atmos. Chem. Phys.*, 14, 831–846, doi:10.5194/acp-14-831-2014,
1088 2014.

1089

1090 Haefele, A., Hocke, K., Kampfer, N., Keckhut, P., Marchand, M., Bekki, S., Morel, B.,
1091 Egorova, T., and Rozanov, E.: Diurnal changes in middle atmospheric H₂O and O₃: Observations in the
1092 Alpine region and climate models, *J. Geophys. Res.*, 113, D17303, doi:10.1029/2008JD009892, 2008.

1093 Harris, N. R. P., et al., Past changes in the Vertical Distribution of Ozone, Part III: Analysis and
1094 interpretation of trends, *Atmos. Chem. Phys.*, in press, 2015.

1095 Hassler, B., Bodeker, G. E., Solomon, S., and Young, P. J.: Changes in the polar vortex: Effects on
1096 Antarctic total ozone observations at various stations, *Geophys. Res. Lett.*, 38, L01805,
1097 doi:10.1029/2010GL045542, 2011.

1098 Hegglin, M. I., Tegtmeier, S., Anderson, J., Froidevaux, L., Fuller, R., Funke, B., Jones, A., Lingenfelter,
1099 G., Lumpe, J., Pendlebury, D., Remsberg, E., Rozanov, A., Toohey, M., Urban, J., von Clarmann, T.,
1100 Walker, K. A., Wang, R., and Weigel, K.: SPARC Data Initiative: Comparison of water vapor
1101 climatologies from international satellite limb sounders, *J. Geophys. Res. Atmos.*, 118, 11,824–11,846,
1102 doi: 10.1002/jgrd.50752, 2013.

1103 Hervig, M., and McHugh, M.: Cirrus detection using HALOE measurements, *Geophys. Res. Lett.*, 26,
1104 No. 6, 719-722, 1999.

1105 Huang, F. T., Mayr, H. G., Russell III, J. M., and Mlynczak, M. G.: Ozone diurnal variations in the
1106 stratosphere and lower mesosphere, based on measurements from SABER on TIMED,
1107 *J. Geophys. Res.*, 115, D24308, doi:10.1029/2010JD014484, 2010.

1108 Hubert, D., et al., Ground-based assesment of the bias and long-term stability of fourteen limb and
1109 occultation ozone profile data records, *Atmos. Meas. Tech.*, in review, 2015.

1110 Hurst, D. F., Lambert, A., Read, W. G., Davis, S. M., Rosenlof, K. H., Hall, E. G., Jordan, A. F., and
1111 Oltmans, S. J.: Validation of Aura Microwave Limb Sounder stratospheric water vapor measurements by
1112 the NOAA frost point hygrometer, *J. Geophys. Res. Atmos.*, 119, 1612-1625,
1113 doi:10.1002/2013JD020757, 2014.

1114 Jiang, J. H., Su, H., Zhai, C., Perun, V. S., Del Genio, A., Nazarenko, L. S., Donner, L. J., Horowitz, L.,
1115 Seman, C., Cole, J., Gettelman, A., Ringer, M. A., Rotstayn, L., Jeffrey, S., Wu, T., Brient, F., Dufresne,

1116 J.-L., Kawai, H., Koshiro, T., Watanabe, M., L'Écuyer, T. S., Volodin, E. M., Iversen, T., Drange, H.,
1117 Mesquita, M. D. S., Read, W. G., Waters, J. W., Tian, B., Teixeira, J., and Stephens, G. L.: Evaluation of
1118 cloud and water vapor simulations in CMIP5 climate models using NASA "A-Train" satellite
1119 observations, *J. Geophys. Res.*, 117, D14105, doi:10.1029/2011JD017237, 2012.

1120 Jones, A., Urban, J., Murtagh, D. P., Eriksson, P., Brohede, S., Haley, C., Degenstein, D., Bourassa, A.,
1121 von. Savigny, C., Sonkaew, T., Rozanov, A., Bovensmann, H., and Burrows, J.: Evolution of
1122 stratospheric ozone and water vapour time series studied with satellite measurements, *Atmos. Chem.*
1123 *Phys.*, 9, 6055-6075, doi:10.5194/acp-9-6055-2009, 2009.

1124 Jones, A., Urban, J., Murtagh, D. P., Sanchez, C., Walker, K. A., Livesey, N. J., Froidevaux, L., and
1125 Santee, M. L.: Analysis of HCl and ClO time series in the upper stratosphere using satellite data sets,
1126 *Atmos. Chem. Phys.*, 11, 5321-5333, doi:10.5194/acp-11-5321-2011, 2011.

1127 Kirgis, G., Leblanc, T., McDermid, I. S., and Walsh, T. D.: Stratospheric ozone interannual variability
1128 (1995–2011) as observed by Lidar and Satellite at Mauna Loa Observatory, HI and Table Mountain
1129 Facility, CA, *Atmos. Chem. Phys.*, 13, 5033–5047, doi:10.5194/acp-13-5033-2013, 2013.

1130

1131 Kley, D., Stone, E. J., Henderson, W. R., Drummond, J. W., Harrop, W. J., Schmeltekopf, A. L.,
1132 Thompson, T. L., and Winkler, R. H.: In Situ Measurements of the Mixing Ratio of Water Vapor in the
1133 Stratosphere, *J. Atmos. Sci.*, 36, 2513-2524, 1979.

1134

1135 Kohlhepp, R., Ruhnke, R., Chipperfield, M. P., De Maziere M., Notholt, J., Barthlott, S., Batchelor, R. L.,
1136 Blatherwick, R. D., Blumenstock, T., Coffey, M. T., Demoulin, P., Fast, H., Feng, W., Goldman, A.,
1137 Griffith, D. W. T., Hamann, K., Hannigan, J. W., Hase, F., Jones, N. B., Kagawa, A., Kaiser, I., Kasai, Y.,
1138 Kirner, O., Kouker, W., Lindenmaier, R., Mahieu, E., Mittermeier, R. L., Monge-Sanz, B., Morino, I.,
1139 Murata, I., Nakajima, H., Palm, M., Paton-Walsh, C., Raffalski, U., Reddmann, T., Rettinger, M.,
1140 Rinsland, C. P., Rozanov, E., Schneider, M., Senten, C., Servais, C., Sinnhuber, B.-M., Smale, D., Strong,
1141 K., Sussmann, R., Taylor, J. R., Vanhaelewyn, G., Warneke, T., Whaley, C., Wiehle, M., and Wood, S.
1142 W.: Observed and simulated time evolution of HCl, ClONO₂, and HF total column abundances, *Atmos.*
1143 *Chem. Phys.*, 12, 3527–3557, doi:10.5194/acp-12-3527-2012, 2012.

1144

1145 Kuttippurath, J., Lefevre, F., Pommereau, J.-P., Roscoe, H. K., Goutail, F., Pazmino, A., and Shanklin, J.
1146 D.: Antarctic ozone loss in 1979–2010: first sign of ozone recovery, *Atmos. Chem. Phys.*, 13, 1625–1635,
1147 doi:10.5194/acp-13-1625-2013, 2013.

1148 Kyrölä, E., Laine, M., Sofieva, V., Tamminen, J., Päivärinta, S.-M., Tukiainen, S., Zawodny, J., and
1149 Thomason, L.: Combined SAGE II-GOMOS ozone profile data set for 1984-2011 and trend analysis of
1150 the vertical distribution of ozone, *Atmos. Chem. Phys.*, 13, 10,645-10,658, doi:10.5194/acp-13-10645-
1151 2013, 2013.

1152 Lambert, A., Read, W. G., Livesey, N. J., Santee, M. L., Manney, G. L., Froidevaux, L.,
1153 Wu, D. L., Schwartz, M. J., Pumphrey, H. C., Jimenez, C., Nedoluha, G. E., Cofield, R. E., Cuddy, D. T.,
1154 Daffer, W. H., Drouin, B. J., Fuller, R. A., Jarnot, R. F., Knosp, B. W., Pickett, H. M., Perun, V. S.,
1155 Snyder, W. V., Stek, P. C., Thurstans, R. P., Wagner, P. A., Waters, J. W., Jucks, K. W., Toon, G. C.,
1156 Stachnik, R. A., Bernath, P. F., Boone, C. D., Walker, K. A., Urban, J., Murtagh, D., Elkins, J. W., and
1157 Atlas, E.: Validation of the Aura Microwave Limb Sounder stratospheric water vapour and nitrous oxide
1158 measurements, *J. Geophys. Res.*, 112, D24S36, doi:10.1029/2007JD008724, 2007.

1159 Livesey, N. J., Read, W. J., Froidevaux, L., Waters, J. W., Santee, M. L., Pumphrey, H. C., Wu, D. L.,
1160 Shippony, Z., and Jarnot, R. F.: The UARS Microwave Limb Sounder version 5 dataset: Theory,
1161 characterization and validation, *J. Geophys. Res.*, 108 (D13), 4378, doi:10.1029/2002JD002273, 2003.

1162 Livesey, N. J., Read, W. G., Froidevaux, L., Lambert, A., Manney, G. L., Pumphrey, H. C., Santee, M.
1163 L., Schwartz, M. J., Wang, S., Cofield, R. E., Cuddy, D. T., Fuller, R. A., Jarnot, R. F., Jiang, J. H.,
1164 Knosp, B. W., Stek, P. C., Wagner, P. A., and Wu, D. L.: EOS MLS Version 3.3/3.4 Level 2 data quality
1165 and description document, Tech. rep., Jet Propulsion Laboratory, available from <http://mls.jpl.nasa.gov/>,
1166 2013.

1167 Mahieu, E., Duchatelet, P., Demoulin, P., Walker, K. A., Dupuy, E., Froidevaux, L., Randall, C., Catoire,
1168 V., Strong, K., Boone, C. D., Bernath, P. F., Blavier, J.-F., Blumenstock, T., Coffey, M., DeMaziere, M.,
1169 Griffith, D., Hannigan, J., Hase, F., Jones, N., Jucks, K. W., Kagawa, A., Kasai, Y., Mebarki, Y.,
1170 Mikuteit, S., Nassar, R., Notholt, J., Rinsland, C. P., Robert, C., Schrems, O., Senten, C., Smale, D.,
1171 Taylor, J., Tetard, C., Toon, G. C., Warneke, T., Wood, S. W., Zander, R., and Servais, C.: Validation of
1172 ACE-FTS v2.2 measurements of HCl, HF, CCl₃F and CCl₂F₂ using space-, balloon- and ground-based
1173 instrument observations, *Atmos. Chem. Phys.*, 8, 6199-6221, doi:10.5194/acp-8-6199-2008, 2008.

1174 Mahieu, E., Zander, R., Bernath, P. F., Boone, C. D., and Walker, K. A.: Recent trend anomaly of
1175 hydrogen chloride (HCl) at northern mid-latitudes derived from Jungfraujoch, HALOE, and ACE-FTS
1176 infrared solar observations, in: *The Atmospheric Chemistry Experiment ACE at 10: a solar occultation*
1177 *anthology*, Bernath, P. (Ed.), Deepak Publishing, Hampton, VA, 239-249, 2013.

1178 Mahieu, E., Chipperfield, M. P., Notholt, J., Anderson, J., Bernath, P. F., Blumenstock, T., Coffey, M. T.,
1179 Dhomse, S., Feng, W., Franco, B., Froidevaux, L., Griffith, D. W. T., Hannigan, J., Hase, F., Hossaini, R.,
1180 Jones, N. B., Morino, I., Murata, I., Nakajima, H., Palm, M., Paton-Walsh, C., Reddman, T.,
1181 Russell III, J. M., Schneider, M., Servais, C., Smale, D., and Walker, K. A.: Increase in northern
1182 stratospheric hydrogen chloride over recent years, submitted, 2014.

1183 McCormick, M. P., Zawodny, J. M., Veiga, R. E., Larsen, J. C., and Wang, P. H.: An overview of SAGE-
1184 I and II ozone measurements, *Planetary and Space Science*, 37, No. 12, 1567-1586, 1989.

1185 McHugh, M., Hervig, M., Magill, B., Thompson, R. E., Remsberg, E., Wrotny, J., and
1186 Russell, J. M.: Improved mesospheric temperature, water vapor, and polar mesospheric cloud extinctions
1187 from HALOE, *Geophys. Res. Lett.*, 30, 8, doi: 10.1029/2002GL016859, 2003.

1188 McLinden, C. A., Tegtmeier, S., and Fioletov, V.: Technical Note: A SAGE-corrected SBUV zonal-mean
1189 ozone data set, *Atmos. Chem. Phys.*, 9, 7963–7972, doi:10.5194/acp-9-7963-2009, 2009.

1190 McPeters, R. D., Bhartia, P. K., Haffner, D., Labow, G. J. and Flynn, L.: The v8.6 SBUV Ozone Data
1191 Record: An Overview, *J. Geophys. Res.*, 118, 8032-8039, doi:10.1002/jgrd.50597, 2013.

1192 Molina, M. J., and Rowland, F. S.: Stratospheric sink for chlorofluoromethane: chlorine atom-catalyzed
1193 destruction of ozone, *Nature*, 249, 810-812, 1974.

1194 Montzka, S. A., Butler, J. H., Elkins, J. W., Thompson, T. M., Clarke, A. D., and Lock, L. T.: Present
1195 and future trends in the atmospheric burden of ozone-depleting halogens, *Nature*, 398, 690-694, 1999.

1196 Morris, G. A., Gleason, J. F., Russell III, J. M., Schoeberl, M. R., and McCormick, M. P.: A comparison
1197 of HALOE V19 with SAGE II V6.00 ozone observations using trajectory mapping, *J. Geophys. Res.*,
1198 107, D13, 4177, doi:10.1029/2001JD000847, 2002.

1199 Mote, P. W., Rosenlof, K. H., McIntyre, M. E., Carr, E. S., Gille, J. C., Holton, J. R., Kinnersley, J. S.,
1200 Pumphrey, H. C., Russell III, J. M., and Waters, J. W.: An atmospheric tape recorder: The imprint of
1201 tropical tropopause temperatures on stratospheric water vapor,
1202 *J. Geophys. Res.*, 101, 3989–4006, 1996.

1203 Nair, P. J., Godin-Beekmann, S., Froidevaux, L., Flynn, L. E., Zawodny, J. M., Russell III, J. M.,
1204 Pazmino, A., Ancellet, G., Steinbrecht, W., Claude, H., Leblanc, T., McDermid, S., van Gijssel, J. A. E.,
1205 Johnson, B., Thomas, A., Hubert, D., Lambert, J.-C., Nakane, H., and Swart, D. P. J.: Relative drifts and
1206 stability of satellite and ground-based stratospheric ozone profiles at NDACC lidar stations, *Atmos.*
1207 *Meas. Tech.*, 5, 1301–1318, doi: 10.5194/amt-5-1301-2012, 2012.

1208 Nair, P. J., Godin-Beekmann, S., Kuttippurath, J., Ancellet, G., Goutail, F., Pazmiño, A., Froidevaux, L.,
1209 Zawodny, J. M., Evans, R. D., Wang, H.-J., Anderson, A., and Pastel, M.: Ozone trends derived from the
1210 total column and vertical profiles at a northern mid-latitude station, *Atmos. Chem. Phys.*, 13, 10373–
1211 10384, doi:10.5194/acp-13-10373-2013, 2013.

1212

1213 Nair, P. J., Froidevaux, L., Kuttippurath, J., Zawodny, J. M., Russell III, J. M., Steinbrecht, W., Claude,
1214 H., Leblanc, T., van Gijssel, J. A. E., Johnson, B., Swart, D. P. J., Thomas, A., Querel, R., Wang, R., and
1215 Anderson, J.: Subtropical and mid-latitude ozone trends in the stratosphere: implications for recovery, *J.*
1216 *Geophys. Res.*, in press, 2015.

1217 Nazaryan, H., McCormick, M. P., and Russell III, J. M.: New studies of SAGE II and HALOE ozone
1218 profile and long-term change comparisons, *J. Geophys. Res.*, 110, D09305, doi:10.1029/2004JD005425,
1219 2005.

1220 Nedoluha, G. E., Gomez, R. M., Hicks, B. C., Bevilacqua, R. M., Russell III, J. M.,
1221 Connor, B. J., and Lambert, A.: A comparison of middle atmospheric water vapor as measured by
1222 WVMS, EOS-MLS, and HALOE, *J. Geophys. Res.*, 112, D24S39, doi:10.1029/2007JD008757, 2007.

1223

1224 Nedoluha, G. E., Gomez, R. M., Hicks, B. C., Wrotny, J. E., Boone, C., and Lambert, A.: Water vapor
1225 measurements in the mesosphere from Mauna Loa over solar cycle 23, *J. Geophys. Res.*, 114, D23303,
1226 doi:10.1029/2009JD012504, 2009.

1227

1228 Nedoluha, G., Gomez, R. M., Hicks, B. C., Helmboldt, J., Bevilacqua, R. M., and Lambert, A.: Ground-
1229 based microwave measurements of water vapor from the midstratosphere to the mesosphere, *J. Geophys.*
1230 *Res.*, 116, D02309, doi:10.1029/2010JD014728., 2011.

1231

1232 Newchurch, M. J., Yang, E. S., Cunnold, D. M., Reinsel, G. C., Zawodny, J. M., and
1233 Russell III, J. M.: Evidence for slowdown in stratospheric ozone loss: First stage of ozone recovery, *J.*

- 1234 Geophys. Res., 108, D16, doi:10.1029/2003JD003471, 2003.
- 1235 Parrish, A., Boyd, I. S., Nedoluha, G. E., Bhartia, P. K., Frith, S. M., Kramarova, N. A.,
1236 Connor, B. J., Bodeker, G. E., Froidevaux, L., Shiotani, M., and Sakazaki, T.: Diurnal variations of
1237 stratospheric ozone measured by ground-based microwave remote sensing at the Mauna Loa NDACC
1238 site: measurement validation and GEOSCCM model comparison, *Atmos. Chem. Phys.*, 7255-7272,
1239 doi:10.5194/acp-14-7255-2014, 2014.
- 1240 Perliski, L. M., Solomon, S., and London, J.: On the interpretation of seasonal variations of stratospheric
1241 ozone, *Planet. Space Sci.*, 37, 12, 1527-1538, 1989.
- 1242 Pumphrey, H. C.: Validation of a new prototype water vapor retrieval for UARS MLS,
1243 *J. Geophys. Res.*, 104 (D8), 9399–9412, 1999.
- 1244 Pumphrey, H. C., Clark, H. L., and Harwood, R. S.: Lower stratospheric water vapor as measured by
1245 UARS MLS, *Geophys. Res. Lett.*, 27, 1691–1694, 2000.
- 1246 Randel, W. J., Wu, F., Oltmans, S. J., Rosenlof, K., and Nedoluha, G. E.: Interannual changes of
1247 stratospheric water vapor and correlations with tropical tropopause temperatures, *J. Atmos. Sci.*, 61,
1248 2133–2148, 2004.
- 1249
1250 Read, W. G., Lambert, A., Bacmeister, J., Cofield, R. E., Christensen, L. E., Cuddy, D. T., Daffer, W.
1251 H., Drouin, B. J., Fetzer, E., Froidevaux, L., Fuller, R., Herman, R., Jarnot, R. F., Jiang, J. H., Jiang, Y.
1252 B., Kelly, K., Knosp, B. W., Kovalenko, L. J., Livesey, N. J., Liu, H.-C., Manney, G. L., Pickett, H. M.,
1253 Pumphrey, H. C., Rosenlof, K. H., Sabouchi, X., Santee, M. L., Schwartz, M. J., Snyder, W. V., Stek, P.
1254 C., Su, H., Takacs, L. L., Thurstans, R. P., Voemel, H., Wagner, P. A., Waters, J. W., Webster, C. R.,
1255 Weinstock, E. M., and Wu, D. L.: Aura Microwave Limb Sounder upper tropospheric and lower
1256 stratospheric H₂O and relative humidity with respect to ice validation, *J. Geophys. Res.*, 112, D24S35,
1257 doi:10.1029/2007JD008752, 2007.
- 1258
1259 Read, W. G., Schwartz, M. J., Lambert, A., Su, H., Livesey, N. J., Daffer, W. H., and
1260 Booe, C. D.: The roles of convection, extratropical mixing, and in-situ freeze-drying in the Tropical
1261 Tropopause Layer, *Atmos. Chem. Phys.*, 8, 6051–6067, doi:10.5194/acp-8-6051-2008, 2008.
- 1262
1263 Remsberg, E.: Observed seasonal to decadal scale responses in mesospheric water vapor,
1264 *J. Geophys. Res.*, 115, D06306, doi:10.1029/2009JD012904, 2010.

1265
1266 Ricaud, P., de La Noë, J., Connor, B. J., Froidevaux, L., Waters, J. W., Harwood, R. S., MacKenzie, I. A.,
1267 and Peckham, G. E.: Diurnal variability of mesospheric ozone as measured by the UARS microwave limb
1268 sounder instrument: Theoretical and ground-based validations, *J. Geophys. Res.*, 101 (D6), 10,077–
1269 10,089, doi:10.1029/95JD02841, 1996.
1270
1271 Rienecker, M., Suarez, M. J., Gelaro, R., Todling, R., Bacmeister, J., Liu, E., Bosilovich, M. G.,
1272 Schubert, S. D., Takacs, L., Kim, G.-K., Bloom, S., Chen, J., Collins, D., Conaty, A.,
1273 da Silva, A., Gu, W., Joiner, J., Koster, R. D., Lucchesi, R., Molod, A., Owens, T., Pawson, S., Pegion,
1274 P., Redder, C. R., Reichle, R., Robertson, J., F. R., Ruddick, A. G., Sienkiewicz, M., and Woollen, J.:
1275 MERRA: NASA's Modern-Era Retrospective Analysis for Research and Applications, *J. Climate*, 24,
1276 3624–3648, doi:10.1175/JCLI-D-11-00015.1, 2011.
1277
1278 Russell III, J. M., Gordley, L. L., Park, J. H., Drayson, S. R., Hesketh, D. H., Cicerone, R. J., Tuck, A. F.,
1279 Frederick, J. E., Harries, J. E., and Crutzen, P.: The Halogen Occultation Experiment, *J. Geophys. Res.*,
1280 98, 10777-10797, 1993.
1281 Russell III, J. M., Deaver, L. E., Luo, M., Park, J. H., Gordley, L. L., Tuck, A. F., Toon, G. C., Gunson ,
1282 M. R., Traub, W. A., Johnson, D. G., Jucks, K. W., Murcray, D. G., Zander, R.,
1283 Nolt, I. G., and Webster, C. R.: Validation of hydrogen chloride measurements made by the Halogen
1284 Occultation Experiment from the UARS platform, *J. Geophys. Res.*, 101 (D6), 10,151– 10,162, 1996.
1285 Sakazaki, T., Fujiwara, M., Mitsuda, C., Imai, K., Manago, N., Naito, Y., Nakamura, T., Akiyoshi, H.,
1286 Kinnison, D., Sano, T., Suzuki, M., and Shiotani, M.: Diurnal ozone variations in the stratosphere
1287 revealed in observations from the Superconducting Submillimeter-Wave Lime-Emission Sounder
1288 (SMILES) on board the International Space Station (ISS), *J. Geophys. Res. Atmos.*, 118, 2991-3006,
1289 doi:10.1002/jgrd.50220, 2013.
1290 Santee, M. L., Lambert, A., Read, W. G., Livesey, N. J., Cofield, R. E., Cuddy, D. T.,
1291 Daffer, W. H., Drouin, B. J., Froidevaux, L., Fuller, R. A., Jarnot, R. F., Knosp, B. W.,
1292 Manney, G. L., Perun, V. S., Snyder, W. V., Stek, P. C., Thurstans, R. P., Wagner, P. A.,
1293 Waters, J. W., Muscari, G., de Zafra, R. L., Dibb, J. E., Fahey, D. W., Popp, P. J., Marcy, T. P., Jucks, K.
1294 W., Toon, G. C., Stachnik, R. A., Bernath, P. F., Boone, C. D., Walker, K. A.,
1295

- 1296 Urban, J., and Murtagh, D.: Validation of the Aura Microwave Limb Sounder HNO₃ measurements, *J.*
1297 *Geophys. Res.*, 112, D24S40, doi:10.1029/2007JD008, 2007.
- 1298 Salby, M., Titova, E., and Deschamps, L.: Rebound of Antarctic ozone, *Geophys. Res. Lett.*, 38, L09702,
1299 doi:10.1029/2011GL047266, 2011.
- 1300 Salby, M. L., Titova, E. A., and Deschamps, L.: Changes of the Antarctic ozone hole: Controlling
1301 mechanisms, seasonal predictability, and evolution, *J. Geophys. Res.*, 117, D10111,
1302 doi:10.1029/2011JD016285, 2012.
- 1303 Schwartz, M. J., Froidevaux, L., Fuller, R. A., and Pawson, S.: GOZCARDS Merged Data for
1304 Temperature Monthly Zonal Means on a Geodetic Latitude and Pressure Grid, version 1.01, Greenbelt,
1305 MD, USA: NASA Goddard Earth Science Data and Information Services Center, accessible from
1306 doi:10.5067/MEASURES/GOZCARDS/DATA3023, 2013.
- 1307 Shepherd, T. G., Plummer, D. A., Scinocca, J. F., Hegglin, M. I., Fioletov, V. E., Reader, M. C., Remsberg,
1308 E., von Clarmann, T., and Wang, H. J.: Reconciliation of halogen-induced ozone loss with the total-
1309 column ozone record, *Nature Geoscience*, 7, 443-449, doi:10.1038/NGEO2155, 2014.
1310
- 1311 Solomon P. M., Barrett, J., Mooney, T., Connor, B., Parrish, A., and Siskind, D. E.: Rise and decline of
1312 active chlorine in the stratosphere, *Geophys. Res. Lett.*, 33, L18807, doi:10.1029/2006GL027029, 2006.
- 1313 Sofieva, V. F., Kalakoski, N., Päivärinta, S.-M., Tamminen, J., Laine, M., and Froidevaux, L.: On
1314 sampling uncertainty of satellite profile ozone measurements, *Atmos. Meas. Tech.*, 7, 1891–1900,
1315 doi:10.5194/amt-7-1891-2014, 2014.
- 1316 Solomon, S.: Stratospheric ozone depletion: A review of concepts and history, *Rev. Geophys.*, 37, 275–
1317 316, doi:10.1029/1999RG900008, 1999.
- 1318 Solomon, S., Rosenlof, K., Portmann, R., Daniel, J., Davis, S., Sanford, T., and Plattner, G.-K.:
1319 Contributions of Stratospheric Water Vapor to Decadal Changes in the Rate of Global Warming, *Science*,
1320 237, 1219-1223, 2010.
- 1321 SPARC: Assessment of Trends in the Vertical Distribution of Ozone, edited by N. Harris, R. Hudson and
1322 C. Phillips, SPARC/IOC/GAW, SPARC Rep. 1, WMO Ozone Res. Monit. Project Rep. 43, 1998.

1323 SPARC WAVAS: Assessment of upper tropospheric and stratospheric water vapour, World Climate
1324 Research Programme, WCRP-113, WMO/TD-No.1043, 261-264, 2000.

1325 Steinbrecht, W., Koehler, U., Claude, H., Weber, M., Burrows, J. P., and van der A, R. J.: Very high
1326 ozone columns at northern mid latitudes in 2010, *Geophys. Res. Lett.*, 38, L06803,
1327 doi:10.1029/2010GL046634, 2011.

1328 Strong, K., Wolff, M. A., Kerzenmacher, T. E., Walker, K. A., Bernath, P. F., Blumenstock, T., Boone,
1329 C., Catoire, V., Coffey, M., De Maziere, M., Demoulin, P., Duchatelet, P., Dupuy, E., Hannigan, J.,
1330 Hopfner, M., Glatthor, N., Griffith, D. W. T., Jin, J. J., Jones, N., Jucks, K., Kuellmann, H., Kuttippurath,
1331 J., Lambert, A., Mahieu, E., McConnell, J. C., Mellqvist, J., Mikuteit, S., Murtagh, D. P., Notholt, J.,
1332 Piccolo, C., Raspollini, P., Ridolfi, M., Robert, C., Schneider, M., Schrems, O., Semeniuk, K., Senten, C.,
1333 Stiller, G. P., Strandberg, A., Taylor, J., Tetard, C., Toohey, M., Urban, J., Warneke, T., and Wood, S.:
1334 Validation of ACE-FTS N₂O measurements, *Atmos. Chem. Phys.*, 8, 4759-4786, doi:10.5194/acp-8-
1335 4759-2008, 2008.

1336 Tegtmeier, S., Hegglin, M. I., Anderson, J., Bourassa, A., Brohede, S., Degenstein, D., Froidevaux, L.,
1337 Fuller, R., Funke, B., Gille, J., Jones, A., Kasai, Y., Krüger, K., Kyrölä, E., Lingenfelser, G., Lumpe, J.,
1338 Nardi, B., Neu, J., Pendlebury, D., Remsberg, E., Rozanov, A., Smith, L., Toohey, M., Urban, J., von
1339 Clarmann, T., Walker, K. A., and Wang, H. J.: The SPARC Data Initiative: A comparison of ozone
1340 climatologies from international satellite limb sounders, *J. Geophys. Res. Atmos.*, 118, 12,229–12,247,
1341 doi: 10.1002/2013JD019877, 2013.

1342 Toohey, M., Hegglin, M. I., Tegtmeier, S., Anderson, J., Añel, J. A., Bourassa, A., Brohede, S.,
1343 Degenstein, D., Froidevaux, L., Fuller, R., Funke, B., Gille, J., Jones, A., Kasai, Y., Krüger, K., Kyrölä,
1344 E., Neu, J. L., Rozanov, A., Smith, L., Urban, J., von Clarmann, T., Walker, K. A., and Wang, R.:
1345 Characterizing sampling bias in the trace gas climatologies of the SPARC Data Initiative, *J. Geophys.*
1346 *Res. Atmos.*, 118, 11,847–11,862, doi: 10.1002/jgrd.5087, 2013.

1347 Tummon, F., Hassler, B., Harris, N. R. P., Staehelin, J., Steinbrecht, W., Anderson, J.,
1348 Bodeker, G. E., Bourassa, A., Davis, S. M., Degenstein, D., Frith, S. M., Froidevaux, L.,
1349 Kyrölä, E., Laine, M., Long, C., Penckwitt, A. A., Sioris, C. E., Rosenlof, K. H., Roth, C.,
1350 Wang, H.-J., and Wild, J.: Intercomparison of vertically resolved merged satellite ozone data sets:
1351 interannual variability and long-term trends, *Atmos. Chem. Phys.*, 15, 3021-3043, doi: 10.5194/acp-15-
1352 3021-2015, 2015.

1353 Urban, J., Lautié, N., Murtagh, D. P., Eriksson, P., Kasai, Y., Lossow, S., Dupuy, E.,
1354 de LaNoë, J., Frisk, U., Olberg, M., Flochmoën, E. Le., and Ricaud, P.: Global observations of middle
1355 atmospheric water vapour by the Odin satellite: An overview, *Planet. Space Sci.*, 55, 9, 1093-1102, 2007.

1356 Urban, J., Lossow, S., Stiller, G., and Read, W.: Another drop in water vapor, *EOS Transactions,*
1357 *American Geophysical Union*, 95, 27, 245-252, doi:10.1002/2014EO270001, 2014.

1358 Veiga, R.E., Cunnold, D. M., Chu, W. P., and McCormick, M. P.: Stratospheric Aerosol and Gas
1359 Experiments I and II comparisons with ozonesondes. *J. Geophys. Res.*, 100 (D5), 9073-9090, 1995.

1360 Voemel, H., Barnes, J. E., Forno, R. N., Fujiwara, M., Hasebe, F., Iwasaki, S., Kivi, R., Komala, N.,
1361 Kyrölä, E., Leblanc, T., Morel, B., Ogino, S.-Y., Read, W. G., Ryan, S. C., Saraspriya, S., Selkirk, H.,
1362 Shiotani, M., Valverde Canossa, J., and Whiteman, D. N.: Validation of Aura Microwave Limb Sounder
1363 water vapor by balloon-borne Cryogenic Frost point Hygrometer measurements, *J. Geophys. Res.*, 112,
1364 D24S37, doi:10.1029/2007JD008698, 2007.

1365 Wang, H. J., Cunnold, D. M., and Bao, X.: A critical analysis of Stratospheric Aerosol and Gas
1366 Experiment ozone trends *J. Geophys. Res.*, 101 (D7), 12495-12514, 1996.

1367 Wang, H. J., Cunnold, D. M., Thomason, L. W., Zawodny, J. M., and Bodeker, G. E.: Assessment of
1368 SAGE version 6.1 ozone data quality, *J. Geophys. Res.*, 107 (D23),
1369 doi: 10.1029/2002JD002418, 2002.

1370 Wang, H. J., Cunnold, D. M., Trepte, C., Thomason, L. W., and Zawodny, J. M.: SAGE III solar ozone
1371 measurements: Initial results, *Geophys. Res. Lett.*, 33, L03805, doi:10.1029/2005GL025099, 2006.

1372 Wang, R., Froidevaux, L., Anderson, J., Fuller, R. A., Bernath, P. F., McCormick, M. P., Livesey, N. J.,
1373 Russell III, J. M., Walker, K. A., and Zawodny, J. M.: GOZCARDS Merged Data for Ozone Monthly
1374 Zonal Means on a Geodetic Latitude and Pressure Grid, version 1.01, Greenbelt, MD, USA: NASA
1375 Goddard Earth Science Data and Information Services Center, accessible from
1376 doi:10.5067/MEASURES/GOZCARDS/DATA3006, 2013.

1377 Waters, J. W., Microwave limb sounding, in *Atmospheric Remote Sensing by Microwave Radiometry*,
1378 ed. by M. Janssen, chap. 8, John Wiley, New York, 1993.

1379 Waters, J. W., Froidevaux, L., Read, W. G., Manney, G. L., Esilon, L. S., Flower, D. A., Jarnot, R. F., and
1380 Harwood, R. S.: Stratospheric ClO and ozone from the Microwave Limb Sounder on the Upper
1381 Atmosphere Research Satellite, *Nature*, 362, 597-602, 1993.

1382 Waters, J. W., Froidevaux, L., Harwood, R. S., Jarnot, R. F., Pickett, H. M., Read, W. G., Siegel, P. H.,
1383 Cofield, R. E., Filipiak, M. J., Flower, D. A., Holden, J. R., Lau, G. K., Livesey, N. J., Manney, G. L.,
1384 Pumphrey, H. C., Santee, M. L., Wu, D. L., Cuddy, D. T., Lay, R. R., Loo, M. S., Perun, V. S., Schwartz,
1385 M. J., Stek, P. C., Thurstans, R. P., Boyles, M. A., Chandra, S., Chavez, M. C., Chen, G.-S., Chudasama,
1386 B. V., Dodge, R., Fuller, R. A., Girard, M. A., Jiang, J. H., Jiang, Y., Knosp, B. W., LaBelle, R. C., Lam,
1387 J. C., Lee, K. A., Miller, M., Oswald, J. E., Patel, N. C., Pukala, D. M., Quintero, O., Scaff, D. M.,
1388 Snyder, W. V., Tope, M. C., Wagner, P. A., and Walch, M. J.: The Earth Observing System Microwave
1389 Limb Sounder (EOS MLS) on the Aura satellite, *IEEE Trans. Geosci. Remote Sens.*, 44 (5), 1075–1092,
1390 doi:10.1109/TGRS.2006.873771, 2006.

1391 Waugh, D. W., Considine, D. B., and Fleming, E. L.: Is Upper Stratospheric Chlorine Decreasing as
1392 Expected?, *Geophys. Res. Lett.*, 28(7), 1187–1190, 2001.

1393 WMO (World Meteorological Organization): Scientific Assessment of Ozone Depletion: 2002, Global
1394 Ozone Research and Monitoring Project – Report No. 47, Geneva, Switzerland, 2003.

1395 WMO (World Meteorological Organization), Scientific Assessment of Ozone Depletion: 2010, Global
1396 Ozone Research and Monitoring Project – Report No. 52, Geneva, Switzerland, 2011.

1397 WMO (World Meteorological Organization), Scientific Assessment of Ozone Depletion: 2014, Global
1398 Ozone Research and Monitoring Project – Report No. 55, Geneva, Switzerland, 2014.

1399 Wohltmann, I., Lehmann, R., Rex, M., Brunner, D., and Mader, J.A.: A process-oriented regression
1400 model for column ozone, *J. Geophys. Res.*, 112, D12304, doi:10.1029/2006JD007573, 2007.

1401 Wolff, M. A., Kerzenmacher, T., Strong, K., Walker, K. A., Toohey, M., Dupuy, E., Bernath, P. F.,
1402 Boone, C. D., Brohede, S., Catoire, V., von Clarmann, T., Coffey, M., Daffer, W. H., De Maziere, M.,
1403 Duchatelet, P., Glatthor, N., Griffith, D. W. T., Hannigan, J., Hase, F., Hopfner, M., Huret, N., Jones, N.,
1404 Jucks, K., Kagawa, A., Kasai, Y., Kramer, I., Kullmann, H., Kuttippurath, J., Mahieu, E., Manney, G.,
1405 McElroy, C. T., McLinden, C., Mebarki, Y., Mikuteit, S., Murtagh, D., Piccolo, C., Raspollini, P.,
1406 Ridolfi, M., Ruhnke, R., Santee, M., Senten, C., Smale, D., Tetard, C., Urban, J., and Wood, S.:
1407 Validation of HNO₃, ClONO₂, and N₂O₅ from the Atmospheric Chemistry Experiment Fourier Transform
1408 Spectrometer (ACE-FTS), *Atmos. Chem. Phys.*, 8, 3529–3562, doi:10.5194/acp-8-3529-2008, 2008.

1409 Yang, E.-S., Cunnold, D. M., Newchurch, M. J., Salawitch, R., McCormick, J. M. P., Russell III, J. M.,
1410 Zawodny, J. M., and Oltmans, S. J.: First stage of Antarctic ozone recovery, *J. Geophys. Res.*, 113,
1411 D20308, doi:10.1029/2007JD009675, 2008.

1412 Ziemke, J. R., and Chandra, S.: Development of a climate record of tropospheric and stratospheric
1413 column ozone from satellite remote sensing: evidence of an early recovery of global stratospheric ozone,
1414 *Atmos. Chem. Phys.*, 12, 5737-5753, doi:10.5194/acp-12-5737-2012, 2012.

1415 Ziemke, J. R., Chandra, S., and Bhartia, P. K.: A 25-year data record of atmospheric ozone from TOMS
1416 Cloud Slicing: Implications for trends in stratospheric and tropospheric ozone, *J. Geophys. Res.*, 110,
1417 D15105, doi:10.1029/2004JD005687, 2005.

1418

1419 **Appendix A**

1420 **A.1. GOZCARDS data provenance**

1421 The general origin of the datasets is summarized here. Data coverage from limb sounders
1422 (including the instruments used here) is displayed nicely in the work by Toohey et al. (2013).

1423 ***SAGE I***

1424 SAGE I was launched February 18, 1979, aboard the Applications Explorer Mission-B
1425 (AEM-B) satellite. SAGE I was a sun photometer using solar occultation (Chu and McCormick,
1426 1979), and it collected a global database for nearly three years on stratospheric aerosol, O₃, and
1427 NO₂. For more information, the reader is referred to <http://sage.nasa.gov/SAGE1>.

1428 ***SAGE II***

1429 SAGE II was launched aboard the Earth Radiation Budget Satellite (ERBS) in October 1984
1430 and its data gathering period ended in August 2005. During each sunrise and sunset, SAGE II
1431 measured stratospheric aerosols, O₃, NO₂, and H₂O via solar occultation. This long dataset has
1432 proven very valuable in determining past ozone trends. For more information on and data access
1433 to the (V6.2) dataset used for GOZCARDS, the reader is referred to <http://sage.nasa.gov/SAGE2>.

1434 ***HALOE***

1435 Since its launch on September 12, 1991 from the Space Shuttle Discovery until November
1436 2005, UARS HALOE collected profiles of atmospheric composition and temperature. HALOE
1437 (Russell et al., 1993) used solar occultation to measure vertical profiles of O₃, HCl, HF, CH₄,
1438 H₂O, NO, NO₂, temperature, aerosol extinction, and aerosol composition and size distribution.
1439 More information and access to the HALOE data can be obtained from <http://haloe.gats-inc.com>
1440 and <http://disc.sci.gsfc.nasa.gov/UARS/data-holdings/HALOE>. For GOZCARDS purposes, we
1441 have used Version 19 HALOE netCDF data files available at <http://haloe.gats-inc.com>.

1442 ***UARS MLS***

1443 This instrument observed the Earth's limb in microwave emission using three radiometers, at
1444 frequencies near 63, 183 and 205 GHz (Waters, 1993; Barath et al., 1993), providing unique

1445 daily global information on stratospheric ClO, along with other profiles, including O₃, H₂O,
1446 HNO₃, temperature, and cloud ice water content. The stratospheric H₂O data ceased on April 15,
1447 1993, after the failure of the 183 GHz radiometer. After March 15, 1994, measurements became
1448 increasingly sparse in order to conserve the life of the MLS antenna scan mechanism and UARS
1449 power. Data exist until July 28, 1999, although for GOZCARDS, only data through mid-June
1450 1997 are used, as data sparseness and degradation of the 63 GHz radiometer led to less ‘trend-
1451 quality’ data after this. Sampling patterns follow the alternating yaw cycles imposed on MLS by
1452 the precessing UARS orbit; MLS measurements were obtained continuously for all latitudes
1453 between 34°S and 34°N, with higher latitudes covered in either the northern or southern
1454 hemisphere with a roughly 36-day cycle. Livesey et al. (2003) provide more information on the
1455 UARS MLS instrument, retrievals, and results. For data access, the reader is directed to the
1456 relevant Goddard Earth Sciences and Information Services Center (GES DISC) data holdings at
1457 <http://disc.sci.gsfc.nasa.gov/UARS/data-holdings/MLS>. L3AT data files were used as the basis
1458 for the production of the GOZCARDS UARS MLS monthly source datasets.

1459 *ACE-FTS*

1460 ACE-FTS is the primary instrument onboard the SCISAT satellite, launched on August 12, 2003.
1461 It is a high spectral resolution (0.02 cm⁻¹) Michelson interferometer operating from 2.2 to
1462 13.3 μm (750-4400 cm⁻¹); see Bernath et al. (2005) for an overview of the ACE mission. The
1463 instrument can simultaneously measure temperature and many trace gases (including all the
1464 species mentioned here for GOZCARDS), thin clouds, and aerosols, using the solar occultation
1465 technique. ACE-FTS data version 2.2, along with the version 2.2 update for ozone, were used
1466 here for GOZCARDS. For access to the public ACE-FTS datasets, with a routine measurement
1467 start date of March 2004, the reader is directed to <http://www.ace.uwaterloo.ca>.

1468 *Aura MLS*

1469 MLS is one of four instruments on NASA's Aura satellite, launched on July 15th 2004. Aura
1470 MLS is a greatly enhanced version of the UARS MLS experiment, providing better spatial
1471 coverage, vertical resolution, and vertical range, along with more continuous data over its
1472 lifetime (and with ongoing measurements at the time of writing). The instrument includes

1473 radiometers at 118, 190, 240, and 640 GHz, and a 2.5 THz module (Waters et al., 2006). Aura
 1474 MLS provides measurements of many chemical species, cloud ice, temperature and geopotential
 1475 height. Continuous measurements have been obtained since August 2004, with the exception of
 1476 OH, for which sparser measurements exist since August 2010, in order to preserve the life of the
 1477 THz module. For more information and access to the Aura MLS datasets, the reader is referred to
 1478 <http://disc.sci.gsfc.nasa.gov/Aura/data-holdings/MLS>. For GOZCARDS, we use the currently
 1479 recommended Aura MLS data versions (version 2.2/2.3 for ozone and 3.3/3.4 for other species).

1480 **A.2. Calculation details for the iterative merging procedure**

1481 Given three time series, the merging procedure that we use first combines two out of the three
 1482 time series, $y_1(i)$ and $y_2(i)$ (where index i represents time for each monthly mean value in a given
 1483 latitude/pressure bin). We first obtain the temporary merged series $m_1(i)$ via:
 1484
$$m_1(i) = (1/2) (y_1(i) + y_2(i)) \quad (1)$$

1485 with the average offsets for $y_1(i)$ and $y_2(i)$ being $(1/(2 n_{12})) \sum (y_1(i) - y_2(i))$ and -1 times this value,
 1486 respectively; n_{12} is the number of overlapping data points between the two time series. Then, we
 1487 merge together the time series $m_1(i)$ and $y_3(i)$, keeping the weightings equal for all 3 time series
 1488 (1/3 for each), so that we calculate the new merged time series $m(i)$ via:

$$1489 \quad m(i) = w_m m_1(i) + w_3 y_3(i) = (1/3) (y_1(i) + y_2(i) + y_3(i)) \quad (2)$$

1490 which will hold if the weights are $w_m = 2/3$ and $w_3 = 1/3$ (given equation (1) for $m_1(i)$). The
 1491 average reference value (to which the adjustments of $m_1(i)$ and $y_3(i)$ in the 2nd step are made) is
 1492 given by $(1/n_m) \sum ((2/3) m_1(i) + (1/3) y_3(i))$, where n_m represents the number of (overlapping
 1493 pairs of) data values used in step 2. For the HCl and H₂O data merging procedure, we always use
 1494 the Aura MLS time series as one of the first two series involved in the initial merging step, for
 1495 example as $y_1(i)$, in order to maximize the overlap between the first two series and obtain more
 1496 robust offset values. Then, we use the 3rd time series; the order used for HALOE and ACE-FTS
 1497 (i.e., whether we use HALOE or ACE-FTS for y_2 or y_3) makes very little difference.

1498 **Calculation of the standard deviation for the merged data values**

1499 The average and standard deviation (square root of variance) for each y_k value (i.e. for each
 1500 monthly zonal mean in a particular lat/p bin) are calculated from equations (3) and (4) below:

1501
$$\bar{y}_k = \frac{1}{n_{yk}} \sum_j y_{kj} \quad (3)$$

1502 and, for the variance,

1503
$$\sigma_{yk}^2 = \frac{1}{n_{yk} - 1} \sum_j (y_{kj} - \bar{y}_k)^2 \quad (4)$$

1504 where index “ j ” corresponds to individual data values within a month, index k represents a given
 1505 instrument (data source), and n is the total number of data values for a given bin and source
 1506 (instrument) time series point in time (or month). Each value \bar{y}_k above is a monthly average
 1507 (although we also use instead the simpler notation y_k), with standard deviation about the mean
 1508 σ_{yk} . Now, given the merged series $u(i)$ (where index i runs over a large number of months), the
 1509 standard deviation of each merged data point (for a given month) can be obtained by considering
 1510 the original datasets y_{kj} that were used to construct u . Specifically, we have the variance for the
 1511 merged dataset

1512
$$\sigma_u^2 = \frac{1}{n_u - 1} \sum_j (u_j - u_{ref})^2 \quad (5)$$

1513 where u_{ref} is the merged value (which is not necessarily chosen to be the average value \bar{u}) and
 1514 the u_j values represent the union of adjusted data values that make up the merged product, with
 1515 the index j for this combined dataset covering all values (up to the total n_u) obtained from the
 1516 original source values y_{kj} . In practice, we do not keep track of the individual data values that
 1517 went into making the averages for the series y_k that are being merged, and we need to obtain σ_u
 1518 based solely on the values \bar{y}_k , σ_{yk} , and the original number of points for each dataset y_k ,
 1519 namely n_{yk} . If we consider all the original values, we have a combined dataset with n_u points,
 1520 such that $n_u = \sum_k n_{yk}$. Now, expanding equation (5), we get

1521
$$(n_u - 1) \sigma_u^2 = \sum_j (u_j^2 + u_{ref}^2 - 2u_{ref} u_j) \quad (6)$$

1522 or

1523 $(n_u - 1) \sigma_u^2 = \sum_j u_j^2 + n_u u_{ref}^2 - 2u_{ref} \sum_j u_j$ (7)

1524 Expanding (4) for each individual dataset y_k , we get

1525 $(n_{yk} - 1) \sigma_{yk}^2 = \sum_j y_{kj}^2 + \bar{y}_k^2 - 2\bar{y}_k \sum_j y_{kj}$ (8)

1526 which leads to

1527 $\sum_j u_j^2 = \sum_{k,j} y_{kj}^2 = \sum_k (n_{yk} - 1) \sigma_{yk}^2 + \sum_k n_{yk} \bar{y}_k^2$, (9)

1528 so that extracting the variance from equation (7) now leads to

1529 $\sigma_u^2 = \frac{1}{(n_u - 1)} \left(\sum_k (n_{yk} - 1) \sigma_{yk}^2 + \sum_k n_{yk} \bar{y}_k^2 + n_u u_{ref}^2 - 2u_{ref} \sum_k n_{yk} \bar{y}_k \right)$ (10)

1530 The adjusted time series are obtained from the original series y_k as Y_k , and we can write

1531 Equation (4) in the same manner for the Y_k data values, namely

1532 $\sigma_{Yk}^2 = \frac{1}{n_{yk} - 1} \sum_j (Y_{kj} - \bar{Y}_k)^2$ (11)

1533 with $\sigma_{Yk} = \sigma_{yk}$ as the adjustments (offsets) are performed in an additive manner; if these

1534 adjustments were performed using multiplicative factors, those factors would also have to be

1535 considered in a multiplicative way to get the new σ_{Yk} values. We can thus write (10) for the

1536 adjusted datasets as:

1537 $\sigma_u^2 = \frac{1}{(n_u - 1)} \left(\sum_k (n_{yk} - 1) \sigma_{yk}^2 + \sum_k n_{yk} \bar{Y}_k^2 + n_u U_{ref}^2 - 2U_{ref} \sum_k n_{yk} \bar{Y}_k \right)$ (12)

1538 Equation (12) for the standard deviation of the merged dataset simplifies if the original datasets

1539 are adjusted to exactly the same reference value ref ($\bar{Y}_k = ref$) and the merged value U_{ref} is

1540 also equal to that value, as the sum of the last 3 terms in Eq. (10) (with Y_k replacing y_k) then

1541 reduces to $n_u ref^2 + n_u ref^2 - 2n_u ref^2$, which is zero. In this case, one obtains

1542
$$\sigma_u^2 = \frac{1}{(n_u - 1)} \left(\sum_k (n_{yk} - 1) \sigma_{yk}^2 \right) \quad (13)$$

1543 However, in general, one should use equation (12) for the standard deviation of the merged
 1544 dataset, given the adjusted datasets \overline{Y}_k and the merged (or reference) value U_{ref} . Also, we often
 1545 use a merged value equal to the average of the original data (over a given overlap period), so that

1546
$$U_{ref} = \frac{1}{n_y} \sum_k \overline{y}_k \quad (14)$$

1547 where n_y is the total number of datasets (y_k), as opposed to having the merged value place more
 1548 weight on the larger datasets (e.g., for emission-type measurements versus occultation-type), in
 1549 which case one would consider using $U_{ref} = \frac{1}{n_u} \sum_k n_{yk} \overline{y}_k$. For ozone, we use a particular dataset
 1550 (SAGE II ozone) as the primary reference, but equation (12) can be used to obtain the standard
 1551 deviation for the merged dataset (about the SAGE II reference) in that case also. While it is
 1552 useful to have the formalism above for obtaining the merged dataset standard deviation σ_u , we
 1553 often find significant differences between the standard deviations of various datasets, so that this
 1554 effect will have the greatest influence on the results, as opposed to the impact of the last 3 terms
 1555 in the summation (in (12)). Finally, it is easy to test equation (12) (and we have done so) by
 1556 using synthetic series and calculating the standard deviation of the combined set. In reality, the
 1557 standard deviations of the time series monthly mean values are typically larger for MLS than for
 1558 ACE-FTS, mainly because of the more complete sampling of variability from the daily global
 1559 measurements acquired by MLS. Sample plots for standard deviations and standard errors in the
 1560 case of HCl are shown in Fig. A1. As expected, merged standard deviations follow the standard
 1561 deviations from HALOE HCl before Aug. 2004 and those from MLS HCl after this time.
 1562 However, the merged standard errors for the MLS time period follow the smaller MLS standard
 1563 errors, because these values vary inversely with the square root of the number of values sampled,
 1564 and are therefore made smaller by the significantly larger daily and monthly MLS sampling rate
 1565 and coverage.

1566

1567 **A.3. Procedural details for GOZCARDS HCl, H₂O, and O₃**

1568 Data screening procedures for the GOZCARDS source datasets, following previously described
1569 methods, are provided (with references) in Table A1, along with certain species-related specifics.
1570 Other GOZCARDS data characteristics and details are provided below for each species.

1571 **A.3.1. HCl**

- 1572 - The vertical data range for valid HCl merged values is between 0.46 hPa and 147 hPa
1573 (inclusive), as a result of data sparseness or data quality issues outside these ranges.
- 1574 - At 147 hPa, no merged HCl values exist for latitude bins from 35°S to 35°N inclusive,
1575 because of unrealistically large Aura MLS HCl values in this region; also, there is not enough
1576 data at this level to provide a meaningful product from HALOE and ACE-FTS data alone.
- 1577 - Because of occasional small negative merged values during southern hemisphere polar
1578 winter, we did not apply HCl data offsets in the lower stratosphere for the 65°S through 85°S
1579 bins from June through September and for pressures larger than or equal to 15 hPa. For
1580 vertical continuity purposes, we applied this method to all lower stratospheric pressure levels,
1581 although the small negative merged values only occurred in a small fraction of cases.
- 1582 - As Aura MLS and ACE-FTS data exist in the 85°N and 85°S bins, but there are no HALOE
1583 measurements, we simply extended the offsets from the adjacent bins (at 75°N and 75°S) to
1584 these two bins to obtain a merged record after 2004 that exhibits continuity versus latitude.
- 1585 - At 100 hPa, we used HCl offsets from the 5°S bin for the 5°N bin, as there was insufficient
1586 data from the combined data in the latter bin to calculate meaningful offsets. This procedure
1587 seems reasonable, given that the time series in these two adjacent tropical latitude bins
1588 (during years outside the 2004/2005 overlap period) look continuous and stable enough to
1589 justify identical adjustments in both bins and to avoid a data gap in the merged series at 5°N.

1590

1591 **A.3.2. H₂O**

- 1592 - The vertical data range for valid H₂O merged values is between 0.01 hPa and 147 hPa
1593 (inclusive). While H₂O data exist at 147 hPa for low latitudes, more careful work would be
1594 needed to extend the merged data globally in such a region.

- 1595 - Users should keep in mind the PMC-related caveats mentioned in Sect. 4 for summer at high
1596 latitudes in the upper mesosphere, prior to the end of the HALOE dataset (Nov. 2005).
- 1597 - As for HCl, we could not use our standard merging procedure at the two most poleward
1598 latitude bins; we simply extended the offsets from the adjacent bins (at 75°N and 75°S) to
1599 these polar bins to obtain a merged record after 2004 that exhibits continuity versus latitude.
- 1600 - Also as for HCl, at 100 hPa, we used H₂O offsets from the 5°S bin for the 5°N bin, as there
1601 was insufficient data from the combined datasets in the latter bin to calculate meaningful
1602 offsets and merge the datasets. This procedure avoids a data gap in the merged series at 5°N.

1603 **A.3.3. O₃**

- 1604 - The vertical range for valid O₃ merged data is from 0.2 hPa to 215 hPa (inclusive), with the
1605 lower altitude bound varying with latitude; the merged product at 147 and 215 hPa has valid
1606 data only for the 35° to 85° latitude bins, with values mostly larger than ~ 0.1 ppmv. The
1607 upper troposphere is more of a merging challenge, given smaller abundances, more difficult
1608 measurements, and a larger impact from different instrument resolutions. Also, while we
1609 suggest (see main text) that GOZCARDS merged ozone data should not be subject to a large
1610 impact from diurnal variations, the highest altitude region should be treated with caution.
- 1611 - SAGE I monthly mean source data are used for the merged dataset in the tropical bins (25°S
1612 to 25°N) from 1 through 68 hPa only and, at higher latitudes, from 1 through 100 hPa only.
- 1613 - We omitted the use of UARS MLS at 100 hPa for low latitudes (from 25°S to 25°N), as these
1614 monthly values are biased quite high and also exhibit too large a seasonal cycle amplitude, in
1615 comparison to HALOE and SAGE II data; this appears to relate to a UARS MLS artifact.
- 1616 - Since there is no (monthly) overlap between SAGE II and HALOE versus UARS MLS or
1617 Aura MLS in the 85°N and 85°S latitude bins, the same offsets as for 75°N and 75°S
1618 (respectively) are applied for these bins, in order to minimize discontinuities.
- 1619 - Because of discontinuities that appeared in merged O₃ at high latitudes above the stratopause,
1620 particularly in the 75°S bin, we flagged merged values for 75° and 85° (N and S) as bad, for
1621 pressures less than 1 hPa. This issue could be the result of a few bad data points or not
1622 enough data overlap. To minimize artifacts, we left the resolution of this issue for future
1623 investigations; also, the reduced amount of occultation data at these high latitudes makes the

1624 usefulness of a merged product with poorly sampled seasonal changes somewhat marginal
1625 (for certain years at least, the number of monthly values drops significantly at high latitudes).
1626
1627

1628 **Table 1.** Characteristics of instrument datasets used to create GOZCARDS ESDRs (version ev1.01).

Instrument and Data Versions	Platform	Type of measurement	Time period (GOZCARDS source files)	Vertical Resolution (km)	Retrieved quantity and stratospheric vertical grid spacing
SAGE I V5.9_rev O ₃	AEM-2	Solar occultation VIS/UV and near-IR	Feb. 1979 - Nov. 1981	1	Density on altitude grid 1 km spacing
SAGE II V6.2 O ₃	ERBS	Solar occultation VIS/UV and near-IR	Oct. 1984 - Aug. 2005	0.5 - 1	Density on altitude grid 0.5 km spacing
HALOE V19	UARS	Solar occultation mid-IR	Oct. 1991 - Nov. 2005	2.5	Volume Mixing Ratio on pressure grid with 30 levels per decade (LPD) change in p
MLS V5 O ₃ V6 H ₂ O	UARS	Limb emission microwave / sub-mm	Oct. 1991 - June 1997 (May 1993 end for strat. H ₂ O)	H₂O 3 - 4 (strat.) 5 - 12 (mes.) O₃ 3.5 - 5 (strat.) 5 - 8 (mes.)	Volume Mixing Ratio on pressure grid with 6 LPD in stratosphere 6 LPD in stratosphere
ACE-FTS V2.2 (V2.2 update for O ₃)	SCISAT	Solar occultation mid-IR	Mar. 2004 through Sep. 2010 (2009 for O ₃)	3 - 4	Volume Mixing Ratio on 1 km grid spacing (height and p provided)
MLS V3.3 V2.2 O ₃	Aura	Limb emission microwave / sub-mm	Aug. 2004 through 2012	HCl 3 - 5 H₂O 3 - 4 (p > 0.1 hPa) 5 - 9 (0.1-0.01 hPa) O₃ 3	Volume Mixing Ratio on pressure grid with 6 LPD 12 LPD 6 LPD

1630 **Table 2.** Products and instrument source data making up the available GOZCARDS data records.

Merged Products and pressure range	Source Datasets (and years used)
HCl 147 – 0.5 hPa	HALOE (1991-2005), ACE-FTS (2004-2010), Aura MLS (2004 onward) Note: MLS data for p < 10 hPa not used for merged time series
H₂O 147 – 0.01 hPa	HALOE (1991-2005), UARS MLS (1991-1993), ACE-FTS (2004-2010), Aura MLS (2004 onward)
O₃ 215 – 0.2 hPa	SAGE I (1979-1981), SAGE II (1984-2005), HALOE (1991-2005), UARS MLS (1991-1997), ACE-FTS (2004-2009), Aura MLS (2004 onward)
HNO₃ 215 – 1 hPa	ACE-FTS (2004-2010), Aura MLS (2004 onward)
N₂O 100 – 0.5 hPa	ACE-FTS (2004-2010), Aura MLS (2004 onward)
Temperature 1000 – 0.015 hPa	GMAO MERRA (1979 onward)

1631

1632

1633

1634

1635

1636

1637

1638

1639 **Table A1.** Data screening procedures and related references used for the source dataset generation.

Instrument	Data Screening Issue / Method	Reference
SAGE I (O ₃)	Aerosol interference issue: Remove values at altitudes below which the 1 μm extinction > 10 ⁻³ km ⁻¹ .	L. Thomason (personal communication, 2012)
SAGE II (O ₃)	Remove entire profile if any error value exceeds 10% of VMR (for 30 to 50 km altitude); this occurred mainly in 1993 & 1994 ("short events"). Use aerosol extinctions and extinction ratios to remove data affected by clouds or by aerosols (from Mt. Pinatubo). Remove anomalously low values resulting from very small SAGE II transmittances (errors are capped at 300% as a flag). Remove profiles under high beta angle conditions.	Wang et al. (2002) See also Wang et al. (1996)
HALOE	Remove cloud-contaminated values. Also remove profiles that may contain artifacts from faulty trip angle or constant lockdown angle registration. Remove aerosol contamination (O ₃ and HCl).	Hervig and McHugh (1999) haloe.gats-inc.com/user_docs/index.php Bhatt et al. (1999)
UARS MLS	Use screening guidelines based on instrument status, retrieval quality flags, and sign of precision values.	Livesey et al. (2003)
Aura MLS	Use screening guidelines based on instrument status, retrieval quality and convergence flags, and sign of precision values.	Livesey et al. (2013)
ACE-FTS	Remove occultations listed as bad. Remove data when error value > VMR or error value < 10 ⁻⁴ xVMR. Use a data screening procedure (see Sect. 2.1) to identify and remove the largest outliers. V2.2 data after Sep. 2010 (2009 for ozone) are not used because of a data processing issue.	databace.scisat.ca/validation/data_issues.php K. Walker (personal communication, 2012)

1641 **Fig. 1.** Merging procedure illustration for HCl. Top left panel shows the HCl monthly mean source data
1642 during the overlap period (Aug. 2004 - Nov. 2005) for HALOE, ACE-FTS, and Aura MLS. Top right
1643 panel illustrates step 1 in the merging procedure, with the temporary merged data values (orange)
1644 resulting from the adjustment of ACE-FTS and Aura MLS values to the mean reference indicated by the
1645 black dashed line (time mean of co-located ACE-FTS/Aura MLS points). Also, the cyan dashed line is
1646 the mean of the ACE-FTS points and the red dashed line is the mean of MLS points co-located with
1647 ACE-FTS. Middle left panel shows step 2 results, namely the merged values arising from merging
1648 HALOE data with the temporary merged data; the black dashed line is the new average reference value,
1649 obtained from a 2/3 and 1/3 weighting of the dashed orange (mean of orange points co-located with
1650 HALOE) and dashed blue line (mean of HALOE) values, respectively. Middle right panel shows all the
1651 source data and the final merged values during the overlap period. Bottom panel shows the source and
1652 merged time series from 1991 through 2012 after the calculated additive offsets are applied to the whole
1653 source datasets, which are then merged (averaged) together wherever overlap between instruments exists.

1654 **Fig. 2.** Offsets applied to the HCl source datasets (top panels for HALOE, middle panels for ACE-FTS,
1655 bottom panels for Aura MLS) as a function of latitude and pressure. The left column gives offsets in ppbv
1656 and the right column provides offsets as a percent of the zonal average merged mixing ratios during the
1657 overlap period (Aug. 2004 – Nov. 2005) used here to compute the average offsets.

1658 **Fig. 3.** Example of HCl time series analyses for 50°N-60°N and 32 hPa. (a) HCl monthly mean source
1659 data from ACE-FTS and Aura MLS; the MLS dots are filled when there is time overlap with ACE-FTS,
1660 and open if no such overlap exists. Simple linear fits are shown as colored lines for
1661 ACE-FTS and for Aura MLS (orange line for all red dots and red line for filled red dots only).
1662 Correlation coefficient values (R values) for the two time series are provided in the title.
1663 (b) Deseasonalized anomalies for both ACE-FTS and Aura MLS, with corresponding linear fits (and R
1664 values). (c) Difference of deseasonalized anomalies (ACE-FTS minus Aura MLS), with linear fit.

1665 **Fig. 4.** Latitude/pressure contours of time series diagnostics obtained from analyses illustrated in
1666 Fig. 3 for HCl from Aura MLS and ACE-FTS. Top panel: Correlation coefficient for the deseasonalized
1667 time series. Bottom panel: Ratio of the slope of the difference between deseasonalized series over the
1668 error in this slope.

1669 **Fig. 5.** Illustration of GOZCARDS HCl monthly averages with systematic error estimates (grey shading)
1670 at 46 hPa for 30°S-40°S; see text for the meaning of this shaded region. The source data from HALOE,
1671 Aura MLS, and ACE-FTS are shown in different colors (see legend), along with the merged values.

1672 **Fig. 6.** Systematic error estimates for GOZCARDS HCl. One error (left panels) is relevant for values
1673 lower than (below) the merged values, and one (right panels) for values larger than the merged values; the

1674 top panels give the error estimates in ppbv, and the bottom panel errors are expressed as percent of the
1675 average merged values over the relevant time periods (see text). These error bars provide a range within
1676 which 95% of the source data values lie.

1677 **Fig. 7.** Time series of the GOZCARDS monthly-averaged merged HCl abundance for 3 different latitude
1678 bin averages (see color legend in panel (a)) for (a) 0.7 hPa, (b) 10 hPa, (c) 32 hPa, and (d) 68 hPa.

1679 **Fig. 8.** The average rate of change (percent per year) for HCl as a function of pressure for different
1680 latitude bin averages (see legend) for time periods corresponding to the appropriate GOZCARDS HCl
1681 values (see text) in the upper stratosphere (Jan. 1997 - Sep. 2010) and lower stratosphere (Jan. 1997 -
1682 Dec. 2012). Deseasonalized monthly data were used to obtain a long-term trend for these time periods;
1683 two-sigma error bars are shown.

1684 **Fig. 9.** Rates of change for GOZCARDS HCl (connected open circles) are given as a function of latitude
1685 in 10° latitude bins for sliding 6-year periods centered on Jan. 1 of each year (e.g., the 1998 point is an
1686 average for data from 1995 through 2000, and the 2011 point is for data from 2008 through 2013). (a) is
1687 for changes in upper stratospheric HCl at 0.7 hPa and (b) is for the change in the integrated HCl column
1688 between 68 hPa and 10 hPa. The two additional curves in (a) represent the rates of change in the
1689 estimated surface total chlorine from NOAA data (green is for a 6-year time shift, and purple for a 7-year
1690 time shift, to account for transport time to the upper stratosphere); see text for more details. Error bars
1691 indicate twice the standard errors in the means.

1692 **Fig. 10.** Offsets applied to the H₂O source datasets as a function of latitude and pressure, similar to
1693 Fig. 2 for HCl.

1694 **Fig. 11.** Latitude/pressure contours of time series diagnostics for H₂O from Aura MLS and ACE-FTS;
1695 this is similar to Fig. 4 for HCl.

1696 **Fig. 12.** A depiction of the “tape recorder” evolution for tropical water vapor abundances from 147 to
1697 10 hPa for October 1991 through December 2013. This plot was produced from GOZCARDS merged
1698 H₂O time series anomalies (differences from the long-term means) for the average of the 4 tropical bins
1699 covering 20°S to 20°N.

1700 **Fig. 13.** Systematic error estimates for GOZCARDS H₂O (similar to Fig. 6 for HCl).

1701 **Fig. 14.** Variations in stratospheric water vapor from the GOZCARDS H₂O merged data records (1992
1702 through 2013) averaged from (a) 60°S to 60°N and (b) 20°S to 20°N. Monthly average values and annual
1703 averages are shown by thin and thick lines (connecting similarly-colored dots), respectively, for the
1704 pressure levels indicated in the plot legend.

1705 **Fig. 15.** Stratospheric water vapor variability on decadal timescales for 1992 through 2013 for tropical
1706 (20°S-20°N in black) and mid-latitude (20°N-60°N in red and 20°S-60°S in blue) zonal means, based on
1707 the GOZCARDS merged H₂O data record. The variability is expressed here as the difference between
1708 maximum and minimum annual average abundances, from 100 to 1 hPa, in ppmv (left panel) and percent
1709 (right panel).

1710 **Fig. 16.** (a) Variations in upper mesospheric (0.01 hPa) water vapor mixing ratios averaged from 60°S to
1711 60°N for Oct. 1991 through Dec. 2013, based on the GOZCARDS merged H₂O data records. Monthly
1712 average values and annual averages are shown by connected brown dots and connected black dots,
1713 respectively. (b) GOZCARDS merged H₂O annual averages (connected filled symbols) from 60°S to
1714 60°N for 1992 through 2013 at pressure levels between 0.1 and 0.01 hPa. A time series of annually-
1715 averaged Lyman α solar flux values (open circles), scaled to arbitrary units, is also displayed (see text).

1716 **Fig. 17.** Time series of monthly zonal mean O₃ for 10°S - 20°S between 1 hPa and 6.8 hPa (with pressure
1717 values given by "pre") from SAGE I, SAGE II, HALOE, UARS MLS, Aura MLS, and ACE-FTS, all
1718 color-coded following the legend in top left panel.

1719 **Fig. 18.** Schematic diagram describing the creation of the merged GOZCARDS monthly zonal mean
1720 ozone data record from various satellite datasets. Instruments represented in red inside the boxes are used
1721 as a reference. Instruments whose measurements have already been adjusted to a reference are indicated
1722 with a "*" superscript. AMLS refers to Aura MLS and UMLS to UARS MLS. See text for more details.
1723

1724 **Fig. 19.** Offsets applied to the O₃ source datasets, similar to Fig. 2 for HCl.

1725 **Fig. 20.** Latitude/pressure contours of time series diagnostics for O₃ from Aura MLS and ACE-FTS; this
1726 is similar to Fig. 4 for HCl. The correlation coefficients (R values) and slope trend diagnostics are
1727 provided for HALOE versus SAGE II in the top two panels (for 1993-1999 as the trend issue for
1728 converted SAGE II data occurs after mid-2000 and to avoid Pinatubo-related data gaps before 1993) and
1729 for ACE-FTS versus Aura MLS in the bottom two panels (for 2005-2009).

1730 **Fig. 21.** Systematic error estimates for GOZCARDS O₃ (similar to Fig. 6 for HCl).

1731 **Fig. 22.** Near-global (60°S to 60°N) results for average column ozone (total and stratospheric, from
1732 *Ziemke and Chandra, 2012*) compared to GOZCARDS O₃ columns above 68 hPa. Stratospheric columns
1733 are offset to better match the total column values, in order to more easily compare relative variations

1734 versus time; the black dots and red crosses are referenced to the 1980 total column values, while the cyan
1735 curves are referenced to 2007 to better illustrate the fits in the later years.

1736 **Fig. 23.** Time evolution (Aug. 2004 through 2012) versus latitude of GOZCARDS merged N₂O (ppbv) at
1737 (a) 6.8 hPa and (b) 100 hPa.

1738 **Fig. 24.** Sample results display the time evolution of satellite-retrieved HNO₃ (ppbv) for two different
1739 periods, 1992-1997 in (a) and (c) versus 2004-2013 in (b) and (d). Panels (a) and (b) are contour plots at
1740 46 hPa from UARS MLS global data and the merged GOZCARDS global data after 2004, respectively;
1741 (c) and (d) show time series at 32 hPa and for the 40°N-50°N latitude bin, with (a) from UARS MLS data,
1742 and (d) from ACE-FTS, Aura MLS, and the merged combination (between the two source data sets).

1743 **Fig. A1.** Illustration of the standard deviations (in (a)) and standard errors (in (b)) for monthly mean
1744 GOZCARDS HCl (source and merged records) at 46 hPa for 30°S-40°S. Source data from HALOE, Aura
1745 MLS, and ACE-FTS are given by the filled colored dots (see legend); each standard deviation is simply
1746 obtained from the range of values measured during the month. The large open brown circles give standard
1747 deviations for the merged HCl product; this Appendix provides the formulae to calculate these quantities.

1748

1749 **Fig. S1:** Illustration of the latitudinal dependence of the HCl offsets for HALOE, ACE-FTS, and Aura
1750 MLS at two pressure levels (top panel for 0.46 hPa, bottom panel for 46 hPa). Error bars represent twice
1751 the standard error in the derived offsets (based on variability during the overlapping period). Larger
1752 standard error values indicate that there were either fewer points of overlap or larger offset variability
1753 (standard deviations); we found that both of these factors contribute.

1754 **Fig. S2:** Latitude/pressure contours of the fitted mean annual amplitudes (ppbv) from HCl time series for
1755 HALOE, ACE-FTS, and Aura MLS, based on their respective measurement periods (see text).

1756 **Fig. S3:** Time evolution (Oct. 1991 through 2013) versus latitude of GOZCARDS merged HCl (ppbv) at
1757 46 hPa.

1758 **Fig. S4:** HALOE sunrise measurements of H₂O versus the 3.46 μm extinction coefficient for 1992, 1993,
1759 and 1999 at 22 hPa. The green vertical line represents the aerosol extinction value ($5 \times 10^{-4} \text{ km}^{-1}$) used to
1760 screen anomalous HALOE H₂O values. It is apparent that anomalously low H₂O values occurred in 1992
1761 when the 3.46 μm aerosol extinction exceeded about $5 \times 10^{-4} \text{ km}^{-1}$. These artifacts were confined to 1991
1762 and 1992; for these years, and for pressure levels at and below 22 hPa, the corresponding H₂O data values

1763 were excluded. This screening method eliminates about 10% of the global (lower stratospheric)
1764 measurements in 1992.

1765 **Fig. S5:** Merging procedure illustration for H₂O at 5°N and 22hPa. This is similar to Fig. 2 (for HCl), but
1766 an additional step is illustrated for the end of this procedure, whereby stratospheric H₂O data from UARS
1767 MLS are adjusted to the early portion of the merged time series that was obtained after the 2nd step; this
1768 adds more coverage (more brown dots in the bottom panel for 1991-1993).

1769 **Fig. S6:** Latitude/pressure contours of the fitted mean annual amplitudes (ppmv) from H₂O time series for
1770 HALOE, ACE-FTS, and Aura MLS, based on their respective measurement periods.

1771 **Fig. S7:** Time evolution (Oct. 1991 through 2013) versus latitude of GOZCARDS merged H₂O (ppmv) at
1772 3.2 hPa (top panel) and 68 hPa (bottom panel).

1773 **Fig. S8:** Monthly zonal mean ozone differences (%) between SAGE II and (a) HALOE,
1774 (b) UARS MLS (UMLS for short), (c) Aura MLS (AMLS for short), and (d) ACE-FTS during their
1775 respective overlap periods. Differences are expressed (in percent) as $100 \times [(SAGE II - Other) / (Other)]$.
1776 Shaded areas indicate negative values.

1777 **Fig. S9:** Monthly zonal mean temperature differences between NCEP (used by SAGE II) and HALOE
1778 temperatures relative to MERRA for 10°S - 20°S between 1 and 6.8 hPa, per color-coding indicated in
1779 bottom left panel; “pre” represents the pressure value. From 1 to 2.1 hPa, differences between NCEP and
1780 MERRA are generally within $\pm 4K$ before mid-2000. After that time, NCEP temperatures show a sharp
1781 increase and are systematically higher than MERRA values by 5 to 10K. However, this divergence and
1782 trend are not seen in HALOE temperatures. NCEP temperatures between 3.2 and 6.8 hPa are smaller than
1783 MERRA after mid-2000; negative trends (versus MERRA) also occur in the HALOE data at these levels.

1784 **Fig. S10:** Relative trends (K/decade) in zonal mean temperature differences for NCEP – MERRA and
1785 HALOE – MERRA (color-coded as in Fig. S9) in the upper stratosphere. NCEP temperatures show
1786 positive trends versus MERRA of $\sim 2-5$ K/decade between 2.1 and 1 hPa for all latitudes. However,
1787 HALOE temperatures show no significant trends versus MERRA, except at 1.5 hPa in the southern
1788 hemisphere. For pressures between 3.2 and 6.8 hPa, the temperature analyses are not conclusive; although
1789 NCEP values show negative trends of $\sim 2-3$ K/decade versus MERRA, they agree with HALOE.

1790 **Fig. S11:** Mean differences and standard deviations (horizontal bars) between SAGE II and Aura MLS
1791 ozone in three different latitude bins: 20°S to 60°S (left panel), 20°S to 20°N (middle panel), and 20°N to
1792 60°N (right panel). Results based on monthly zonal mean and coincident profiles (see text for coincidence
1793 criteria) during overlap periods are shown in red and blue, respectively. To choose collocated profiles,

1794 coincidence criteria of $\pm 1^\circ$ in latitude and $\pm 8^\circ$ in longitude were used; the time difference criterion was
1795 chosen as 12 hours, but only nighttime measurements from Aura MLS were used.

1796 **Fig. S12:** Latitude/pressure contours of the fitted mean annual amplitudes (ppmv) from O₃ time series for
1797 SAGE II, HALOE, ACE-FTS, and Aura MLS, based on their respective measurement periods.

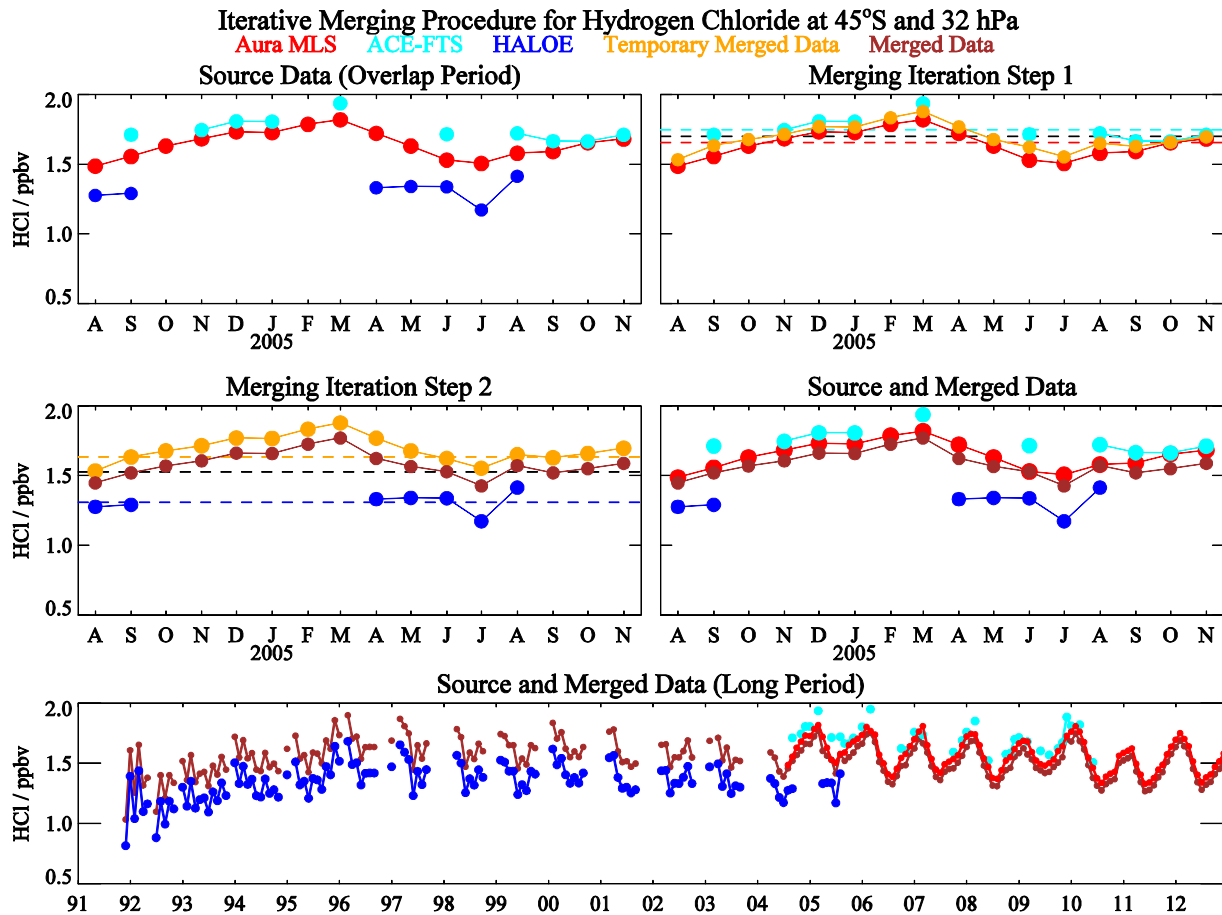
1798 **Fig. S13:** Illustration of the time evolution of the GOZCARDS merged O₃ data field versus latitude at
1799 68 hPa (top panel) and versus pressure for the 40°N-50°N latitude bin (bottom panel).

1800 **Fig. S14:** Offsets applied to the N₂O source datasets (top panels for ACE-FTS, bottom panels for Aura
1801 MLS) as a function of latitude and pressure. The left column gives offsets in ppbv and the right column
1802 provides offsets as a percent of the zonal average merged mixing ratios during the overlap period (Aug.
1803 2004 – Sep. 2010) used here to compute the average offsets.

1804 **Fig. S15:** Latitude/pressure contours of time series diagnostics derived from Aura MLS and ACE-FTS
1805 N₂O data comparisons (and obtained from analyses similar to those illustrated in Fig. 6 for HCl). Top
1806 panel: Correlation coefficient for the deseasonalized time series. Bottom panel: Ratio of the slope of the
1807 difference between deseasonalized series over the error in this slope.

1808 **Fig. S16:** Offsets applied to the HNO₃ source datasets (top panels for ACE-FTS, bottom panels for Aura
1809 MLS) as a function of latitude and pressure. The left column gives offsets in ppbv and the right column
1810 provides offsets as a percent of the zonal average merged mixing ratios during the overlap period (Aug.
1811 2004 – Sep. 2010) used here to compute the average offsets.

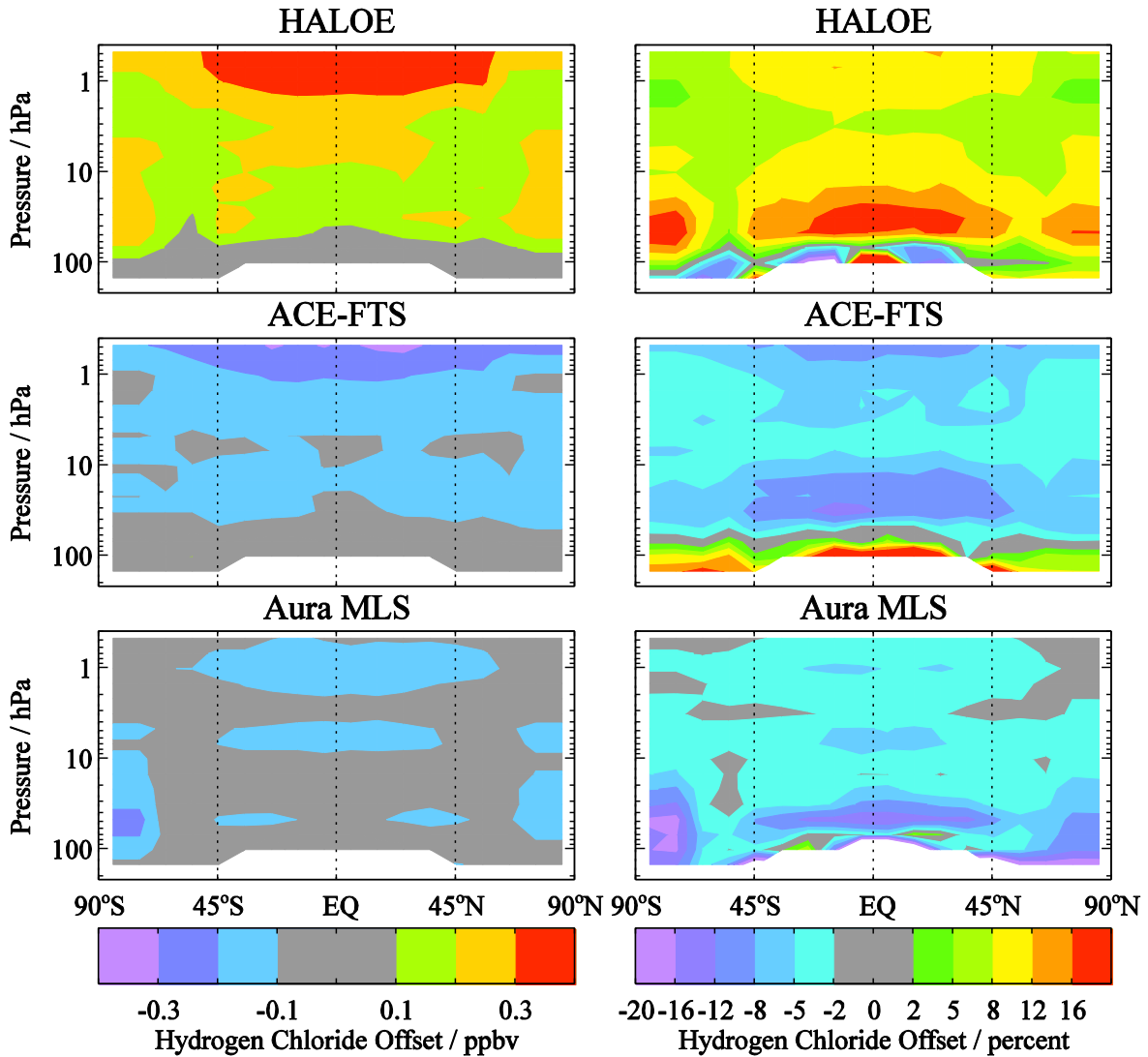
1812 **Fig. S17:** Latitude/pressure contours of time series diagnostics derived from Aura MLS and ACE-FTS
1813 HNO₃ data comparisons (and obtained from analyses similar to those illustrated in Fig. 6 for HCl). Top
1814 panel: Correlation coefficient for the deseasonalized time series. Bottom panel: Ratio of the slope of the
1815 difference between deseasonalized series over the error in this slope.



2

3

4 **Fig. 1.** Merging procedure illustration for HCl. Top left panel shows the HCl monthly mean source data
 5 during the overlap period (Aug. 2004 - Nov. 2005) for HALOE, ACE-FTS, and Aura MLS. Top right
 6 panel illustrates step 1 in the merging procedure, with the temporary merged data values (orange)
 7 resulting from the adjustment of ACE-FTS and Aura MLS values to the mean reference indicated by the
 8 black dashed line (time mean of co-located ACE-FTS/Aura MLS points). Also, the cyan dashed line is
 9 the mean of the ACE-FTS points and the red dashed line is the mean of MLS points co-located with
 10 ACE-FTS. Middle left panel shows step 2 results, namely the merged values arising from merging
 11 HALOE data with the temporary merged data; the black dashed line is the new average reference value,
 12 obtained from a 2/3 and 1/3 weighting of the dashed orange (mean of orange points co-located with
 13 HALOE) and dashed blue line (mean of HALOE) values, respectively. Middle right panel shows all the
 14 source data and the final merged values during the overlap period. Bottom panel shows the source and
 15 merged time series from 1991 through 2012 after the calculated additive offsets are applied to the whole
 16 source datasets, which are then merged (averaged) together wherever overlap between instruments exists.

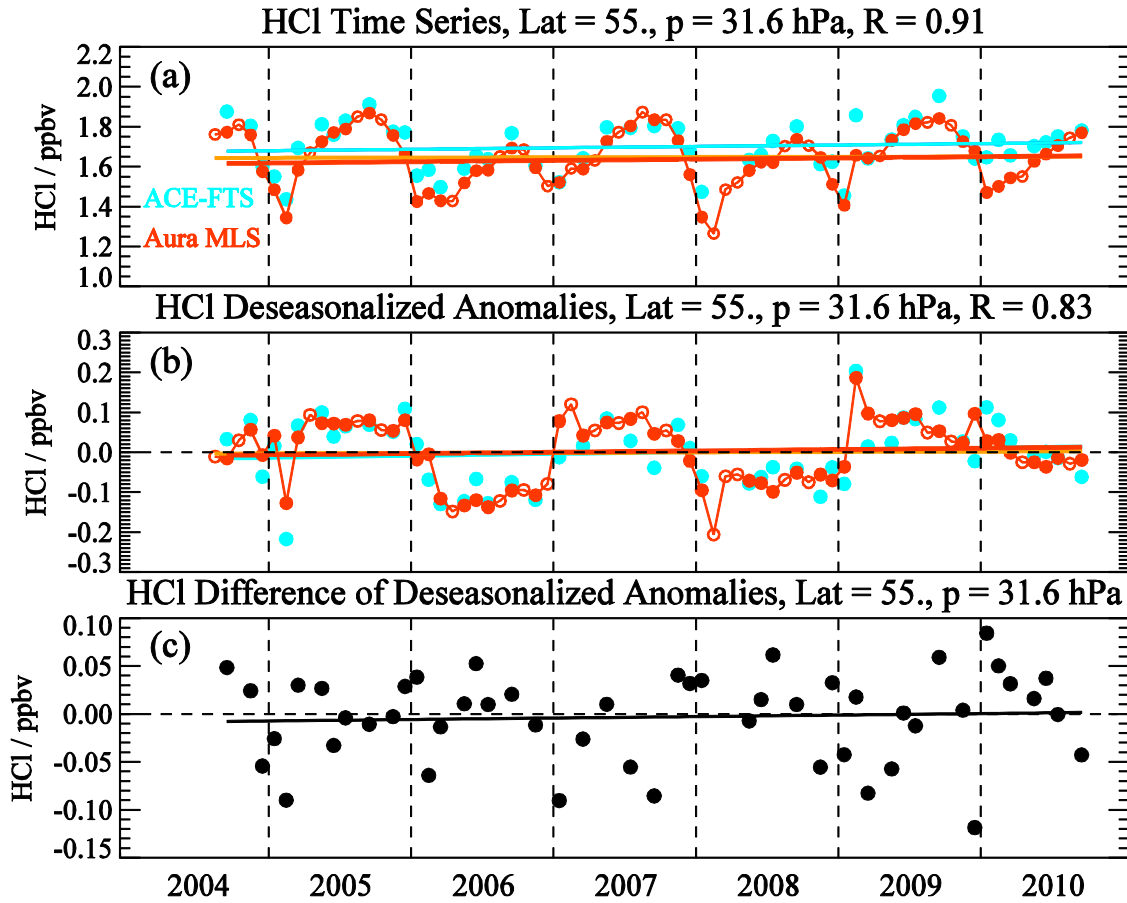


17

18

19 **Fig. 2.** Offsets applied to the HCl source datasets (top panels for HALOE, middle panels for ACE-FTS,
 20 bottom panels for Aura MLS) as a function of latitude and pressure. The left column gives offsets in ppbv
 21 and the right column provides offsets as a percent of the zonal average merged mixing ratios during the
 22 overlap period (Aug. 2004 – Nov. 2005) used here to compute the average offsets.

23



24

25

26

27

28

29

30

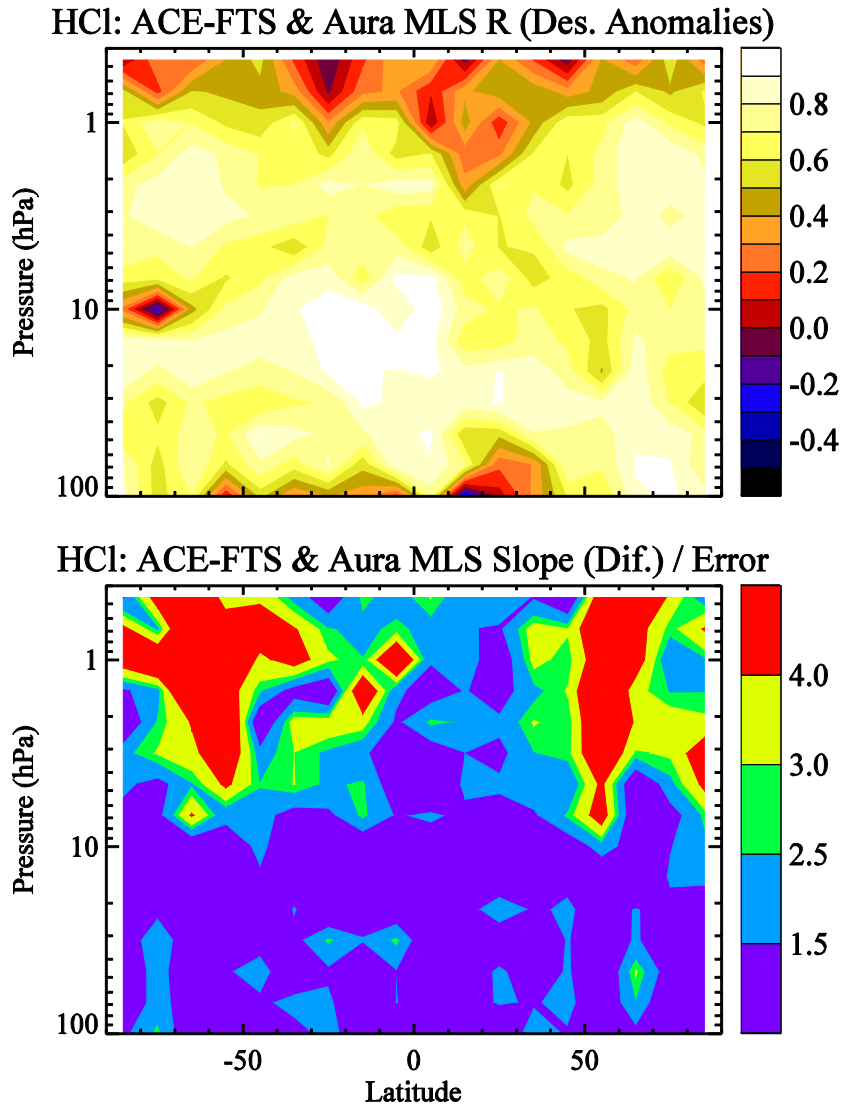
31

32

33

34

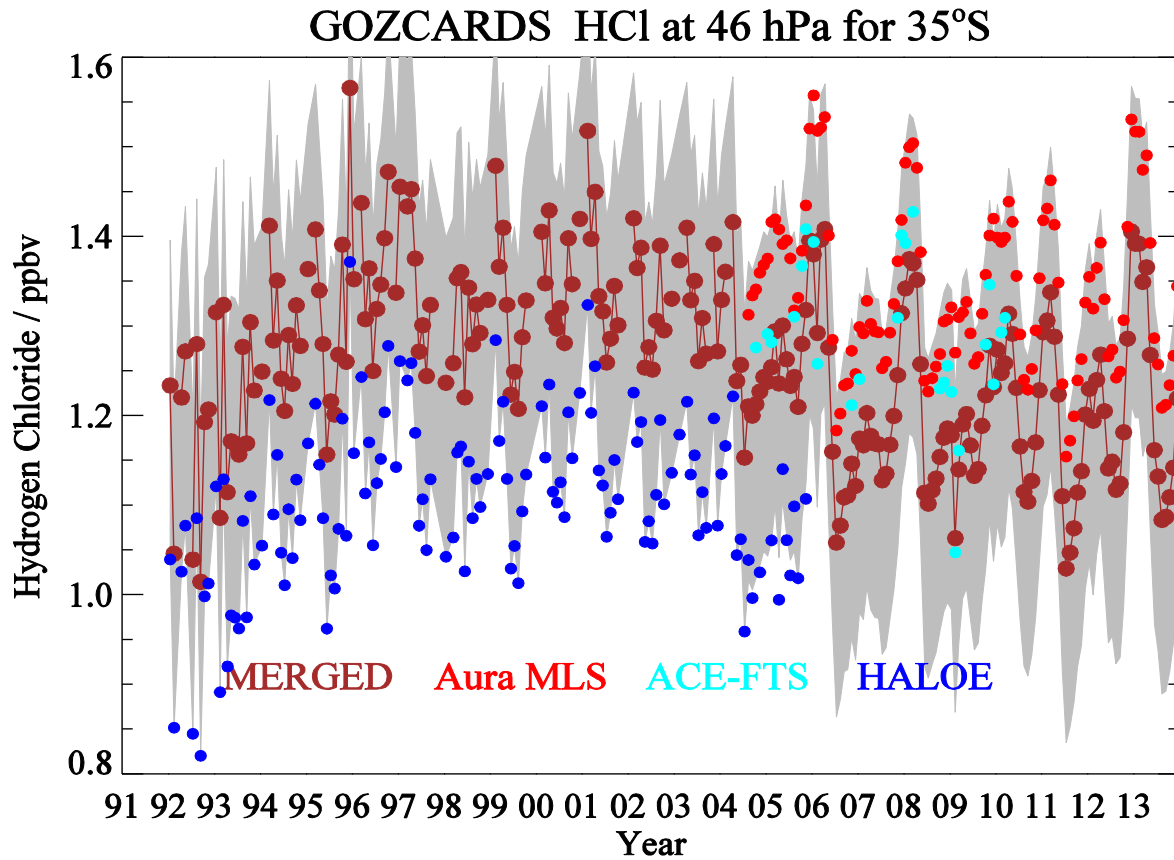
Fig. 3. Example of HCl time series analyses for 50°N-60°N and 32 hPa. (a) HCl monthly mean source data from ACE-FTS and Aura MLS; the MLS dots are filled when there is time overlap with ACE-FTS, and open if no such overlap exists. Simple linear fits are shown as colored lines for ACE-FTS and for Aura MLS (orange line for all red dots and red line for filled red dots only). Correlation coefficient values (R values) for the two time series are provided in the title. (b) Deseasonalized anomalies for both ACE-FTS and Aura MLS, with corresponding linear fits (and R values). (c) Difference of deseasonalized anomalies (ACE-FTS minus Aura MLS), with linear fit.



35
 36 **Fig. 4.** Latitude/pressure contours of time series diagnostics obtained from analyses illustrated in
 37 Fig. 3 for HCl from Aura MLS and ACE-FTS. Top panel: Correlation coefficient for the deseasonalized
 38 time series. Bottom panel: Ratio of the slope of the difference between deseasonalized series over the
 39 error in this slope.

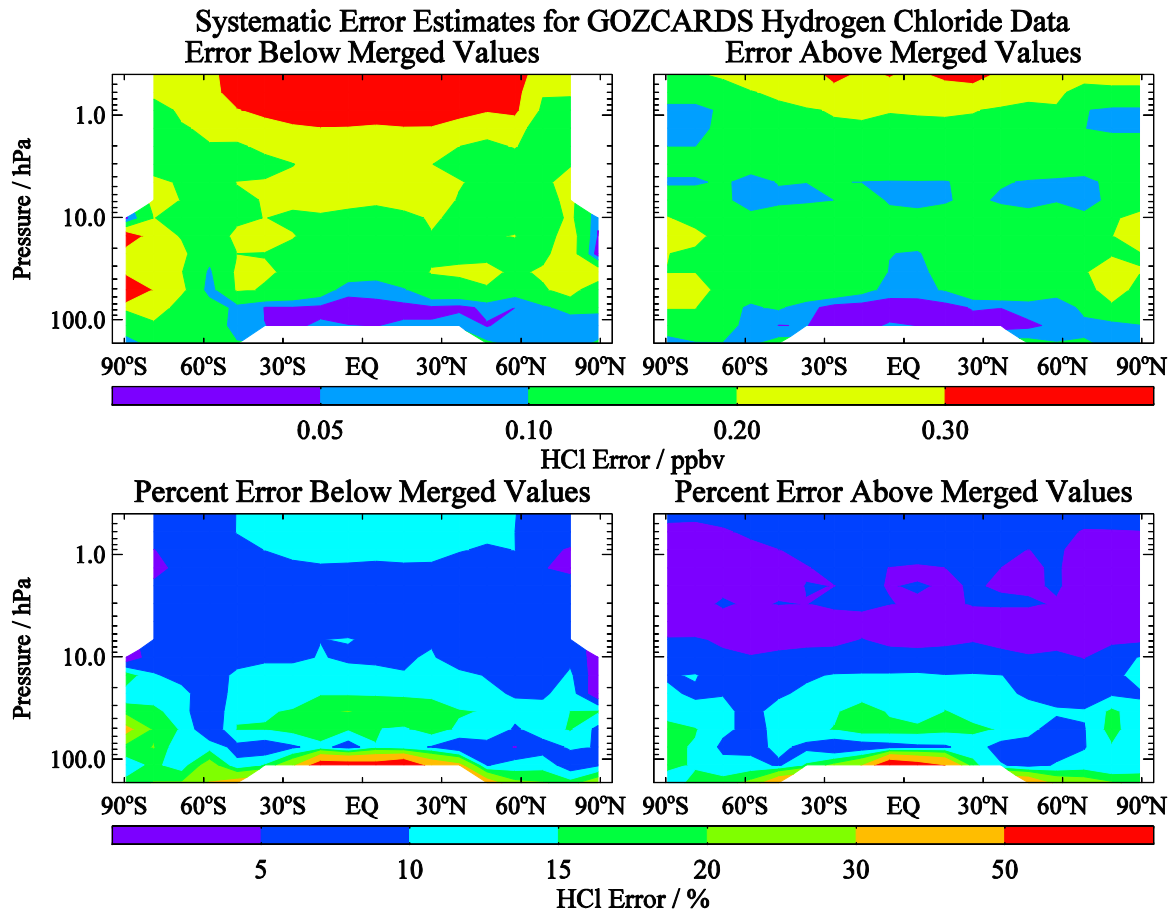
40

41



42
 43
 44
 45
 46
 47
 48
 49
 50
 51
 52
 53
 54
 55
 56
 57

Fig. 5. Illustration of GOZCARDS HCl monthly averages with systematic error estimates (shown as grey shading) at 46 hPa for 30°S-40°S; see text for the meaning of this shaded region. The source data from HALOE, Aura MLS, and ACE-FTS are shown in different colors (see legend), along with the merged values.



58

59

60 **Fig. 6.** Systematic error estimates for GOZCARDS HCl. One error (left panels) is relevant for values
 61 lower than (below) the merged values, and one (right panels) for values larger than the merged values; the
 62 top panels give the error estimates in ppbv, and the bottom panel errors are expressed as percent of the
 63 average merged values over the relevant time periods (see text). These error bars provide a range within
 64 which 95% of the source data values lie.

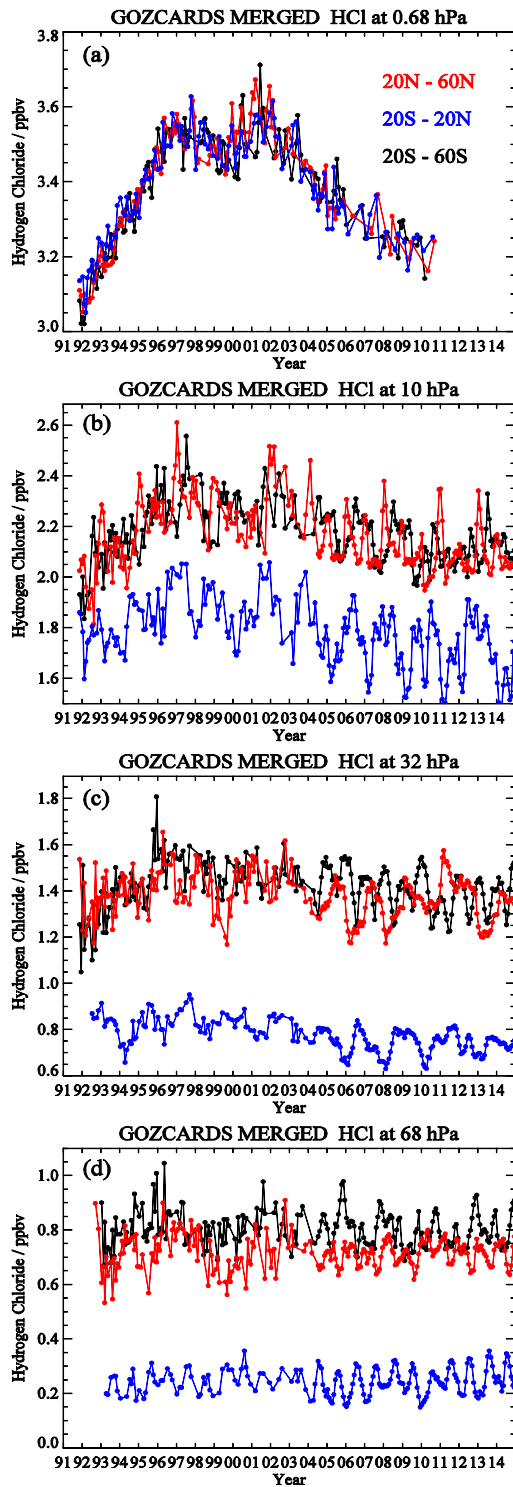
65

66

67

68

69

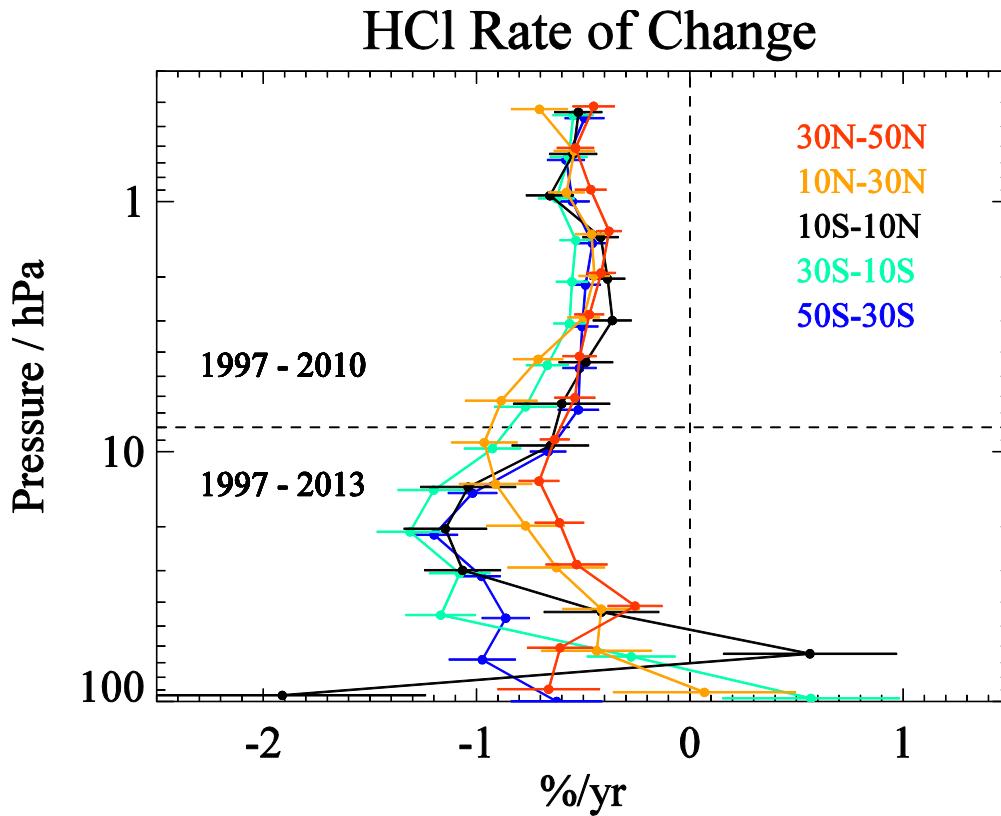


71

72

73 **Fig. 7.** Time series of the GOZCARDS monthly-averaged merged HCl abundance for 3 different latitude

74 bin averages (see color legend in panel (a)) for (a) 0.7 hPa, (b) 10 hPa, (c) 32 hPa, and (d) 68 hPa.



76

77

78 **Fig. 8.** The average rate of change (percent per year) for HCl as a function of pressure for different
 79 latitude bin averages (see legend) for time periods corresponding to the appropriate GOZCARDS HCl
 80 values (see text) in the upper stratosphere (Jan. 1997 - Sep. 2010) and lower stratosphere (Jan. 1997 -
 81 Dec. 2012). Deseasonalized monthly data were used to obtain a long-term trend for these time periods;
 82 two-sigma error bars are shown.

83

84

85

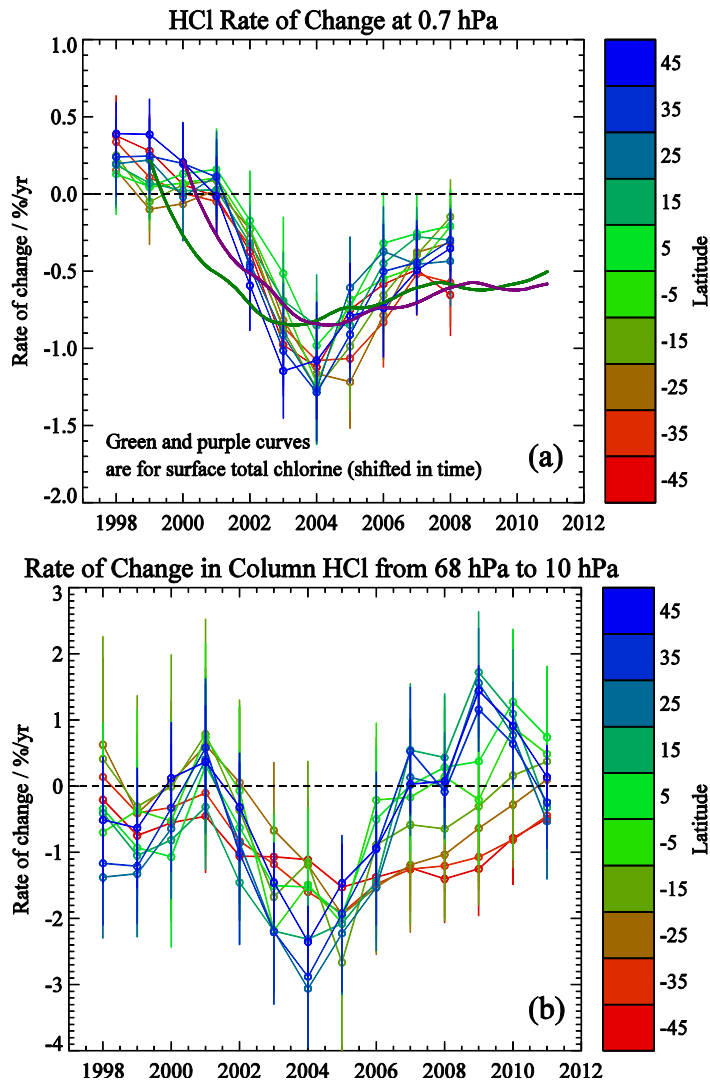
86

87

88

89

90



92

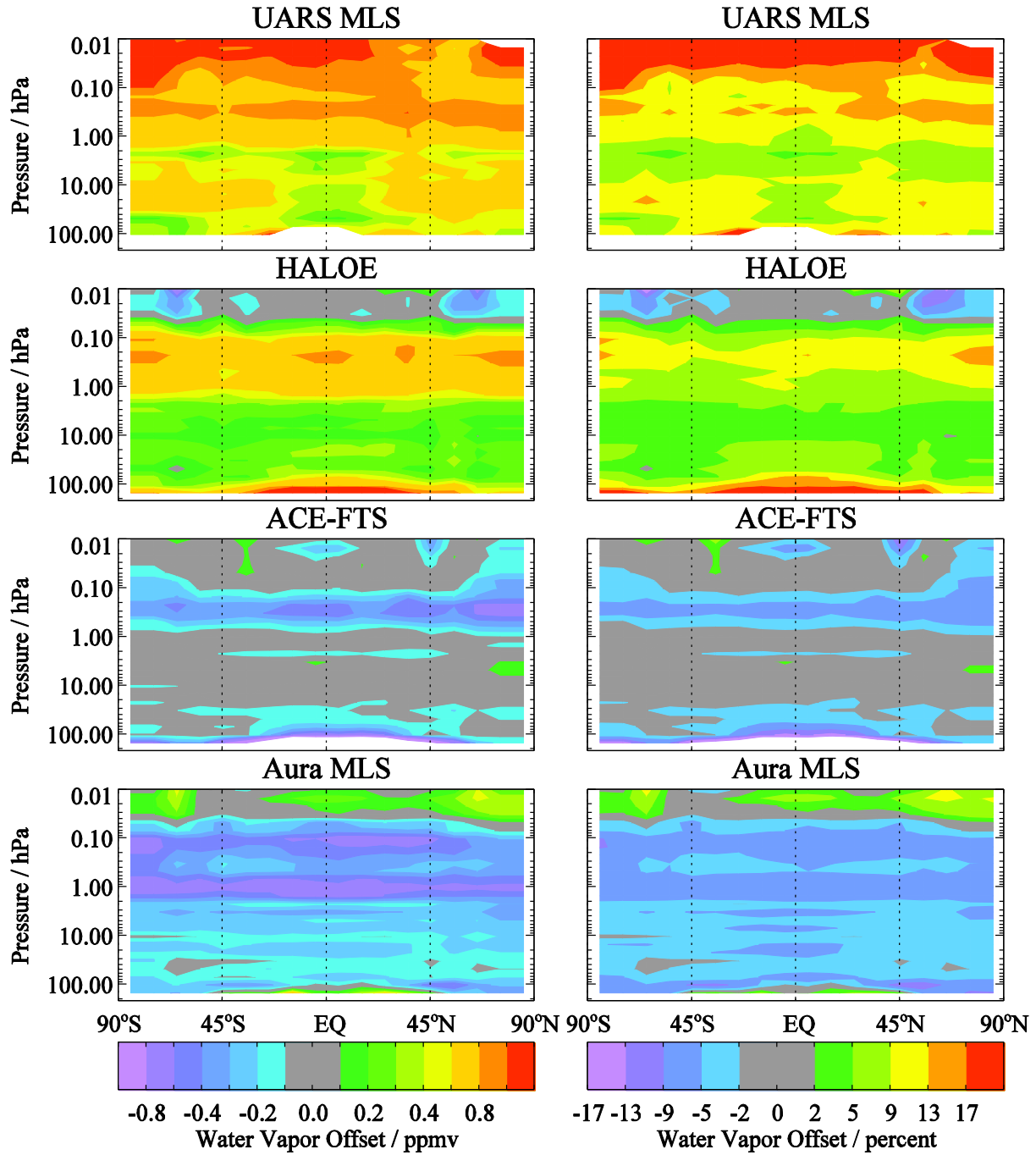
93

94 **Fig. 9.** Rates of change for GOZCARDS HCl (connected open circles) are given as a function of latitude
 95 in 10° latitude bins for sliding 6-year periods centered on Jan. 1 of each year (e.g., the 1998 point is an
 96 average for data from 1995 through 2000, and the 2011 point is for data from 2008 through 2013). (a) is
 97 for changes in upper stratospheric HCl at 0.7 hPa and (b) is for the change in the integrated HCl column
 98 between 68 hPa and 10 hPa. The two additional curves in (a) represent the rates of change in the
 99 estimated surface total chlorine from NOAA data (green is for a 6-year time shift, and purple for a
 100 7-year time shift, to account for transport time to the upper stratosphere); see text for more details. Error
 101 bars indicate twice the standard errors in the means.

102

103

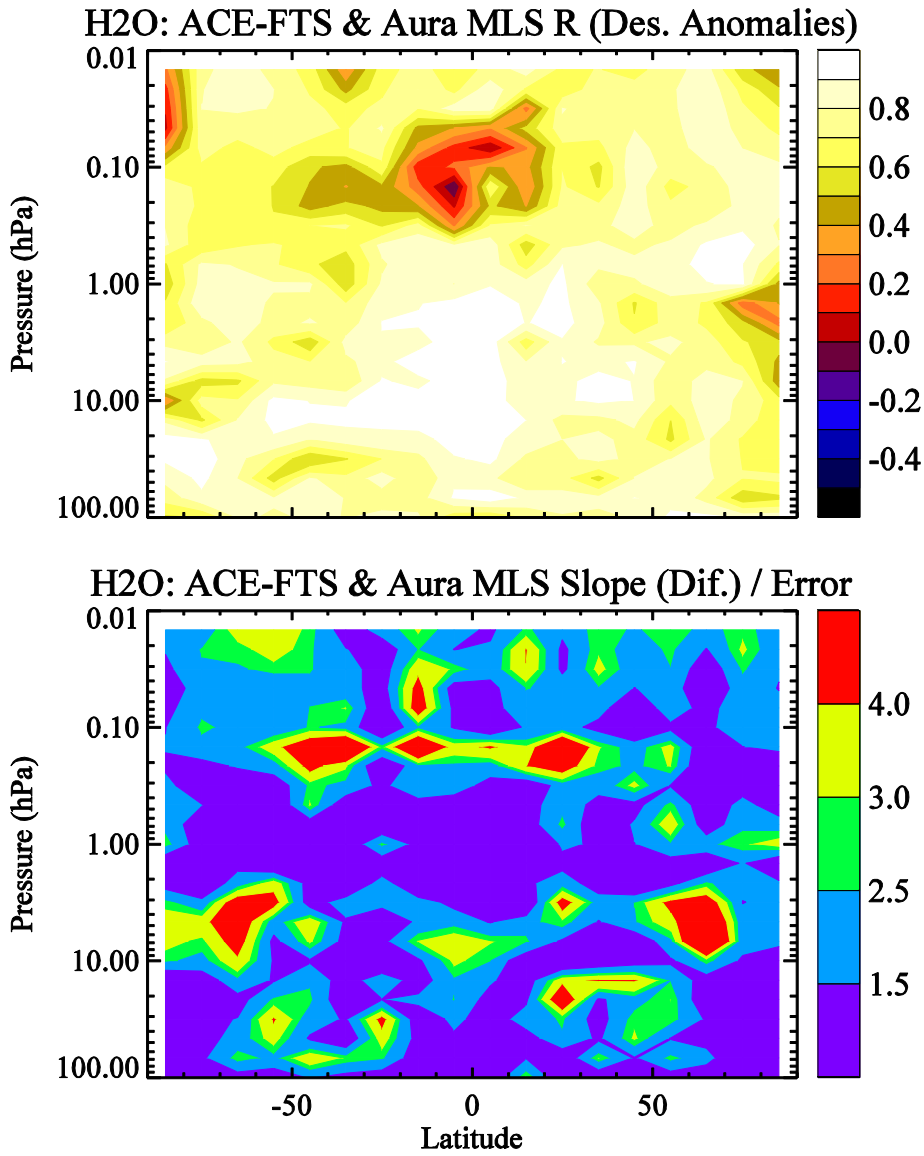
104



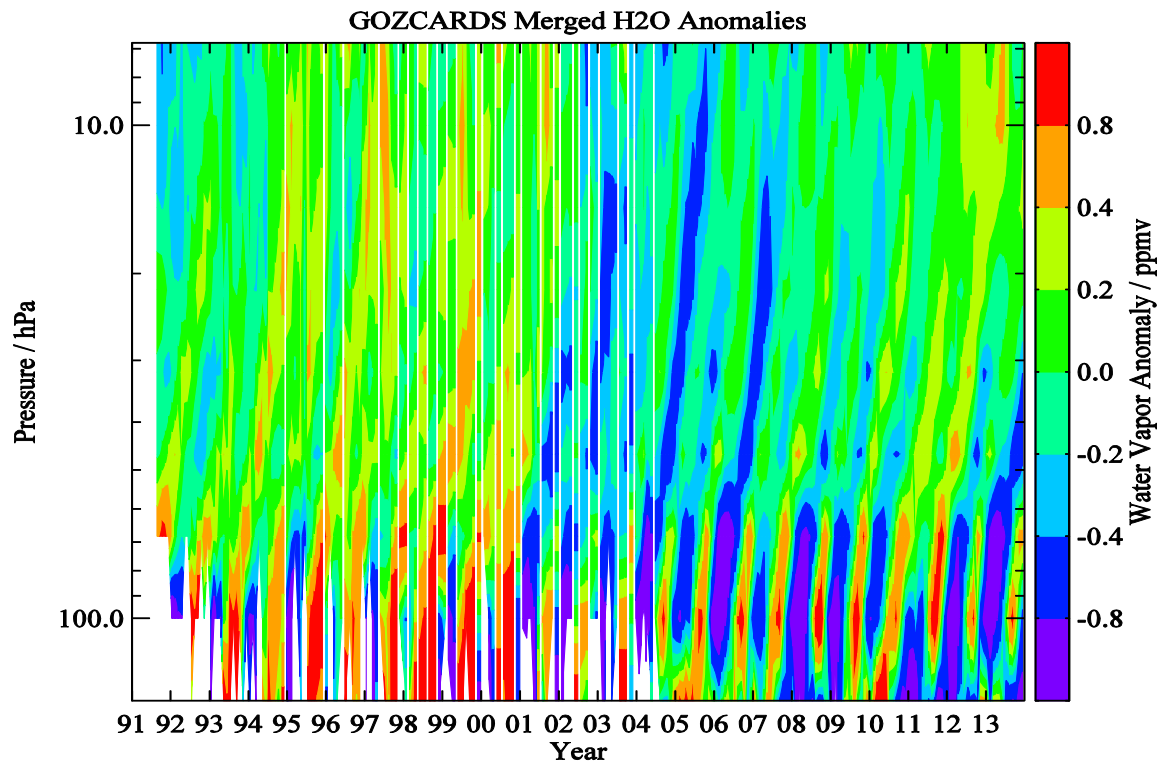
105
 106
 107
 108
 109
 110

Fig. 10. Offsets applied to the H₂O source datasets as a function of latitude and pressure, similar to Fig. 2 for HCl.

111
112
113



114
115 **Fig. 11.** Latitude/pressure contours of time series diagnostics for H₂O from Aura MLS and ACE-FTS;
116 this is similar to Fig. 4 for HCl.



117

118

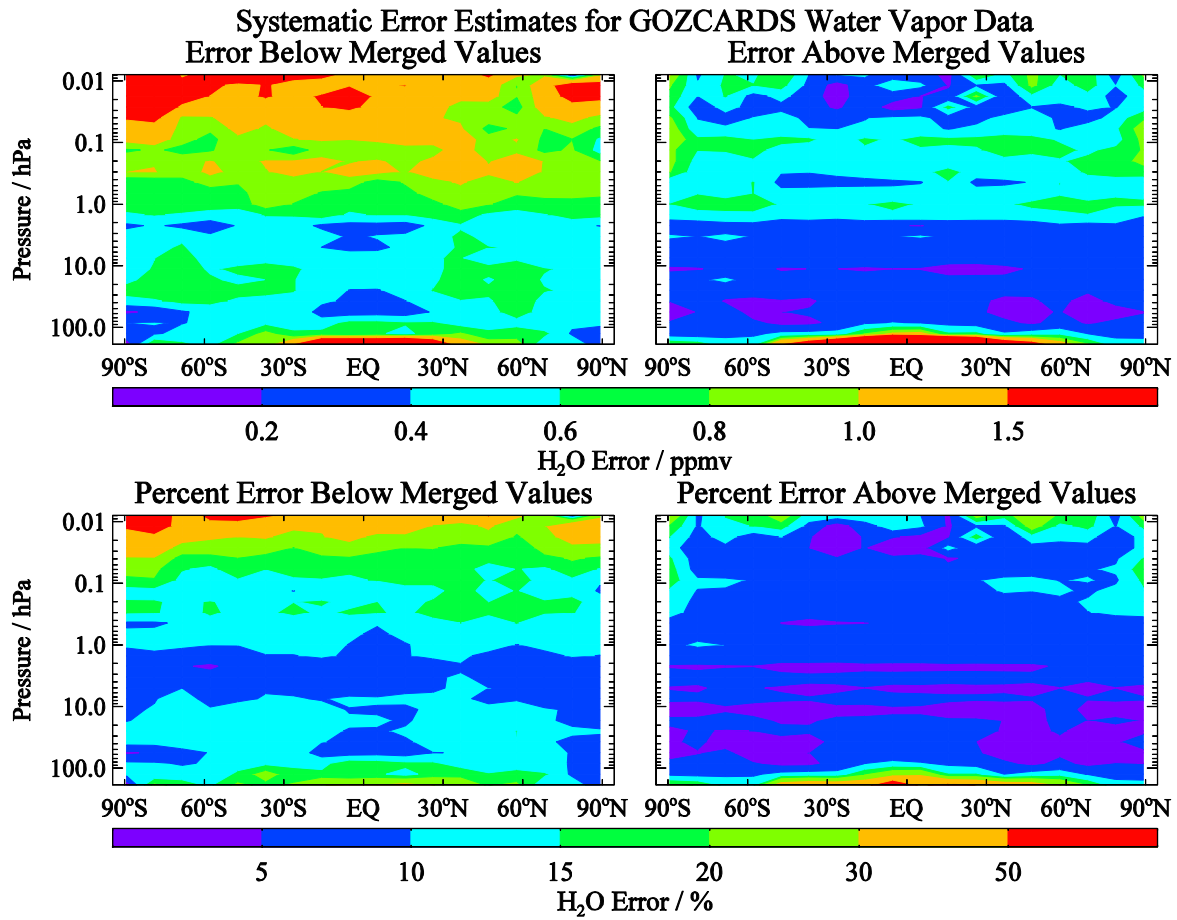
119 **Fig. 12.** A depiction of the “tape recorder” evolution for tropical water vapor abundances from 147 to
120 10 hPa for October 1991 through December 2013. This plot was produced from GOZCARDS merged
121 H₂O time series anomalies (differences from the long-term means) for the average of the 4 tropical bins
122 covering 20°S to 20°N.

123

124

125

126



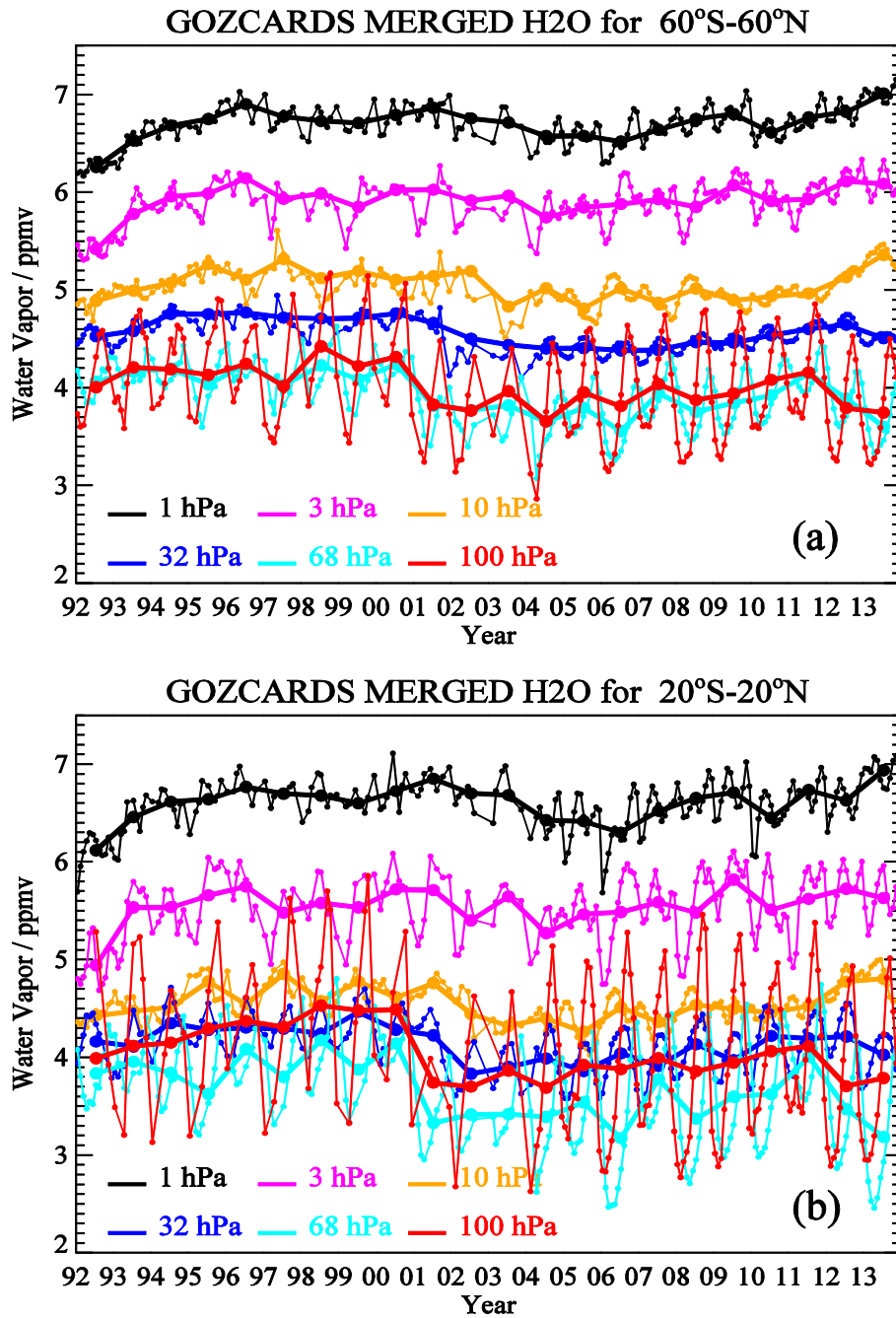
127

128

129 **Fig. 13.** Systematic error estimates for GOZCARDS H₂O (similar to Fig. 6 for HCl).

130

131



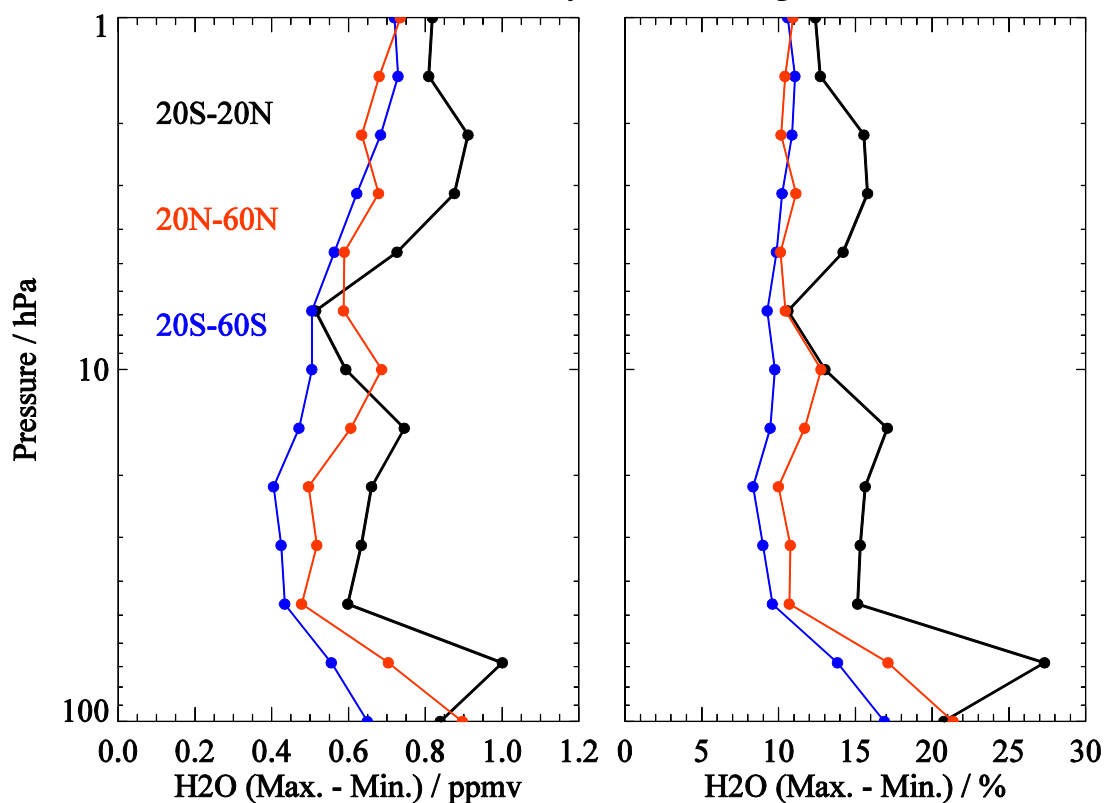
133

134 **Fig. 14.** Variations in stratospheric water vapor from the GOZCARDS H₂O merged data records (1992
 135 through 2013) averaged from (a) 60°S to 60°N and (b) 20°S to 20°N. Monthly average values and annual
 136 averages are shown by thin and thick lines (connecting similarly-colored dots), respectively, for the
 137 pressure levels indicated in the plot legend.

138

139

H2O Variability: 1992 through 2013



140

141

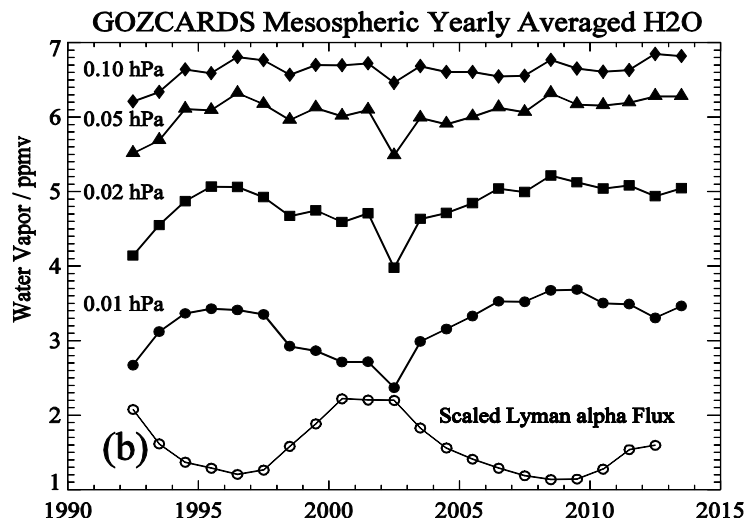
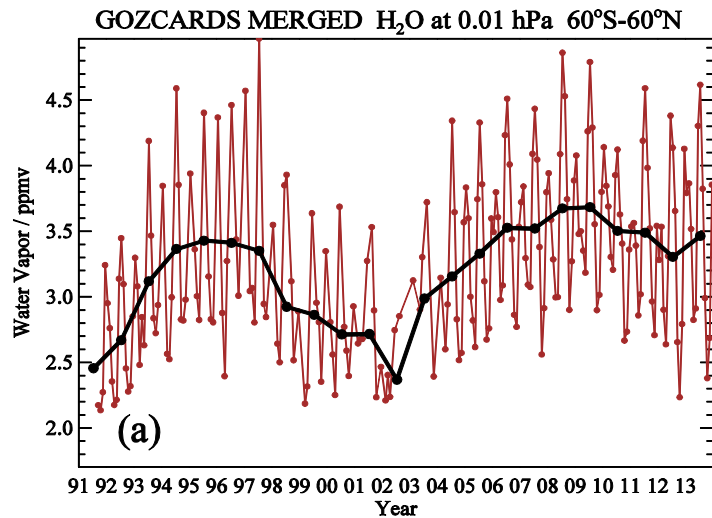
142 **Fig. 15.** Stratospheric water vapor variability on decadal timescales for 1992 through 2013 for tropical
143 (20°S-20°N in black) and mid-latitude (20°N-60°N in red and 20°S-60°S in blue) zonal means, based on
144 the GOZCARDS merged H₂O data record. The variability is expressed here as the difference between
145 maximum and minimum annual average abundances, from 100 to 1 hPa, in ppmv (left panel) and percent
146 (right panel).

147

148

149

150



151

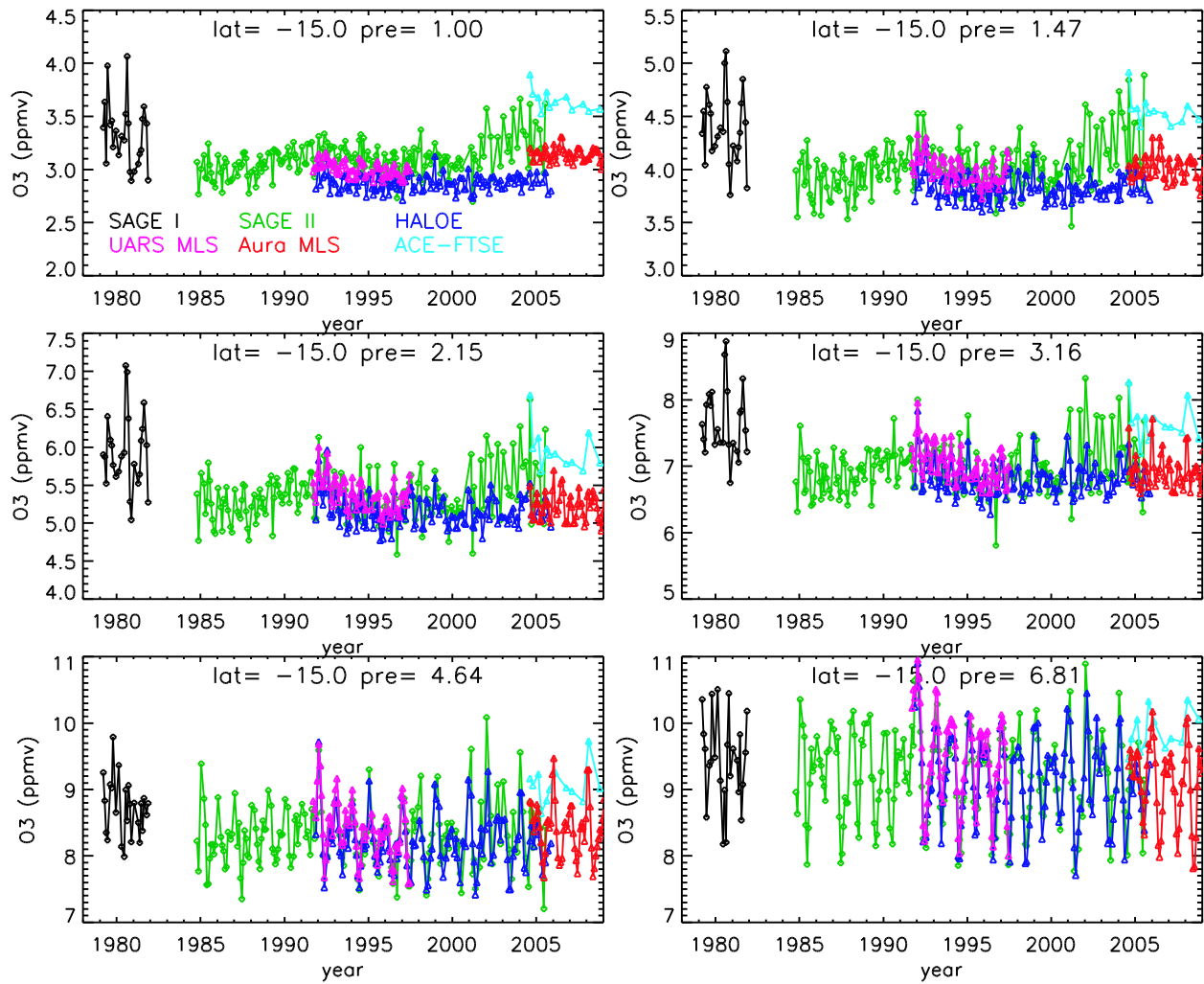
152

153 **Fig. 16.** (a) Variations in upper mesospheric (0.01 hPa) water vapor mixing ratios averaged from 60°S to
 154 60°N for Oct. 1991 through Dec. 2013, based on the GOZCARDS merged H₂O data records. Monthly
 155 average values and annual averages are shown by connected brown dots and connected black dots,
 156 respectively. (b) GOZCARDS merged H₂O annual averages (connected filled symbols) from 60°S to
 157 60°N for 1992 through 2013 at pressure levels between 0.1 and 0.01 hPa. A time series of annually-
 158 averaged Lyman α solar flux values (open circles), scaled to arbitrary units, is also displayed (see text).

159

160

161



162

163

164 **Fig. 17.** Time series of monthly zonal mean O₃ for 10°S - 20°S between 1 hPa and 6.8 hPa (with pressure
 165 values given by "pre") from SAGE I, SAGE II, HALOE, UARS MLS, Aura MLS, and ACE-FTS, all
 166 color-coded following the legend in top left panel.

167

168

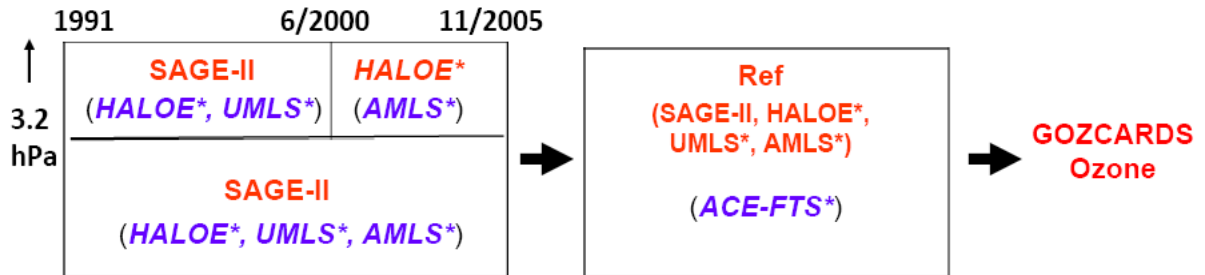
169

170

171

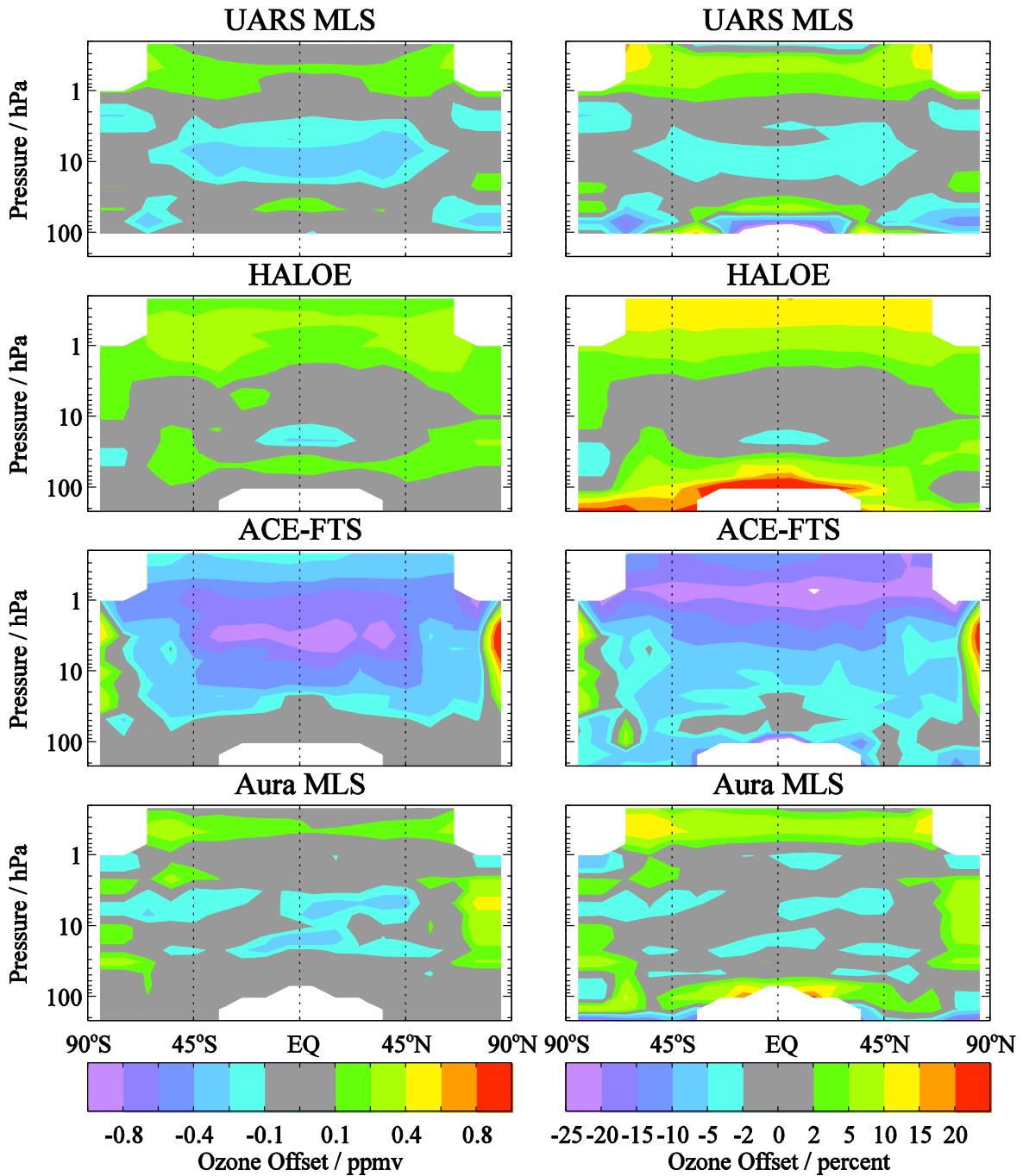
172

173 .
174
175



176
177
178
179
180
181
182
183
184
185

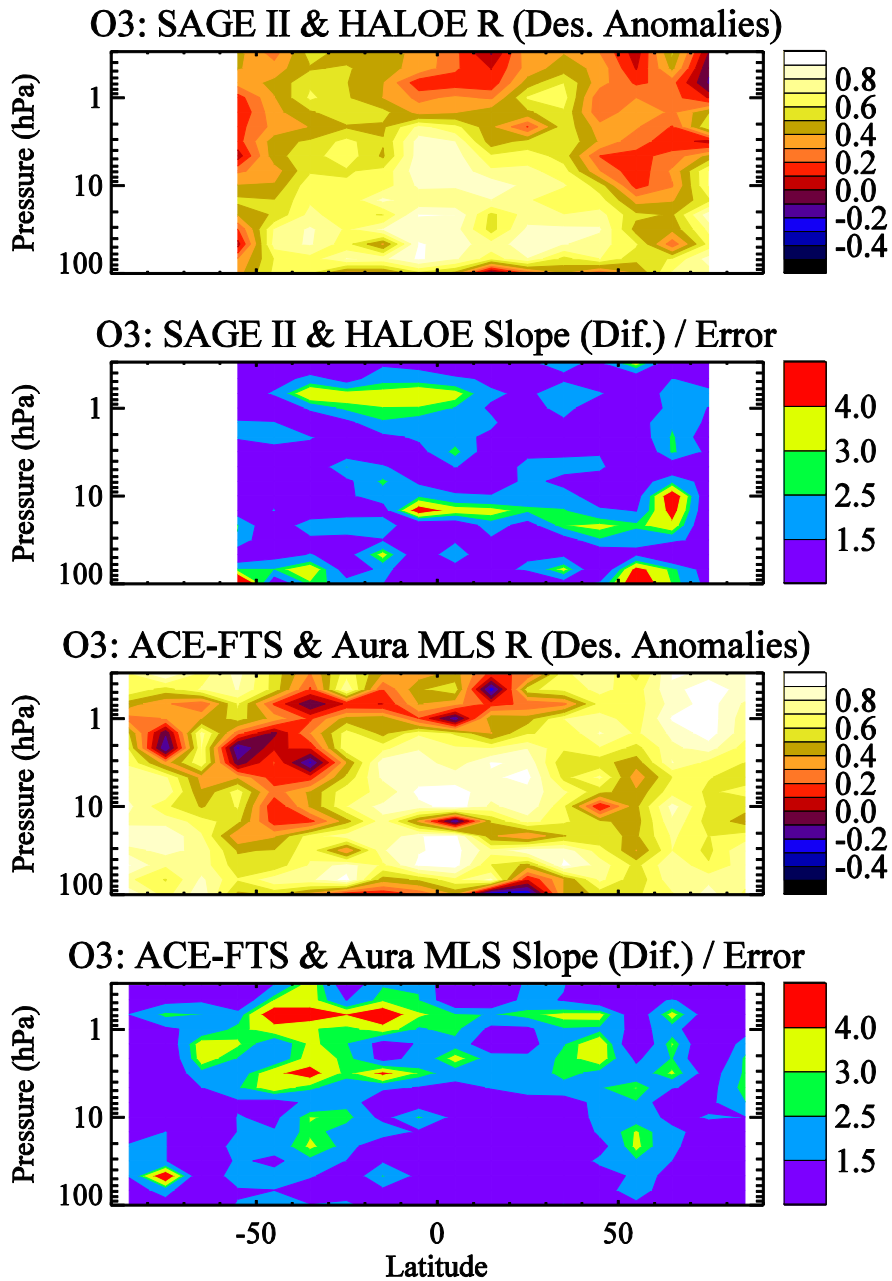
Fig. 18. Schematic diagram describing the creation of the merged GOZCARDS monthly zonal mean ozone data record from various satellite datasets. Instruments represented in red inside the boxes are used as a reference. Instruments whose measurements have already been adjusted to a reference are indicated with a “*” superscript. AMLS refers to Aura MLS and UMLS to UARS MLS. See text for more details.



186

187 **Fig. 19.** Offsets applied to the O₃ source datasets, similar to Fig. 2 for HCl.

188

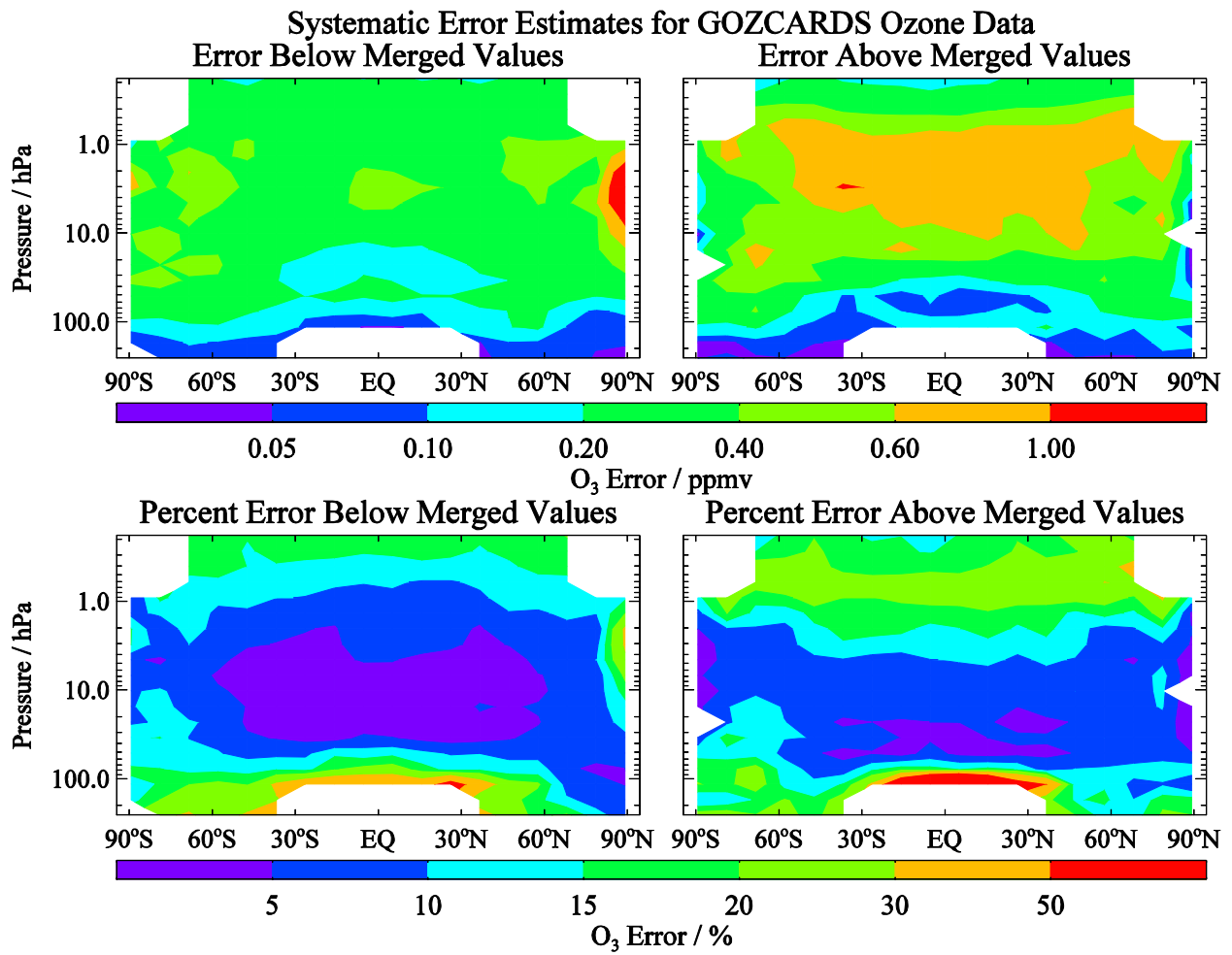


190

191 **Fig. 20.** Latitude/pressure contours of time series diagnostics for O₃ from Aura MLS and ACE-FTS; this
 192 is similar to Fig. 4 for HCl. The correlation coefficients (R values) and slope trend diagnostics are
 193 provided for HALOE versus SAGE II in the top two panels (for 1993-1999 as the trend issue for
 194 converted SAGE II data occurs after mid-2000 and to avoid Pinatubo-related data gaps before 1993) and
 195 for ACE-FTS versus Aura MLS in the bottom two panels (for 2005-2009).

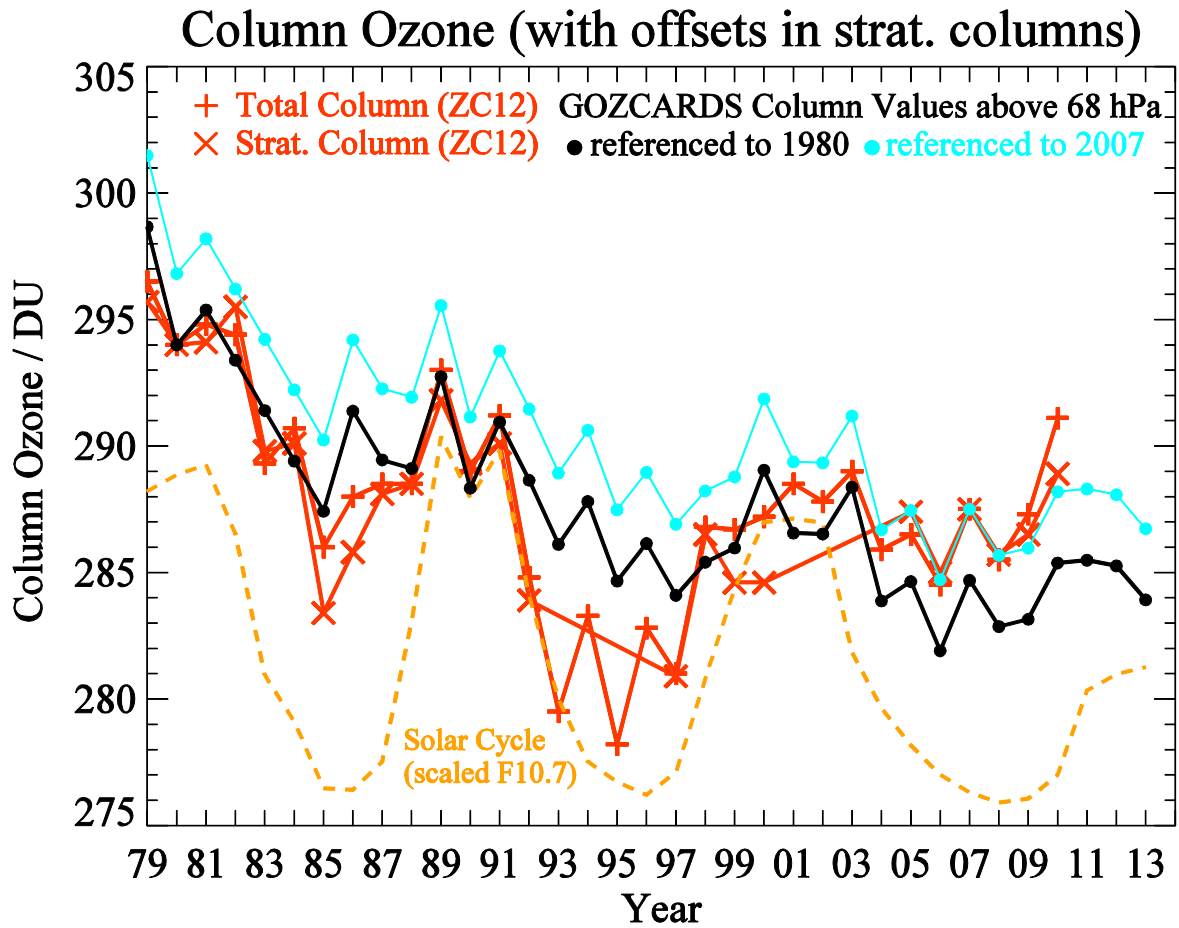
196

197
198
199



200
201
202
203
204

Fig. 21. Systematic error estimates for GOZCARDS O₃ (similar to Fig. 6 for HCl).



206

207

208 **Fig. 22.** Near-global (60°S to 60°N) results for average column ozone (total and stratospheric, from
 209 *Ziemke and Chandra, 2012*) compared to GOZCARDS O₃ columns above 68 hPa. Stratospheric columns
 210 are offset to better match the total column values, in order to more easily compare relative variations
 211 versus time; the black dots and red crosses are referenced to the 1980 total column values, while the cyan
 212 curves are referenced to 2007 to better illustrate the fits in the later years.

213

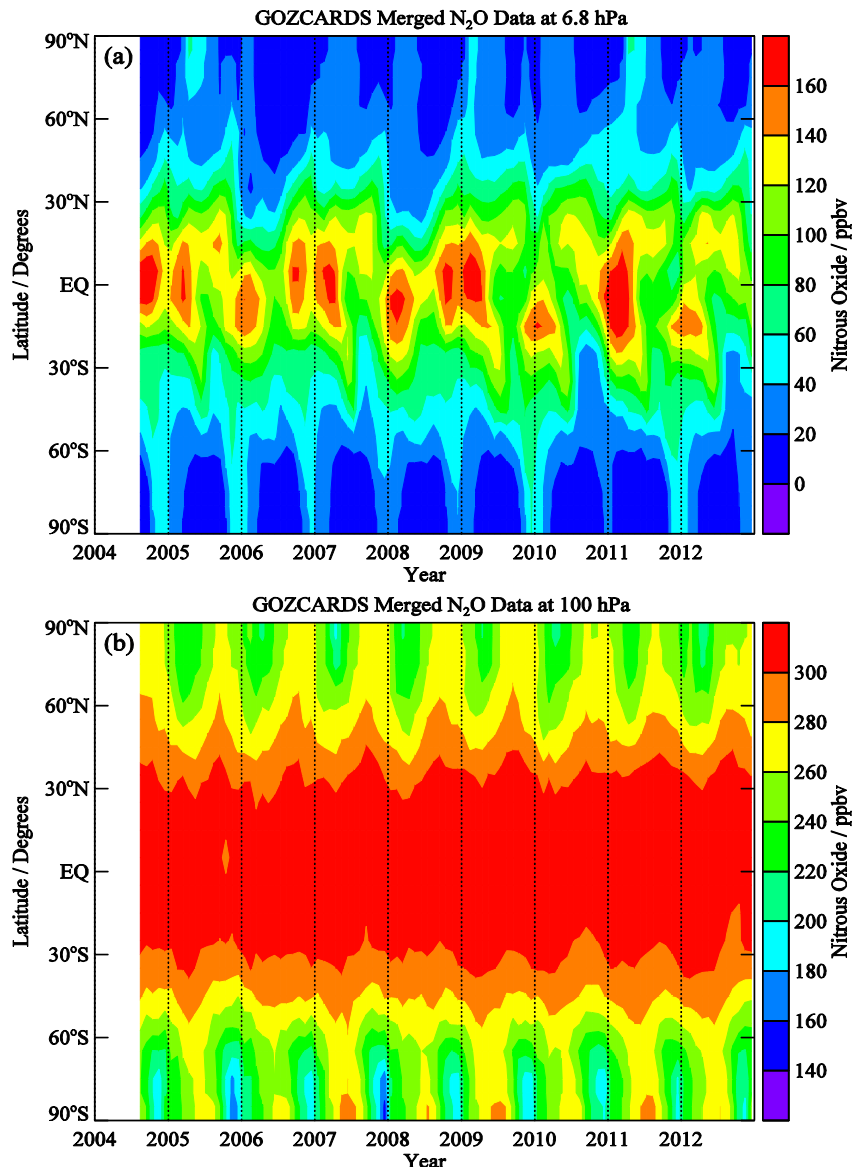
214

215

216

217

218



219

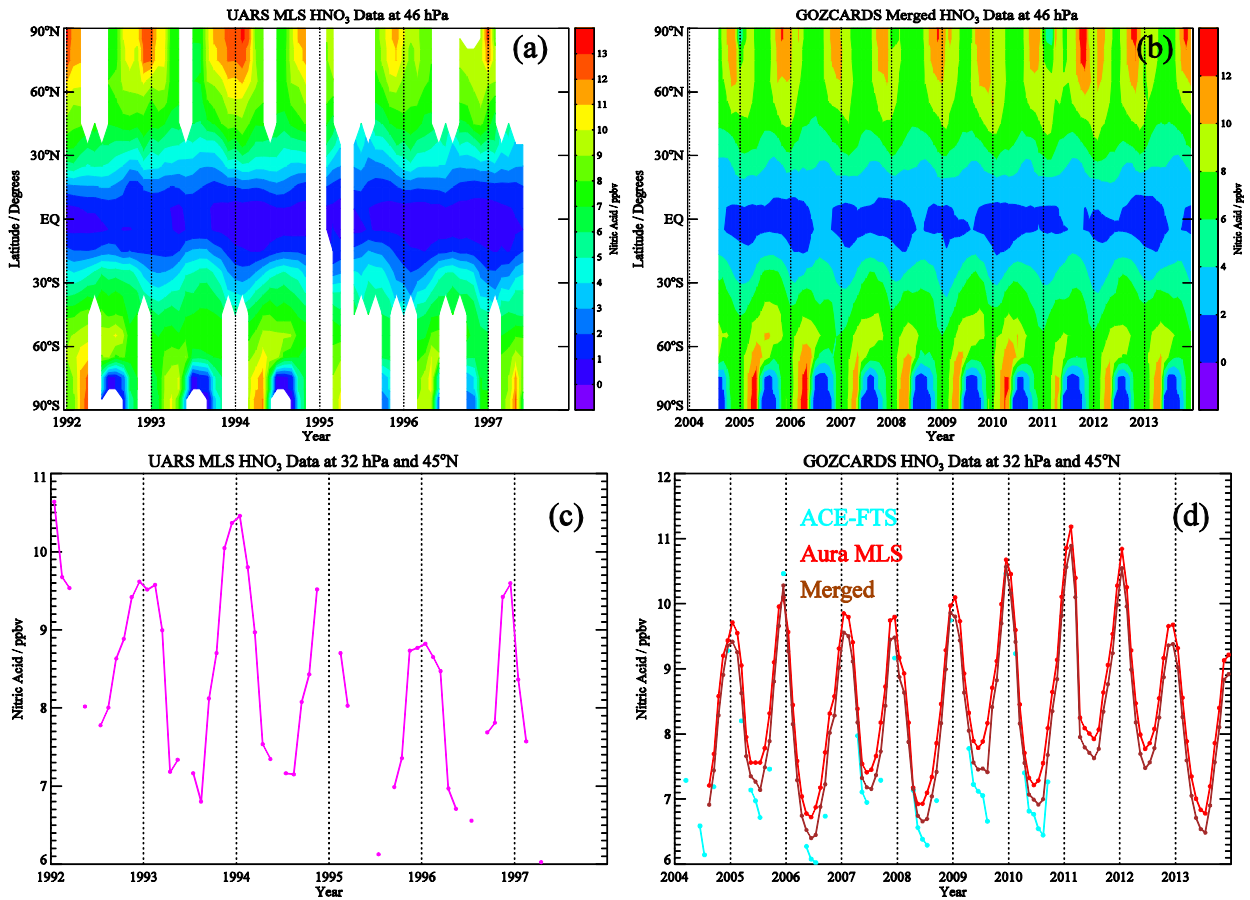
220 **Fig. 23.** Time evolution (Aug. 2004 through 2012) versus latitude of GOZCARDS merged N_2O (ppbv) at
 221 (a) 6.8 hPa and (b) 100 hPa.

222

223

224

225



226

227

228 **Fig. 24.** Sample results display the time evolution of satellite-retrieved HNO₃ (ppbv) for two different
229 periods, 1992-1997 in (a) and (c) versus 2004-2013 in (b) and (d). Panels (a) and (b) are contour plots at
230 46 hPa from UARS MLS global data and the merged GOZCARDS global data after 2004, respectively;
231 (c) and (d) show time series at 32 hPa and for the 40°N-50°N latitude bin, with (a) from UARS MLS data,
232 and (d) from ACE-FTS, Aura MLS, and the merged combination (between the two source data sets).

233

234

1 **Global Ozone Chemistry And Related Datasets for the**
2 **Stratosphere (GOZCARDS): methodology and sample results**
3 **with a focus on HCl, H₂O, and O₃**

4 **L. Froidevaux¹, J. Anderson², H.-J. Wang³, R. A. Fuller¹, M. J. Schwartz¹,**
5 **M. L. Santee¹, N. J. Livesey¹, H. C. Pumphrey⁴, P. F. Bernath⁵,**
6 **J. M. Russell III², and M. P. McCormick²**

7 ¹Jet Propulsion Laboratory, California Institute of Technology, Pasadena, CA, USA

8 ²Hampton University, Hampton, VA, USA

9 ³Georgia Institute of Technology, Atlanta, GA, USA

10 ⁴The University of Edinburgh, Edinburgh, UK

11 ⁵Old Dominion University, Norfolk, VA, USA

12 *Correspondence to:* L. Froidevaux (lucief@jpl.nasa.gov)

13

14

15

16

17

18

19

20

21

22

23

24 **Abstract**

25 We describe the publicly available dataset from the Global OZone Chemistry And Related
26 Datasets for the Stratosphere (GOZCARDS) project, and provide some results, with a focus on
27 hydrogen chloride (HCl), water vapor (H₂O), and ozone (O₃). This dataset is a global long-term
28 stratospheric Earth System Data Record (ESDR), consisting of monthly zonal mean time series
29 starting as early as 1979. The data records are based on high quality measurements from several
30 NASA satellite instruments and ACE-FTS on SCISAT. We examine consistency aspects
31 between the various datasets. To merge ozone records, the time series are debiased by calculating
32 average offsets with respect to SAGE II during periods of measurement overlap, whereas for
33 other species, the merging derives from an averaging procedure based on overlap periods. The
34 GOZCARDS files contain mixing ratios on a common pressure/latitude grid, as well as standard
35 errors and other diagnostics; we also present estimates of systematic uncertainties in the merged
36 products. Monthly mean temperatures for GOZCARDS were also produced, based directly on
37 data from the Modern-Era Retrospective analysis for Research and Applications (MERRA).

38 The GOZCARDS HCl merged product comes from HALOE, ACE-FTS and (for the lower
39 stratosphere) Aura MLS data. After a rapid rise in upper stratospheric HCl in the early 1990s, the
40 rate of decrease in this region for 1997-2010 was between 0.4 and 0.7%/yr. On shorter timescales
41 (6 to 8 years), the rate of decrease peaked in 2004-2005 at about 1%/yr, and has since levelled
42 off, at ~0.5%/yr. With a delay of 6-7 years, these changes roughly follow total surface chlorine,
43 whose behavior versus time arises from inhomogeneous changes in the source gases. Since the
44 late 1990s, HCl decreases in the lower stratosphere have occurred with pronounced latitudinal
45 variability at rates sometimes exceeding 1-2%/yr. *There has been a significant reversal in the
46 changes of lower stratospheric HCl abundances and columns for 2005-2010, in particular at
47 northern midlatitudes and in the deep tropics, where short-term increases are observed. However,
48 lower stratospheric HCl tendencies appear to be reversing after about 2011, with (short-term)
49 decreases at northern midlatitudes and some increasing tendencies at southern midlatitudes.*

50 For GOZCARDS H₂O, covering the stratosphere and mesosphere, the same instruments as for
51 HCl are used, along with UARS MLS stratospheric H₂O data (1991-1993). We display seasonal
52 to decadal-type variability in H₂O from 22 years of data. In the upper mesosphere, the anti-

53 correlation between H₂O and solar flux is now clearly visible over two full solar cycles. Lower
54 stratospheric tropical H₂O has exhibited two periods of increasing values, followed by fairly
55 sharp drops, the well-documented 2000-2001 decrease, and another recent decrease in 2011-
56 2013. Tropical decadal variability peaks just above the tropopause. Between 1991 and 2013, both
57 in the tropics and on a near-global basis, H₂O has decreased by ~5-10% in the lower
58 stratosphere, but about a 10% increase is observed in the upper stratosphere and lower
59 mesosphere. However, recent tendencies may not hold for the long-term, and the addition of a
60 few years of data can significantly modify trend results.

61 For ozone, we used SAGE I, SAGE II, HALOE, UARS and Aura MLS, and ACE-FTS data to
62 produce a merged record from late 1979 onward, using SAGE II as the primary reference for
63 aligning (debiasing) the other datasets. ~~Other adjustments were needed in the upper stratosphere
64 to circumvent temporal drifts in SAGE II O₃ after June 2000, as a result of the (temperature-
65 dependent) data conversion from a density/altitude to a mixing ratio/pressure grid.~~ Unlike the 2
66 to 3% increase in near-global column ozone after the late 1990s reported by some, GOZCARDS
67 stratospheric column O₃ values do not show a recent upturn of more than 0.5 to 1%; continuing
68 studies of changes in global ozone profiles, as well as ozone columns, are warranted.

69 A brief mention is also made of other currently available, commonly-formatted GOZCARDS
70 satellite data records for stratospheric composition, namely those for N₂O and HNO₃.

71 **1 Introduction**

72 The negative impact of anthropogenic chlorofluorocarbon emissions on the ozone layer,
73 following the early predictions of Molina and Rowland (1974), stimulated interest in the trends
74 and variability of stratospheric ozone, a key absorber of harmful ultraviolet radiation. The
75 discovery of the ozone hole in ground-based data records (Farman et al., 1985) and the
76 associated dramatic ozone changes during southern hemisphere winter and spring raised the level
77 of research and understanding regarding the existence of new photochemical processes (see
78 Solomon, 1999). This research was corroborated by analyses of aircraft and satellite datasets
79 (e.g., Anderson et al., 1989; Waters et al., 1993), and by independent ground-based data. Global
80 total column ozone averages in 2006-2009 were measured to be smaller than during 1964-1980
81 by ~3%, and larger more localized decreases over the same periods reached ~6% in the southern

82 hemisphere midlatitudes (WMO, 2011). Halogen source gas emissions have continued to
83 decrease as a result of the Montreal Protocol and its amendments. Surface loading of total
84 chlorine peaked in the early 1990s (WMO, 2011), and subsequent decreases in global
85 stratospheric HCl and ClO have been measured from satellite-based sensors (Anderson et al.,
86 2000; Froidevaux et al., 2006; Jones et al., 2011) as well as from the ground (e.g., Solomon et
87 al., 2006, Kohlhepp et al., 2012). A slow recovery of the ozone layer is expected between the
88 late 1990s and several decades from now, towards pre-1985 levels (WMO, 2011); **the robust
89 determination of a long-term global trend requires a sufficiently long and accurate data record. It
90 is desirable to use high quality datasets for ozone and related stratospheric species for a robust
91 documentation of past variations and as constraints for global atmospheric models.**

92 The history of global stratospheric observations includes a large suite of satellite-based
93 instruments, generally well-suited for the elucidation of long-term global change. A review of
94 differences between past and ongoing satellite measurements of atmospheric composition has
95 been the focus of the Stratosphere-troposphere Processes And their Role in Climate (SPARC)
96 Data Initiative (DI); results for stratospheric water vapor and ozone intercomparisons have been
97 published by Hegglin et al. (2013) and Tegtmeier et al. (2013), respectively, to be followed by a
98 larger report on intercomparisons of multiple species. Systematic biases reported in these recent
99 papers tend to mirror past validation work. However, these investigations have not pursued data
100 merging aspects or the creation of long-term records.

101 Under the Global OZone Chemistry And Related Datasets for the Stratosphere (GOZCARDS)
102 project, we have created monthly zonally averaged datasets of stratospheric composition on a
103 common latitude/pressure grid, using satellite-based limb viewing instruments launched as early
104 as 1979 (for ozone data in particular) and now continuing with instruments launched about a
105 decade ago. The creation of this Earth System Data Record stays close to the data values
106 themselves. Therefore, spatial or temporal gaps are typically not filled in; various methods can
107 be used to try to produce continuous fits to time series, but we viewed this as being outside the
108 scope of this data record creation. The GOZCARDS products arise from several high quality
109 satellite datasets, namely from Stratospheric Aerosol and Gas Experiment instruments (SAGE I
110 and SAGE II), the Halogen Occultation Experiment (HALOE) which flew aboard the Upper
111 Atmosphere Research Satellite (UARS), the UARS Microwave Limb Sounder (MLS), the

112 Atmospheric Chemistry Experiment Fourier Transform Spectrometer (ACE-FTS) on SCISAT,
113 and the Aura MLS experiment. Table 1 provides characteristics of the original datasets;
114 validation papers from the instrument teams and other related studies give a certain degree of
115 confidence in these datasets. However, the existence of validation references does not imply that
116 there are no caveats or issues with a particular measurement suite. In this project, we have strived
117 to optimize data screening and mitigate some undesirable features, such as the impact of outlier
118 values or the effects of clouds or aerosols. All source datasets still have shortcomings or
119 imperfections, but we have refrained from arbitrarily removing specific monthly means.

120 Based on original profiles from the various instruments, GOZCARDS “source” monthly
121 zonal mean values were derived. After data screening, monthly average profiles were created by
122 vertical interpolation onto the GOZCARDS pressure levels, followed by binning and averaging
123 into monthly sets. In order to accommodate the lower vertical resolution of some limb viewers,
124 such as UARS MLS, the GOZCARDS pressure grid was chosen as

$$125 \quad p(i) = 1000 \cdot 10^{-\frac{i}{6}} (\text{hPa}) \quad (1)$$

126 with i varying from 0 to a product-dependent top; this grid width corresponds to ~ 2.7 km. The
127 high resolution SAGE O₃ profiles were smoothed vertically onto this grid (see Sect. 5). Given
128 the sampling of solar occultation instruments, which typically provide 15 sunrise (SR) and 15
129 sunset (SS) profiles every day (versus the emission-based sampling from MLS), we used latitude
130 bins of width 10° (18 bins from 80°S-90°S to 80°N-90°N) to construct the monthly zonal means.

131 After the production of GOZCARDS source data files on the above grid, merged (combined)
132 products were created. This involves the calculation of average biases between monthly zonal
133 means from different source data during periods of overlap, followed by an adjustment (using
134 calculated average offsets) of the time series. Non-zero biases always exist between datasets
135 from different instruments for various reasons, such as systematic errors arising from Level 1
136 (radiances) or Level 2 (retrievals), different vertical resolutions, or sampling effects. A useful
137 reference regarding the sampling effects, which can arise spatially (within a latitude bin) or
138 temporally (within a month), is the recent work by Toohey et al. (2013). They studied sampling
139 biases from a large suite of satellite-based stratospheric profiling instruments, based on
140 simulations using fully-sampled model abundance averages versus averaged sampled results
141 from sub-orbital track locations. The magnitude of such sampling errors is typically inversely

142 related to the number of available profiles routinely sampled, so that larger sampling errors arise
143 from occultation than from emission measurements, which often sample thousands of profiles
144 per day. Toohey et al. (2013) found that sampling-related biases can reach 10-15% in some
145 regions/periods, notably at high latitudes when larger atmospheric variability exists. Sofieva et
146 al. (2014) have also discussed sampling uncertainty issues for satellite ozone datasets.

147 We have observed very good correlations between GOZCARDS ozone and other long-term
148 ozone datasets, such as the Stratospheric Water vapor and OzOne Satellite Homogenized
149 (SWOOSH) dataset (Davis et al., in preparation) and homogenized Solar Backscatter Ultraviolet
150 (SBUV) data; these analyses (along with related work on H₂O) will be discussed elsewhere.
151 Results from GOZCARDS and other data relating to midlatitude ozone trends have appeared
152 (e.g., Nair et al., 2013). Dissemination of trend results arising from analyses of GOZCARDS
153 and other ozone profile data is planned as part of the SI²N initiative, which stands for
154 Stratospheric Processes And their Role in Climate (SPARC), International Ozone Commission
155 (IOC), Integrated Global Atmospheric Chemistry Observations (IGACO-O₃), and the Network
156 for the Detection of Atmospheric Composition Change (NDACC). Recent results on such ozone
157 profile trend comparisons can be found in Tummon et al. (2014) and Harris et al. (2014).

158 This paper starts with a discussion of general data screening issues (Sect. 2), and then
159 describes the GOZCARDS data production approach and methodology, followed by some
160 atmospheric results for HCl (Sect. 3), H₂O (Sect. 4), and O₃ (Sect. 5). We provide specific
161 diagnostics that indicate generally good correlations and small relative drifts between the main
162 datasets being used to create the longer-term GOZCARDS merged time series. Section 6 briefly
163 mentions the availability of a few other GOZCARDS products, namely N₂O, HNO₃, and
164 temperatures derived from MERRA fields. The version of GOZCARDS described here is
165 referred to as ESDR version 1.01 or ev1.01. ~~Each product's public GOZCARDS data record has
166 an associated digital object identifier (DOI) along with a relevant dataset reference.~~

167

168 **2 GOZCARDS source data and data screening**

169 Data provenance information regarding the various measurements used as inputs for
170 GOZCARDS is provided in Appendix A (Sect. A.1).

171 2.1 GOZCARDS data screening and binning

172 The screening of profiles for GOZCARDS has largely followed guidelines recommended by
173 the various instrument teams and/or relevant publications; such screening procedures are rarely
174 all described in one convenient location, so we review this briefly here for the various data sets.
175 Data screening can reduce the total number of good profiles below our chosen threshold for
176 flagging zonal monthly means; unless otherwise noted, we only provide monthly means
177 constructed from 15 or more values in a given latitude/pressure bin.

178 ~~For HALOE, cloud contamination may add retrieval artifacts and HALOE profiles were~~
179 ~~screened for clouds, following procedures described in Hervig and McHugh (1999); values at~~
180 ~~and below the cloud level (found in the netCDF files) were excluded. Also, HALOE profiles that~~
181 ~~may occasionally contain artifacts associated with either a faulty trip angle or constant lockdown~~
182 ~~angle registration were screened out, per recommendations from the HALOE data processing~~
183 ~~team (see http://haloc.gats-inc.com/user_docs/index.php for details).~~

184 ~~—For UARS MLS, we used screening recommendations documented by Livesey et al. (2003).~~
185 ~~In particular, MLS data points whose retrieved precisions are flagged with a negative sign were~~
186 ~~discarded, ensuring only a negligible contribution to the retrieval from a priori. Also, our data~~
187 ~~filtering followed the recommendations regarding the “MMAF_STAT” flag for operational~~
188 ~~status (we only used values of ‘G’, ‘t’, or ‘T’ for this flag) and the product-specific~~
189 ~~“QUALITY” flag (for which we only used values equal to 4, thus eliminating bad radiance fits).~~

190 ~~—For Aura MLS data screening, the procedures are generally as follows: we only use profiles~~
191 ~~with even values of the Status field, Quality values larger than documented thresholds (indicating~~
192 ~~good radiance fits), Convergence values smaller than documented thresholds (indicating good~~
193 ~~convergence), and positive (unflagged) values of the estimated precisions. Species-specific~~
194 ~~validation papers give data screening recommendations, with appropriate flag values for Quality~~
195 ~~and Convergence; see Livesey et al. (2013) for such references and v3.3 data screening updates.~~

196 ~~—For ACE FTS, a list of profiles with data issues is provided by the ACE FTS team (see~~
197 ~~https://database.seisat.ca/validation/data_issues_table.php) and these have been removed from~~
198 ~~our database. However, we also found it necessary to remove occasional large outlier values that~~
199 ~~could significantly impact monthly zonal means by adding a bias (or “noise”) to the time series if~~

200 such screening were not performed; such outliers are not otherwise routinely removed from the
201 original ACE-FTS profiles. Our outlier screening procedure removed values outside 2.5 times
202 the standard deviation, as measured from the median values in each latitude/pressure bin, for
203 each year of data. This was deemed close to optimum by comparing the results to Aura MLS
204 time series (which usually are not impacted by such outliers), as well as to independent zonal
205 means (using 5° latitude bins) provided by the ACE-FTS instrument team. Up to 5% of the
206 profile values in each bin in any given month were typically discarded as a result of this
207 procedure, but the maximum percentage of discarded values can be close to 10% for a few
208 months of ACE-FTS version 2.2 data, depending on year and species. Moreover, because of poor
209 ACE-FTS sampling in the tropics, the threshold value for minimum number of (good) ACE-FTS
210 profiles determining a monthly zonal average was allowed to be as low as 10 for mid- to high
211 latitudes, and as low as 6 for low latitudes (bins centered from 25°S to 25°N). Our zonal mean
212 datasets for ACE-FTS would become too sparse in some years if such lower threshold values
213 were not used; ~~such data sparseness can introduce limitations (larger error bars) in the~~
214 ~~determination of trends, for example, although we also performed comparisons versus Aura MLS~~
215 ~~monthly means to provide some level of confidence in the results. In addition, ACE-FTS single~~
216 ~~profile values were discarded if the associated error was larger than the mixing ratio or smaller~~
217 ~~than 10^{-4} times the mixing ratio, following recommendations from the ACE-FTS team.~~

218 The binning of profiles occurs after the screened values are averaged (in each
219 latitude/pressure bin). Negative monthly means have been flagged (set to -999.0) in the
220 GOZCARDS files; while a negative mixing ratio that is smaller (in absolute value) than its
221 associated standard error (or a few times this standard error) can in theory be meaningful, we
222 deem that occasional small negative monthly means are unlikely to be very useful, scientifically.

223 The organization of profiles on a common pressure grid is straightforward when pressure
224 values are present in the original files, as is the case for most data used here. Also, the vertical
225 resolutions are similar for most of the instruments used for GOZCARDS (see more details in
226 each species-specific section). The UARS MLS, HALOE, and Aura MLS native pressure grids
227 are either the same as or a superset of the GOZCARDS pressure grid, so these datasets were
228 readily sampled for the construction of the GOZCARDS monthly means. For ACE-FTS profiles,
229 pressures are provided along with the fixed altitude grid, and we used linear interpolation versus

230 log(pressure) to convert profiles to the GOZCARDS grid. More details are provided in the O₃
231 section for SAGE I and SAGE II, for which density versus altitude is the native representation.

232

233 **3 GOZCARDS HCl**

234 **3.1 GOZCARDS HCl source data records**

235 We used HCl datasets from HALOE, ACE-FTS and Aura MLS to generate the monthly zonal
236 mean source products for GOZCARDS HCl.

237 For the screening of HALOE HCl profiles, in addition to the procedures mentioned in
238 Sect. 2, a first-order aerosol screening was applied: all HCl values at and below a level where the
239 5.26 μm aerosol extinction exceeds 10⁻³ km⁻¹ were excluded.

240 For Aura MLS, the ongoing standard HCl product is retrieved using band 14 rather than band
241 13, which was used to measure HCl for the first 1.5 years after launch, but started deteriorating
242 rapidly after Feb. 2006. Validation and error characterization for the Aura MLS HCl product
243 (version 2.2) were provided by Froidevaux et al. (2008). The MLS version 3.3/3.4 HCl data used
244 here (see Livesey et al., 2013) compare quite well with v2.2, with average biases within 5% in
245 general. A high bias exists in MLS HCl versus aircraft data at 147 hPa at low latitudes
246 (Froidevaux et al., 2008). Such regions with large uncertainties and biases are avoided (flagged)
247 for the production of the GOZCARDS merged HCl dataset.

248 The use of the GOZCARDS source files for Aura MLS HCl, like the use of original Level 2
249 MLS HCl files, is not recommended for obtaining realistic trends in the upper stratosphere (at
250 pressures < 10 hPa), even if monthly mean MLS HCl in this region displays reasonable values in
251 comparison to other satellite-based measurements. Aura MLS switched to a backup band (band
252 14) to retrieve the daily HCl measurements after band 13 (originally targeted specifically for
253 HCl) showed signs of rapid degradation in early 2006; as the remaining lifetime for band 13 is
254 expected to be very short (days as opposed to weeks), this band has only been turned on for a
255 few days since February 2006. However, for pressures ≥ 10 hPa, the long-term (band 14) HCl
256 data now being routinely produced is deemed to be robust (because of the broader emission line

257 in this region, in comparison to the measurement bandwidth). These considerations have
258 implications for how we treat MLS HCl upper stratospheric data in terms of the merging process.

259 Past validation studies have compared MLS HCl (v2.2), ACE-FTS (v2.2) and HALOE (v19)
260 datasets using coincident pairs of profiles; such work was described by Froidevaux et al. (2008)
261 for MLS HCl validation and by Mahieu et al. (2008) for ACE-FTS HCl validation. HALOE HCl
262 values were found to be biased low by ~10-15% relative to both MLS and ACE-FTS, especially
263 in the upper stratosphere; this low bias versus other (balloon- and space-based) measurements
264 had been noted in past HALOE validation studies (Russell et al., 1996). Also, HALOE (v19) and
265 ACE-FTS (v2.2) HCl data tend to lose sensitivity and reliability for pressures less than ~0.4 hPa.

266 **3.2 GOZCARDS HCl merged data records**

267 HCl is a good candidate for merging the main satellite data that have provided this measurement
268 since 1991. Indeed, one can benefit from the strengths of all datasets in the lower stratosphere,
269 but rely on HALOE and ACE-FTS for upper stratospheric trends, because of the Aura MLS HCl
270 trend detection issue mentioned above. Aura MLS HCl time series were not included in the
271 merging at pressures less than 10 hPa, so after November 2005, the GOZCARDS HCl upper
272 stratospheric trends are dictated only by changes in ACE-FTS abundances. However, in order to
273 derive the systematic offsets needed to adjust the time series from these three instruments in a
274 continuous way (in the pressure dimension), we used the absolute Aura MLS HCl measurements
275 at all pressure levels in 2004 and 2005, during the overlap period between the three instruments.

276 Figure 1 illustrates the merging process for HCl at 32 hPa for the 45°S latitude bin (which
277 covers 40°S to 50°S). Given that there exists very little overlap between the three sets of
278 measurements in the same months in 2004 and 2005, especially in the tropics, a simple 3-way
279 averaging of the datasets is not practical and would lead to significant data gaps. Our
280 methodology is equivalent to averaging all three datasets during this period (if one had full
281 coverage from all datasets), but we use Aura MLS as a transfer dataset. This was done by first
282 averaging ACE-FTS and Aura MLS data, where the datasets overlap, and then including the
283 third dataset (HALOE) into the merging process with the intermediate (temporary) merged data.
284 Although HALOE HCl is believed to be biased too low, modifying the HALOE values to
285 somehow match ACE-FTS or Aura MLS values or a combination of these two datasets was

286 deemed to be too subjective. The combined weight of the other two datasets leads to a merged
287 HCl dataset that is generally further away from HALOE than it is from either ACE-FTS or Aura
288 MLS. The top left panel in Fig. 1 shows monthly zonal average GOZCARDS source data for
289 HALOE, ACE-FTS, and Aura MLS during the overlap period, from Aug. 2004 (when Aura
290 MLS data started) through Nov. 2005 (when HALOE data ended). The top right panel illustrates
291 the result of step 1 in the merging procedure, with the temporary merged data values (orange)
292 resulting from the adjustment of ACE-FTS and Aura MLS values to the mean reference
293 indicated by the black dashed line; this reference is simply the average (over the overlap period)
294 of these two datasets, formed from the average of the points which overlap during the same
295 months, meaning whenever ACE-FTS obtained monthly data (since Aura MLS HCl means exist
296 every month). The middle left panel shows the result of step 2, namely the merged values
297 (brown) that arise from merging HALOE values with the temporary merged values (orange)
298 from step 1. In this second averaging step, we weigh the intermediate merged values by $2/3$ and
299 HALOE values by $1/3$ (leading to a mean reference illustrated by the dashed black line), in order
300 for this process to be equivalent to averaging all three datasets, each with a weight of $1/3$. The
301 middle right panel shows the source data along with the final merged values during the overlap
302 period. A simple mathematical description of the above procedure is provided in Appendix A.
303 The bottom panel shows the same datasets but for 1991 through 2012, after the calculated
304 additive offsets are applied to the whole source series, thus debiasing the datasets; these adjusted
305 time series are then merged (averaged) together wherever overlap exists. We tested this
306 procedure by using one or the other of the two occultation datasets as the initial one in step 1,
307 and results were not found to differ appreciably. This methodology is used as well for the same
308 three datasets for the H_2O merging; we have also checked our procedures and results by using
309 two independent calculations from different institutions. We also found that the use of
310 multiplicative adjustments generally produces very similar results as additive offsets. Some
311 issues were found on occasion with multiplicative offsets, when combining very low mixing
312 ratios, but additive offsets can also have drawbacks if the merged values end up being slightly
313 negative, notably as a result of changes that modify the already low HCl values during Antarctic
314 polar winter. This occurs on occasion as additive offsets tend to be weighted more heavily by the
315 larger mixing ratios found during non-winter seasons; as a result, we decided not to offset the

316 lower stratospheric HCl source datasets in the polar winter seasons at high latitudes for any of
317 the years (for interannual consistency). Procedural details regarding the merging of HCl data are
318 summarized in the Supplementary material.

319 In Fig. 2, we display the offsets that were applied to the three HCl source datasets as a result
320 of the merging process in each latitude/pressure bin; a positive value means that a dataset is
321 biased low and needs to be increased (on average) by the offset value. These offsets show that in
322 general, ACE-FTS and Aura MLS HCl values were adjusted down by 0.1-0.2 ppbv (a decrease
323 of about 2-10%), while HALOE HCl was adjusted upward by 0.2-0.4 ppbv. Offset values tend
324 to be fairly constant with latitude and the sum of the offsets equals zero. The generally
325 homogeneous behaviour versus latitude is a good sign, as large discontinuities would signal
326 potential issues in the merging (e.g., arising from large variability or lack of sufficient statistics).
327 Figure S1 provides more detailed examples of some of these (upper and lower stratospheric)
328 offsets versus latitude, including standard errors based on the variability in the offsets from
329 month to month during the overlap period. Error bars in the offsets provide an indication of the
330 results' robustness. Another indication of first-order compatibility between datasets is provided
331 by a comparison of annual cycles. Figure S2 provides average annual cycle amplitudes obtained
332 from simple regression model fits to HALOE, ACE-FTS, and Aura MLS series over their
333 respective periods. While there are a few regions where noise or spikes exist (mainly for ACE-
334 FTS), large annual amplitudes in the polar regions occur in all the time series; this arises from
335 HCl decreases in polar winter, followed by springtime increases.

336 A more detailed analysis of interannual variability and trend consistency is provided from
337 results in Fig. 3, which shows an example of ACE-FTS and Aura MLS time series. ~~We note that
338 no v2.2 ACE-FTS data (for any species) are used after September 2010, because of a data
339 processing problem; a fully updated version of ACE-FTS data was not available when the
340 GOZCARDS data records were constructed.~~ We have used coincident points from these time
341 series to compare the deseasonalized anomalies (middle panel in Fig. 3) from both instrument
342 series; correlation coefficient values (R values) are also computed. In the Fig. 3 example, very
343 good correlations are obtained and no significant trend difference between the anomalies (bottom
344 panel) is found for ACE-FTS and Aura MLS HCl. A global view for all latitude/pressure bins of
345 these correlations and drifts is provided in Fig. 4, where the top panel gives R values for

346 deseasonalized anomalies, and the bottom panel gives the ratio of the difference trends over the
347 error in these trends. The results in Fig. 4 confirm that there are significant trend differences
348 between the upper stratospheric HCl time series from ACE-FTS and that of Aura MLS (as a
349 reminder, we did not use Aura MLS HCl for pressures less than 10 hPa). Fig. 4 also shows very
350 low correlation coefficients from the deseasonalized HCl series in the uppermost stratosphere,
351 because Aura MLS HCl exhibits unrealistically flat temporal behavior, whereas ACE-FTS HCl
352 varies more. In the lower stratosphere, there is generally good agreement between the ACE-FTS
353 and Aura MLS HCl time series, with R values typically larger than 0.7 and difference trend to
354 error ratios smaller than 1.5. The few low R values for 100 hPa at low latitudes likely reflect
355 more infrequent ACE-FTS sampling and some (possibly related) outlier data screening issues.

356 Figure S3 illustrates GOZCARDS merged 46 hPa HCl variations versus time; there is clearly
357 a much more complete global view (with no monthly gaps) after the launch of Aura MLS. Gaps
358 at low latitudes in 1991 and 1992 are caused by post-Pinatubo aerosol-related issues in the
359 HALOE record, and gaps in later years arise from the decrease in coverage from UARS. In the
360 upper stratosphere, there are more gaps compared to 10 hPa and below, as a result of the much
361 poorer tropical coverage from ACE-FTS and the elimination of MLS data in this region.

362 An indication of systematic errors in the merged values can be obtained by providing
363 estimates of the range of available monthly mean source data. We have made such a calculation,
364 although these error values are not part of the public GOZCARDS data files. For each bin, we
365 computed the ranges of monthly means above and below the merged values that include 95% of
366 the available source data monthly means. These error bars are not usually symmetric about the
367 merged values, especially if one dataset is biased significantly in relation to merged values. We
368 did not have enough datasets here to consider a more statistical approach (such as actual standard
369 deviations among source datasets). Figure 5 shows the result of such a systematic error
370 calculation at 46 hPa for the 35°S latitude bin. The lower shaded region range gives the lower
371 bound, determined by HALOE data, and the upper limit of the grey shading originates from
372 ACE-FTS data. Figure 6 shows contour plots of these estimated systematic errors in HCl for all
373 latitudes and pressures. These are fairly conservative error bars; however, even the source data
374 averages at the 95% boundaries have their own systematic errors (rarely smaller than 5%), so our
375 estimates do not really encompass all error sources. Error bars representing a range within which

376 95% of the source data values reside (see Figs. 5 and 6) can be a useful guide for data users or
377 model comparisons; users can readily calculate such ranges (or we can provide these values).

378 ~~Other quantities are provided in the netCDF GOZCARDS files, which are composed of one~~
379 ~~set of individual yearly files for all source datasets, and one set of yearly files for the merged~~
380 ~~products. The main data quantities are monthly averages, plus standard deviations and standard~~
381 ~~errors for these means. The GOZCARDS source files also provide the number of days sampled~~
382 ~~each month as well as minimum and maximum values for the source datasets. Other information~~
383 ~~includes average solar zenith angles and local solar times for individual sources. Note that for the~~
384 ~~species discussed here, sunset and sunrise occultation values in the same latitude bin during a~~
385 ~~given month are averaged together. Finally, formulae for monthly standard deviations of the~~
386 ~~merged data are given in Appendix A, where sample time series of the standard deviations and~~
387 ~~standard errors (not systematic errors) for both source and merged HCl data are also shown.~~

388 **3.3 GOZCARDS HCl sample results and discussion**

389 Stratospheric HCl is important because it is the main reservoir of gaseous chlorine and it can be
390 used to follow the chlorine budget evolution over the past decades. This includes a significant
391 increase before the mid-1990s as a result of anthropogenic chlorofluorocarbon (CFC) production,
392 followed by a slower decrease as a result of the Montreal Protocol and subsequent international
393 agreements to limit surface emissions that were correctly predicted to be harmful to the ozone
394 layer (Molina and Rowland, 1974; Farman et al., 1985).

395 In Fig. 7, we provide an overview of the HCl evolution since 1991, based on GOZCARDS
396 average merged HCl for 3 different latitude regions at 4 pressure levels, from the upper
397 stratosphere to the lower stratosphere. In the upper stratosphere (at 0.7 hPa shown here), the
398 rapid early rise in HCl was followed by a period of stabilization (1997-2000) and subsequent
399 decreases. ~~The GOZCARDS HCl time series for pressures less than 10 hPa stop in September~~
400 ~~2010 because after this, v2.2 ACE FTS data were halted, due to technical retrieval issues with~~
401 ~~that data version.~~ Rates of decrease for stratospheric HCl and total chlorine have been
402 documented based on such satellite-based upper stratospheric abundances, which tend to follow
403 tropospheric source gas trends with a time delay of order 6 years, with some uncertainties in the
404 modeling of this time delay and related age of air issues (Waugh et al., 2001; Engel et al., 2002;

405 Froidevaux et al., 2006). As summarized in WMO (2011), the average rate of decrease in
406 stratospheric HCl has typically been measured at $-0.6\%/yr$ to $-0.9\%/yr$, in reasonable agreement
407 with estimated rates of change in surface total chlorine; see also the HCl upper stratospheric
408 results provided by Anderson et al. (2000) for HALOE, Froidevaux et al. (2006) for the one and
409 a half year Aura MLS data record (from the initially used primary band), and Jones et al. (2009)
410 and Brown et al. (2011) for a combination of HALOE and ACE-FTS datasets. The WMO (2011)
411 summary of trends also includes results from column HCl data at various NDACC Fourier
412 transform infrared (FTIR) measurement sites; see Kohlhepp et al. (2012) for a comprehensive
413 discussion of ground-based results, showing some scatter as a function of latitude. Figure 7
414 demonstrates that a global-scale decline in mid- to lower stratospheric HCl is visible since about
415 1997. We also notice that at 68 hPa in the tropics, the long-term rate of change appears to be
416 near-zero or slightly positive. In addition, there are shorter-term periods in recent years when an
417 average increasing “trend” would be inferred rather than a decrease, in particular, see the
418 northern hemisphere data from 2005 through 2012 at 32 hPa.

419 To quantify the rates of change further, we created deseasonalized GOZCARDS merged
420 monthly zonal mean HCl data for the different latitudes, and we show in Fig. 8 the linear rate of
421 change that results from simple fits through such series (averaged into 20° -wide latitude bins).
422 The long-term trends (1997 through 2013 for the lower stratosphere, and 1997 through 2010 for
423 the upper stratosphere) are generally negative and between about $-0.5\%/yr$ in the upper
424 stratosphere and $-1\%/yr$ in the lower stratosphere, depending on latitude. Some separation
425 between northern and southern hemisphere results is observed in the lower stratosphere, with
426 smaller trends in the northern hemisphere. Also, the scatter increases for 68 to 100 hPa and some
427 positive (or essentially zero) trends occur at low latitudes in this region; however, we have less
428 confidence in the results at 100 hPa, given the larger scatter and error bars in that region (and the
429 smaller abundances). ~~Results at more polar latitudes (not shown here) tend to follow the adjacent~~
430 ~~midlatitude bin results, but with more scatter (and larger error bars), especially for shorter time~~
431 ~~periods. To explore these rates of change in the lower stratosphere in more detail, Fig. 9 shows~~
432 ~~the same type of analysis as Fig. 8 for three other time periods and for pressures of 10 hPa or~~
433 ~~more: (a) for a decade of data from 2003 through 2012, (b) for a shorter 6-yr period from 2006~~
434 ~~through 2011, and (c) for the most recent 6-yr period from 2008 through 2013. For the results in~~

435 ~~(a), a decadal decrease is still observed for the southern hemisphere bins and some of the tropics~~
436 ~~in the upper region, but increases can be detected in the northern hemisphere and at the higher~~
437 ~~pressures in the tropics. In (b), we see an accentuation of this hemispheric asymmetry in the~~
438 ~~short-term rates of change, with large positive changes in the northern hemisphere, and values on~~
439 ~~both negative and positive sides between 1 and 3 %/yr in many cases; during this past decade,~~
440 ~~this 6-yr period (2006–2011) is near the temporal peak of this asymmetric lower stratospheric~~
441 ~~behavior. In the most recent 6-yr period, however (see (c)), the rates of change have decreased~~
442 ~~for all the latitude bins shown, with all results from 10 to 68 hPa under 0.5 to 1%/yr (absolute~~
443 ~~value).~~ Without assigning an exact linear “trend” from these simple analyses, we illustrate here
444 that there is considerable variability in lower stratospheric HCl short-term behavior, especially
445 after 2005. Such lower stratospheric changes in HCl have been captured in column HCl FTIR
446 data, as demonstrated by Mahieu et al. (2013, 2014). In the latter reference, it is shown that total
447 column (FTIR) results and GOZCARDS lower stratospheric HCl trends agree quite well; also,
448 these authors’ analyses imply that a relative slowdown in the northern hemispheric circulation is
449 responsible for these observed recent changes in the lower stratosphere. However, we note from
450 Fig. 7, that such changes in lower stratospheric HCl appear to be fairly short-term in nature, with
451 an apparent reversal in behavior occurring at both northern and southern midlatitudes since 2011
452 (e.g., at 32 hPa). The lower stratospheric changes are distinct from the upper stratospheric long-
453 term decrease, which we expect to continue, as long as the Montreal Protocol agreements are
454 fulfilled worldwide and total surface chlorine emissions keep decreasing.

455 The rate of change analyses above were repeated and shown in Fig. 10 for sliding time
456 periods centered on different years (e.g., a 6-yr average for 2004 means an average from 2001
457 through 2006) in the upper and lower stratosphere for various latitude bins (covering 50°S to
458 50°N in 10° steps). As observed in Fig. 10(a), the sliding 6-yr results indicate that there has been
459 an acceleration in the rate of decrease of upper stratospheric HCl between 2000 and 2004,
460 followed by a flatter period until 2010 (this being the last year of GOZCARDS data available for
461 the upper stratosphere, with a 6-yr period centered at the start of 2008). The rate of upper
462 stratospheric HCl change reached a maximum close to -1%/yr, and has retreated to values near -
463 0.5%/yr in more recent years. This is roughly in agreement with time-shifted curves showing the
464 rates of change for surface total chlorine based on National Oceanic and Atmospheric

465 Administration (NOAA) surface data (Montzka et al., 1999), as shown in Fig. 10 (upper panels,
466 green and purple curves) with the Earth System Research Laboratory Global Monitoring
467 Division (website) data, time shifted by 6 or 7 years to approximately account for transport
468 delays into the upper stratosphere. The tropospheric source gases for chlorine have also shown a
469 reduction in the rate of decrease during the 2nd half of the past decade, as discussed by Montzka
470 et al. (1999) and summarized more recently in WMO (2011). As discussed in the latter report,
471 this arises from a combination of factors, including the initial rapid decrease in methyl
472 chloroform (which now plays a much smaller role), slower rates of decrease from the sum of
473 CFCs in more recent years, and increases in hydrochlorofluorocarbons (HCFCs), along with
474 small contributions from very short-lived species, all of which requires continued monitoring. In
475 Fig. 10, the lower stratospheric response is summarized (panel (b)) by considering the rates of
476 change in partial column density between 68 hPa and 10 hPa. The lower stratospheric rates of
477 change show more variability with latitude than in the upper stratosphere for short (6-yr) time
478 periods, and a hemispheric asymmetry exists, peaking in 2009, when positive tendencies are seen
479 in the northern hemisphere, as opposed to decreases in the south. ~~Figure 10 (panels (e) and (d))~~
480 ~~also displays the sensitivity to the time period chosen, as we average the different latitudinal~~
481 ~~results (from the left panels) and add 8-yr sliding periods to this analysis of HCl changes.~~ The
482 near-global results are not too dependent on whether 6-yr or 8-yr periods are used, but longer
483 periods tend to smooth out the rates of change; interannual changes, including those arising from
484 the quasi-biennial oscillation (QBO), will affect short-term results, especially in the lower
485 stratosphere. It is worth noting (Fig. 10) that the patterns in the upper and lower stratosphere are
486 qualitatively similar, and that rates of change in surface emissions will impact both regions, but
487 carefully disentangling this from changes in the dynamics and in other constituents (e.g., CH₄)
488 that can affect the partitioning of chlorine species will require more analyses and modeling.

489

490 **4 GOZCARDS H₂O**

491 **4.1 GOZCARDS H₂O source data records**

492 We used water vapor datasets from HALOE, UARS MLS, ACE-FTS, and Aura MLS to generate
493 the monthly zonal mean source products for GOZCARDS H₂O.

494 In addition to the data screening procedures mentioned in Sect. 2, screening of HALOE H₂O
495 data for high aerosol extinction values was performed, in a way very similar to the method used
496 for the creation of merged H₂O for the Stratospheric Water vapor and OzOne Satellite
497 Homogenized (SWOOSH) dataset (Sean Davis, personal communication, 2013). This method
498 (see Fig. S4) screens out anomalous HALOE H₂O values that occurred mainly in 1991-1992,
499 when the aerosol extinction near 22 hPa exceeded $5 \times 10^{-4} \text{ km}^{-1}$; for pressure levels at and below
500 22 hPa, we have excluded the corresponding H₂O values. Also, for upper mesospheric HALOE
501 data used here, care should be taken during high latitude summer months, as no screening was
502 applied for the effect of polar mesospheric clouds (PMCs). High biases (by tens of percent) in
503 H₂O above ~70 km have been shown to occur as a result of PMCs in the HALOE field of view
504 (McHugh et al., 2003). Indeed, monthly mean values larger than 8-10 ppmv are observed in
505 GOZCARDS H₂O merged data and in HALOE source data for pressures less than ~0.03 hPa. A
506 more recent HALOE data version (version 20), or the version labeled VPMC based on the above
507 reference, could be used to largely correct such PMC-related effects, although this was not
508 implemented for GOZCARDS H₂O. The Aura MLS and ACE-FTS measurements, obtained at
509 longer wavelengths than those from HALOE, do not yield such large H₂O values; a rough
510 threshold value of 8.5 ppmv could also be used (by GOZCARDS data users) to flag the pre-2005
511 merged dataset.

512 UARS MLS stratospheric H₂O for GOZCARDS was obtained from V6 (or V600) H₂O data.
513 This data version is identical to the original prototype (named V0104) from Pumphrey (1999),
514 who noted that UARS MLS H₂O often exhibits drier values (by 5-10%) than HALOE H₂O (see
515 also Pumphrey et al., 2000). The resulting GOZCARDS H₂O monthly zonal means span the
516 period from Sep. 1991 through April, 1993. We note that a significant fraction of UARS MLS
517 tropical data values at 100 hPa are flagged bad (as a result of diminishing sensitivity).

518 Summarizing briefly past validation results, SPARC WAVAS (2000) analyses pointed out the
519 existence of a small low bias in HALOE stratospheric data versus most other measurements
520 (from satellites or other means), except for UARS MLS. Lambert et al. (2007) showed
521 agreement within 5-10% between Aura MLS version 2.2 stratospheric H₂O and other satellite
522 data, including ACE-FTS H₂O (see also Carleer et al., 2008), as well as for comparisons between
523 Aura MLS and balloon data; Aura MLS H₂O values are slightly larger than HALOE H₂O in the

524 stratosphere, with differences increasing to 10-15% in the mesosphere. Changes from MLS v2.2
525 to v3.3 led to an increase of 0.2-0.3 ppmv in stratospheric values (Livesey et al., 2013). Past
526 disagreements between aircraft water vapor measurements have made those datasets somewhat
527 difficult to use as absolute validation of satellite-derived H₂O in the upper troposphere and lower
528 stratosphere (UTLS) (Read et al., 2007, Weinstock et al., 2009). An intercomparison of
529 measurements under controlled chamber conditions has helped to better constrain this issue
530 (Fahey et al., 2014). Very good agreement exists between Aura MLS UTLS H₂O and
531 measurements from Cryogenic Frost point Hygrometers (CFH), as discussed by Read et al.
532 (2007) and Voemel et al. (2007) for MLS v2.2 data. At the lowest level (147 hPa) used here for
533 merged H₂O, the latter study showed a dry bias (by ~10%) in the MLS v2.2 data versus CFH.
534 Recent comparisons by Hurst et al. (2014) of MLS v3.3 H₂O data versus Boulder CFH time
535 series show excellent overall agreement, and no significant trend differences between coincident
536 profile sets. There is therefore support for systematic uncertainties as low as 5% for lower
537 stratospheric MLS data. Aura MLS stratospheric H₂O v3.3 values are slightly larger (by up to
538 ~5%) than the multi-instrument average from a number of satellite datasets, as discussed in
539 SPARC Data Initiative comparisons by Hegglin et al. (2013). No large disagreements in
540 interannual variations were noted by these authors for the GOZCARDS datasets ($p < 150$ hPa).
541 From the mid-stratosphere to the upper mesosphere, excellent agreement between ground-based
542 data from the Water Vapor Millimeter-wave Spectrometer (WVMS) and H₂O profiles from Aura
543 MLS and ACE-FTS has been demonstrated by Nedoluha et al. (2007, 2009, 2011).

544 **4.2 GOZCARDS H₂O merged data records**

545 The merging process for H₂O is nearly identical to the method used for HCl. The main difference
546 is an additional step that merges UARS MLS data with the already combined datasets from
547 HALOE, ACE-FTS, and Aura MLS, by simply adjusting UARS MLS values to the average of
548 the previously merged series during the early (1991-1993) overlap period; see Fig. S5 for an
549 illustration at 22 hPa for the 5°N latitude bin. Typically, this requires an upward adjustment of
550 the UARS MLS H₂O data, as these values are biased low versus most other datasets;
551 nevertheless, the fairly short but global record from UARS MLS helps to fill the time series.
552 After considering the channel drift issues for SAGE II H₂O (and following past advice from the

553 SAGE II team itself), we decided to use caution and did not include that dataset for GOZCARDS
554 merging, as some trend results could be affected to an unknown extent. Also, there is probably
555 some remaining retrieval contamination from volcanic aerosol effects for some time after the
556 volcanic eruptions of El Chichon (1982) and Mt. Pinatubo (1991), as well as after several smaller
557 eruptions; see Bauman et al. (2003) for a review of stratospheric aerosol climatology (1984-
558 1999) and Thomason et al. (2008) for the SAGE II stratospheric aerosol dataset.

559 Minor procedural merging details or issues for H₂O are included in the Supplement. Also,
560 data users should be aware of effects from unequal latitudinal sampling when no MLS data exist,
561 for regions where large latitudinal variations occur, as for H₂O at 147 hPa (the largest pressure
562 value). Indeed, global or latitudinal averages can be significantly biased in certain months and
563 month-to-month variability for such averages increases. This is because of poor sampling of the
564 full latitudinal variability, prior to Aug. 2004; after this, regular sampling exists from MLS every
565 month. Such variations in sampling can become an issue for temporal analyses of latitudinal or
566 global averages, unless additional fits or interpolations to mitigate such effects are undertaken.

567 In Fig. 11, we display the average offsets that were applied to the four H₂O source datasets;
568 these offsets follow previously known relative data biases (mentioned earlier). For example, low
569 biases in UARS MLS H₂O, especially in the mesosphere, were discussed by Pumphrey (1999)
570 and the UARS MLS offsets (see Fig. 11) correct that dataset upward. The application of offsets
571 derived for HALOE and UARS MLS raises the H₂O time series from these instruments, whereas
572 negative offsets lower the H₂O source data from ACE-FTS and Aura MLS. As we found for
573 HCl, the offset values generally display small variations versus latitude and are therefore fairly
574 stable systematic adjustments to the time series. Figure S6 displays the amplitudes of the fitted
575 annual cycles for HALOE, ACE-FTS, and Aura MLS. As for HCl, similar patterns emerge for
576 these datasets. Wintertime descent into the polar vortex regions is responsible for large annual
577 cycles at high latitudes, especially in the mesosphere; also, the seasonal impact of dehydration in
578 the lower stratospheric Antarctic region causes a large annual cycle in Aura MLS high southern
579 latitude data. Figure 12 provides some statistical information, as done for HCl in Sect. 3.2,
580 regarding the correlations and trend differences between ACE-FTS and Aura MLS. There are a
581 few regions with noisier relationships. While slow increases in H₂O are generally observed by
582 both instruments in the stratosphere and mesosphere, the tropical region near 0.1 hPa shows a

583 slight decreasing trend for the ACE-FTS points, thus leading to larger discrepancies; it is not
584 clear what the source of these discrepancies is. While the tropical ACE-FTS data are generally
585 sampled with a significantly lower temporal frequency, the same applies for all pressure levels;
586 however, a few outlier points can have a much larger impact when sampling is poorer. There are
587 also a few other spots, such as near 65°S and 65°N and near 5 hPa with a poor trend value for the
588 difference series, in comparison to the errors; this may be caused by a combination of poorer
589 sampling by ACE-FTS and higher atmospheric variability, which can lead to more scatter. At the
590 highest latitudes in the lower stratosphere, the observed slope differences are more within error
591 bars, but the larger variability means that a longer record is needed to determine if two time
592 series really trend differently. The main point here is to show the dataset characteristics and to
593 point out where the agreement is better or worse than typical. The merged dataset tends to be
594 much closer to Aura MLS in terms of trends because there are usually many more months of
595 Aura MLS data than ACE-FTS data, including the fact that the ACE-FTS time series (data
596 version 2.2) used here was halted for data after late 2010 due to technical retrieval issues.
597 Therefore, the overall impact of ACE-FTS data on the merged H₂O series is fairly small.

598 Figure S7 provides a visual representation of the merged GOZCARDS H₂O fields at
599 3 hPa and 68 hPa, respectively. Well-known features are displayed in these plots, given the good
600 global coverage in the post-2004 period in particular. In the upper stratosphere, descent at high
601 latitudes during the winter months leads to larger H₂O values, and low latitude QBO features are
602 also observed. In the lower stratosphere, one observes dehydration evidence at high southern
603 latitudes in the winter months, as well as a low latitude seasonal “tape recorder” signal; this
604 phenomenon is driven by tropopause temperatures and has been measured in satellite data since
605 the early 1990s (Mote et al., 1996; Pumphrey, 1999). A vertical cross-section of this lower
606 stratospheric tropical (20°S to 20°N) tape recorder in GOZCARDS merged H₂O for 1991-2013
607 is shown in Fig. 13; periods of positive anomalies alternate with negative anomalies, including
608 the post-2000 lows, as well as the most recent decreases in 2012-2013 (see also next section).

609 As we discussed for HCl, we have estimated systematic errors for the merged H₂O product.
610 This is illustrated by the contour plots in Fig. 14; these ranges encompass at least 95% of the
611 monthly mean source data values from HALOE, UARS MLS, ACE-FTS, and Aura MLS above
612 or below the merged series. These errors typically span 5 to 15% of the mean between 100 and

613 0.1 hPa; errors larger than 30% exist in the tropical upper troposphere (147 hPa), and similarly,
614 large values in the upper mesosphere arise from the low bias in UARS MLS H₂O.

615 **4.3 GOZCARDS H₂O sample results and discussion**

616 Stratospheric H₂O variations have garnered attention in the past two decades, because of the
617 radiative impacts of water vapor in the UTLS and the connection to climate change, as well as
618 the stratospheric chemical significance of H₂O oxidation products. H₂O can influence changes in
619 stratospheric and mesospheric ozone via the HO_x catalytic cycles. H₂O in the UTLS has a
620 significant radiative impact (e.g., Forster and Shine, 2002) and has the potential to influence
621 surface temperature changes in ways that could mitigate surface warming (Solomon et al., 2010)
622 if H₂O exhibits a significant drop, as was observed right after 2000. A decrease of about 1 ppmv
623 was also observed in *in situ* data (Fujiwara et al., 2010; Hurst et al., 2011; Kunz et al., 2013).
624 Randel et al. (2004, 2006) correlated this post-2000 decrease with a decline in tropical cold point
625 temperatures. An increasing trend in stratospheric H₂O since the 1950s (see Rosenlof et al.,
626 2001) will have a surface warming tendency. We expect to see continued studies of the influence
627 of cold point temperatures on stratospheric H₂O and the possible connections to changes in sea
628 surface temperatures (see Rosenlof and Reid, 2008; Garfinkel et al., 2013). Efforts to better
629 understand past changes in H₂O, and their causes and expected impacts, include the references
630 above, and (among others) Dvortsov and Solomon (2001), Shindell (2001), Nedoluha et al.
631 (2003), Urban et al. (2007), Dhomse et al. (2008), Scherer et al. (2008), Read et al. (2008), Tian
632 et al. (2009), Schoeberl et al. (2012), Fueglistaler (2012), Fueglistaler et al. (2013), and the
633 recent review of the tropical tropopause layer by Randel and Jensen (2013). The reconciliation of
634 long-term trends in tropopause temperatures with changes in lower stratospheric water vapor is a
635 task worthy of continued study, using additional datasets as well as model studies.

636 Individual water vapor datasets have been used here to produce a merged record now
637 spanning more than two decades. Linear trend estimates can be quite sensitive to the starting and
638 ending points of the time series, even for 22 years of data, and simple linear trends do not best
639 describe the variations in stratospheric H₂O over the past two decades. We do not attempt here to
640 characterize trends or to imply that recent tendencies will carry into the next decade or two.
641 Rather, as variability is also of interest to climate modelers, we provide information below

642 regarding observed decadal-type (longer-term) variability in stratospheric water vapor. Figure 15
643 illustrates monthly, annual, and longer-term changes in stratospheric water vapor, based on the
644 global GOZCARDS merged H₂O series; this shows the well-known H₂O minimum in the lower
645 tropical stratosphere as well as an increasing vertical gradient in the upper stratosphere (as a
646 result of methane oxidation). As we know from past studies (e.g., Randel et al., 2004), medium-
647 to long-term changes in H₂O are large-scale in nature. However, lower stratospheric H₂O
648 variations are more accentuated at low latitudes, in comparison to near-global (60°S-60°N)
649 results. It has long been known (e.g., from the *in situ* balloon-borne measurements of Kley et al.,
650 1979) that the hygropause is typically located a few km higher than the thermal tropopause; this
651 is consistent with the tape recorder and Brewer-Dobson circulation concepts. We observe low
652 water vapor mixing ratios at 68 hPa in the tropics, in comparison to 100 hPa values (near the
653 tropopause). According to the 22-year GOZCARDS data record, annually-averaged H₂O values
654 in the tropics (20°S-20°N) have varied between about 3.2 and 4.2 ppmv at 68 hPa. The rapid
655 drop between 2000 and 2001 is observed at 100 and 68 hPa, with some dilution of this effect at
656 higher altitudes. There is a clear difference in long-term behavior between the upper
657 stratosphere, where changes in methane should have the clearest influence, and the lower
658 stratosphere, especially in a narrow vertical region above the tropopause, where cold point
659 temperatures and dynamical changes have a significant impact. To first-order, the last few years
660 show ~10% larger values in the upper stratosphere than in the early 1990s, while the opposite
661 holds in the lowest stratospheric region, where a decrease of order 10% is observed over the
662 same period. The long-term upper stratospheric increase carries into the mesosphere (see below).
663 Figure 15 also shows that month-to-month and seasonal variations (thin lines) are usually
664 somewhat larger than the long-term changes in the lower stratosphere, most notably at 100 hPa.

665 In order to provide longer-term variability diagnostics for water vapor, we show in Fig. 16 the
666 minimum to maximum spread in annual averages (tropics and mid-latitudes) from Fig. 15. These
667 variability diagnostics are provided for the 22-yr period (1992 to 2013) and also separated into
668 the two 11-yr periods (thin and dashed lines); as expected, the 22-yr variability is always larger
669 than the variability in either of the two decadal period subsets. We also note that the tropical
670 variability is largest just above the tropopause (here this means at the 68 hPa GOZCARDS

671 level), where it reaches 20-28% (or 0.8 to 1 ppmv) depending on the time period. Such
672 variability diagnostics should be useful for comparisons to various chemistry climate models.

673 The longer-term variability in water vapor increases above the stratopause and reaches close
674 to 30% in the uppermost mesosphere, as seen in Fig. 17(a); this plot shows the monthly and
675 annual near-global (60°S-60°N) H₂O variations at 0.01 hPa. Large seasonal changes in this
676 region are driven by vertical advection associated with the mesospheric circulation, with each
677 hemisphere's summertime peaks contributing to the maxima (two per year) in these near-global
678 averages; such seasonal variations were compared to model results by Chandra et al. (1997),
679 based on the first few years of HALOE H₂O data. The strong upper mesospheric variability in
680 annual-mean H₂O is known from previous studies of ground-based and satellite H₂O data
681 (Chandra et al., 1997; Nedoluha et al., 2009; Remsberg, 2010), and this region is where the solar
682 (Lyman α) influence on H₂O is strongest. Figure 17(b) displays the near-global variations in
683 annual upper mesospheric H₂O from 0.1 to 0.01 hPa. We clearly see increased variability in the
684 uppermost mesosphere, and decreases in the mixing ratios as a result of H₂O photodissociation.

685 **5 GOZCARDS ozone**

686 A number of discussions relating to signs of ozone recovery have been presented before
687 (Newchurch et al., 2003; Wohltmann et al., 2007; Yang et al., 2008; Jones et al., 2009; Hassler
688 et al., 2011; Salby et al., 2011, 2012; Ziemke and Chandra, 2012; Gebhardt et al., 2013;
689 Kuttipurath et al., 2013; Kirgis et al., 2013; Nair et al., 2013, 2014; Shepherd et al., 2014, Frith et
690 al., 2014). While there are some indications of small increases in O₃ in the past 10-15 years,
691 further confirmation of an increase in global O₃ and its correlation with column increases, is
692 needed, in order to more clearly distinguish between long-term forcings, notably from the 11-yr
693 solar cycle, slow changes in halogen source gases, temperature changes, and shorter-term
694 variability. Continuing, good long-term ozone datasets are clearly needed for such studies.

695 **5.1 GOZCARDS ozone source data records**

696 We used ozone datasets from SAGE I, SAGE II, HALOE, UARS MLS, ACE-FTS, and Aura
697 MLS to generate the monthly zonal mean source products for GOZCARDS. Due to time
698 constraints, we did not use the newer SAGE II version 7 ozone (see Damadeo et al., 2013) as
699 part of the GOZCARDS merged dataset. Our studies indicate that there are systematic

700 differences of a few percent between SAGE II V6.2 and V7 O₃ on their native coordinates
701 (number density versus altitude). However, these 2 versions will exhibit different trends, mainly
702 in the upper stratosphere, after the data are converted to mixing ratios on pressure surfaces (as
703 shown later). These differences result mainly from different temperature trends between
704 MERRA and analyses from the National Centers for Environmental Prediction (NCEP), which
705 are used by the SAGE II V7 and V6.2 retrievals, respectively; the main differences between
706 MERRA and NCEP temperatures occur in the upper stratosphere for time periods before 1989
707 and after mid-2000. ~~After June 2000, SAGE II V6.2 O₃ at upper stratospheric pressures (≤ 3 hPa)
708 is not included in our merged data (see discussions in Sect. 5.2). In addition to the general data
709 screening methods (Sect. 2), HALOE O₃ was screened for aerosols based on recommendations
710 from Bhatt et al. (1999). Specifically, the O₃ profiles were screened for instances when either the
711 5.26 μm aerosol extinction exceeded 10^{-3} km^{-1} or a local aerosol extinction minimum was
712 present near the tropopause; all O₃ values at or below the identified levels were flagged bad.~~

713 **5.1.1 Treatment of SAGE ozone profiles**

714 Both SAGE I and SAGE II used solar occultations during satellite sunrise and sunset to measure
715 vertical profiles of ozone, along with other composition data and aerosol extinction (McCormick
716 et al., 1989; Cunnold et al., 1989). It takes about 1 month for SAGE I and II to provide near
717 global coverage (about 80°N to 80°S), with some dependence on season. The SAGE I
718 measurements started in February 1979 and stopped in November 1981, while SAGE II provided
719 data between October 1984 and August 2005. In the middle of July 2000, SAGE II had a
720 problem in its azimuth gimbal system. Although this was corrected by November 2000, the
721 instrument operation was switched to a 50% duty cycle, with either sunrise or sunset occultations
722 occurring in monthly alternating periods, until the end of the mission.

723 It has been known that there were altitude registration errors in SAGE I (V5.9) data
724 (Veiga et al., 1995; Wang et al., 1996). To correct this problem, an empirical altitude correction
725 method based on Wang et al. (1996) had been applied to SAGE I (V5.9) data; these corrected
726 SAGE I V5.9 profiles, which had been evaluated in previous trend studies (e.g. SPARC Report,
727 1998; WMO, 2003), were used to create the GOZCARDS SAGE I product (denoted as version
728 V5.9_rev). We did not use reprocessed version 6.1 SAGE I data (L. W. Thomason, personal

729 communication) because the altitude registration problems had not been completely fixed and
730 new altitude correction criteria should be derived and validated.

731 Ozone data screening details for the original SAGE I and SAGE II datasets are provided in
732 the Supplementary material. The number density profiles were converted to mixing ratios on
733 pressure levels by using NCEP temperature and pressure data provided with each profile.
734 Derived ozone profiles were then interpolated to fixed pressure levels on the following grid:

$$735 \quad p(i) = 1000 \times 10^{-\frac{i}{30}} \text{ (hPa)} \quad i = 0, 1, 2, \dots \quad (2)$$

736 Ozone values at each of the 5 levels centered on every GOZCARDS pressure level were then
737 averaged (weighted by pressure) to derive mixing ratios at each GOZCARDS pressure level. By
738 doing this, the SAGE profiles were smoothed to a vertical resolution comparable to that of the
739 other satellite instruments used in this GOZCARDS work. Monthly zonal means were then
740 computed for the SAGE ozone datasets on the GOZCARDS-compatible grid.

741 **5.1.2 Comparisons of ozone zonal means**

742 O₃ differences between SAGE II and other satellites are shown in Fig. S8. Zonal mean
743 differences between SAGE II and HALOE are generally within 5% for 1.5 to 68 hPa at mid-
744 latitudes, and for 1.5 to 46 hPa in the tropics. The relative biases are larger outside those ranges
745 and increase to ~10% near the tropopause and also near 1 hPa. SAGE II data show better
746 agreement with UARS and Aura MLS in the upper stratosphere and lower mesosphere, within
747 5% up to 0.68 hPa and for latitudes outside the polar regions. Aura MLS O₃ compares better with
748 SAGE II data than does UARS MLS in the tropics for pressures larger than 68 hPa; the high bias
749 in UARS MLS O₃ at 100 hPa has been discussed previously (Livesey et al., 2003). There are no
750 months that include both SAGE II and ACE-FTS data in the northern hemisphere tropics (see the
751 gap in Fig. S8, bottom right panel), largely due to the poorer coverage from ACE-FTS in the
752 tropics. ACE-FTS O₃ shows the largest positive bias (greater than 10%) with respect to SAGE II,
753 for pressures less than 1.5 hPa. The high bias in upper stratospheric ACE-FTS ozone has been
754 mentioned in past validation work using ACE-FTS data (e.g., Froidevaux et al., 2008; Dupuy et
755 al., 2008). The biases shown here are also consistent with recent O₃ intercomparison studies from
756 a comprehensive array of satellite instruments by Tegtmeier et al. (2013). It has been known for
757 some time that the HALOE and SAGE II ozone datasets, which govern the main variations of the

758 GOZCARDS merged ozone values before 2005, agree quite well (within 5%) in absolute value,
759 and also in terms of temporal trends (Nazaryan et al., 2005), and versus ozonesondes (mostly
760 above ~20 km or ~50 hPa). Larger percentage differences occur in the lowest region of the
761 stratosphere at low latitudes, and especially in the upper troposphere, where HALOE values
762 become significantly smaller than SAGE II data, which are already biased low (by ~50%) versus
763 sondes (Wang et al., 2002); see also Morris et al. (2002), as well as results of SAGE II and
764 HALOE comparisons versus solar occultation UV-Visible spectrometer measurements from long
765 duration balloons (Borchi et al., 2005). We should note here that in this GOZCARDS merging
766 work, we have largely avoided the upper tropospheric region.

767 Zonal mean differences between SAGE II and Aura MLS show some latitudinal structure
768 between 1 and 3 hPa, with larger (5-10%) biases in the southern hemisphere, especially for 0 to
769 30°S (see Fig. S8). There are no such features between SAGE II and HALOE or UARS MLS.
770 We found that this results from anomalous NCEP temperatures after 2000, which affect SAGE II
771 data converted from number density/altitude to GOZCARDS VMR/pressure coordinates.
772 Figure 18 shows an example of the ozone series from SAGE II and other satellite data for 10°S to
773 20°S from 1 to 6.8 hPa. At 1 hPa, SAGE II ozone drifts and is elevated after mid-2000, when
774 compared to HALOE. Similar features are found down to pressures near 3 hPa. These anomalous
775 values can be attributed to abnormal NCEP temperature trends compared to MERRA and
776 HALOE during the same time period (for detailed views, see Figs. S9 and S10). Issues relating
777 to anomalous upper stratospheric NCEP temperature trends were noted by McLinden et al.
778 (2009). Because such NCEP-related artifacts are confirmed by both MERRA and HALOE, we
779 decided not to include in the merging process any SAGE II O₃ values after June 30, 2000 for
780 pressures equal to or less than 3.2 hPa. SAGE II ozone is not significantly affected by the
781 conversion to mixing ratio/pressure coordinates at 4.6 and 6.8 hPa (Fig. 18).

782 **5.2 GOZCARDS ozone merged data records**

783 **5.2.1 Methodology for GOZCARDS merged ozone**

784 Ozone measurements from SAGE I, SAGE II, HALOE, UARS MLS, Aura MLS and ACE-FTS,
785 as described in Sect. 5.1, were used to establish a near-continuous monthly zonal mean record

786 from late 1979 through 2012 for the GOZCARDS merged O₃ product (ESDR version 1.01). ~~The~~
787 ~~monthly means from each instrument were produced after applying the screening described in~~
788 ~~Sect. 5.1.~~ The SAGE II dataset was used as a reference standard, since it has the longest period
789 of measurements and has been extensively validated. A GOZCARDS ozone merged data record
790 is constructed by combining these measurements after removing systematic biases with respect
791 to SAGE II. This is done by applying additive offsets to all other instrument series, as
792 determined from average differences between monthly zonal means and SAGE II during overlap
793 time periods. The merged data are then derived by averaging all available adjusted datasets.
794 Because there are gaps in overlap between SAGE II and ACE-FTS monthly mean data in some
795 latitudes (Fig. S7), and as SAGE II ozone VMRs obtained from the vertical grid transformation
796 were affected by anomalous NCEP temperatures after mid-2000 for pressures smaller than or
797 equal to 3.2 hPa, a two-step approach is used to generate the merged product. First, SAGE II data
798 are used as reference for pressures larger than 3.2 hPa to adjust HALOE, UARS MLS and Aura
799 MLS based on overlapping months between 1991 and Nov. 2005; see the method overview
800 schematic in Fig. 19. For $p \leq 3.2$ hPa, SAGE II O₃ is still used as a reference through June 2000,
801 and HALOE and UARS MLS data are adjusted accordingly. This eliminates the effect of
802 anomalous NCEP temperatures on SAGE II ozone and leads to more accurate offsets based on
803 HALOE values, after they have been adjusted to SAGE II. The adjusted HALOE data (denoted
804 as HALOE* in Fig. 19) are then used as a reference to derive estimated offsets for Aura MLS O₃,
805 using the overlap period with HALOE from Aug. 2004 to Nov. 2005. In step 2, a new reference
806 value is derived by averaging all available data from SAGE II, HALOE*, UARS MLS* and
807 Aura MLS*. This new reference value is then used to adjust the ACE-FTS ozone values based
808 on all overlapping months between March 2004 and Nov. 2005. By including Aura MLS in the
809 dataset created in step 1, we obtain more complete spatial and temporal coverage than possible
810 with SAGE II and HALOE, and ensure that there are overlapping months between this combined
811 dataset and ACE-FTS source data. At the end of step 2, the final merged ozone is derived by
812 averaging the temporary merged dataset from step 1 with the adjusted ACE-FTS data values.

813 **5.2.2 Further considerations regarding GOZCARDS merged ozone data**

814 ~~Diurnal changes in ozone can affect measurement comparisons and could impact data merging.~~
815 ~~Measurements and models of the ozone diurnal variation from the lower stratosphere to the~~

816 mesosphere have been discussed previously (Ricaud et al., 1996; Haefele et al., 2008; Huang et
817 al., 2010). Sakazaki et al. (2013) presented diurnal changes measured by the Superconducting
818 Submillimeter Wave Limb Emission Sounder (SMILES), and Parrish et al. (2014) have analyzed
819 ground-based microwave ozone profile variations versus local time in conjunction with satellite
820 datasets. These studies indicate that ozone diurnal variations range from a few percent in the
821 lower stratosphere to more than 10% in the upper stratosphere and lower mesosphere. SAGE II
822 and other occultation instruments observe ozone at local sunrise or sunset, and the retrieved
823 values are generally closer to nighttime values in the upper stratosphere and mesosphere. To
824 characterize systematic differences between satellite data, coincident profiles with small
825 differences in space and time are most often used; an example of mean differences and standard
826 deviations between SAGE II and Aura MLS using both coincident profile and zonal mean
827 methods is provided in Fig. S11. SAGE II and coincident Aura MLS nighttime O_3 values agree
828 within $\sim 5\%$ between 0.46 and 100 hPa, except in the tropical lower stratosphere where
829 comparisons are noisier due to weak O_3 signals and strong dynamical variability. Differences
830 between zonal mean SAGE II and Aura MLS data are very close to the differences from
831 averaged coincident values, except for pressures less than 2 hPa, where differences between the
832 methods increase from a few % to $\sim 10\%$ at 0.3 hPa, consistent with what one expects from the
833 diurnal cycle. Biases between SAGE II and Aura MLS based on coincident profiles versus zonal
834 means could be different by more than 5% in the upper stratosphere and above. Zonal mean
835 differences are likely to be less representative of “true” differences between the two instruments.
836 By combining SAGE II with Aura MLS data adjusted by zonal mean biases, we provide a series
837 adjusted to the average of sunrise and sunset, as measured by SAGE II. However, if Aura MLS
838 data were adjusted by biases obtained using the coincident method, an upper stratospheric offset
839 of several percent and artificial trends due to such a diurnal cycle effect could be introduced.

840 —Even in the absence of diurnal variations, measurements from occultation sensors can yield
841 larger sampling errors than those from more densely sampled emission measurements (Toohey
842 et al., 2013). The use of long term data with consistent sampling should be an advantage for
843 trend detection. Avoiding SAGE II data after mid-2000 also mitigates potential artifacts arising
844 from different SAGE II sunrise/sunset sampling patterns versus time. The HALOE sampling
845 remained fairly balanced between SR and SS events over its mission duration, although there

846 ~~were also more data gaps in the later years. Similarly, the Aura MLS ozone data generated here~~
847 ~~are averaged from local times roughly in the middle of the day and the middle of the night, with~~
848 ~~repeatable and stable patterns over the years; ACE-FTS sampling patterns are also quite stable.~~

849 Figure 20 displays the average ozone offsets obtained from the calculated biases versus
850 SAGE II data. The effect of a high bias in upper stratospheric and lower mesospheric ozone from
851 ACE-FTS relative to other datasets is made evident by the need to apply a negative offset as
852 large as 25% to the ACE-FTS series. Most of the stratospheric offsets applied to the other
853 instrument datasets are in the 5-10% range; a lowering of O₃ from UARS MLS, HALOE, and
854 Aura MLS in the lower mesosphere is generally required to match the SAGE II values. Sampling
855 differences and data sparseness may be responsible for larger offsets at the highest latitudes. In
856 these regions, more caution is required with the merged data, which is also less amenable to
857 long-term analyses because of data gaps and larger variability (especially prior to 2004).

858 As shown in the Supplement (Fig. S12), we observe strong similarities in the ozone annual
859 cycle amplitude patterns from SAGE II, HALOE, ACE-FTS, and Aura MLS over their
860 respective measurement periods (e.g., peaks at midlatitudes near 10 hPa and 1.5 hPa). The
861 middle stratospheric peaks are a result of the annual cycle in oxygen photolysis, whereas
862 temperature variations drive the annual cycle in the upper stratosphere (Perliski et al., 1989).
863 This sort of comparison provides some (first-order) reassurance regarding the consistency of the
864 various datasets. For further details, Fig. 21 provides diagnostics similar to those presented for
865 HCl and H₂O, namely the correlation coefficients and significance ratios for the slopes of the
866 deseasonalized anomaly time series from SAGE II versus HALOE as well as from ACE-FTS
867 versus Aura MLS (for 1992 through 1999, and 2005 through 2009, respectively). These
868 diagnostic results for ACE-FTS and Aura MLS are of a quality that is comparable to the
869 HALOE/SAGE II results; poorer fits occur mostly at high latitudes and in the upper stratosphere.
870 Poorer correlations at upper altitude appear largely tied to a decrease in the amount of valid data
871 in this region (especially at high latitudes), coupled with a relatively small variability. For
872 regions with poorer agreement between ACE-FTS and Aura MLS, we often see small variability
873 in the series from Aura MLS but larger changes (scatter) in the ACE-FTS series. Larger
874 differences in trends between SAGE II and HALOE were noted by Nazaryan et al. (2005) at low
875 latitudes near 50 km; this is also indicated by our simple linear fits (not shown here) to the

876 GOZCARDS source datasets from these two instruments and the existence of poorer agreements
877 in Fig. 21 (2nd panel from top) for the slope of the differenced (anomaly) series in that region.
878 The existence of good correlations in interannual ozone variations between a large number of
879 satellite measurements was discussed by Tegtmeier et al. (2013). Regarding temporal drifts, Nair
880 et al. (2012) have shown that small drifts (mostly within about $\pm 0.5\%/yr$ for the 20-35 km
881 region) exist between most of the datasets from six ozone lidar sites and coincident HALOE,
882 SAGE II, and Aura MLS measurements; similar results were obtained at two of these sites by
883 Kirgis et al. (2013). Other recent or ongoing studies (in particular, the comprehensive study by
884 Hubert et al., 2015) corroborate the very good stability of the longer-term ozone datasets used for
885 GOZCARDS, which relies most heavily on data from SAGE II and Aura MLS. Jones et al.
886 (2009) also studied the consistency of various satellite datasets (including SAGE II and HALOE)
887 for 1979-2008; they concluded that small relative drifts existed between their averaged series and
888 individual instrument series, although they did find that larger inter-instrument drifts exist in the
889 extra-tropical upper stratosphere. While we feel justified in the use of the longer-term time series
890 and generally robust datasets chosen for GOZCARDS O₃, data users should still note the
891 existence of a few regions with poorer correlations or trend agreement (and, therefore, larger
892 uncertainties) between different satellite ozone datasets, as indicated in Fig. 21. Long-term
893 merged datasets from GOZCARDS and other sources should undergo continued scrutiny from
894 the community, as done recently for trends by Tummon et al. (2014) and Harris et al. (2014).
895 Sample cross-sectional views of two slices through the GOZCARDS merged O₃ field are
896 provided in the Supplement (Fig. S13). Figure 22 shows estimated systematic errors from our
897 calculation of the 95% ranges for the monthly mean source data used here, both above and below
898 the merged values. In this case, as SAGE II is used as a reference dataset, the applied offsets
899 (Fig. 20) correlate quite well with this plot depicting the ranges about SAGE II values. Minimum
900 error bars can be slightly lower than 5% for the middle stratosphere at low latitudes, where ozone
901 values are largest. This view of systematic error bars is generally consistent with results by
902 Tegtmeier et al. (2013), who used a standard deviation measure, based on the larger set of
903 satellite datasets analyzed for the SPARC Data Initiative. They also found that the regions with
904 lowest errors (scatter) are in the middle stratosphere at low to mid-latitudes, where most monthly
905 mean satellite data fit within $\pm 5\%$ of the multi-instrument mean.

906 **5.3 GOZCARDS ozone sample results and discussion**

907 Nair et al. (2013) used regression analyses to compare profile trend results from GOZCARDS
908 merged O₃ at northern midlatitudes versus a combined O₃ dataset from lidar and coincident
909 satellite data at the Observatoire de Haute Provence (OHP), France. They showed that good
910 consistency exists for the decreasing ozone time period, from the early 1980s to 1997, and for the
911 upper stratospheric increase since 1997, but some differences exist in the lower stratosphere
912 during this second time period, when the GOZCARDS results show a near-zero trend in
913 comparison to small positive trends from the combined (and more localized) dataset. The above
914 results for the declining time period agree broadly with earlier work (for the 1979-1997 period)
915 by Jones et al. (2009), who averaged various satellite ozone datasets and produced trend
916 estimates; however, these authors obtained only a small positive, but statistically insignificant,
917 linear trend for the post-1997 phase, most likely because of too short a time series at that time.
918 Gebhardt et al. (2013) analyzed ozone profile trends from SCIAMACHY on ENVISAT, and
919 compared this to trends from Aura MLS, Optical Spectrograph and InfraRed Imager System
920 (OSIRIS) on the Odin satellite, and sondes; their results include the detection of localized ozone
921 increases in the mid-stratosphere at low latitudes; see also Bourassa et al. (2014), who analyzed
922 merged SAGE II and (OSIRIS) observations for 1984-2013, as well as results from Kyrölä et al.
923 (2013) on combined SAGE II and Global Ozone Monitoring by Occultation of Stars (GOMOS)
924 records for 1984-2012, and Eckert et al. (2014), who investigated ENVISAT MIPAS trends for
925 2002-2012. The shortness of data records since 1997, coupled with relative variability and
926 potential drifts between various measurements may explain some differences in recent trend
927 results, notably for the post-1997 period. More comprehensive analyses from the SI²N initiative
928 have focused on an intercomparison of profile changes from a variety of datasets, including
929 GOZCARDS and other merged records (Tummon et al., 2014; Harris et al., 2014).

930 Here, we investigate ozone column results based on the global GOZCARDS dataset, given
931 the work by Ziemke and Chandra (2012), hereafter generally referenced to as ZC12; these
932 authors analyzed total column and stratospheric column data from satellite measurements, and
933 their analyses yielded a rather strong near-global (60°S-60°N) average ozone increase since
934 1998. Their stratospheric column measurements depend on the convective-cloud differential
935 (CCD) method, which uses Total Ozone Mapping Spectrometer (TOMS) and Ozone Monitoring

936 Instrument (OMI) column ozone data over convective clouds near the tropopause; below the
937 clouds, little sensitivity exists, so the method can lead to stratospheric column estimates,
938 especially in the tropics, where good cloud-related data of this kind exist. For midlatitudes, their
939 methodology has focused on ozone data over the Pacific, along with a few assumptions relating
940 to cloud heights and longitudinal invariance, in order to try to represent zonal mean stratospheric
941 columns (see also Ziemke et al., 2005). In Fig. 23, we show the near-global total and
942 stratospheric column values from ZC12 (J. Ziemke, private communication, 2013), along with
943 (unscaled) GOZCARDS column densities down to three pressure levels (68, 100, and 215 hPa)
944 for mid-latitudes (30°S-60°S and 30°N-60°N), low latitudes (30°S-30°N), and a near-global
945 range (60°S-60°N). In an absolute sense, the GOZCARDS near-global columns above 215 hPa
946 are larger than the ZC12 stratospheric columns, but quite close to the total column amounts from
947 ZC12. Not too surprisingly, the GOZCARDS column values above 100 hPa are slightly lower
948 than the stratospheric columns from ZC12, as the latter columns (estimated down to cloud tops)
949 will capture more of the lower stratosphere in the extra-tropics. Most of the near-global decrease
950 comes from the midlatitudes, as more of the lower stratospheric column resides in these regions,
951 in an absolute sense. Randel and Thompson (2011) obtained small decreases (-2 to -4% per
952 decade) in tropical lower stratospheric ozone for 1985-2009, from a combination of SAGE II
953 ozone and sonde data from the Southern Hemisphere Additional Ozonesondes (SHADOZ)
954 network. A fairly strong increase is observed from 2008 to 2010 at northern midlatitudes (orange
955 curves); Steinbrecht et al. (2011) attributed large ozone enhancements in that region in 2010 to a
956 coupling between the quasi-biennial and Arctic oscillations (and the North Atlantic oscillation).
957 Long-term halogen source gas reductions that have occurred since the mid-1990s should only
958 lead to an ozone increase of a few DU since 1997 (Steinbrecht et al., 2011).

959 In Fig. 24, we compare the changes in 60°S-60°N ZC12 column ozone data to the
960 GOZCARDS column amounts above 68 hPa for that region; note that GOZCARDS values do
961 not provide for a continuous long-term time series down to pressures of 100 hPa (or more) in the
962 SAGE I years (1979-1981). To eliminate biases between stratospheric columns as calculated
963 using the CCD methodology and the GOZCARDS fixed bottom pressure approach, we reference
964 all stratospheric columns to the 1980 total column value. These column series include the SAGE
965 I data record and are linearly interpolated between 1981 and 1984, when no GOZCARDS source

966 datasets exist. We observe that the relative changes in GOZCARDS columns follow the ZC12
967 curves within a few DU in the downward phase until about 1992, but the 1992-1997 decrease in
968 total columns does not compare very well. Some of this discrepancy may be because total
969 columns capture a stronger decrease from levels below 68 hPa, not fully represented in
970 GOZCARDS columns; there are also gaps in ZC12 stratospheric columns in 1993-1996 and
971 other years. Focusing on the late period for GOZCARDS data from Aura MLS and ACE-FTS,
972 we also show the GOZCARDS columns above 68 hPa, referenced to 2007 instead of 1980.
973 There is a good match in the variations between GOZCARDS and ZC12 columns during 2005-
974 2010, in agreement with the fact that very good correlations were obtained by ZC12 between
975 Aura MLS column variations and stratospheric column data from the CCD technique. The ZC12
976 values for stratospheric and total columns are in good agreement, although the stratospheric
977 values have gaps when not enough data were present for near-global estimates. Also, the large
978 increase in ZC12 data from 1997 to 1998 is not matched very well by GOZCARDS column data.

979 We removed the solar cycle from the deseasonalized anomalies, as was done in the ZC12
980 study, namely via a regression fit and subtraction of that component from the time series. In the
981 resulting plots (see Fig. 25), a 3-year smoothing is also applied (as done by ZC12). We focus in
982 these plots on the total time period from 1979 onward, and therefore, on the GOZCARDS
983 columns above 68 hPa. While agreement exists at the few DU level between the ZC12 relative
984 changes and the GOZCARDS columns, the apparent ‘recovery’ in the ZC12 datasets is quite
985 large (~3%) and is not matched by the changes in GOZCARDS columns. The latter columns
986 show an increase of less than 0.8% between 2001 and 2011, with some decrease (by ~ 0.5%)
987 from 2011 to 2013. We note that the recent analyses by Sheperd et al. (2014), who used a
988 chemistry-climate model constrained by observed meteorology to investigate potential causes of
989 long-term total column ozone variations, show a partial return, in 2010, towards the 1980 ozone
990 levels (for 60°S-60°N), but not nearly as much as implied by ZC12, neither in the model, nor in
991 the observations. It is possible that the discrepancies lie in the various datasets and their merging;
992 for example, it would be worthwhile to check if homogenized SBUV column O₃ data show
993 results that are substantially different from those of ZC12. Alternatively, the discrepancies could
994 mainly reflect differences between the coverage or meaning of the different ozone columns used
995 here (because of different methodologies, grids and/or sampling to properly determine a near-

996 global result). Although most column discrepancies are not that large as a percent of the total
997 column values, a better consensus regarding the recovery of near-global ozone columns (and
998 profile values discussed in other recent references) will be desirable in the future.

999 **6 Other GOZCARDS data records**

1000 We now briefly mention the three other datasets that were part of the delivery of GOZCARDS
1001 records for public dissemination in 2013, namely N₂O, HNO₃, and temperature. For N₂O and
1002 HNO₃, the somewhat simpler merging procedure consisted of averaging the source datasets from
1003 ACE-FTS and Aura MLS over the overlap time period (Aug. 2004 through Sep. 2010) to obtain
1004 the additive offsets for each of the two individual records. We then simply used the
1005 correspondingly-adjusted and averaged series to create the merged results; this procedure is the
1006 same as we described for the first step in the HCl (or H₂O) merging process.

1007 **6.1 N₂O**

1008 This data set starts in August 2004, when the Aura MLS data record began; the only dataset after
1009 Sep. 2010 is the Aura MLS N₂O (version 3.3) data record, because we no longer had ACE-FTS
1010 version 2.2 data after that time due to ACE-FTS data processing issues mentioned earlier.
1011 Because of degradation in the main target MLS N₂O band (near 640 GHz) after the first few
1012 months of 2013, the N₂O standard MLS product will be reprocessed for the whole Aura MLS
1013 period using an alternate measurement band and an updated software version. As discontinuities
1014 in the version 3.3 MLS data are introduced after mid-2013, when the standard N₂O product was
1015 replaced with results from the 190 GHz band, there are currently no GOZCARDS N₂O zonal
1016 mean data after 2012 based on the original (640 GHz) MLS N₂O measurement band.

1017 Validation results for the first few years of Aura MLS and ACE-FTS N₂O data were provided
1018 by Lambert et al. (2007) and Strong et al. (2008), respectively. Livesey et al. (2013) provided a
1019 minor update regarding the v3.3 Aura MLS N₂O data used here, which show typically small
1020 differences (within $\pm 5\%$) in comparison to v2.2 data. The references mentioned above showed
1021 that excellent agreement (mostly within 5%) exists between the stratospheric ACE-FTS and Aura
1022 MLS N₂O profiles. Plots showing the average offsets applied to both MLS and ACE-FTS N₂O
1023 series as a function of latitude and pressure are provided in Fig. S14. These plots are in

1024 agreement (in magnitude and in sign) with the above-referenced studies; the two datasets yield
1025 typical offsets (one half of the average differences) of less than 5%. Also, very good temporal
1026 agreement between these two time series (for 2004-2010) is illustrated by the quality of the N₂O
1027 diagnostic information displayed in Fig. S15 (computed as for other MLS and ACE-FTS
1028 comparisons discussed in this work). This generally shows very highly correlated fields, with
1029 insignificant drifts between the two separate time series of deseasonalized N₂O data; the poorest
1030 correlations are obtained near 100 hPa in the tropics.

1031 Figure 26 shows sample contour plots for the N₂O merged field (2004-2012); as seen from the
1032 bottom panel (100 hPa), wintertime descent brings low N₂O values down at high latitudes (inside
1033 the polar vortices). N₂O is a conserved tracer in the lower stratosphere and its variations near the
1034 tropopause have implications regarding age of air. Variations in upper stratospheric N₂O are
1035 clearly affected by seasonal and dynamical effects; this is evident from the striking semi-annual,
1036 annual and QBO-related patterns displayed in Fig. 26 for the 6.8 hPa level (top panel).

1037 **6.2 HNO₃**

1038 As for N₂O, we merged the HNO₃ data from ACE-FTS (version 2.2) and Aura MLS (version
1039 3.3) from Aug. 2004 onward, and included only the adjusted MLS dataset after Sep. 2010. The
1040 average offsets applied to MLS and ACE-FTS time series as a function of latitude and pressure
1041 for HNO₃ are provided in Fig. S16. The typical offsets (one half of the average differences) for
1042 HNO₃ are less than ~10% (and less than 0.5 ppbv). Despite somewhat larger percent absolute
1043 differences than for N₂O between Aura MLS and ACE-FTS HNO₃, there is very good agreement
1044 as a function of time between these two datasets in the stratosphere. This is illustrated by the
1045 quality of the HNO₃ diagnostic information provided in Fig. S17; the poorest correlations are
1046 obtained at or below the tropical tropopause.

1047 Comparisons of v3.3 Aura MLS and v2.2 ACE-FTS nitric acid profiles have shown good
1048 agreement (see also Livesey et al., 2013), as the MLS HNO₃ v3.3 values are now generally larger
1049 than in v2.2, for which validation results were provided by Santee et al. (2007). Wolff et al.
1050 (2008) also compared MLS (v2.2) and ACE-FTS (v2.2) coincident profiles, and obtained similar
1051 results; in addition, they demonstrated that very good agreement exists between the HNO₃
1052 profiles from ACE-FTS and coincident profiles from MIPAS on Envisat. Also, comparisons

1053 between Aura MLS HNO₃ (v3.3) profiles and wintertime HNO₃ profiles retrieved by a Ground-
1054 based Millimeter-wave Spectrometer (GBMS) in Thule, Greenland, during the first 3 months of
1055 2010, 2011, and 2012 have shown good agreement, mostly within 10-15% (Fiorucci et al., 2013).

1056 Figure 27 (top two panels) displays the HNO₃ fields at 46 hPa from the UARS MLS period
1057 (1991-1997) as well as from the 2004-2013 period, for which a merged GOZCARDS product
1058 was produced, based on Aura MLS and ACE-FTS source datasets. Also shown (bottom two
1059 panels) are time series for 45°N and 32 hPa from both these periods; the bottom right panel
1060 includes the source and merged time series. We have performed additional investigations (not
1061 shown here) which lead us to believe that small upward adjustments to the UARS MLS HNO₃
1062 values (by about 10%) are needed to better cross-correlate these datasets across the two distinct
1063 time periods; such relative biases are within the expected systematic errors. This is based on a
1064 consideration of ground-based Fourier Transform infrared column HNO₃ data covering the full
1065 time period, as well as past GBMS HNO₃ profile retrievals. Also, Aura MLS and ACE-FTS
1066 HNO₃ data match ground-based and other correlative data quite well, and typically better than
1067 the (intrinsically poorer quality) UARS MLS HNO₃ data. However, obtaining an optimum global
1068 set of adjustments for the UARS MLS nitric acid field will be limited by the number of sites with
1069 such ground-based data (as well as by the different vertical resolutions for these datasets versus
1070 MLS). More collaborative work regarding such analyses is needed in order to find the optimum
1071 adjustments to help tie together these two time periods for this species. Although we did not
1072 deliver the UARS MLS HNO₃ source data files for GOZCARDS, we could provide these
1073 monthly zonal mean series upon request, keeping the above caveats in mind.

1074 **6.3 Temperature**

1075 Finally, in terms of the initial set of delivered GOZCARDS products, and for the convenience of
1076 stratospheric composition data users, we have used temperatures (T) from the Modern-Era
1077 Retrospective Analysis for Research and Applications (MERRA) to produce a monthly mean
1078 GOZCARDS temperature data set from 1979 onward. MERRA is a NASA Goddard reanalysis
1079 (Rienecker et al., 2011) for the satellite era using Goddard Earth Observing System Data
1080 Assimilation System version 5 (GEOS-5); T is from the DAS 3d analyzed state MAI6NVANA,
1081 version 5.2 files (such as MERRA300.prod.assim.inst6_3d_ana_Nv.20110227.hdf). Data from

1082 four daily MERRA files (for 00, 06, 12, and 18 hr UT) were averaged to provide daily mean
1083 temperature fields (appropriate for a mean time of 09 hr). Vertical interpolation was performed
1084 onto the GOZCARDS pressure grid, which, for temperature, covers 30 pressures levels from
1085 1000 hPa to 0.0147 hPa. Averaged values were stored for the 10° GOZCARDS latitude bins, and
1086 daily results were binned to create the GOZCARDS monthly temperature data set (version 1.0).

1087 **7 Summary and conclusions**

1088 We have reviewed the MEaSURES GOZCARDS project's production of merged data records of
1089 stratospheric composition using carefully screened satellite data, starting in 1979 with SAGE I
1090 O₃ and continuing with Aura MLS and ACE-FTS data. The source datasets have a high degree of
1091 maturity, and we have reinforced our confidence in their usefulness through investigations of
1092 various diagnostics (offsets, annual cycle amplitudes, temporal correlations and trend differences
1093 of deseasonalized series). We have focused here on the relatively long-term data records for HCl,
1094 H₂O, and O₃. These records are publicly available as GOZCARDS ESDR version 1.01 and can
1095 be referenced using DOI numbers (Froidevaux et al., 2013b, Anderson et al., 2013, and Wang et
1096 al., 2013, for the above species, respectively). The other GOZCARDS data records mentioned
1097 here also have dataset references, namely Schwartz et al. (2013) for the MERRA-based
1098 temperature records, and Froidevaux et al. (2013c, 2013d) for N₂O and HNO₃, respectively.
1099 Table 2 provides a summary of the monthly mean datasets produced for GOZCARDS. Yearly
1100 netCDF files were delivered to the GES DISC for public access (see
1101 <http://mirador.gsfc.nasa.gov>, where a README document is also available, see Froidevaux et
1102 al., 2013a). Temperature records based on MERRA are also included on the GOZCARDS grid
1103 (see Sect. 1). The merging methodology follows from the determination of mean biases (for each
1104 pressure level and 10° latitude bin) between satellite instrument datasets, based on the overlap
1105 periods between the various series. Each species is treated separately: for ozone, SAGE II data
1106 are the chosen reference, whereas for other species, the approach is equivalent to an average of
1107 the datasets during the periods of overlap. The merged data files contain the average offset
1108 values that were applied to each source data time series, along with standard deviations and
1109 standard errors. The GOZCARDS README document provides more details about the
1110 GOZCARDS data file quantities, including local time and solar zenith angle information, and a
1111 list of days with available data for each month. We have also presented here a compilation of

1112 systematic error estimates about the merged values. While it is difficult to identify error sources
1113 specifically, we find that typical estimated systematic errors (ranging from ~5% to 15% for
1114 composition data) are consistent with the magnitude of observed relative biases.

1115 The GOZCARDS HCl merged record in the upper stratosphere enables us to track long-term
1116 changes in this reservoir for stratospheric chlorine, and by implication, total stratospheric
1117 chlorine. The long-term increase in HCl prior to the late 1990s, and the subsequent gentler
1118 decrease in the 21st century, are delayed manifestations of changes in the sum of the surface
1119 source gas abundances as a result of regulations from the Montreal Protocol (and its
1120 amendments). From 1997 to 2010, the average rate of change in upper stratospheric HCl (50°S to
1121 50°N) was about -0.4 to -0.7%/yr. There are smaller rates of decrease and a flattening or slight
1122 turn-around after 2003. In the lower stratosphere, where Aura MLS data weigh in heavily, recent
1123 short-term variations have shown a flattening out and, in particular for northern midlatitudes and
1124 at 50-70 hPa for the deep tropics, a significant reversal and increasing trend, compared to the
1125 decrease from the late 1990s to about 2004. Mahieu et al. (2014) have discussed the reversal in
1126 total column HCl trends for 2007-2012 (for northern, not southern midlatitudes), based on
1127 ground-based FTIR series at various sites; they also showed that column trends agree with those
1128 from lower stratospheric GOZCARDS abundances for the appropriate latitude bands. However,
1129 lower stratospheric HCl tendencies appear to be reversing in recent years (2011-2014), with
1130 decreases at northern midlatitudes (see Fig. 7 for 32 hPa) and some increasing tendencies at
1131 southern midlatitudes (Fig. 7). Continued data will be needed to track such short-term changes in
1132 HCl, but we expect to see long-term global HCl decreases in both upper and lower stratosphere,
1133 as long as the Montreal Protocol and its amendments are adhered to; also, surface chlorine shows
1134 smaller rates of decrease in recent years, for reasons that are largely understood (Sect. 3).

1135 For water vapor, we have merged monthly mean datasets for 1991-2013 from the same
1136 satellite instruments as for HCl using the same basic methodology, except for the addition of
1137 1991-1993 UARS MLS data, and the inclusion of Aura MLS H₂O data for all pressures. Mostly
1138 at the uppermost (mesospheric) altitudes, large variations that are anti-correlated with solar flux
1139 are clearly observed over the past two 11-yr solar cycles, as discussed previously by others,
1140 using shorter data records. Net long-term trends in lower stratospheric water vapor are quite
1141 small if one considers the past 22 years, but there has been considerable interannual change, as

1142 mentioned also in past work using satellite data and Boulder sonde records. Notably, the steep
1143 drop (by 0.5-0.8 ppmv depending on latitude and pressure from 46 to 100 hPa) from 2000 to
1144 2001 is clearly visible in the GOZCARDS record. While the trends have been generally positive
1145 in the decade following 2001 (see Sect. 3), the 68 and 100 hPa levels show equally steep
1146 decreases again from 2011 to 2013 (from ~ 0.5 ppmv for 60°S to 60°N averages to ~ 0.8 ppmv in
1147 the 20°S - 20°N bin at 68 hPa); see also Urban et al. (2014). Long-term stratospheric trends may
1148 be observable most readily in the upper stratosphere. In the past 22 years, long-term global H_2O
1149 increases of order 10% are observed in the upper stratosphere and lower mesosphere, whereas a
1150 decrease of nearly 10% has occurred in the lower stratosphere (near 70-100 hPa). However, there
1151 is no regular monotonic change on decadal timescales, especially in the tropical lower
1152 stratosphere, where fairly sharp decreases followed by steadier increases may be a recurrent
1153 pattern. This remains to be better understood, with ongoing global datasets; Fueglistaler (2012)
1154 recently discussed the possibility of stepwise changes in water vapor. We have displayed the
1155 seasonal and decadal variability in stratospheric and mesospheric H_2O based on the GOZCARDS
1156 records for the past 22 years. As one might expect from the well-documented temperature
1157 influence on the tropical lower stratosphere, the H_2O variability based on maximum minus
1158 minimum yearly averages, is largest in the tropics and just above the tropopause. The elucidation
1159 of lower stratospheric water vapor changes over multiple decades is complicated by the
1160 significant low frequency variability in this region, and the occurrence of sudden changes; the
1161 addition of a few years of data can significantly modify trend results. More accurate studies of
1162 seasonal to decadal water vapor variability will be enabled by continuing merged H_2O data from
1163 the lower stratosphere to the upper mesosphere. A reduction in model spread for stratospheric
1164 H_2O is likely easier to achieve than tighter model results for water vapor (and ice water content)
1165 in the upper troposphere (for this region, see the data/model comparisons by Jiang et al., 2012).
1166 We should continue to improve model comparison results for H_2O (see, for example, Gettelman
1167 et al., 2010), although some studies should still focus on non-zonal aspects such as the Asian
1168 monsoon or Western Pacific regions, rather than zonal means like GOZCARDS.

1169 For ozone, we have used measurements from SAGE I, SAGE II, HALOE, UARS MLS, Aura
1170 MLS and ACE-FTS to produce a merged data record from late 1979 onward, after adjusting the
1171 monthly zonal mean series to SAGE II averages. Some complications arose because of the

1172 conversion of the original SAGE II profiles from a density/altitude grid to the GOZCARDS
1173 mixing ratio/pressure grid. In particular, we observed temperature-related temporal drifts in the
1174 converted SAGE II series, as a result of the NCEP temperature data used in this conversion,
1175 mostly in the upper stratosphere after June 2000 (see also McLinden et al., 2009). To circumvent
1176 this issue, we used HALOE upper stratospheric O₃ (p < 4 hPa) as a reference for July 2000 to
1177 November 2005, after applying offsets to the HALOE series. Aura MLS and ACE-FTS provide
1178 the continuing data past 2004. The resulting GOZCARDS merged ozone profiles for northern
1179 midlatitudes have recently been used in regression analyses (Nair et al., 2013) to reveal
1180 significant decreases in the whole stratosphere during 1984-1996. Nair et al. (2014) extended this
1181 work to a broader range of latitudes; they found significant increasing trends in upper
1182 stratospheric GOZCARDS ozone since 1997, but no significant positive trends in the lower
1183 stratosphere. Studies of GOZCARDS (and other) O₃ profile trends have been recently discussed
1184 as part of the SI²N analyses (Tummon et al., 2014; Harris et al., 2014), among other efforts.

1185 Here, we looked into the consistency of column ozone data between stratospheric
1186 GOZCARDS results and the study by Ziemke and Chandra (2012), who noted, using a simple
1187 regression model, that a fairly rapid change (“recovery”) in near-global ozone columns from
1188 TOMS and OMI data could be inferred since the mid-1990s. We show here that, unlike the 2 to
1189 3% net increase in near-global column ozone reported by ZC12 after the late 1990s, the similarly
1190 analyzed GOZCARDS record does not show such a strong reversal (or an upturn of more than
1191 0.5-1% since that period). Reasons for these differences could include data coverage or
1192 merging-related issues in either dataset, as well as differences in column sensitivities, as column
1193 ozone data down to certain pressures (as used in GOZCARDS analyses) cannot be exactly
1194 equivalent to stratospheric or total column estimates from ZC12; for example, changes that occur
1195 at the lowest altitudes may not be that well captured (for all latitudes) by GOZCARDS-derived
1196 columns. Further studies regarding the consistency of various column ozone results and a
1197 recovery tendency are warranted; a recent global total ozone study (Sheperd et al., 2014) also
1198 points to less of a return towards the 1980 levels than implied by ZC12.

1199 We also briefly described the creation of N₂O and HNO₃ GOZCARDS data records, based on
1200 Aura MLS and ACE-FTS monthly mean time series. The agreement between these two
1201 instruments’ datasets for these species was shown to be generally very good. For HNO₃, UARS

1202 MLS HNO₃ source datasets in the GOZCARDS format are available from the authors. However,
1203 a small upward adjustment (of order 10%) to the UARS MLS values is most likely needed based
1204 on our preliminary work comparing these time series to HNO₃ column results from FTIR
1205 measurements. More detailed work should help determine if adjustments can indeed be made in
1206 a more generalized way to the global UARS MLS HNO₃ dataset; lacking this, one should ensure
1207 that the error bars reflect the likely biases that can affect the continuity between satellite HNO₃
1208 datasets before and after 2000, given the multi-year gap in satellite coverage for this species.

1209 **There is a Supplement related to this article.**

1210 *Acknowledgements.* We dedicate this work to the memory of Professor Derek Cunnold (Georgia
1211 Institute of Technology) who was a member of the original GOZCARDS proposal. The
1212 GOZCARDS data generation could not have been possible without the past work from
1213 instrument teams for SAGE I, SAGE II, HALOE, UARS MLS, Aura MLS, and ACE-FTS, and
1214 related data usage documentation. At JPL, we thank Joe Waters for his leadership role in making
1215 MLS instruments and datasets possible and Bill Read for his key role; thanks to Vince Perun for
1216 MERRA-related work, and to Brian Knosp and Robert Thurstans for database and computer
1217 management assistance. Work at JPL was performed under contract with the National
1218 Aeronautics and Space Administration. We also thank Kaley Walker and Ashley Jones for
1219 comments regarding ACE-FTS data, Gloria Manney and William Daffer for help in making the
1220 original ACE-FTS data profiles available, and Joe Zawodny and Larry Thomason for their
1221 contributions and comments regarding SAGE data. We acknowledge the work of the GMAO
1222 team responsible for MERRA data used to generate the GOZCARDS temperatures, specifically,
1223 Steven Pawson and Jianjun Jin for discussions and cross-checks regarding temperature data. We
1224 acknowledge Jerry Ziemke for the ozone column data (from Ziemke and Chandra, 2012), and
1225 Sean Davis for discussions on data usage and screening, and the creation of long-term series. For
1226 early HNO₃-related work connecting ground-based data to MLS datasets, we thank Giovanni
1227 Muscari and Irene Fiorucci. We are thankful for the NOAA Earth System Research Laboratory
1228 (ESRL) Global Monitoring Division (GMD) website information and data on total surface
1229 chlorine. We obtained solar flux data for the Ottawa/Penticton sites from the NOAA National
1230 Geophysical Data Center (NGDC) website (www.ngdc.noaa.gov), for which we also
1231 acknowledge the National Research Council of Canada.

1232 **References**

1233

1234 Anderson, J. G., Brune, W. H., and Proffitt, M. H.: Ozone destruction by chlorine radicals within the
1235 Antarctic vortex: The spatial and temporal evolution of ClO–O₃ anticorrelation based on in situ ER-2
1236 data, *J. Geophys. Res.*, 94, 11,465-11,479, 1989.

1237 Anderson, J., Russell, J. M., Solomon, S., and Deaver, L. E.: HALOE confirmation of stratospheric
1238 chlorine decreases in accordance with the Montreal Protocol, *J. Geophys. Res.*, 105, 4483-4490, 2000.

1239 Anderson, J., Froidevaux, L., Fuller, R. A., Bernath, P. F., Livesey, N. J., Pumphrey, H. C., Read, W. G.,
1240 and Walker, K. A.: GOZCARDS Merged Data for Water Vapor Monthly Zonal Means on a Geodetic
1241 Latitude and Pressure Grid, version 1.01, Greenbelt, MD, USA: NASA Goddard Earth Science Data and
1242 Information Services Center, accessible from doi:10.5067/MEASURES/GOZCARDS/DATA3003, 2013.

1243 Barath, F., Chavez, M. C., Cofield, R. E., Flower, D. A., Frerking, M. A., Gram, M. B.,
1244 Harris, W. M., Holden, J. R., Jarnot, R. F., Kloezeman, W. G., Klose, G. J., Lau, G. K.,
1245 Loo, M. S., Maddison, B. J., Mattauch, R. J., McKinney, R. P., Peckham, G. E., Pickett, H. M., Siebes,
1246 G., Soltis, F. S., Suttie, R. A., Tarsala, J. A., Waters, J. W., and Wilson, W. J.: The Upper Atmosphere
1247 Research Satellite Microwave Limb Sounder Experiment, *J. Geophys. Res.*, 98, 10751-10762, 1993.

1248 Bauman, J. J., Russell, P. B., Geller, M. A., and Hamill, P.: A stratospheric aerosol climatology from
1249 SAGE II and CLAES measurements: 2. Results and comparisons, 1984–1999, *J. Geophys. Res.*, 108
1250 (D13), 4383, doi:10.1029/2002JD002993, 2003.

1251 Bernath, P. F., McElroy, C. T., Abrams, M. C., Boone, D., Butler, M., Camy-Peyret, C.,
1252 Carleer, M., Clerbaux, C., Coheur, P.-F., Colin, R., DeCola, P., DeMaziere, M., Drummond, J. R.,
1253 Dufour, D., Evans, W. F. J., Fast, H., Fussen, D., Gilbert, K., Jennings, D. E., Llewellyn, E. J., Lowe, R.
1254 P., Mahieu, E., McConnell, J. C., McHugh, M., McLeod, S. D., Michaud, R., Midwinter, C., Nassar, R.,
1255 Nichitiu, F., Nowlan, C., Rinsland, C. P., Rochon, Y. J., Rowlands, N., Semeniuk, K., Simon, P., Skelton,
1256 R., Sloan, J. J., Soucy, M.-A., Strong, K., Tremblay, P., Turnbull, D., Walker, K. A., Walkty, I., Wardle,
1257 D. A., Wehrle, V., Zander, R., and Zou, J.: Atmospheric Chemistry Experiment (ACE): Mission
1258 overview, *Geophys. Res. Lett.*, 32, L15S01, doi:10.1029/2005GL022386, 2005.

1259 Bhatt, P. P., Remsberg, E. E., Gordley, L. L., McInerney, J. M., Brackett, V. G., and
1260 Russell, III, J. M.: An evaluation of the quality of Halogen Occultation Experiment ozone profiles in the
1261 lower stratosphere, *J. Geophys. Res.*, 104 (D8), 9261-9275, 1999.

- 1262 Borchi, F., Pommereau, J.-P., Garnier, A., and Pinharanda, M.: Evaluation of SHADOZ sondes, HALOE
1263 and SAGE II ozone profiles at the tropics from SAOZ UV-Vis remote measurements onboard long
1264 duration balloons, *Atmos. Chem. Phys.*, 5, 1381-1397, 2005.
- 1265 Bourassa, A. E., Degenstein, D. A., Randel, W. J., Zawodny, J. M., Kyrölä, E., McLinden, C. A., Sioris,
1266 C. E., and Roth, C. Z., Trends in stratospheric ozone derived from merged SAGE II and Odin-OSIRIS
1267 satellite observations, *Atmos. Chem. Phys.*, 14, 6983-6994, doi:10.5194/acp-14-6983-2014, 2014.
- 1268 Brown, A. T., Chipperfield, M. P., Boone, C., Wilson, C., Walker, K. A., and Bernath, P.: Trends in
1269 atmospheric halogen containing gases since 2004, *J. Quant. Spec. Rad. Trans.*, 112, 2552-2566, 2011.
- 1270 Carleer, M. R., Boone, C. D., Walker, K. A., Bernath, P. F., Strong, K., Sica, R. J., Randall, C., Vomel, E.
1271 H., Kar, J., Hopfner, M., Milz, M., von Clarmann, T., Kivi, R., Valverde-Canossa, J., Sioris, C. E., Izawa,
1272 M. R. M., Dupuy, E., McElroy, C. T., Drummond, J. R., Nowlan, C. R., Zou, J., Nichitiu, F., Lossow, S.,
1273 Urban, J., Murtagh, D., and Dufour, D. G.: Validation of water vapour profiles from the Atmospheric
1274 Chemistry Experiment (ACE), *Atmos. Chem. Phys. Discuss.*, 8, 4499-4559, 2008.
- 1275 Chandra, S., Jackman, C. H., Fleming, E. L., and Russell, J. M.: The seasonal and long term changes in
1276 mesospheric water vapor, *Geophys. Res. Lett.*, 24, No. 6, 639-642, 1997.
- 1277 Chu, W. P., and McCormick, M. P.: Inversion of Stratospheric Aerosol and Gaseous Constituents From
1278 Spacecraft Solar Extinction Data in the 0.38-1.0 μm Wavelength Region, *Appl. Opt.*, 18, No. 9, 1404-
1279 1413, 1979.
- 1280 Cunnold, D. M., Chu, W. P., Barnes, R. A., McCormick, M. P., and Veiga, R. E.: Validation of SAGE II
1281 ozone measurements, *J. Geophys. Res.*, 94, 8447-8460, 1989.
- 1282 Damadeo, R. P., Zawodny, J. M., Thomason, L. W., and Iyer, N.: SAGE version 7.0 algorithm:
1283 application to SAGE II, *Atmos. Meas. Tech.*, 6, 3539-3561, doi:10.5194/amt-6-3539-2013, 2013.
- 1284 Davis, S., et al., in preparation, 2014.
- 1285 Dhomse, S., Weber, M., and Burrows, J.: The relationship between tropospheric wave forcing and
1286 tropical lower stratospheric water vapor, *Atmos. Chem. Phys.*, 8, 471-480, doi:10.5194/acp-8-471-2008,
1287 2008.

1288 Dupuy, E., Walker, K. A., Kar, J., Boone, C. D., McElroy, C. T., Bernath, P. F.,
 1289 Drummond, J. R., Skelton, R., McLeod, S. D., Hughes, R. C., Nowlan, C. R., Dufour, D. G., Zou, J.,
 1290 Nichitiu, F., Strong, K., Baron, P., Bevilacqua, R. M., Blumenstock, T., Bodeker, G. E., Borsdorff, T.,
 1291 Bourassa, A. E., Bovensmann, H., Boyd, I. S., Bracher, A., Brogniez, C., Burrows, J. P., Catoire, V.,
 1292 Ceccherini, S., Chabrillat, S., Christensen, T., Coffey, M. T., Cortesi, U., Davies, J., De Clercq, C.,
 1293 Degenstein, D. A., De Maziere, M., Demoulin, P., Dodion, J., Firanski, B., Fischer, H., Forbes, G.,
 1294 Froidevaux, L., Fussen, D., Gerard, P., Godin-Beekmann, S., Goutail, F., Granville, J., Griffith, D.,
 1295 Haley, C. S., Hannigan, J. W., Hopfner, M., Jin, J. J., Jones, A., Jones, N. B., Jucks, K., Kagawa, A.,
 1296 Kasai, Y., Kerzenmacher, T. E., Kleinbohl, A., Klekociuk, A. R., Kramer, I., Kullmann, H.,
 1297 Kuttippurath, J., Kyrölä, E., Lambert, J.-C., Livesey, N. J., Llewellyn, E. J., Lloyd, N. D., Mahieu, E.,
 1298 Manney, G. L., Marshall, B. T., McConnell, J. C., McCormick, M. P., McDermid, I. S., McHugh, M.,
 1299 McLinden, C. A., Mellqvist, J., Mizutani, K., Murayama, Y., Murtagh, D. P., Oelhaf, H., Parrish, A.,
 1300 Petelina, S. V., Piccolo, C., Pommereau, J.-P., Randall, C. E., Robert, C., Roth, C., Schneider, M., Senten,
 1301 C., Steck, T., Strandberg, A., Strawbridge, K. B., Sussmann, R., Swart, D. P. J., Tarasick, D. W., Taylor,
 1302 J. R., Tetard, C., Thomason, L. W., Thompson, A. M., Tully, M. B., Urban, J., Vanhellefont, F.,
 1303 Vigouroux, C., von Clarmann, T., von der Gathen, P., von Savigny, C., Waters, J. W., Witte, J. C., Wolff,
 1304 M., and Zawodny, J. M.: Validation of ozone measurements from the Atmospheric Chemistry Experiment
 1305 (ACE), *Atmos. Chem. Phys.*, 9, 287–343, doi:10.5194/acp-9-287-2009, 2009.

1306 Dvortsov, V. L. and Solomon, S.: Response of the stratospheric temperatures and ozone to past and future
 1307 increases in stratospheric humidity. *J. Geophys. Res.*, 106, 7505-7514, 2001.

1308 Eckert, E., von Clarmann, T., Kiefer, M., Stiller, G. P., Lossow, S., Glatthor, N., Degenstein, D. A.,
 1309 Froidevaux, L., Godin-Beekmann, S., Leblanc, T., McDermid, S., Pastel, M., Steinbrecht, W., Swart, D.
 1310 P. J., Walker, K. A., and Bernath, P. F.: Drif-corrected trends and periodic variations in MIPAS IMK/IAA
 1311 ozone measurements, *Atmos. Chem. Phys.*, 14, 2571-2589, doi:10.5194/acp-14-2571-2014, 2014.

1312 Engel, A., Strunk, M., Muller, M., Haase, H.-P., Poss, C., Levin, I., and Schmidt, U.: The temporal
 1313 development of total chlorine in the high latitude stratosphere based on reference distributions of mean
 1314 age derived from CO₂ and SF₆, *J. Geophys. Res.*, 107, 4136, doi:10.1029/2001JD000584, 2002.

1315 Fahey, D. W., Gao, R.-S., Möhler, O., Saathoff, H., Schiller, C., Ebert, V., Krämer, M., Peter, T.,
 1316 Amarouche, N., Avallone, L. M., Bauer, R., Bozoki, Z., Christensen, L. E., Davis, S. M., Durrey, G.,
 1317 Dyroff, C., Herman, R. L., Hunsmann, S., Khaykin, S. M., Mackrodt, P., Meyer, J., Smith, J. B., Spelten,
 1318 N., Troy, R. F., Vömel, H., Wagner, S., and Wienhold, F. G.: The AquaVIT-1 intercomparison of

- 1319 atmospheric water vapor measurement techniques, *Atm. Meas. Tech. Discuss.*, 7, 3159-3251,
1320 doi:10.5194/amtd-7-3159-2014, 2014.
- 1321 Farman, J. C., Gardiner, B. G., and Shanklin, J. D.: Large losses of total ozone in Antarctica reveal
1322 seasonal ClOx/NOx interaction, *Nature*, 315, 207-210, 1985.
- 1323 Fiorucci, I., Muscari, G., Froidevaux, L., and Santee, M. L.: Ground-based stratospheric O₃ and HNO₃
1324 measurements at Thule, Greenland: an intercomparison with Aura MLS observations, *Atmos. Meas.*
1325 *Tech.*, 6, 2441–2453, doi:10.5194/amt-6-2441-2013, 2013.
- 1326 Forster, P. M. de F., and Shine, K. P.: Assessing the climate impact of trends in stratospheric water vapor,
1327 *Geophys. Res. Lett.*, 29 (6), 1086, doi:10.1029/2001GL013909, 2002.
- 1328 Frith, S. M., Kramarova, N. A., Stolarski, R. S., McPeters, R. D., Bhartia, P. K., and Labow, G. J.: Recent
1329 changes in total column ozone based on the SBUV Version 8.6 Merged Ozone Data Set, *J. Geophys.*
1330 *Res.*, 119, 9735-9751, doi:10.1029/2014JD021889, 2014.
- 1331 Froidevaux, L., Livesey, N. J., Read, W. G., Salawitch, R. J., Waters, J. W., Drouin, B., MacKenzie, I. A.,
1332 Pumphrey, H. C., Bernath, P., Boone, C., Nassar, R., Montzka, S., Elkins, J., Cunnold, D., and
1333 Waugh, D.: Temporal decrease in upper atmospheric chlorine, *Geophys. Res. Lett.*, 33, L23813,
1334 doi:10.1029/2006GL027600, 2006.
- 1335 Froidevaux, L., Jiang, Y. B., Lambert, A., Livesey, N. J., Read, W. G., Waters, J. W.,
1336 Browell, E. V., Hair, J. W., Avery, M. A., McGee, T. J., Tiwgg, L. W., Sumnicht, G. K., Jucks, K. W.,
1337 Margitan, J. J., Sen, B., Stachnik, R. A., Toon, G. C., Bernath, P. F., Boone, C. D., Walker, K. A.,
1338 Filipiak, M. J., Harwood, R. S., Fuller, R. A., Manney, G. L., Schwartz, M. J., Daffer, W. H., Drouin, B. J.,
1339 Cofield, R. E., Cuddy, D. T., Jarnot, R. F., Knosp, B. W., Perun, V. S., Snyder, W. V., Stek, P. C.,
1340 Thurstans, R. P., and Wagner, P. A.: Validation of Aura Microwave Limb Sounder stratospheric and
1341 mesospheric ozone measurements, *J. Geophys. Res.*, 113, doi:10.1029/2007JD008771, D15S20, 2008.
- 1342 Froidevaux, L., Fuller, R., Schwartz, M., Anderson, J., and Wang, R.: README Document for the
1343 Global OZoneChemistry And Related trace gas Data records for the Stratosphere (GOZCARDS) project,
1344 Goddard Earth Sciences Data and Information Services Center (GES DISC), <http://disc.gsfc.nasa.gov>,
1345 NASA Goddard Space Flight Center, Code 610.2, Greenbelt, MD 20771 USA, 2013a.
- 1346 Froidevaux, L., Anderson, J., Fuller, R. A., Bernath, P. F., Livesey, N. J., Russell III, J. M., and
1347 Walker, K. A.: GOZCARDS Merged Data for Hydrogen Chloride Monthly Zonal Means on a Geodetic

1348 Latitude and Pressure Grid, version 1.01, Greenbelt, MD, USA: NASA Goddard Earth Science Data and
1349 Information Services Center, accessible from doi:10.5067/MEASURES/GOZCARDS/DATA3002,
1350 2013b.

1351 Froidevaux, L., Fuller, R. A., Lambert, A., Livesey, N. J., Bernath, P. F., Livesey, N. J., and Walker,
1352 K.A.: GOZCARDS Merged Data for Nitrous Oxide Monthly Zonal Means on a Geodetic Latitude and
1353 Pressure Grid, version 1.01, Greenbelt, MD, USA: NASA Goddard Earth Science Data and Information
1354 Services Center, accessible from doi:10.5067/MEASURES/GOZCARDS/DATA3013, 2013c.

1355 Froidevaux, L., Fuller, R. A., Santee, M. L., Manney, G. L., Livesey, N. J., Bernath, P. F., and Walker,
1356 K.A.: GOZCARDS Merged Data for Nitric Acid Monthly Zonal Means on a Geodetic Latitude and
1357 Pressure Grid, version 1.01, Greenbelt, MD, USA: NASA Goddard
1358 Earth Science Data and Information Services Center, accessible from
1359 doi:10.5067/MEASURES/GOZCARDS/DATA3008, 2013d.

1360 Fueglistaler, S.: Step-wise changes in stratospheric water vapor? *J. Geophys. Res.*, 117, D13302,
1361 doi:10.1029/2012JD017582, 2012.

1362 Fueglistaler, S., Liu, Y. S., Flannaghan, T. J., Haynes, P. H., Dee, D. P., Read, W. J., Remsberg, E. E.,
1363 Thomason, L. W., Hurst, D. F., Lanzante, J. R., and Bernath, P. F.: The relation between atmospheric
1364 humidity and temperature trends for stratospheric water, *J. Geophys. Res.*, 118, 1052–1074,
1365 doi:10.1002/jgrd.50157, 2013.

1366

1367 Fujiwara, M., Vomel, H., Hasebe, F., Shiotani, M., Ogino, S.- Y., Iwasaki, S., Nishi, N.,
1368 Shibata, T., Shimizu, K., Nishimoto, E., Valverde Canossa, J. M., Selkirk, H. B., and
1369 Oltmans, S. J.: Seasonal to decadal variations of water vapour in the tropical lower stratosphere observed
1370 with balloon-borne cryogenic frost point hygrometers, *J. Geophys. Res.*, 115, D18304,
1371 doi:10.1029/2010JD014179, 2010.

1372

1373 Garfinkel, C. I., Waugh, D. W., Oman, L. D., Wang, L., and Hurwitz, M. M.: Temperature trends in the
1374 tropical upper troposphere and lower stratosphere: Connections with sea surface temperatures and
1375 implications for water vapor and ozone, *J. Geophys. Res. Atmos.*, 118, 9658–9672,
1376 doi:10.1002/jgrd.50772, 2013.

1377

1378 Gebhardt, C., Rozanov, A., Hommel, R., Weber, M., Bovensmann, H., Burrows, J. P., Degenstein, D.,

1379 Froidevaux, L., and Thompson, A. M.: Stratospheric ozone trends and variability as seen by
1380 SCIAMACHY from 2002 to 2012, *Atmos. Chem. Phys.*, 14, 831–846, doi:10.5194/acp-14-831-2014,
1381 2014.

1382

1383 Gettelman, A., Hegglin, M. I., Son, S.-W., Kim, J., Fujiwara, M., Birner, T., Kremser, S.,
1384 Rex, M., Añel, J. A., Akiyoshi, H., Austin, J., Bekki, S., Braesike, P., Brühl, C., Butchart, N.,
1385 Chipperfield, M., Dameris, M., Dhomse, S., Garny, H., Hardiman, S. C., Jöckel, P.,
1386 Kinnison, D. E., Lamarque, J. F., Mancini, E., Marchand, M., Michou, M., Morgenstern, O., Pawson, S.,
1387 Pitari, G., Plummer, D., Pyle, J. A., Rozanov, E., Scinocca, J., Shepherd, T. G., Shibata, K., Smale, D.,
1388 Teyssèdre, H., and Tian, W.: Multimodel assessment of the upper troposphere and lower stratosphere:
1389 Tropics and global trends, *J. Geophys. Res.*, 115, D00M08, doi:10.1029/2009JD013638, 2010.

1390 Gordley, L. L., Russell III, J. M., Mickley, L. J., Frederick, J. E., Park, J. H., Stone, K. A., Beaver, G. M.,
1391 McNerney, J. M., Deaver, L. E., Toon, G. C., Murcray, F. J., Blatherwick, R. D., Gunson, M. R., Abbatt,
1392 J. P. D., Mauldin III, R. L., Mount, G. H., Sen, B., and Blavier, J.-F.: Validation of nitric oxide and
1393 nitrogen dioxide measurements made by the Halogen Occultation Experiment for UARS platform, *J.*
1394 *Geophys. Res.*, 101, 10241-10266, 1996.

1395 Haefele, A., Hocke, K., Kampfer, N., Keckhut, P., Marchand, M., Bekki, S., Morel, B.,
1396 Egorova, T., and Rozanov, E.: Diurnal changes in middle atmospheric H₂O and O₃: Observations in the
1397 Alpine region and climate models, *J. Geophys. Res.*, 113, D17303, doi:10.1029/2008JD009892, 2008.

1398 Harris, N. R. P., et al., Past changes in the Vertical Distribution of Ozone, Part III: Analysis and
1399 interpretation of trends, in preparation, 2014.

1400 Hassler, B., Bodeker, G. E., Solomon, S., and Young, P. J.: Changes in the polar vortex: Effects on
1401 Antarctic total ozone observations at various stations, *Geophys. Res. Lett.*, 38, L01805,
1402 doi:10.1029/2010GL045542, 2011.

1403 Hegglin, M. I., Tegtmeier, S., Anderson, J., Froidevaux, L., Fuller, R., Funke, B., Jones, A., Lingenfelter,
1404 G., Lumpe, J., Pendlebury, D., Remsberg, E., Rozanov, A., Toohey, M., Urban, J., von Clarmann, T.,
1405 Walker, K. A., Wang, R., and Weigel, K.: SPARC Data Initiative: Comparison of water vapor
1406 climatologies from international satellite limb sounders, *J. Geophys. Res. Atmos.*, 118, 11,824–11,846,
1407 doi: 10.1002/jgrd.50752, 2013.

1408 Hervig, M., and McHugh, M.: Cirrus detection using HALOE measurements, *Geophys. Res. Lett.*, 26,
1409 No. 6, 719-722, 1999.

1410 Huang, F. T., Mayr, H. G., Russell III, J. M., and Mlynczak, M. G.: Ozone diurnal variations in the
1411 stratosphere and lower mesosphere, based on measurements from SABER on TIMED,
1412 *J. Geophys. Res.*, 115, D24308, doi:10.1029/2010JD014484, 2010.

1413 Hubert, D., et al., Ground-based assesment of the bias and long-term stability of fourteen limb and
1414 occultation ozone profile data records, in preparation, 2014.

1415 Hurst, D. F., Oltmans, S. J., Vomel, H., Rosenlof, K. H., Davis, S. M., Ray, E. A., Hall, E. G., and
1416 Jordan, A. F.: Stratospheric water vapor trends over Boulder, Colorado: Analysis of the 30 year Boulder
1417 record, *J. Geophys. Res.*, 116, D02306, doi:10.1029/2010JD015065, 2011.

1418 Hurst, D. F., Lambert, A., Read, W. G., Davis, S. M., Rosenlof, K. H., Hall, E. G., Jordan, A. F., and
1419 Oltmans, S. J.: Validation of Aura Microwave Limb Sounder stratospheric water vapor measurements by
1420 the NOAA frost point hygrometer, *J. Geophys. Res. Atmos.*, 119, 1612-1625,
1421 doi:10.1002/2013JD020757, 2014.

1422 Jiang, J. H., Su, H., Zhai, C., Perun, V. S., Del Genio, A., Nazarenko, L. S., Donner, L. J., Horowitz, L.,
1423 Seman, C., Cole, J., Gettelman, A., Ringer, M. A., Rotstayn, L., Jeffrey, S., Wu, T., Brient, F., Dufresne,
1424 J.-L., Kawai, H., Koshiro, T., Watanabe, M., L'Écuyer, T. S., Volodin, E. M., Iversen, T., Drange, H.,
1425 Mesquita, M. D. S., Read, W. G., Waters, J. W., Tian, B., Teixeira, J., and Stephens, G. L.: Evaluation of
1426 cloud and water vapor simulations in CMIP5 climate models using NASA "A-Train" satellite
1427 observations, *J. Geophys. Res.*, 117, D14105, doi:10.1029/2011JD017237, 2012.

1428 Jiang, Y. B., Froidevaux, L., Lambert, A., Livesey, N. J., Read, W. G., Waters, J. W.,
1429 Bojkov, B., Leblanc, T., McDermid, I. S., Godin-Beekmann, S., Filipiak, M. J., Harwood, R. S.,
1430 Fuller, R. A., Daffer, W. H., Drouin, B. J., Cofield, R. E., Cuddy, D. T., Jarnot, R. F., Knosp, B. W.,
1431 Perun, V. S., Schwartz, M. J., Snyder, W. V., Stek, P. C., Thurstans, R. P., Wagner, P. A., Allaart, M.,
1432 Andersen, S. B., Bodeker, G., Calpini, B., Claude, H., Coetzee, G., Davies, J., De Backer, H., Dier, H.,
1433 Fujiwara, M., Johnson, B., Kelder, H., Leme, N. P., Koenig-Langlo, G., Kyrölä, E., Laneve, G.,
1434 Fook, L.S., Merrill, J., Morris, G., Newchurch, M., Oltmans, S., Parrondos, M.C., Posny, F., Schmidlin, F.,
1435 Skrivankova, P., Stubi, R., Tarasick, D., Thompson, A., Thouret, V., Viatte, P., Vomel, H., von Der
1436 Gathen, P., Yela, M., and Zablocki, G.: Validation of the Aura Microwave Limb Sounder Ozone by

1437 Ozonesonde and Lidar Measurements, *J. Geophys. Res.*, 112, D24S34, , doi:10.1029/2007JD008776,
1438 2007.

1439 Jones, A., Urban, J., Murtagh, D. P., Eriksson, P., Brohede, S., Haley, C., Degenstein, D., Bourassa, A.,
1440 von. Savigny, C., Sonkaew, T., Rozanov, A., Bovensmann, H., and Burrows, J.: Evolution of
1441 stratospheric ozone and water vapour time series studied with satellite measurements, *Atmos. Chem.*
1442 *Phys*, 9, 6055-6075, doi:10.5194/acp-9-6055-2009, 2009.

1443 Jones, A., Urban, J., Murtagh, D. P., Sanchez, C., Walker, K. A., Livesey, N. J., Froidevaux, L., and
1444 Santee, M. L.: Analysis of HCl and ClO time series in the upper stratosphere using satellite data sets,
1445 *Atmos. Chem. Phys.*, 11, 5321-5333, doi:10.5194/acp-11-5321-2011, 2011.

1446 Kirgis, G., Leblanc, T., McDermid, I. S., and Walsh, T. D.: Stratospheric ozone interannual variability
1447 (1995–2011) as observed by Lidar and Satellite at Mauna Loa Observatory, HI and Table Mountain
1448 Facility, CA, *Atmos. Chem. Phys.*, 13, 5033–5047, doi:10.5194/acp-13-5033-2013, 2013.

1449

1450 Kley, D., Stone, E. J., Henderson, W. R., Drummond, J. W., Harrop, W. J., Schmeltekopf, A. L.,
1451 Thompson, T. L., and Winkler, R. H.: In Situ Measurements of the Mixing Ratio of Water Vapor in the
1452 Stratosphere, *J. Atmos. Sci.*, 36, 2513-2524, 1979.

1453

1454 Kohlhepp, R., Ruhnke, R., Chipperfield, M. P., De Maziere M., Notholt, J., Barthlott, S., Batchelor, R. L.,
1455 Blatherwick, R. D., Blumenstock, T., Coffey, M. T., Demoulin, P., Fast, H., Feng, W., Goldman, A.,
1456 Griffith, D. W. T., Hamann, K., Hannigan, J. W., Hase, F., Jones, N. B., Kagawa, A., Kaiser, I., Kasai, Y.,
1457 Kirner, O., Kouker, W., Lindenmaier, R., Mahieu, E., Mittermeier, R. L., Monge-Sanz, B., Morino, I.,
1458 Murata, I., Nakajima, H., Palm, M., Paton-Walsh, C., Raffalski, U., Reddman, T., Rettinger, M.,
1459 Rinsland, C. P., Rozanov, E., Schneider, M., Senten, C., Servais, C., Sinnhuber, B.-M., Smale, D., Strong,
1460 K., Sussmann, R., Taylor, J. R., Vanhaelewyn, G., Warneke, T., Whaley, C., Wiehle, M., and Wood, S.
1461 W.: Observed and simulated time evolution of HCl, ClONO₂, and HF total column abundances, *Atmos.*
1462 *Chem. Phys.*, 12, 3527–3557, doi:10.5194/acp-12-3527-2012, 2012.

1463

1464 Kunz, A., Müller, R., Homonnai, V., Jánosi, I. M., Hurst, D., Rap, A., Forster, P. M., Rohrer, F., Spelten,
1465 N., and Riese, M.: Extending water vapor trend observations over Boulder into the tropopause region:
1466 Trend uncertainties and resulting radiative forcing, *J. Geophys. Res. Atmos.*, 118,
1467 doi:10.1002/jgrd.50831, 2013.

1468 Kuttippurath, J., Lefevre, F., Pommereau, J.-P., Roscoe, H. K., Goutail, F., Pazmino, A., and Shanklin, J.
1469 D.: Antarctic ozone loss in 1979–2010: first sign of ozone recovery, *Atmos. Chem. Phys.*, 13, 1625–1635,
1470 doi:10.5194/acp-13-1625-2013, 2013.

1471 Kyrölä, E., Laine, M., Sofieva, V., Tamminen, J., Päivärinta, S.-M., Tukiainen, S., Zawodny, J., and
1472 Thomason, L.: Combined SAGE II-GOMOS ozone profile data set for 1984-2011 and trend analysis of
1473 the vertical distribution of ozone, *Atmos. Chem. Phys.*, 13, 10,645-10,658, doi:10.5194/acp-13-10645-
1474 2013, 2013.

1475 Lambert, A., Read, W. G., Livesey, N. J., Santee, M. L., Manney, G. L., Froidevaux, L.,
1476 Wu, D. L., Schwartz, M. J., Pumphrey, H. C., Jimenez, C., Nedoluha, G. E., Cofield, R. E., Cuddy, D. T.,
1477 Daffer, W. H., Drouin, B. J., Fuller, R. A., Jarnot, R. F., Knosp, B. W., Pickett, H. M., Perun, V. S.,
1478 Snyder, W. V., Stek, P. C., Thurstans, R. P., Wagner, P. A., Waters, J. W., Jucks, K. W., Toon, G. C.,
1479 Stachnik, R. A., Bernath, P. F., Boone, C. D., Walker, K. A., Urban, J., Murtagh, D., Elkins, J. W., and
1480 Atlas, E.: Validation of the Aura Microwave Limb Sounder stratospheric water vapour and nitrous oxide
1481 measurements, *J. Geophys. Res.*, 112, D24S36, doi:10.1029/2007JD008724, 2007.

1482 Livesey, N. J., Read, W. J., Froidevaux, L., Waters, J. W., Santee, M. L., Pumphrey, H. C., Wu, D. L.,
1483 Shippony, Z., and Jarnot, R. F.: The UARS Microwave Limb Sounder version 5 dataset: Theory,
1484 characterization and validation, *J. Geophys. Res.*, 108 (D13), 4378, doi:10.1029/2002JD002273, 2003.

1485 Livesey, N. J., Read, W. G., Froidevaux, L., Lambert, A., Manney, G. L., Pumphrey, H. C., Santee, M.
1486 L., Schwartz, M. J., Wang, S., Cofield, R. E., Cuddy, D. T., Fuller, R. A., Jarnot, R. F., Jiang, J. H.,
1487 Knosp, B. W., Stek, P. C., Wagner, P. A., and Wu, D. L.: EOS MLS Version 3.3/3.4 Level 2 data quality
1488 and description document, Tech. rep., Jet Propulsion Laboratory, available from <http://mls.jpl.nasa.gov/>,
1489 2013.

1490 Mahieu, E., Duchatelet, P., Demoulin, P., Walker, K. A., Dupuy, E., Froidevaux, L., Randall, C., Catoire,
1491 V., Strong, K., Boone, C. D., Bernath, P. F., Blavier, J.-F., Blumenstock, T., Coffey, M., DeMaziere, M.,
1492 Griffith, D., Hannigan, J., Hase, F., Jones, N., Jucks, K. W., Kagawa, A., Kasai, Y., Mebarki, Y.,
1493 Mikuteit, S., Nassar, R., Notholt, J., Rinsland, C. P., Robert, C., Schrems, O., Senten, C., Smale, D.,
1494 Taylor, J., Tetard, C., Toon, G. C., Warneke, T., Wood, S. W., Zander, R., and Servais, C.: Validation of
1495 ACE-FTS v2.2 measurements of HCl, HF, CCl₃F and CCl₂F₂ using space-, balloon- and ground-based
1496 instrument observations, *Atmos. Chem. Phys.*, 8, 6199-6221, doi:10.5194/acp-8-6199-2008.

1497 Mahieu, E., Zander, R., Bernath, P. F., Boone, C. D., and Walker, K. A.: Recent trend anomaly of
1498 hydrogen chloride (HCl) at northern mid-latitudes derived from Jungfraujoch, HALOE, and ACE-FTS
1499 infrared solar observations, in: *The Atmospheric Chemistry Experiment ACE at 10: a solar occultation*
1500 *anthology*, Bernath, P. (Ed.), Deepak Publishing, Hampton, VA, 239-249, 2013.

1501 Mahieu, E., Chipperfield, M. P., Notholt, J., Anderson, J., Bernath, P. F., Blumenstock, T., Coffey, M. T.,
1502 Dhomse, S., Feng, W., Franco, B., Froidevaux, L., Griffith, D. W. T., Hannigan, J., Hase, F., Hossaini, R.,
1503 Jones, N. B., Morino, I., Murata, I., Nakajima, H., Palm, M., Paton-Walsh, C., Reddman, T.,
1504 Russell III, J. M., Schneider, M., Servais, C., Smale, D., and Walker, K. A.: Increase in northern
1505 stratospheric hydrogen chloride over recent years, submitted, 2014.

1506 McCormick, M. P., Zawodny, J. M., Veiga, R. E., Larsen, J. C., and Wang, P. H.: An overview of SAGE-
1507 I and II ozone measurements, *Planetary and Space Science*, 37, No. 12, 1567-1586, 1989.

1508 McHugh, M., Hervig, M., Magill, B., Thompson, R. E., Remsberg, E., Wrotny, J., and
1509 Russell, J. M.: Improved mesospheric temperature, water vapor, and polar mesospheric cloud extinctions
1510 from HALOE, *Geophys. Res. Lett.*, 30, 8, doi: 10.1029/2002GL016859, 2003.

1511 McLinden, C. A., Tegtmeier, S., and Fioletov, V.: Technical Note: A SAGE-corrected SBUV zonal-mean
1512 ozone data set, *Atmos. Chem. Phys.*, 9, 7963–7972, doi:10.5194/acp-9-7963-2009, 2009.

1513 McPeters, R. D., Bhartia, P. K., Haffner, D., Labow, G. J. and Flynn, L.: The v8.6 SBUV Ozone Data
1514 Record: An Overview, *J. Geophys. Res.*, 118, 8032-8039, doi:10.1002/jgrd.50597, 2013.

1515 Molina, M. J., and Rowland, F. S.: Stratospheric sink for chlorofluoromethane: chlorine atom-catalyzed
1516 destruction of ozone, *Nature*, 249, 810-812, 1974.

1517 Montzka, S. A., Butler, J. H., Elkins, J. W., Thompson, T. M., Clarke, A. D., and Lock, L. T.: Present
1518 and future trends in the atmospheric burden of ozone-depleting halogens, *Nature*, 398, 690-694, 1999.

1519 Morris, G. A., Gleason, J. F., Russell III, J. M., Schoeberl, M. R., and McCormick, M. P.: A comparison
1520 of HALOE V19 with SAGE II V6.00 ozone observations using trajectory mapping, *J. Geophys. Res.*,
1521 107, D13, 4177, doi:10.1029/2001JD000847, 2002.

1522 Mote, P. W., Rosenlof, K. H., McIntyre, M. E., Carr, E. S., Gille, J. C., Holton, J. R., Kinnersley, J. S.,
1523 Pumphrey, H. C., Russell III, J. M., and Waters, J. W.: An atmospheric tape recorder: The imprint of
1524 tropical tropopause temperatures on stratospheric water vapor,
1525 *J. Geophys. Res.*, 101, 3989–4006, 1996.

1526 Nair, P. J., Godin-Beekmann, S., Froidevaux, L., Flynn, L. E., Zawodny, J. M., Russell III, J. M.,
1527 Pazmino, A., Ancellet, G., Steinbrecht, W., Claude, H., Leblanc, T., McDermid, S., van Gijssel, J. A. E.,
1528 Johnson, B., Thomas, A., Hubert, D., Lambert, J.-C., Nakane, H., and Swart, D. P. J.: Relative drifts and
1529 stability of satellite and ground-based stratospheric ozone profiles at NDACC lidar stations, *Atmos.*
1530 *Meas. Tech.*, 5, 1301–1318, doi: 10.5194/amt-5-1301-2012, 2012.

1531 Nair, P. J., Godin-Beekmann, S., Kuttippurath, J., Ancellet, G., Goutail, F., Pazmiño, A., Froidevaux, L.,
1532 Zawodny, J. M., Evans, R. D., Wang, H.-J., Anderson, A., and Pastel, M.: Ozone trends derived from the
1533 total column and vertical profiles at a northern mid-latitude station, *Atmos. Chem. Phys.*, 13, 10373–
1534 10384, doi:10.5194/acp-13-10373-2013, 2013.

1535

1536 Nair, P. J., Froidevaux, L., Kuttippurath, J., Zawodny, J. M., Russell III, J. M., Steinbrecht, W., Claude,
1537 H., Leblanc, T., van Gijssel, J. A. E., Johnson, B., Swart, D. P. J., Thomas, A., Querel, R., Wang, R., and
1538 Anderson, J.: Subtropical and mid-latitude ozone trends: implications for recovery, submitted, 2014.

1539 Nazaryan, H., McCormick, M. P., and Russell III, J. M.: New studies of SAGE II and HALOE ozone
1540 profile and long-term change comparisons, *J. Geophys. Res.*, 110, D09305, doi:10.1029/2004JD005425,
1541 2005.

1542 Nedoluha, G. E., Bevilacqua, R. M., Gomez, R. M., Hicks, B. C., Russell III, J. M., and
1543 Connor, B. J.: An evaluation of trends in middle atmospheric water vapor as measured by HALOE,
1544 WVMS, and POAM, *J. Geophys. Res.*, 108 (D13), 4391, doi:10.1029/2002JD003332, 2003.

1545 Nedoluha, G. E., Gomez, R. M., Hicks, B. C., Bevilacqua, R. M., Russell III, J. M.,
1546 Connor, B. J., and Lambert, A.: A comparison of middle atmospheric water vapor as measured by
1547 WVMS, EOS-MLS, and HALOE, *J. Geophys. Res.*, 112, D24S39, doi:10.1029/2007JD008757, 2007.

1548

1549 Nedoluha, G. E., Gomez, R. M., Hicks, B. C., Wrotny, J. E., Boone, C., and Lambert, A.: Water vapor
1550 measurements in the mesosphere from Mauna Loa over solar cycle 23, *J. Geophys. Res.*, 114, D23303,
1551 doi:10.1029/2009JD012504, 2009.

1552

1553 Nedoluha, G., Gomez, R. M., Hicks, B. C., Helmboldt, J., Bevilacqua, R. M., and Lambert, A.: Ground-
1554 based microwave measurements of water vapor from the midstratosphere to the mesosphere, *J. Geophys.*
1555 *Res.*, 116, D02309, doi:10.1029/2010JD014728., 2011.

1556

1557 Newchurch, M. J., Yang, E. S., Cunnold, D. M., Reinsel, G. C., Zawodny, J. M., and
1558 Russell III, J. M.: Evidence for slowdown in stratospheric ozone loss: First stage of ozone recovery, *J.*
1559 *Geophys. Res.*, 108, D16, doi:10.1029/2003JD003471, 2003.

1560 Parrish, A., Boyd, I. S., Nedoluha, G. E., Bhartia, P. K., Frith, S. M., Kramarova, N. A.,
1561 Connor, B. J., Bodeker, G. E., Froidevaux, L., Shiotani, M., and Sakazaki, T.: Diurnal variations of
1562 stratospheric ozone measured by ground-based microwave remote sensing at the Mauna Loa NDACC
1563 site: measurement validation and GEOSCCM model comparison, *Atmos. Chem. Phys.*, 7255-7272,
1564 doi:10.5194/acp-14-7255-2014, 2014.

1565 Perliski, L. M., Solomon, S., and London, J.: On the interpretation of seasonal variations of stratospheric
1566 ozone, *Planet. Space Sci.*, 37, 12, 1527-1538, 1989.

1567 Pumphrey, H. C.: Validation of a new prototype water vapor retrieval for UARS MLS,
1568 *J. Geophys. Res.*, 104 (D8), 9399–9412, 1999.

1569 Pumphrey, H. C., Clark, H. L., and Harwood, R. S.: Lower stratospheric water vapor as measured by
1570 UARS MLS, *Geophys. Res. Lett.*, 27, 1691–1694, 2000.

1571 Randel, W. J., Wu, F., Oltmans, S. J., Rosenlof, K., and Nedoluha, G. E.: Interannual changes of
1572 stratospheric water vapor and correlations with tropical tropopause temperatures, *J. Atmos. Sci.*, 61,
1573 2133–2148, 2004.

1574
1575 Randel, W. J., Wu, F., Voemel, H., Nedoluha, G. E., and Forster, P.: Decreases in stratospheric water
1576 vapor after 2001: links to changes in the tropical tropopause and the Brewer-Dobson circulation, *J.*
1577 *Geophys. Res.*, 111, D12312, doi:10.1029/2005JD006744, 2006.

1578
1579 Randel, W.J., and Jensen, E. J.: Physical processes in the tropical tropopause layer and their role in a
1580 changing climate, *Nature Geosci.*, 6, 169-176, doi:10.1038/ngeo1733, 2013.

1581
1582 Randel, W. J., and Thompson, A. M.: Interannual variability and trends in tropical ozone derived from
1583 SAGE II satellite data and SHADOZ ozonesondes, *J. Geophys. Res.*, 116, D07303,
1584 doi:10.1029/2010JD015195, 2011.

1585
1586 Read, W. G., Lambert, A., Bacmeister, J., Cofield, R. E., Christensen, L. E., Cuddy, D. T., Daffer, W.
1587 H., Drouin, B. J., Fetzer, E., Froidevaux, L., Fuller, R., Herman, R., Jarnot, R. F., Jiang, J. H., Jiang, Y.

1588 B., Kelly, K., Knosp, B. W., Kovalenko, L. J., Livesey, N. J., Liu, H.-C., Manney, G. L., Pickett, H. M.,
1589 Pumphrey, H. C., Rosenlof, K. H., Sabouchi, X., Santee, M. L., Schwartz, M. J., Snyder, W. V., Stek, P.
1590 C., Su, H., Takacs, L. L., Thurstans, R. P., Voemel, H., Wagner, P. A., Waters, J. W., Webster, C. R.,
1591 Weinstock, E. M., and Wu, D. L.: Aura Microwave Limb Sounder upper tropospheric and lower
1592 stratospheric H₂O and relative humidity with respect to ice validation, *J. Geophys. Res.*, 112, D24S35,
1593 doi:10.1029/2007JD008752, 2007.

1594

1595 Read, W. G., Schwartz, M. J., Lambert, A., Su, H., Livesey, N. J., Daffer, W. H., and
1596 Booe, C. D.: The roles of convection, extratropical mixing, and in-situ freeze-drying in the Tropical
1597 Tropopause Layer, *Atmos. Chem. Phys.*, 8, 6051–6067, doi:10.5194/acp-8-6051-2008, 2008.

1598

1599 Remsberg, E.: Observed seasonal to decadal scale responses in mesospheric water vapor,
1600 *J. Geophys. Res.*, 115, D06306, doi:10.1029/2009JD012904, 2010.

1601

1602 Ricaud, P., de La Noë, J., Connor, B. J., Froidevaux, L., Waters, J. W., Harwood, R. S., MacKenzie, I. A.,
1603 and Peckham, G. E.: Diurnal variability of mesospheric ozone as measured by the UARS microwave limb
1604 sounder instrument: Theoretical and ground-based validations, *J. Geophys. Res.*, 101 (D6), 10,077–
1605 10,089, doi:10.1029/95JD02841, 1996.

1606

1607 Rienecker, M., Suarez, M. J., Gelaro, R., Todling, R., Bacmeister, J., Liu, E., Bosilovich, M. G.,
1608 Schubert, S. D., Takacs, L., Kim, G.-K., Bloom, S., Chen, J., Collins, D., Conaty, A.,
1609 da Silva, A., Gu, W., Joiner, J., Koster, R. D., Lucchesi, R., Molod, A., Owens, T., Pawson, S., Pegion,
1610 P., Redder, C. R., Reichle, R., Robertson, J., F. R., Ruddick, A. G., Sienkiewicz, M., and Woollen, J.:
1611 MERRA: NASA's Modern-Era Retrospective Analysis for Research and Applications, *J. Climate*, 24,
1612 3624–3648, doi:10.1175/JCLI-D-11-00015.1, 2011.

1613

1614 Rosenlof, K. H., and Reid, G. C.: Trends in the temperature and water vapor content of the tropical lower
1615 stratosphere: Sea surface connection, *J. Geophys. Res.*, 113, D06107, doi:10.1029/2007JD009109, 2008.

1616

1617 Rosenlof, K. H., Chiou, E.-W., Chu, W. P., Johnson, D. G., Kelly, K. K., Michelsen, H. A., Nedoluha, G.
1618 E., Remsberg, E. E., Toon, G. C., and McCormick, M. P.: Stratospheric water vapor increases over the
1619 past half-century, *Geophys. Res. Lett.*, 28, 1195–1198, doi:10.1029/2000GL012502, 2001.

1620 Russell III, J. M., Gordley, L. L., Park, J. H., Drayson, S. R., Hesketh, D. H., Cicerone, R. J., Tuck, A. F.,
 1621 Frederick, J. E., Harries, J. E., and Crutzen, P.: The Halogen Occultation Experiment, *J. Geophys. Res.*,
 1622 98, 10777-10797, 1993.

1623 Russell III, J. M., Deaver, L. E., Luo, M., Park, J. H., Gordley, L. L., Tuck, A. F., Toon, G. C., Gunson ,
 1624 M. R., Traub, W. A., Johnson, D. G., Jucks, K. W., Murcray, D. G., Zander, R.,
 1625 Nolt, I. G., and Webster, C. R.: Validation of hydrogen chloride measurements made by the Halogen
 1626 Occultation Experiment from the UARS platform, *J. Geophys. Res.*, 101 (D6), 10,151– 10,162, 1996.

1627 Sakazaki, T., Fujiwara, M., Mitsuda, C., Imai, K., Manago, N., Naito, Y., Nakamura, T., Akiyoshi, H.,
 1628 Kinnison, D., Sano, T., Suzuki, M., and Shiotani, M.: Diurnal ozone variations in the stratosphere
 1629 revealed in observations from the Superconducting Submillimeter-Wave Lime-Emission Sounder
 1630 (SMILES) on board the International Space Station (ISS), *J. Geophys. Res. Atmos.*, 118, 2991-3006,
 1631 doi:10.1002/jgrd.50220, 2013.

1632 Santee, M. L., Lambert, A., Read, W. G., Livesey, N. J., Cofield, R. E., Cuddy, D. T.,
 1633 Daffer, W. H., Drouin, B. J., Froidevaux, L., Fuller, R. A., Jarnot, R. F., Knosp, B. W.,
 1634 Manney, G. L., Perun, V. S., Snyder, W. V., Stek, P. C., Thurstans, R. P., Wagner, P. A.,
 1635 Waters, J. W., Muscari, G., de Zafra, R. L., Dibb, J. E., Fahey, D. W., Popp, P. J., Marcy, T. P., Jucks, K.
 1636 W., Toon, G. C., Stachnik, R. A., Bernath, P. F., Boone, C. D., Walker, K. A.,
 1637 Urban, J., and Murtagh, D.: Validation of the Aura Microwave Limb Sounder HNO₃ measurements, *J.*
 1638 *Geophys. Res.*, 112, D24S40, doi:10.1029/2007JD008, 2007.

1639 Salby, M., Titova, E., and Deschamps, L.: Rebound of Antarctic ozone, *Geophys. Res. Lett.*, 38, L09702,
 1640 doi:10.1029/2011GL047266, 2011.

1641 Salby, M. L., Titova, E. A., and Deschamps, L.: Changes of the Antarctic ozone hole: Controlling
 1642 mechanisms, seasonal predictability, and evolution, *J. Geophys. Res.*, 117, D10111,
 1643 doi:10.1029/2011JD016285, 2012.

1644 Schoeberl, M. R., Dessler, A. E., and Wang, T.: Simulation of stratospheric water vapor and trends using
 1645 three reanalyses, *Atmos. Chem. Phys.*, 12, 6475–6487, doi:10.5194/acp-12-6475-2012, 2012.

1646 Schwartz, M. J., Froidevaux, L., Fuller, R. A., and Pawson, S.: GOZCARDS Merged Data for
 1647 Temperature Monthly Zonal Means on a Geodetic Latitude and Pressure Grid, version 1.01, Greenbelt,

1648 MD, USA: NASA Goddard Earth Science Data and Information Services Center, accessible from
1649 doi:10.5067/MEASURES/GOZCARDS/DATA3023, 2013.

1650 Scherer, M., Vömel, H., Fueglistaler, S., Oltmans, S. J., and J. Staehelin, J.: Trends and variability of
1651 midlatitude stratospheric water vapour deduced from the re-evaluated Boulder balloon series and
1652 HALOE, *Atmos. Chem. Phys.*, 8, 1391–1402, doi:10.5194/acp-8-1391-2008, 2008.

1653

1654 Sheperd, T. G., Plummer, D. A., Scinocca, J. F., Hegglin, M. I., Fioletov, V. E., Reader, M. C., Remsberg,
1655 E., von Clarmann, T., and Wang, H. J.: Reconciliation of halogen-induced ozone loss with the total-
1656 column ozone record, *Nature Geoscience*, 7, 443-449, doi:10.1038/NGEO2155, 2014.

1657

1658 Shindell, D. T.: Climate and ozone response to increased stratospheric water vapor,
1659 *Geophys. Res. Lett.*, 28, 1551-1554, doi:10.1029/1999GL011197, 2001.

1660 Solomon P. M., Barrett, J., Mooney, T., Connor, B., Parrish, A., and Siskind, D. E.: Rise and decline of
1661 active chlorine in the stratosphere, *Geophys. Res. Lett.*, 33, L18807, doi:10.1029/2006GL027029, 2006.

1662 Sofieva, V. F., Kalakoski, N., Päivärinta, S.-M., Tamminen, J., Laine, M., and Froidevaux, L.: On
1663 sampling uncertainty of satellite profile ozone measurements, *Atmos. Meas. Tech.*, 7, 1891–1900,
1664 doi:10.5194/amt-7-1891-2014, 2014.

1665 Solomon, S.: Stratospheric ozone depletion: A review of concepts and history, *Rev. Geophys.*, 37, 275–
1666 316, doi:10.1029/1999RG900008, 1999.

1667 Solomon, S., Rosenlof, K., Portmann, R., Daniel, J., Davis, S., Sanford, T., and Plattner, G.-K.:
1668 Contributions of Stratospheric Water Vapor to Decadal Changes in the Rate of Global Warming, *Science*,
1669 237, 1219-1223, 2010.

1670 SPARC: Assessment of Trends in the Vertical Distribution of Ozone, edited by N. Harris, R. Hudson and
1671 C. Phillips, SPARC/IOC/GAW, WMO Ozone Research and Monitoring Project Report No. 43, 1998.

1672 SPARC WAVAS: Assessment of upper tropospheric and stratospheric water vapour, World Climate
1673 Research Programme, WCRP-113, WMO/TD-No.1043, 261-264, 2000.

1674 Steinbrecht, W., Koehler, U., Claude, H., Weber, M., Burrows, J. P., and van der A, R. J.: Very high
1675 ozone columns at northern mid latitudes in 2010, *Geophys. Res. Lett.*, 38, L06803,

1676 doi:10.1029/2010GL046634, 2011.

1677 Strong, K., Wolff, M. A., Kerzenmacher, T. E., Walker, K. A., Bernath, P. F., Blumenstock, T., Boone,
1678 C., Catoire, V., Coffey, M., De Maziere, M., Demoulin, P., Duchatelet, P., Dupuy, E., Hannigan, J.,
1679 Hopfner, M., Glatthor, N., Griffith, D. W. T., Jin, J. J., Jones, N., Jucks, K., Kuellmann, H., Kuttippurath,
1680 J., Lambert, A., Mahieu, E., McConnell, J. C., Mellqvist, J., Mikuteit, S., Murtagh, D. P., Notholt, J.,
1681 Piccolo, C., Raspollini, P., Ridolfi, M., Robert, C., Schneider, M., Schrems, O., Semeniuk, K., Senten, C.,
1682 Stiller, G. P., Strandberg, A., Taylor, J., Tetard, C., Toohey, M., Urban, J., Warneke, T., and Wood, S.:
1683 Validation of ACE-FTS N₂O measurements, *Atmos. Chem. Phys.*, 8, 4759-4786, doi:10.5194/acp-8-
1684 4759-2008, 2008.

1685 Tegtmeier, S., Hegglin, M. I., Anderson, J., Bourassa, A., Brohede, S., Degenstein, D., Froidevaux, L.,
1686 Fuller, R., Funke, B., Gille, J., Jones, A., Kasai, Y., Krüger, K., Kyrölä, E., Lingenfelter, G., Lumpe, J.,
1687 Nardi, B., Neu, J., Pendlebury, D., Remsberg, E., Rozanov, A., Smith, L., Toohey, M., Urban, J., von
1688 Clarmann, T., Walker, K. A., and Wang, H. J.: The SPARC Data Initiative: A comparison of ozone
1689 climatologies from international satellite limb sounders, *J. Geophys. Res. Atmos.*, 118, 12,229–12,247,
1690 doi: 10.1002/2013JD019877, 2013.

1691 Thomason, L. W., Burton, S. P., Iyer, N., Zawodny, J. M., and Anderson, J.: A revised water vapor
1692 product for the Stratospheric Aerosol and Gas Experiment (SAGE) II version 6.2 data set,
1693 *J. Geophys. Res.*, 109 (D6), 9, 2004.

1694 Thomason, L. W., Burton, S. P., Luo, B.-P., and Peter, T.: SAGE II measurements of stratospheric
1695 aerosol properties at non-volcanic levels, *Atmos. Chem. Phys.*, 8, 983–995, doi:10.5194/acp-8-983-2008,
1696 2008.

1697 Thomason, L. W., Moore, J. R., Pitts, M. C., Zawodny, J. M., and Chiou, E.-W.: An evaluation of the
1698 SAGE III Version 4 aerosol extinction coefficient and water vapor data products, *Chem. Phys. Discuss.*,
1699 9, 22,177-22,222, 2009.

1700 Tian, W., Chipperfield, M. P., and Lu, D.: Impact of increasing stratospheric water vapor on ozone
1701 depletion and temperature change, *Adv. in Atmos. Sci.*, 26, 3, 423–437, 2009.

1702 Toohey, M., Hegglin, M. I., Tegtmeier, S., Anderson, J., Añel, J. A., Bourassa, A., Brohede, S.,
1703 Degenstein, D., Froidevaux, L., Fuller, R., Funke, B., Gille, J., Jones, A., Kasai, Y., Krüger, K., Kyrölä,
1704 E., Neu, J. L., Rozanov, A., Smith, L., Urban, J., von Clarmann, T., Walker, K. A., and Wang, R.:

1705 Characterizing sampling bias in the trace gas climatologies of the SPARC Data Initiative, *J. Geophys.*
1706 *Res. Atmos.*, 118, 11,847–11,862, doi: 10.1002/jgrd.5087, 2013.

1707 Tummon, F., Hassler, B., Harris, N. R. P., Staehelin, J., Steinbrecht, W., Anderson, J.,
1708 Bodeker, G. E., Bourassa, A., Davis, S. M., Degenstein, D., Frith, S. M., Froidevaux, L.,
1709 Kyrölä, E., Laine, M., Long, C., Penckwitt, A. A., Sioris, C. E., Rosenlof, K. H., Roth, C.,
1710 Wang, H. J., and Wild, J.: Intercomparison of vertically resolved merged satellite ozone data sets:
1711 interannual variability and long-term trends, *Atmos. Chem. Phys. Discuss.*, 14, 25687-25745, doi:
1712 10.5194/acpd-14-25687-2014, 2014.

1713 Urban, J., Lautié, N., Murtagh, D. P., Eriksson, P., Kasai, Y., Lossow, S., Dupuy, E.,
1714 de LaNoë, J., Frisk, U., Olberg, M., Flochmoën, E. Le., and Ricaud, P.: Global observations of middle
1715 atmospheric water vapour by the Odin satellite: An overview, *Planet. Space Sci.*, 55, 9, 1093-1102, 2007.

1716 Urban, J., Lossow, S., Stiller, G., and Read, W.: Another drop in water vapor, *EOS Transactions,*
1717 *American Geophysical Union*, 95, 27, 245-252, doi:10.1002/2014EO270001, 2014.

1718 Veiga, R.E., Cunnold, D. M., Chu, W. P., and McCormick, M. P.: Stratospheric Aerosol and Gas
1719 Experiments I and II comparisons with ozonesondes. *J. Geophys. Res.*, 100 (D5), 9073-9090, 1995.

1720 Voemel, H., Barnes, J. E., Forno, R. N., Fujiwara, M., Hasebe, F., Iwasaki, S., Kivi, R., Komala, N.,
1721 Kyrölä, E., Leblanc, T., Morel, B., Ogino, S.-Y., Read, W. G., Ryan, S. C., Saraspriya, S., Selkirk, H.,
1722 Shiotani, M., Valverde Canossa, J., and Whiteman, D. N.: Validation of Aura Microwave Limb Sounder
1723 water vapor by balloon-borne Cryogenic Frost point Hygrometer measurements, *J. Geophys. Res.*, 112,
1724 D24S37, doi:10.1029/2007JD008698, 2007.

1725 Wang, H. J., Cunnold, D. M., and Bao, X.: A critical analysis of Stratospheric Aerosol and Gas
1726 Experiment ozone trends *J. Geophys. Res.*, 101 (D7), 12495-12514, 1996.

1727 Wang, H. J., Cunnold, D. M., Thomason, L. W., Zawodny, J. M., and Bodeker, G. E.: Assessment of
1728 SAGE version 6.1 ozone data quality, *J. Geophys. Res.*, 107 (D23),
1729 doi: 10.1029/2002JD002418, 2002.

1730 Wang, H. J., Cunnold, D. M., Trepte, C., Thomason, L. W., and Zawodny, J. M.: SAGE III solar ozone
1731 measurements: Initial results, *Geophys. Res. Lett.*, 33, L03805, doi:10.1029/2005GL025099, 2006.

1732 Wang, R., Froidevaux, L., Anderson, J., Fuller, R. A., Bernath, P. F., McCormick, M. P., Livesey, N. J.,
1733 Russell III, J. M., Walker, K. A., and Zawodny, J. M.: GOZCARDS Merged Data for Ozone Monthly
1734 Zonal Means on a Geodetic Latitude and Pressure Grid, version 1.01, Greenbelt, MD, USA: NASA

1735 Goddard Earth Science Data and Information Services Center, accessible from
1736 doi:10.5067/MEASURES/GOZCARDS/DATA3006, 2013.

1737 Waters, J. W., Microwave limb sounding, in *Atmospheric Remote Sensing by Microwave Radiometry*,
1738 ed. by M. Janssen, chap. 8, John Wiley, New York, 1993.

1739 Waters, J. W., Froidevaux, L., Read, W. G., Manney, G. L., Esilon, L. S., Flower, D. A., Jarnot, R. F., and
1740 Harwood, R. S.: Stratospheric ClO and ozone from the Microwave Limb Sounder on the Upper
1741 Atmosphere Reseach Satellite, *Nature*, 362, 597-602, 1993.

1742 Waters, J. W., Froidevaux, L., Harwood, R. S., Jarnot, R. F., Pickett, H. M., Read, W. G., Siegel, P. H.,
1743 Cofield, R. E., Filipiak, M. J., Flower, D. A., Holden, J. R., Lau, G. K., Livesey, N. J., Manney, G. L.,
1744 Pumphrey, H. C., Santee, M. L., Wu, D. L., Cuddy, D. T., Lay, R. R., Loo, M. S., Perun, V. S., Schwartz,
1745 M. J., Stek, P. C., Thurstans, R. P., Boyles, M. A., Chandra, S., Chavez, M. C., Chen, G.-S., Chudasama,
1746 B. V., Dodge, R., Fuller, R. A., Girard, M. A., Jiang, J. H., Jiang, Y., Knosp, B. W., LaBelle, R. C., Lam,
1747 J. C., Lee, K. A., Miller, M., Oswald, J. E., Patel, N. C., Pukala, D. M., Quintero, O., Scaff, D. M.,
1748 Snyder, W. V., Tope, M. C., Wagner, P. A., and Walch, M. J.: The Earth Observing System Microwave
1749 Limb Sounder (EOS MLS) on the Aura satellite, *IEEE Trans. Geosci. Remote Sens.*, 44 (5), 1075–1092,
1750 doi:10.1109/TGRS.2006.873771, 2006.

1751 Waugh, D. W., Considine, D. B., and Fleming, E. L.: Is Upper Stratospheric Chlorine Decreasing as
1752 Expected?, *Geophys. Res. Lett.*, 28(7), 1187–1190, 2001.

1753 Weinstock, E. M., Smith, J. B., Sayres, D. S., Pittman, J. V., Spackman, J. R., Hints, E. J., Hanisco, T.
1754 F., Moyer, E. J., St. Clair, J. M., Sargent, M. R., and Anderson, J. G.: Validation of the Harvard Lyman- α
1755 in situ water vapor instrument: Implications for the mechanisms that control stratospheric water vapor, *J.*
1756 *Geophys. Res.*, 114, D23301, doi:10.1029/2009JD012427, 2009.

1757 WMO (World Meteorological Organization): *Scientific Assessment of Ozone Depletion: 2002*, Global
1758 Ozone Research and Monitoring Project – Report No. 47, Geneva, Switzerland, 2003.

1759 WMO (World Meteorological Organization), *Scientific Assessment of Ozone Depletion: 2010*, Global
1760 Ozone Research and Monitoring Project – Report No. 52, Geneva, Switzerland, 2011.

1761 Wohltmann, I., Lehmann, R., Rex, M., Brunner, D., and Mader, J.A.: A process-oriented regression
1762 model for column ozone, *J. Geophys. Res.*, 112, D12304, doi:10.1029/2006JD007573, 2007.

1763 Wolff, M. A., Kerzenmacher, T., Strong, K., Walker, K. A., Toohey, M., Dupuy, E., Bernath, P. F.,
1764 Boone, C. D., Brohede, S., Catoire, V., von Clarmann, T., Coffey, M., Daffer, W. H., De Maziere, M.,

1765 Duchatelet, P., Glatthor, N., Griffith, D. W. T., Hannigan, J., Hase, F., Hopfner, M., Huret, N., Jones, N.,
1766 Jucks, K., Kagawa, A., Kasai, Y., Kramer, I., Kullmann, H., Kuttippurath, J., Mahieu, E., Manney, G.,
1767 McElroy, C. T., McLinden, C., Mebarki, Y., Mikuteit, S., Murtagh, D., Piccolo, C., Raspollini, P.,
1768 Ridolfi, M., Ruhnke, R., Santee, M., Senten, C., Smale, D., Tetard, C., Urban, J., and Wood, S.:
1769 Validation of HNO₃, ClONO₂, and N₂O₅ from the Atmospheric Chemistry Experiment Fourier Transform
1770 Spectrometer (ACE-FTS), *Atmos. Chem. Phys.*, 8, 3529–3562, doi:10.5194/acp-8-3529-2008, 2008.

1771 Yang, E.-S., Cunnold, D. M., Newchurch, M. J., Salawitch, R., McCormick, J. M. P., Russell III, J. M.,
1772 Zawodny, J. M., and Oltmans, S. J.: First stage of Antarctic ozone recovery, *J. Geophys. Res.*, 113,
1773 D20308, doi:10.1029/2007JD009675, 2008.

1774 Ziemke, J. R., and Chandra, S.: Development of a climate record of tropospheric and stratospheric
1775 column ozone from satellite remote sensing: evidence of an early recovery of global stratospheric ozone,
1776 *Atmos. Chem. Phys.*, 12, 5737-5753, doi:10.5194/acp-12-5737-2012, 2012.

1777 Ziemke, J. R., Chandra, S., and Bhartia, P. K.: A 25-year data record of atmospheric ozone from TOMS
1778 Cloud Slicing: Implications for trends in stratospheric and tropospheric ozone, *J. Geophys. Res.*, 110,
1779 D15105, doi:10.1029/2004JD005687, 2005.

1780

1781 **Appendix A**

1782 **A.1. GOZCARDS data provenance**

1783 The general origin of the datasets is summarized here. Data coverage from limb sounders
1784 (including the instruments used here) is displayed nicely in the work by Toohey et al. (2013).

1785 ***SAGE I***

1786 SAGE I was launched February 18, 1979, aboard the Applications Explorer Mission-B
1787 (AEM-B) satellite. SAGE I was a sun photometer using solar occultation (Chu and McCormick,
1788 1979), and it collected a global database for nearly three years on stratospheric aerosol, O₃, and
1789 NO₂. For more information, the reader is referred to <http://sage.nasa.gov/SAGE1>.

1790 ***SAGE II***

1791 SAGE II was launched aboard the Earth Radiation Budget Satellite (ERBS) in October 1984
1792 and its data gathering period ended in August 2005. During each sunrise and sunset, SAGE II
1793 measured stratospheric aerosols, O₃, NO₂, and H₂O via solar occultation. This long dataset has
1794 proven very valuable in determining past ozone trends. For more information on and data access
1795 to the (V6.2) dataset used for GOZCARDS, the reader is referred to <http://sage.nasa.gov/SAGE2>.

1796 ***HALOE***

1797 Since its launch on September 12, 1991 from the Space Shuttle Discovery until November
1798 2005, UARS HALOE collected profiles of atmospheric composition and temperature. HALOE
1799 (Russell et al., 1993) used solar occultation to measure vertical profiles of O₃, HCl, HF, CH₄,
1800 H₂O, NO, NO₂, temperature, aerosol extinction, and aerosol composition and size distribution.
1801 More information and access to the HALOE data can be obtained from <http://haloe.gats-inc.com>
1802 and <http://disc.sci.gsfc.nasa.gov/UARS/data-holdings/HALOE>. For GOZCARDS purposes, we
1803 have used Version 19 HALOE netCDF data files available at <http://haloe.gats-inc.com>.

1804 ***UARS MLS***

1805 This instrument observed the Earth's limb in microwave emission using three radiometers, at
1806 frequencies near 63, 183 and 205 GHz (Waters, 1993; Barath et al., 1993), providing unique

1807 daily global information on stratospheric ClO, along with other profiles, including O₃, H₂O,
1808 HNO₃, temperature, and cloud ice water content. The stratospheric H₂O data ceased on April 15,
1809 1993, after the failure of the 183 GHz radiometer. After March 15, 1994, measurements became
1810 increasingly sparse in order to conserve the life of the MLS antenna scan mechanism and UARS
1811 power. Data exist until July 28, 1999, although for GOZCARDS, only data through mid-June
1812 1997 are used, as data sparseness and degradation of the 63 GHz radiometer led to less ‘trend-
1813 quality’ data after this. Sampling patterns follow the alternating yaw cycles imposed on MLS by
1814 the precessing UARS orbit; MLS measurements were obtained continuously for all latitudes
1815 between 34°S and 34°N, with higher latitudes covered in either the northern or southern
1816 hemisphere with a roughly 36-day cycle. Livesey et al. (2003) provide more information on the
1817 UARS MLS instrument, retrievals, and results. For data access, the reader is directed to the
1818 relevant Goddard Earth Sciences and Information Services Center (GES DISC) data holdings at
1819 <http://disc.sci.gsfc.nasa.gov/UARS/data-holdings/MLS>. L3AT data files were used as the basis
1820 for the production of the GOZCARDS UARS MLS monthly source datasets.

1821 *ACE-FTS*

1822 ACE-FTS is the primary instrument onboard the SCISAT satellite, launched on August 12, 2003.
1823 It is a high spectral resolution (0.02 cm⁻¹) Michelson interferometer operating from 2.2 to
1824 13.3 μm (750-4400 cm⁻¹); see Bernath et al. (2005) for an overview of the ACE mission. The
1825 instrument can simultaneously measure temperature and many trace gases (including all the
1826 species mentioned here for GOZCARDS), thin clouds, and aerosols, using the solar occultation
1827 technique. ACE-FTS data version 2.2, along with the version 2.2 update for ozone, were used
1828 here for GOZCARDS. For access to the public ACE-FTS datasets, with a routine measurement
1829 start date of March 2004, the reader is directed to <http://www.ace.uwaterloo.ca>.

1830 *Aura MLS*

1831 MLS is one of four instruments on NASA's Aura satellite, launched on July 15th 2004. Aura
1832 MLS is a greatly enhanced version of the UARS MLS experiment, providing better spatial
1833 coverage, vertical resolution, and vertical range, along with more continuous data over its
1834 lifetime (and with ongoing measurements at the time of writing). The instrument includes

1835 radiometers at 118, 190, 240, and 640 GHz, and a 2.5 THz module (Waters et al., 2006). Aura
 1836 MLS provides measurements of many chemical species, cloud ice, temperature and geopotential
 1837 height. Continuous measurements have been obtained since August 2004, with the exception of
 1838 OH, for which sparser measurements exist since August 2010, in order to preserve the life of the
 1839 THz module. For more information and access to the Aura MLS datasets, the reader is referred to
 1840 <http://disc.sci.gsfc.nasa.gov/Aura/data-holdings/MLS>. For GOZCARDS, we use the currently
 1841 recommended Aura MLS data versions (version 2.2/2.3 for ozone and 3.3/3.4 for other species).

1842 **A.2. Calculation details for the iterative merging procedure**

1843 Given three time series, the merging procedure that we use first combines two out of the three
 1844 time series, $y_1(i)$ and $y_2(i)$ (where index i represents time for each monthly mean value in a given
 1845 latitude/pressure bin). We first obtain the temporary merged series $m_1(i)$ via:
 1846
$$m_1(i) = (1/2) (y_1(i) + y_2(i)) \quad (1)$$

 1847 with the average offsets for $y_1(i)$ and $y_2(i)$ being $(1/(2 n_{12})) \sum (y_1(i) - y_2(i))$ and -1 times this value,
 1848 respectively; n_{12} is the number of overlapping data points between the two time series. Then, we
 1849 merge together the time series $m_1(i)$ and $y_3(i)$, keeping the weightings equal for all 3 time series
 1850 (1/3 for each), so that we calculate the new merged time series $m(i)$ via:

$$1851 \quad m(i) = w_m m_1(i) + w_3 y_3(i) = (1/3) (y_1(i) + y_2(i) + y_3(i)) \quad (2)$$

1852 which will hold if the weights are $w_m = 2/3$ and $w_3 = 1/3$ (given equation (1) for $m_1(i)$). The
 1853 average reference value (to which the adjustments of $m_1(i)$ and $y_3(i)$ in the 2nd step are made) is
 1854 given by $(1/n_m) \sum ((2/3) m_1(i) + (1/3) y_3(i))$, where n_m represents the number of (overlapping
 1855 pairs of) data values used in step 2. For the HCl and H₂O data merging procedure, we always use
 1856 the Aura MLS time series as one of the first two series involved in the initial merging step, for
 1857 example as $y_1(i)$, in order to maximize the overlap between the first two series and obtain more
 1858 robust offset values. Then, we use the 3rd time series; the order used for HALOE and ACE-FTS
 1859 (i.e., whether we use HALOE or ACE-FTS for y_2 or y_3) makes very little difference.

1860 **Calculation of the standard deviation for the merged data values**

1861 The average and standard deviation (square root of variance) for each y_k value (i.e. for each
 1862 monthly zonal mean in a particular lat/p bin) are calculated from equations (3) and (4) below:

1863
$$\bar{y}_k = \frac{1}{n_{yk}} \sum_j y_{kj} \quad (3)$$

1864 and, for the variance,

1865
$$\sigma_{yk}^2 = \frac{1}{n_{yk} - 1} \sum_j (y_{kj} - \bar{y}_k)^2 \quad (4)$$

1866 where index “ j ” corresponds to individual data values within a month, index k represents a given
 1867 instrument (data source), and n is the total number of data values for a given bin and source
 1868 (instrument) time series point in time (or month). Each value \bar{y}_k above is a monthly average
 1869 (although we also use instead the simpler notation y_k), with standard deviation about the mean
 1870 σ_{yk} . Now, given the merged series $u(i)$ (where index i runs over a large number of months), the
 1871 standard deviation of each merged data point (for a given month) can be obtained by considering
 1872 the original datasets y_{kj} that were used to construct u . Specifically, we have the variance for the
 1873 merged dataset

1874
$$\sigma_u^2 = \frac{1}{n_u - 1} \sum_j (u_j - u_{ref})^2 \quad (5)$$

1875 where u_{ref} is the merged value (which is not necessarily chosen to be the average value \bar{u}) and
 1876 the u_j values represent the union of adjusted data values that make up the merged product, with
 1877 the index j for this combined dataset covering all values (up to the total n_u) obtained from the
 1878 original source values y_{kj} . In practice, we do not keep track of the individual data values that
 1879 went into making the averages for the series y_k that are being merged, and we need to obtain σ_u
 1880 based solely on the values \bar{y}_k , σ_{yk} , and the original number of points for each dataset y_k ,
 1881 namely n_{yk} . If we consider all the original values, we have a combined dataset with n_u points,
 1882 such that $n_u = \sum_k n_{yk}$. Now, expanding equation (5), we get

1883
$$(n_u - 1) \sigma_u^2 = \sum_j (u_j^2 + u_{ref}^2 - 2u_{ref} u_j) \quad (6)$$

1884 or

1885 $(n_u - 1) \sigma_u^2 = \sum_j u_j^2 + n_u u_{ref}^2 - 2u_{ref} \sum_j u_j$ (7)

1886 Expanding (4) for each individual dataset y_k , we get

1887 $(n_{y_k} - 1) \sigma_{y_k}^2 = \sum_j y_{kj}^2 + \bar{y}_k^2 - 2\bar{y}_k \sum_j y_{kj}$ (8)

1888 which leads to

1889 $\sum_j u_j^2 = \sum_{k,j} y_{kj}^2 = \sum_k (n_{y_k} - 1) \sigma_{y_k}^2 + \sum_k n_{y_k} \bar{y}_k^2$, (9)

1890 so that extracting the variance from equation (7) now leads to

1891 $S_u^2 = \frac{1}{(n_u - 1)} (\underset{k}{\overset{\circ}{\mathbf{a}}}(n_{y_k} - 1) S_{y_k}^2 + \underset{k}{\overset{\circ}{\mathbf{a}}} n_{y_k} \bar{y}_k^2 + n_u u_{ref}^2 - 2u_{ref} \underset{k}{\overset{\circ}{\mathbf{a}}} n_{y_k} \bar{y}_k)$ (10)

1892 The adjusted time series are obtained from the original series y_k as Y_k , and we can write

1893 Equation (4) in the same manner for the Y_k data values, namely

1894 $\sigma_{Y_k}^2 = \frac{1}{n_{y_k} - 1} \sum_j (Y_{kj} - \bar{Y}_k)^2$ (11)

1895 with $\sigma_{Y_k} = \sigma_{y_k}$ as the adjustments (offsets) are performed in an additive manner; if these

1896 adjustments were performed using multiplicative factors, those factors would also have to be

1897 considered in a multiplicative way to get the new σ_{Y_k} values. We can thus write (10) for the

1898 adjusted datasets as:

1899 $S_u^2 = \frac{1}{(n_u - 1)} (\underset{k}{\overset{\circ}{\mathbf{a}}}(n_{y_k} - 1) S_{y_k}^2 + \underset{k}{\overset{\circ}{\mathbf{a}}} n_{y_k} \bar{Y}_k^2 + n_u U_{ref}^2 - 2U_{ref} \underset{k}{\overset{\circ}{\mathbf{a}}} n_{y_k} \bar{Y}_k)$ (12)

1900 Equation (12) for the standard deviation of the merged dataset simplifies if the original datasets

1901 are adjusted to exactly the same reference value ref ($\bar{Y}_k = ref$) and the merged value U_{ref} is

1902 also equal to that value, as the sum of the last 3 terms in Eq. (10) (with Y_k replacing y_k) then

1903 reduces to $n_u ref^2 + n_u ref^2 - 2n_u ref^2$, which is zero. In this case, one obtains

1904
$$s_u^2 = \frac{1}{(n_u - 1)} \left(\sum_k (n_{yk} - 1) s_{yk}^2 \right) \quad (13)$$

1905 However, in general, one should use equation (12) for the standard deviation of the merged
 1906 dataset, given the adjusted datasets \bar{Y}_k and the merged (or reference) value U_{ref} . Also, we often
 1907 use a merged value equal to the average of the original data (over a given overlap period), so that

1908
$$U_{ref} = \frac{1}{n_y} \sum_k \bar{y}_k \quad (14)$$

1909 where n_y is the total number of datasets (y_k), as opposed to having the merged value place more
 1910 weight on the larger datasets (e.g., for emission-type measurements versus occultation-type), in
 1911 which case one would consider using $U_{ref} = \frac{1}{n_u} \sum_k n_{yk} \bar{y}_k$. For ozone, we use a particular dataset
 1912 (SAGE II ozone) as the primary reference, but equation (12) can be used to obtain the standard
 1913 deviation for the merged dataset (about the SAGE II reference) in that case also. While it is
 1914 useful to have the formalism above for obtaining the merged dataset standard deviation σ_u , we
 1915 often find significant differences between the standard deviations of various datasets, so that this
 1916 effect will have the greatest influence on the results, as opposed to the impact of the last 3 terms
 1917 in the summation (in (12)). Finally, it is easy to test equation (12) (and we have done so) by
 1918 using synthetic series and calculating the standard deviation of the combined set. In reality, the
 1919 standard deviations of the time series monthly mean values are typically larger for MLS than for
 1920 ACE-FTS, mainly because of the more complete sampling of variability from the daily global
 1921 measurements acquired by MLS. Sample plots for standard deviations and standard errors in the
 1922 case of HCl are shown in Fig. A1. As expected, merged standard deviations follow the standard
 1923 deviations from HALOE HCl before Aug. 2004 and those from MLS HCl after this time.
 1924 However, the merged standard errors for the MLS time period follow the smaller MLS standard
 1925 errors, because these values vary inversely with the square root of the number of values sampled,
 1926 and are therefore made smaller by the significantly larger daily and monthly MLS sampling rate
 1927 and coverage.

1928

1929 **A.3. Procedural merging details for GOZCARDS HCl, H₂O, and O₃**

1930 **A.3.1. HCl**

- 1931 - The vertical data range for valid HCl merged values is between 0.46 hPa and 147 hPa
1932 (inclusive), as a result of data sparseness or data quality issues outside these ranges.
- 1933 - At 147 hPa, no merged HCl values exist for latitude bins from 35°S to 35°N inclusive,
1934 because of unrealistically large Aura MLS HCl values in this region; also, there is not enough
1935 data at this level to provide a meaningful product from HALOE and ACE-FTS data alone.
- 1936 - Because of occasional small negative merged values during southern hemisphere polar
1937 winter, we did not apply HCl data offsets in the lower stratosphere for the 65°S through 85°S
1938 bins from June through September and for pressures larger than or equal to 15 hPa. For
1939 vertical continuity purposes, we applied this method to all lower stratospheric pressure levels,
1940 although the small negative merged values only occurred in a small fraction of cases and the
1941 impact on the merged values is not large. Seasonal variations in other bins are milder and did
1942 not lead to such an Antarctic winter issue; also, this issue did not affect other species.
- 1943 - As Aura MLS and ACE-FTS data exist in the 85°N and 85°S bins, but there are no HALOE
1944 measurements, we could not use our standard merging procedure there. We simply extended
1945 the offsets from the adjacent bins (at 75°N and 75°S) to these two bins to obtain a merged
1946 record after 2004 that exhibits continuity versus latitude.
- 1947 - At 100 hPa, we used HCl offsets from the 5°S bin for the 5°N bin, as there was insufficient
1948 data from the three combined datasets in the latter bin to calculate meaningful offsets and
1949 merge the datasets. This procedure seems reasonable, given that the time series in these two
1950 adjacent tropical latitude bins (during years outside the 2004/2005 overlap period) look
1951 continuous and stable enough to justify identical adjustments in both bins and to avoid a data
1952 gap in the merged series at 5°N, although this does imply somewhat larger error bars at 5°N.

1953

1954 **A.3.2. H₂O**

- 1955 - The vertical data range for valid H₂O merged values is between 0.01 hPa and 147 hPa
1956 (inclusive). Some H₂O data exist at 147 hPa for low latitudes, but more careful work would
1957 be needed to extend the merged data globally in such a region.

- 1958 - Users should keep in mind the PMC-related caveats mentioned in Sect. 4 for summer at high
1959 latitudes in the upper mesosphere, prior to the end of the HALOE dataset (Nov. 2005).
- 1960 - As for HCl, we could not use our standard merging procedure at the two most poleward
1961 latitude bins; we simply extended the offsets from the adjacent bins (at 75°N and 75°S) to
1962 these polar bins to obtain a merged record after 2004 that exhibits continuity versus latitude.
- 1963 - Also as for HCl, at 100 hPa, we used H₂O offsets from the 5°S bin for the 5°N bin, as there
1964 was insufficient data from the combined datasets in the latter bin to calculate meaningful
1965 offsets and merge the datasets. This procedure avoids a data gap in the merged series at 5°N.

1966 **A.3.3. O₃**

1967 *Screening of SAGE O₃ data*

1968 For SAGE I O₃, the main uncertainty is aerosol interference, especially below 15 to 20 km. All
1969 SAGE I values below (in altitude) where the aerosol extinction at 1.0 μm reaches a value larger
1970 than $1.0 \times 10^{-3} \text{ km}^{-1}$ are removed from the analysis (L. W. Thomason, personal communication).

1971 For SAGE II ozone, the screening steps are based on Wang et al (2002) as follows:

- 1972 - We removed the entire ozone profile when any reported error bar value exceeded 10%
1973 between 30 and 50 km, in order to filter out outliers affected by “short events” (Wang et al.,
1974 2002), which mainly occurred between mid-1993 and mid-1994, when SAGE II had a battery
1975 problem. In order to preserve power, sunset measurements were started later than normal
1976 while sunrise measurements were ended earlier. These “short events” had fewer
1977 extraterrestrial solar irradiance measurements for calibration and normalization.
- 1978 - We used aerosol extinctions and extinction ratios to remove data affected by clouds, and
1979 aerosols from the June 1991 Mt. Pinatubo eruption. O₃ data were removed when the aerosol
1980 extinction at 0.525 μm exceeded $6 \times 10^{-3} \text{ km}^{-1}$, thus removing data affected by this eruption
1981 for months and even years, in the lower stratosphere. For cases with extinctions less than
1982 $6 \times 10^{-3} \text{ km}^{-1}$ but greater than $1 \times 10^{-3} \text{ km}^{-1}$, and extinction ratios ($0.525 \text{ μm} / 1.02 \text{ μm}$) ≤ 1.4 , the
1983 corresponding data were removed for additional filtering. Although more stringent criteria
1984 could be used to remove a few more outliers, this would also remove many more “good”
1985 ozone data that are not affected by aerosol/cloud. Fortunately, any artifacts from these few
1986 unfiltered data values are greatly reduced after binning the data into monthly zonal means.

- 1987 - We removed anomalously low O₃ values resulting from very small SAGE II transmittances;
1988 O₃ error values in these cases were capped at 300% by the algorithm. Such low O₃ values
1989 (sometimes low by 2-3 orders of magnitude) generally occur close to the tropopause and in
1990 the troposphere, and can be identified by using this 300% error flag (Wang et al., 2002).
1991 - It was found that SAGE II ozone data could be affected during high sun-orbit beta angle
1992 conditions (Wang et al., 1996). SAGE II profiles immediately following fully sunlit orbits
1993 with absolute values of beta greater than 40° are eliminated from monthly zonal means.

1994

1995 *Other merging details for O₃*

- 1996 - SAGE I monthly mean source data are used for the merged dataset in the tropical bins (25°S
1997 to 25°N) from 1 through 68 hPa only and, at higher latitudes, from 1 through 100 hPa only.
1998 - The vertical range for valid O₃ merged values is between 0.2 hPa and 215 hPa (inclusive),
1999 with the lower altitude bound varying with latitude. The merged product at 147 and 215 hPa
2000 has valid data only for the 35° to 85° latitude bins. Indeed, we limited merged data mostly to
2001 stratospheric values (larger than ~ 0.1 ppmv); the upper troposphere is more of a challenge
2002 for such a merging activity, given smaller abundances, more challenging measurements, and
2003 a larger impact from different instrument resolutions. The upper range limit was chosen to
2004 enable studies of the upper stratosphere and lower mesosphere, even if this is a region where
2005 diurnal ozone change occurs; arguments we have presented (see main text) suggest that the
2006 GOZCARDS merged ozone time series variations should not be subject to a large impact
2007 from diurnal variations, although high altitude regions should still be treated with caution.
2008 - We omitted the use of UARS MLS at 100 hPa for low latitudes (from 25°S to 25°N), as these
2009 monthly values are biased quite high and also exhibit too large a seasonal cycle amplitude, in
2010 comparison to HALOE and SAGE II data; this appears to relate to a UARS MLS artifact.
2011 - Since there is no (monthly) overlap between SAGE II and HALOE versus UARS MLS or
2012 Aura MLS in the 85°N and 85°S latitude bins, the same offsets as for 75°N and 75°S
2013 (respectively) are applied to the datasets at these two extreme latitude bins, in order to
2014 minimize latitudinal discontinuities in the merged data record.

2015 - Because of discontinuities that appeared in merged O₃ at high latitudes above the stratopause,
2016 particularly in the 75°S bin, we flagged merged values for 75° and 85° (N and S) as bad, for
2017 pressures less than 1 hPa. This issue could be the result of a few bad data points or not
2018 enough data overlap. To minimize artifacts, we left the resolution of this issue for future
2019 investigations; also, the reduced amount of occultation data at these high latitudes makes the
2020 usefulness of a merged product with poorly sampled seasonal changes somewhat marginal
2021 (for certain years at least, the number of monthly values drops significantly at high latitudes).
2022
2023

Table 1. Characteristics of instrument datasets used to create GOZCARDS ESDRs (version ev1.01).

Instrument and Data Versions	Platform	Type of measurement	Time period (GOZCARDS source files)	Vertical Resolution (km)	Retrieved quantity and stratospheric vertical grid spacing
SAGE I V5.9_rev O ₃	AEM-2	Solar occultation VIS/UV and near-IR	Feb. 1979 - Nov. 1981	1	Density on altitude grid 1 km spacing
SAGE II V6.2 O ₃	ERBS	Solar occultation VIS/UV and near-IR	Oct. 1984 - Aug. 2005	0.5 - 1	Density on altitude grid 0.5 km spacing
HALOE V19	UARS	Solar occultation mid-IR	Oct. 1991 - Nov. 2005	2.5	Volume Mixing Ratio on pressure grid with 30 levels per decade (LPD) change in p
MLS V5 O ₃ V6 H ₂ O	UARS	Limb emission microwave / sub-mm	Oct. 1991 - June 1997 (May 1993 end for strat. H ₂ O)	H₂O 3 - 4 (strat.) 5 - 12 (mes.) O₃ 3.5 - 5 (strat.) 5 - 8 (mes.)	Volume Mixing Ratio on pressure grid with 6 LPD in stratosphere 6 LPD in stratosphere
ACE-FTS V2.2 (V2.2 update for O ₃)	SCISAT	Solar occultation mid-IR	Mar. 2004 through Sep. 2010 (2009 for O ₃)	3 - 4	Volume Mixing Ratio on 1 km grid spacing (height and p provided)
MLS V3.3 V2.2 O ₃	Aura	Limb emission microwave / sub-mm	Aug. 2004 through 2012	HCl 3 - 5 H₂O 3 - 4 (p > 0.1 hPa) 5 - 9 (0.1-0.01 hPa) O₃ 3	Volume Mixing Ratio on pressure grid with 6 LPD 12 LPD 6 LPD

2027 **Table 2.** Products and instrument source data making up the available GOZCARDS data records.

Merged Products and pressure range	Source Datasets (and years used)
HCl 147 – 0.5 hPa	HALOE (1991-2005), ACE-FTS (2004-2010), Aura MLS (2004 onward)
H₂O 147 – 0.01 hPa	HALOE (1991-2005), UARS MLS (1991-1993), ACE-FTS (2004-2010), Aura MLS (2004 onward)
O₃ 215 – 0.2 hPa	SAGE I (1979-1981), SAGE II (1984-2005), HALOE (1991-2005), UARS MLS (1991-1997), ACE-FTS (2004-2009), Aura MLS (2004 onward)
HNO₃ 215 – 1 hPa	ACE-FTS (2004-2010), Aura MLS (2004 onward)
N₂O 100 – 0.5 hPa	ACE-FTS (2004-2010), Aura MLS (2004 onward)
Temperature 1000 – 0.015 hPa	GMAO MERRA (1979 onward)

2028

2029

2030

2031 **Fig. 1.** Merging procedure illustration for HCl. Top left panel shows the HCl monthly mean source data
2032 during the overlap period (Aug. 2004 - Nov. 2005) for HALOE, ACE-FTS, and Aura MLS. Top right
2033 panel illustrates step 1 in the merging procedure, with the temporary merged data values (orange)
2034 resulting from the adjustment of ACE-FTS and Aura MLS values to the reference indicated by the black
2035 dashed line. Middle left panel shows the result of step 2, namely the merged values arising from merging
2036 HALOE data with the temporary merged values from step 1; the black dashed line is the new average
2037 reference value, obtained from a 2/3 and 1/3 weighting of the dashed orange and dashed blue line values,
2038 respectively (see text). Middle right panel shows all the source data and the final merged values during
2039 the overlap period. Bottom panel shows the source and merged time series from 1991 through 2012 after
2040 the calculated additive offsets are applied to the whole source datasets, which are then merged (averaged)
2041 together wherever overlap between instruments exists.

2042
2043 **Fig. 2.** Offsets applied to the HCl source datasets (top panels for HALOE, middle panels for ACE-FTS,
2044 bottom panels for Aura MLS) as a function of latitude and pressure. The left column gives offsets in ppbv
2045 and the right column provides offsets as a percent of the zonal average merged mixing ratios during the
2046 overlap period (Aug. 2004 – Nov. 2005) used here to compute the average offsets.

2047
2048 **Fig. 3.** Example of HCl time series analyses for 50°N-60°N and 32 hPa. (a) HCl monthly mean source
2049 data from ACE-FTS and Aura MLS; the MLS dots are filled when there is time overlap with ACE-FTS,
2050 and open if no such overlap exists. Simple linear fits are shown as colored lines for
2051 ACE-FTS and for Aura MLS (orange line for all red dots and red line for filled red dots only).
2052 Correlation coefficient values (R values) for the two time series are provided in the title.
2053 (b) Deseasonalized anomalies for both ACE-FTS and Aura MLS, with corresponding linear fits (and R
2054 values). (c) Difference of deseasonalized anomalies (ACE-FTS minus Aura MLS), with linear fit.

2055
2056 **Fig. 4.** Latitude/pressure contours of time series diagnostics obtained from analyses illustrated in
2057 Fig. 3 for HCl from Aura MLS and ACE-FTS. Top panel: Correlation coefficient for the deseasonalized
2058 time series. Bottom panel: Ratio of the slope of the difference between deseasonalized series over the
2059 error in this slope.

2060

2061

2062 **Fig. 5.** Illustration of GOZCARDS HCl monthly averages with systematic error estimates (shown as grey
2063 shading) at 46 hPa for 30°S-40°S; see text for the meaning of this shaded region. The source data from
2064 HALOE, Aura MLS, and ACE-FTS are shown in different colors (see legend), along with the merged
2065 values.

2066
2067 **Fig. 6.** Systematic error estimates for GOZCARDS HCl. One error (left panels) is relevant for values
2068 lower than (below) the merged values, and one (right panels) for values larger than the merged values; the
2069 top panels give the error estimates in ppbv, and the bottom panel errors are expressed as percent of the
2070 average merged values over the relevant time periods (see text). These error bars provide a range within
2071 which 95% of the source data values lie.

2072
2073 **Fig. 7.** Time series of the GOZCARDS monthly-averaged merged HCl abundance for 3 different latitude
2074 bin averages (see color legend in panel (a)) for (a) 0.7 hPa, (b) 10 hPa, (c) 32 hPa, and (d) 68 hPa.

2075
2076 **Fig. 8.** The average rate of change (percent per year) for HCl as a function of pressure for different
2077 latitude bin averages (see legend) for time periods corresponding to the appropriate GOZCARDS HCl
2078 values (see text) in the upper stratosphere (Jan. 1997 - Sep. 2010) and lower stratosphere (Jan. 1997 -
2079 Dec. 2012). Deseasonalized monthly data were used to obtain a long-term trend for these time periods;
2080 two-sigma error bars are shown.

2081
2082 **Fig. 9.** Same as Fig. 8, but for the lower stratosphere only and using different time periods to illustrate
2083 shorter-term changes in this region. Average rates of change in HCl are given for (a) 2003 through 2012,
2084 a decade exhibiting significant differences between northern and southern hemispheric change, (b) the
2085 6-year period 2006 through 2011, when the largest changes occurred, and (c) the most recent 6-year
2086 period 2008 through 2013, when a significant decrease in the variability took place.

2087

2088

2089

2090

2091 **Fig. 10.** Rates of change for GOZCARDS HCl (connected open circles) are given as a function of latitude
2092 in 10° latitude bins for sliding 6-year periods centered on Jan. 1 of each year (e.g., the 1998 point is an
2093 average for data from 1995 through 2000, and the 2011 point is for data from 2008 through 2013). (a) is
2094 for changes in upper stratospheric HCl at 0.7 hPa and (b) is for the change in the integrated HCl column
2095 between 68 hPa and 10 hPa. The two additional curves in (a) represent the rates of change in the
2096 estimated surface total chlorine from NOAA data (green is for a 6-year time shift, and purple for a
2097 7-year time shift, to account for transport time to the upper stratosphere); see text for more details. Panels
2098 (c) and (d) are similar to (a) and (b), respectively, in terms of the pressure levels used, but the rates of
2099 change are averaged over all latitude bins covering 50°S to 50°N for two sets of sliding time periods
2100 (black is for 6-year periods, red is for 8-year periods). As in (a), surface total chlorine variations are also
2101 displayed in panel (c). Error bars indicate twice the standard errors in the means.

2102
2103 **Fig. 11.** Offsets applied to the H₂O source datasets as a function of latitude and pressure, similar to
2104 Fig. 2 for HCl.

2105
2106 **Fig. 12.** Latitude/pressure contours of time series diagnostics for H₂O from Aura MLS and ACE-FTS;
2107 this is similar to Fig. 4 for HCl.

2108
2109 **Fig. 13.** A depiction of the “tape recorder” evolution for tropical water vapor abundances from 147 to
2110 10 hPa for October 1991 through December 2013. This plot was produced from GOZCARDS merged
2111 H₂O time series anomalies (differences from the long-term means) for the average of the 4 tropical bins
2112 covering 20°S to 20°N.

2113
2114 **Fig. 14.** Systematic error estimates for GOZCARDS H₂O (similar to Fig. 6 for HCl).

2115
2116 **Fig. 15.** Variations in stratospheric water vapor from the GOZCARDS H₂O merged data records (1992
2117 through 2013) averaged from (a) 60°S to 60°N and (b) 20°S to 20°N. Monthly average values and annual
2118 averages are shown by thin and thick lines (connecting similarly-colored dots), respectively, for the
2119 pressure levels indicated in the plot legend.

2120

2121 **Fig. 16.** Stratospheric water vapor variability on decadal timescales for 1992 through 2013 (thick lines)
2122 for tropical (20°S-20°N in black) and mid-latitude (20°N-60°N in red and 20°S-60°S in blue) zonal
2123 means, based on the GOZCARDS merged H₂O data record. The variability is expressed here as the
2124 difference between maximum and minimum annual average abundances, from 100 to 1 hPa, in ppmv (left
2125 panel) and percent (right panel). The 22-year period is broken up into two 11-year periods to illustrate
2126 how the variability changes from the 1st period (dashed lines) to the 2nd period (thin solid lines).

2127

2128 **Fig. 17.** (a) Variations in upper mesospheric (0.01 hPa) water vapor mixing ratios averaged from 60°S to
2129 60°N for Oct. 1991 through Dec. 2013, based on the GOZCARDS merged H₂O data records. Monthly
2130 average values and annual averages are shown by connected brown dots and connected black dots,
2131 respectively. (b) GOZCARDS merged H₂O annual averages (connected filled symbols) from 60°S to
2132 60°N for 1992 through 2013 at pressure levels between 0.1 and 0.01 hPa. A time series of annually-
2133 averaged Lyman α solar flux values (open circles), scaled to arbitrary units, is also displayed (see text).

2134

2135 **Fig. 18.** Time series of monthly zonal mean O₃ for 10°S - 20°S between 1 hPa and 6.8 hPa (with pressure
2136 values given by "pre") from SAGE I, SAGE II, HALOE, UARS MLS, Aura MLS, and ACE-FTS, all
2137 color-coded following the legend in top left panel.

2138

2139 **Fig. 19.** Schematic diagram describing the creation of the merged GOZCARDS monthly zonal mean
2140 ozone data record from various satellite datasets. Instruments represented in red inside the boxes are used
2141 as a reference. Instruments whose measurements have already been adjusted to a reference are indicated
2142 with a "*" superscript. AMLS refers to Aura MLS and UMLS to UARS MLS. See text for more details.

2143

2144 **Fig. 20.** Offsets applied to the O₃ source datasets, similar to Fig. 2 for HCl.

2145

2146

2147

2148 **Fig. 21.** Latitude/pressure contours of time series diagnostics for O₃ from Aura MLS and ACE-FTS; this
2149 is similar to Fig. 4 for HCl. The correlation coefficients (R values) and slope trend diagnostics are
2150 provided for HALOE versus SAGE II in the top two panels (for 1993-1999 as the trend issue for
2151 converted SAGE II data occurs after mid-2000 and to avoid Pinatubo-related data gaps before 1993) and
2152 for ACE-FTS versus Aura MLS in the bottom two panels (for 2005-2009).

2153

2154 **Fig. 22.** Systematic error estimates for GOZCARDS O₃ (similar to Fig. 6 for HCl).

2155

2156 **Fig. 23.** Column ozone values (DU) from ZC12 (in red) for 60°S-60°N and from GOZCARDS averages
2157 in different latitude bins (see legend). The connected dots are for GOZCARDS column ozone densities
2158 above 68 hPa from 1979 through 2013. The lines with no symbols and the connected open dots are also
2159 for GOZCARDS columns, but for values above 100 hPa and above 215 hPa, respectively, for 1985
2160 through 2013; there are no blue open dots because of the lack of GOZCARDS merged ozone data in the
2161 tropics for pressures larger than 100 hPa, during 1985-2013.

2162

2163 **Fig. 24.** Near-global (60°S to 60°N) results for average column ozone (total and stratospheric, from
2164 *Ziemke and Chandra, 2012*) compared to GOZCARDS O₃ columns above 68 hPa. Stratospheric columns
2165 are offset in order to more easily compare relative variations versus time; the black dots and red crosses
2166 are referenced to the 1980 total column values, while the cyan curves are referenced to 2007 to better
2167 illustrate the fits in the later years.

2168

2169 **Fig. 25.** Change in column ozone after removal of solar cycle signal and with 3-year smoothing applied;
2170 (a) gives relative changes in DU, and (b) shows percent changes relative to the average GOZCARDS
2171 stratospheric columns in 1979. Black symbols are from the GOZCARDS column values above 68 hPa,
2172 averaged over 60°S-60°N. Red symbols, for comparison, are from the ZC12 data over the same latitude
2173 range (after removal of the fitted solar cycle signal).

2174

2175 **Fig. 26.** Time evolution (Aug. 2004 through 2012) versus latitude of GOZCARDS merged N₂O (ppbv) at
2176 (a) 6.8 hPa and (b) 100 hPa.

2177

2178 **Fig. 27.** Sample results display the time evolution of satellite-retrieved HNO_3 (ppbv) for two different
2179 periods, 1992-1997 in (a) and (c) versus 2004-2013 in (b) and (d). Panels (a) and (b) are contour plots at
2180 46 hPa from UARS MLS global data and the merged GOZCARDS global data after 2004, respectively;
2181 (c) and (d) show time series at 32 hPa and for the 40°N - 50°N latitude bin, with (a) from UARS MLS data,
2182 and (d) from ACE-FTS, Aura MLS, and the merged combination (between the two source data sets).

2183

2184

2185

2186

2187 **Fig. A1.** Illustration of the standard deviations (in (a)) and standard errors (in (b)) for monthly
2188 mean GOZCARDS HCl (source and merged records) at 46 hPa for 30°S - 40°S . Source data from
2189 HALOE, Aura MLS, and ACE-FTS are given by the filled colored dots (see legend); each
2190 standard deviation is simply obtained from the range of values measured during the month. The
2191 large open brown circles give standard deviations for the merged HCl product; this Appendix
2192 provides the formulae to calculate these quantities.

2193

2194

2195

2196 **Fig. S1:** Illustration of the latitudinal dependence of the HCl offsets for HALOE, ACE-FTS, and Aura
2197 MLS at two pressure levels (top panel for 0.46 hPa, bottom panel for 46 hPa). Error bars represent twice
2198 the standard error in the derived offsets (based on variability during the overlapping period). Larger
2199 standard error values indicate that there were either fewer points of overlap or larger offset variability
2200 (standard deviations); we found that both of these factors contribute.

2201
2202 **Fig. S2:** Latitude/pressure contours of the fitted mean annual amplitudes (ppbv) from HCl time series for
2203 HALOE, ACE-FTS, and Aura MLS, based on their respective measurement periods (see text).

2204
2205 **Fig. S3:** Time evolution (Oct. 1991 through 2013) versus latitude of GOZCARDS merged HCl (ppbv) at
2206 46 hPa.

2207
2208 **Fig. S4:** HALOE sunrise measurements of H₂O versus the 3.46 μm extinction coefficient for 1992, 1993,
2209 and 1999 at 22 hPa. The green vertical line represents the aerosol extinction value ($5 \times 10^{-4} \text{ km}^{-1}$) used to
2210 screen anomalous HALOE H₂O values. It is apparent that anomalously low H₂O values occurred in 1992
2211 when the 3.46 μm aerosol extinction exceeded about $5 \times 10^{-4} \text{ km}^{-1}$. These artifacts were confined to 1991
2212 and 1992; for these years, and for pressure levels at and below 22 hPa, the corresponding H₂O data values
2213 were excluded. This screening method eliminates about 10% of the global (lower stratospheric)
2214 measurements in 1992.

2215
2216 **Fig. S5:** Merging procedure illustration for H₂O at 5°N and 22hPa. This is similar to Fig. 2 (for HCl), but
2217 an additional step is illustrated for the end of this procedure, whereby stratospheric H₂O data from UARS
2218 MLS are adjusted to the early portion of the merged time series that was obtained after the 2nd step; this
2219 adds more coverage (more brown dots in the bottom panel for 1991-1993).

2220
2221 **Fig. S6:** Latitude/pressure contours of the fitted mean annual amplitudes (ppmv) from H₂O time series for
2222 HALOE, ACE-FTS, and Aura MLS, based on their respective measurement periods.

2223

2224 **Fig. S7:** Time evolution (Oct. 1991 through 2013) versus latitude of GOZCARDS merged H₂O (ppmv) at
2225 3.2 hPa (top panel) and 68 hPa (bottom panel).

2226

2227 **Fig. S8:** Monthly zonal mean ozone differences (%) between SAGE II and (a) HALOE,
2228 (b) UARS MLS (UMLS for short), (c) Aura MLS (AMLS for short), and (d) ACE-FTS during their
2229 respective overlap periods. Differences are expressed (in percent) as $100 \times [(SAGE II - Other) / (Other)]$.
2230 Shaded areas indicate negative values.

2231

2232 **Fig. S9:** Monthly zonal mean temperature differences between NCEP (used by SAGE II) and HALOE
2233 temperatures relative to MERRA for 10°S - 20°S between 1 and 6.8 hPa, per color-coding indicated in
2234 bottom left panel; “pre” represents the pressure value. From 1 to 2.1 hPa, differences between NCEP and
2235 MERRA are generally within $\pm 4K$ before mid-2000. After that time, NCEP temperatures show a sharp
2236 increase and are systematically higher than MERRA values by 5 to 10K. However, this divergence and
2237 trend are not seen in HALOE temperatures. NCEP temperatures between 3.2 and 6.8 hPa are smaller than
2238 MERRA after mid-2000; negative trends (versus MERRA) also occur in the HALOE data at these levels.

2239

2240 **Fig. S10:** Relative trends (K/decade) in zonal mean temperature differences for NCEP – MERRA and
2241 HALOE – MERRA (color-coded as in Fig. S9) in the upper stratosphere. NCEP temperatures show
2242 positive trends versus MERRA of $\sim 2-5$ K/decade between 2.1 and 1 hPa for all latitudes. However,
2243 HALOE temperatures show no significant trends versus MERRA, except at 1.5 hPa in the southern
2244 hemisphere. For pressures between 3.2 and 6.8 hPa, the temperature analyses are not conclusive; although
2245 NCEP values show negative trends of $\sim 2-3$ K/decade versus MERRA, they agree with HALOE.

2246

2247 **Fig. S11:** Mean differences and standard deviations (horizontal bars) between SAGE II and Aura MLS
2248 ozone in three different latitude bins: 20°S to 60°S (left panel), 20°S to 20°N (middle panel), and 20°N to
2249 60°N (right panel). Results based on monthly zonal mean and coincident profiles (see text for coincidence
2250 criteria) during overlap periods are shown in red and blue, respectively. To choose collocated profiles,
2251 coincidence criteria of $\pm 1^\circ$ in latitude and $\pm 8^\circ$ in longitude were used; the time difference criterion was
2252 chosen as 12 hours, but only nighttime measurements from Aura MLS were used.

2253

2254 **Fig. S12:** Latitude/pressure contours of the fitted mean annual amplitudes (ppmv) from O₃ time series for
2255 SAGE II, HALOE, ACE-FTS, and Aura MLS, based on their respective measurement periods.

2256

2257 **Fig. S13:** Illustration of the time evolution of the GOZCARDS merged O₃ data field versus latitude at
2258 68 hPa (top panel) and versus pressure for the 40°N-50°N latitude bin (bottom panel).

2259

2260 **Fig. S14:** Offsets applied to the N₂O source datasets (top panels for ACE-FTS, bottom panels for Aura
2261 MLS) as a function of latitude and pressure. The left column gives offsets in ppbv and the right column
2262 provides offsets as a percent of the zonal average merged mixing ratios during the overlap period (Aug.
2263 2004 – Sep. 2010) used here to compute the average offsets.

2264

2265 **Fig. S15:** Latitude/pressure contours of time series diagnostics derived from Aura MLS and ACE-FTS
2266 N₂O data comparisons (and obtained from analyses similar to those illustrated in Fig. 6 for HCl). Top
2267 panel: Correlation coefficient for the deseasonalized time series. Bottom panel: Ratio of the slope of the
2268 difference between deseasonalized series over the error in this slope.

2269

2270 **Fig. S16:** Offsets applied to the HNO₃ source datasets (top panels for ACE-FTS, bottom panels for Aura
2271 MLS) as a function of latitude and pressure. The left column gives offsets in ppbv and the right column
2272 provides offsets as a percent of the zonal average merged mixing ratios during the overlap period (Aug.
2273 2004 – Sep. 2010) used here to compute the average offsets.

2274

2275 **Fig. S17:** Latitude/pressure contours of time series diagnostics derived from Aura MLS and ACE-FTS
2276 HNO₃ data comparisons (and obtained from analyses similar to those illustrated in Fig. 6 for HCl). Top
2277 panel: Correlation coefficient for the deseasonalized time series. Bottom panel: Ratio of the slope of the
2278 difference between deseasonalized series over the error in this slope.

2279

2280